# MIMO Communication Using Single Feed Antenna Arrays

Alrabadi, Osama

*Publication date:*
2011

*Document Version*
Accepted author manuscript, peer reviewed version

Osama N. Alrabadi

MIMO Communication Using Single Feed Antenna Arrays

Osama N. Alrabadi

MIMO Communication Using Single Feed Antenna Arrays

Osama N. Alrabadi

The dissertation proposes an alternative approach for MIMO transmission using a fast switching antenna system with a single RF chain. One approach merely switches the RF excitation point at the modulation rate and thus encodes some information onto the active antenna index; however complex signal formats may not be encoded in this manner. A sophisticated reactance-assisted antenna system is proposed for addressing the complex signaling problem. Using a 3-element reactance-assisted antenna system, the dissertation proposes a universal encoding scheme for encoding multi PSK signals directly on the array far-field.

A proof of concept antenna prototype at 2.6 GHz has been designed. The MIMO functionality has been demonstrated, where two BPSK datastreams at a rate of 800 kbps were successfully multiplexed and demultiplexed via a single radio at the transmit side and a conventional uniform linear array on the receiver side.

2011
Aalborg University
Department of Electronic Systems
Center for TeleInfFrastrktur (CTiF)
ISBN: 978-87-92328-57-1

MIMO Communication Using Single Feed Antenna Arrays

AAU

Center for TeleInfFrastrktur (CTiF)
Department of Electronic Systems
Aalborg University

# MIMO Communication Using Single Feed Antenna Arrays

Osama N. Alrabadi
Department of Electronic Systems
Aalborg University

***A Dissertation Submitted to the Department of Electronic Systems and the Committee on Graduate Studies of Aalborg University in Partial Fulfillment of the Requirements for the Degree of Doctor of Philosophy***

January, 2011

# Abstract

Multi-input-multi-output (MIMO) communication has emerged as a promising technology for meeting the increasing demand on higher data rates. The technology exploits the spatial resource dimension by sending the datastreams to different locations in the multi element array (MEA) domain while decoding the signals at the receive end based on the signalsŠ unique spatial signatures. To this end, the MEA is conventionally assumed to be attached to a number of radios for independently modulating and up-converting (demodulating and down-converting) the set of signals at the transmit (receive) end.

While the implementation of a MIMO system is affordable at basestations (BS) and access points (AP), this is not true when considering simple, low-cost, battery-based mobile terminals with limited physical area. It is the subject of this thesis to bring a new philosophy regarding the design of reduced complexity MIMO systems by revisiting the MIMO wireless propagation from a signal space point of view. The main objective is to enable MIMO transmit functionalities with a sole radio and a single RF chain.

The general approach for achieving the aforementioned objective is to modulate one datastream conventionally to a single antenna element while modulating the other datastreams in the analogue RF domain, using simple switched antenna systems (SAS) or sophisticated reactance-assisted antenna systems.

The use of a SAS is found simple to implement, but can hardly handle high order signal formats, and is best suited for binary phase shift keying (BPSK) signal formats. The idea there is to encode the remaining datastreams to the active antenna index by moving the excitation point using an RF switch.

In the second case, reactance-assisted antenna systems are found important for scaling the single-radio MIMO objective to high order signaling dimensions. The idea is to exploit a number of passive radiators surrounding the central driving one for creating the desired multiplexing relations of a set of predefined basis beams. By this, information is encoded over the angular variations of the beampattern, which finally conveys the datastreams over the propagation channel to the intended receiver. However the second technique requires a complex baseband control circuitry when compared to the SAS approach. The proposed approach is finally validated in an indoor office environment using a 2.6 GHz prototype. The experiments show that

the proposed beamspace MIMO approach provides performance comparable to a conventional MIMO system, but at a reduced size and hardware complexity.

## English-Danish Short Summary

The dissertation proposes an alternative approach for MIMO transmission using a fast switching antenna system with a single RF chain. One approach merely switches the RF excitation point at the modulation rate and thus encodes some information onto the active antenna index; however complex signal formats may not be encoded in this manner. A sophisticated reactance-assisted antenna system is proposed for addressing the complex signalling problem. Using a 3-element reactance-assisted antenna system, the dissertation proposes a universal encoding scheme for encoding multi PSK signals directly on the array far-field.

A proof of concept antenna prototype at 2.6 GHz has been designed. The MIMO functionality has been demonstrated, where two BPSK datastreams at a rate of 800 kbps were successfully multiplexed and demultiplexed via a single radio at the transmit side and a conventional uniform linear array on the receiver side.

Denne afhandling foreslår en alternativ tilgang for MIMO transmissioner der anvender hurtigt switched antenne systemer med en enkel RF kåde. En af metoderne switcher blot mellem RF excitationspunktet ved den givne modulationshastighed og koder derfor informationer på det aktive antenne indeks; nogle komplekse signalformater kan dog ikke kodes på denne måde. Et sofistikeret reaktanstilpasset antenne system er foreslået for at kunne addressere problemet med de komplekse signaler. Ved brug af et tre elements reaktanstilpasset antenne system, foreslår afhandlingen en universel kodningsmetode til at kode multi PSK signaler direkte på fjernfeldts arrays.

En antenne prototype til verificering af konceptet ved 2.6 GHz er designet. MIMO funktionaliteten er blevet demonstreret, hvor to BPSK datastrømme med en hastighed på 800 kbps med success er multiplekset og demultiplekset via en enkelt radio på den transmitterende side og et konventionel uniform linear array på modtager siden.

TO MY PARENTS

# Acknowledgements

First I would like to express my deep gratitude to my thesis advisors: Professor Ramjee Prasad, Professor Constantinos Papadias, Professor Antonis Kalis and Dr. Nicola Marchetti for their help and encouragement throughout the last three years, the discussion with them has always been inspiring for my thesis project.

Thanks to the BWiSe members for their help on demonstrating the core idea of my PhD and special thanks to Elpiniki Tsakalaki for the collaborative research and for co-authoring more than eight papers with her. I would also like to thank Dr. Julien Perruisseau-Carrier from Ecole Polytechnique Fédérale de Lausanne (EPFL), for the seamless collaboration on designing the antenna system and for co-authoring some papers with me.

I would also like to express my gratitude to Howard Huang and Reinaldo Valenzuela at Lucent Bell labs for an exciting summer internship that extended my expertise to multi user cellular systems.

Finally, deepest gratitude is due to my family for their support and understanding during my study and stay abroad.

# Contents

# List of Figures

## LIST OF FIGURES

# List of Tables

## LIST OF TABLES

# 1

# Introduction

## 1.1 Background

MIMO array processing has been established as an effective means to achieve remarkable spectral efficiency. The capacity of such space-time (ST) wireless channels has been shown to increase almost linearly with the minimum number of transmit-receive antennas (GF98; Tel99). The average mutual information of a wireless MIMO system of many transmit and receive antennas scales as

$$\Im_{av} \approx \min(\mathcal{K}_R, \mathcal{K}_T) \log_2(1 + \rho \frac{\mathcal{K}_R}{\mathcal{K}_T}) \tag{1.1}$$

where $\mathcal{K}_R, \mathcal{K}_T$ are the number of the receive and transmit antennas, respectively and $\rho$ is the average signal-to-noise ratio (SNR) per receive antenna.

Since the emergence of the MIMO technology, the classical approach has been assuming a transmitter with a number of transmit RF chains in order to independently map a set of signals onto a corresponding set of antennas. The receiver on the other hand performs some complex signal processing so as to decode the linear mixture of the signals and extract the useful data. However, having multiple RF chains at the user mobile terminal is rather costly. For example, in the future standard of mobile terminals as in the LTE system (L1)(L2), a single antenna will be used for the uplink transmission whereas four antennas will be used for the downlink reception. The asymmetry in the number of the antennas is mainly intended for avoiding the costly power amplifiers (PA's) in the transmit RF chains. Although antenna selection is a terminal option, it requires instantaneous channel state information from the receiver back to the transmitter, which is a burden on the wireless communication system. Consequently, classical MIMO transmission especially in uplink scenarios may not be supported due to the practical limitations of the portable RF units.

## Conventional MIMO Under Compactness Constraints

MIMO systems, characterized by multi antennas at the transmit and the receive sides, have demonstrated the potential for increased capacity in rich multipath environments (Win87; HM99; CR98). As per (1.1), the capacity scales linearly with the minimum number of the transmit-receive antennas under rich scattering conditions besides the assumption of having a large wireless MIMO system (i.e. many uncorrelated transmit and/or receive antennas). The results are quite ideal in the sense that

- A rich scattering environment is almost impossible when considering a base-station (BS) on top of a clutter. For example, it is stated in (AV03) that the multipath concentration seen by a BS in a rural area is only within $2^\circ$ and within $5-7^\circ$ in urban environments.
- A MIMO system intended for a mobile terminal (where the rich scattering assumption makes sense) requires a minimum decorrelation distance of half the carrier wavelength between every two adjacent antennas (VLT05), leading to impractical large array implementations. In this work we are concerned with the second problem i.e. efficient MIMO system design under compactness constraints. In fact, it was found that the mutual coupling (MC) effect among a set of antennas is unavoidable when considering portable units with limited physical area (WSW04). It was first noted in (YTE91) that MC decorrelates the received signals, however MC also results in impedance mismatch and thus degrades the maximum average power the antenna system can extract from the field (ea05).

  This part discusses the main design challenges of MIMO systems intended for portable RF units within a limited physical area. The limitations can be summarized as follows:

  - RF hardware cost & complexity: The need for multiple radios where every RF chain has its own analogue-to-digital converter (ADC), digital-to-analogue converter (DAC), low-noise amplifier (LNA), PA and the intermediate frequency (IF)/RF filters etc., is rather costly especially as the cost of such analogue components *does not* scale down as in the case of silicon based components.
  - Circuit energy consumption: which is the DC power consumption of the PA, the DAC, the mixer, the active filters in the transmit chain, the frequency synthesizer, the LNA, the IF amplifier, the ADC and the active filters in the receive chain.
  - Spatial correlation: Closely spaced antennas emit signals of correlated spatial signatures, resulting in reduced channel capacity. In fact, (1.1) assumes a high rank channel i.e. $\text{rank}(\mathbf{H}) = \min(\mathcal{K}_R, \mathcal{K}_T)$. A low-rank channel has an average mutual information approximated by

$$\Im_{av} \approx \log_2(1 + \rho\mathcal{K}_R) \tag{1.2}$$

i.e. the channel behaves like a point-to-point channel with $\mathcal{K}_R$ times the received signal power due to the antenna array, achieved by simple maximum ratio combining (MRC) at the receiver. For the system to achieve the performance promised by (1.1) under rich scattering conditions, the antenna elements need to have a typical inter-element spacing of half the carrier wavelength[1] (VLT05), thus leading to large array realizations.

– Antenna system efficiency - Due to the strong MC among the closely spaced antenna elements, the input impedance seen by the RF ports is altered, thus leading to a mismatch loss (i.e. some of the incident power is reflected back to the source). Moreover, some of the radiated power will be absorbed by the neighboring antennas[2] as being terminated (matched) by a resistive impedance. The two losses (reflection plus absorption) are accounted for by the matching efficiency. The matching efficiency $\eta_M$ in the transmit mode is the ratio of the transmitted power $P_t$ to the input power $P_i$ and can be related to the matching network and the antenna array parameters by the general expression in (MKAL06)

– Inter-chain interference: The use of non-ideal (dirty) RF components will result in a leakage (cross talk) among the parallel RF chains leading to reduced system capacity (JM05b).

The negative impact of the signals correlation and antennas MC can be jointly mitigated by incorporating a decoupling and matching (DMN) network just before the antenna system (HSB$^+$06; CWC08), within what is referred to as multi-port conjugate matching or bilateral Hermitian matching (JW04). However, such a sophisticated network is difficult to design when considering many antenna elements, besides its negative impact on the antenna system bandwidth (MKAL06). Consequently, the classical uncoupled matching techniques like the

1. characteristic impedance (or $Z_0$) termination, which is the simplest type of termination, and the
2. self-impedance termination which is optimal under no MC,

are preferred for their simple deployments though provide suboptimal performance under MC. An alternative optimal single-port matching technique was proposed in (ea08c; LA06), where the ports of the antenna system are matched *individually* without any shunt connections either for a high power gain or low correlation with small negative impact on the antenna system bandwidth. For example, in (ea08c),

[1] As mentioned before, a spacing of half the carrier wavelength is enough for decorrelating the signals under rich scattering conditions, but not under narrow angular spreads where sometimes a spacing of ten times the carrier wavelength is required!

[2] However, the average power absorbed by a neighboring antenna terminated by a reactive load is zero.

it was shown that a *balanced uncoupled* matching of two closely spaced electrical dipoles can be optimized either for the maximum received power with high output correlation, or for zero correlation with an excess power loss of 1.5 dB. In both scenarios, the optimized parameter (received power or output correlation) was shown to slightly change with the *reactive part* of the optimal loading impedance i.e. negligible effect on the system bandwidth.

Other techniques for reducing the MC level among a set of closely spaced antennas include the insertion of a defected ground plane between the neighboring elements (CGK09) and the direct control of the effective mutual impedance matrix (TAPP10), etc. On the other side, several techniques have been already proposed in the literature for decorrelating the signals emitted or captured by a set of closely spaced antennas, e.g. the reader may refer to (RBD05) where the authors discuss three different techniques for decorrelationg the signals.

The aforementioned techniques help decouple and decorrelate co-polar antenna elements, however cross-polar antennas might seem attractive for some wireless portable devices, though require a bigger physical area as compared to the co-polar case. In fact, polarized antenna systems have already been proposed for realizing compact MIMO systems, for example in (AG05), the authors investigate the capacity performance of the MIMO cube with twelve edges of center-fed electrical dipole antennas. This geometry allows benefiting from space, polarization and pattern diversities jointly in a somehow small volume. In fact, a comparable performance to the case of i.i.d. Rayleigh fading channel has been found using such configuration.

Another feasible approach is the use of multimode antennas, which have been heavily researched in the recent years (EK08; Kle09; EK05). Multimode antennas are a strong candidate for compact MIMO systems as they provide a diversity action within a miniaturized physical area. The modes of an antenna system are the different solutions of Maxwell equations under the same boundary conditions. The modal patterns in the far-field show angular dependence, which is the source of the aforementioned diversity action i.e. the modal patterns are weakly correlated. Multimode MIMO systems have been evaluated during the reception mode, via different mode combining techniques. It is understood from (EK07) that the covariance rather than the correlation matrix should be used when evaluating the performance of such kind of MIMO systems as the modal patterns are generally imbalanced.

The aforementioned techniques enable the MIMO functionality within a small area, however they don't address the cost and complexity issues of such systems. In fact, a reduced complexity ST processing (i.e ST processing with a smaller number of RF chains than the number of the available antennas) may fall in one of the following contexts:

- State selection: The transceiver switches to a different state (state $\equiv$ antenna, mode or polarization) that corresponds to the strongest channel (the

most common approach in wireless MIMO is antenna selection(NS04)). In case state selection is implemented by the transmitter, a kind of channel knowledge at the transmit side should be available.

- Spatial oversampling: In (WIK04; IWF02) the authors propose a reduced complexity receiver architecture by oversampling the linear mixture of the received signals using a number of antennas and a single RF chain. Notice that such approach leads to bandwidth expansion making the receiver sensitive to the channel interference. Although such approach is useful for demultiplexing the mixed signals, it is not clear how it could be useful during transmission.
- Spatial combining/Analogue beamforming: In this approach the multi-antennas are simultaneously attached to a single RF chain. By controlling the time/phase delay and gain of the signals in each antenna path independently in the analogue domain (using RF phase shifters and attenuators), the multi-antenna system can improve the SNR, and requirements on the PA can be also relaxed through spatial power combining (LPL06). The spatial combining can be used as analogue beamformer, however having RF components in the path of every antenna increases somehow the cost, RF complexity and more importantly the RF insertion losses, a draw back addressed by the following alternative analogue beamforming approach.

### Analogue Beamforming via Reactance-Assisted Antenna Systems

As already mentioned, analogue beamforming is an approach for directly controlling the signals in the RF domain. One way to do it is to use RF phase shifters and attenuators so as to control the phases and amplitudes of the high frequency signals. An alternative approach for analogue beamforming is proposed in (LOT96; GO00), using a tunable reactance-assisted antenna system. This idea was first demonstrated by Ohira at the ATR labs in Japan using the well-known 7-element ESPAR antenna. The ESPAR is a smart antenna system that is able to control its beam pattern as any smart antenna system, while being implemented using a single active antenna element and a number of parasitic elements (PEs) placed on a circle around the active one (OG00). The PEs are short-circuited and loaded with variable reactors (varactors) that control the imaginary part of the PEs' input impedances. By adjusting the varactors' values, the radiation pattern of the ESPAR antenna system can be controlled to direct its beams and nulls toward certain directions in an adaptive or predefined fashion. ESPAR antennas present an attractive solution for wireless devices (ea03b) due to the simplicity of the antenna feeding network and the small inter-element spacing that can be as small as $0.05\lambda$ (ea06). They have already been used for receive diversity schemes (LDP06; OTIS04), where the antenna is controlled in a way that maximizes the received signal-to-noise-and-interference-ratio (SNIR). In this thesis we focus on

using reactance-assisted antenna systems at the transmit side for implementing reduced complexity MIXO (X={M,S}) transmitters.

### From Analogue Beamforming to Analogue MIMO

The current work proposes an approach for making multi antenna technology feasible for low profile wireless devices of a limited physical area by addressing some of the aforementioned design challenges encountered when bringing the antennas within a small volume. Multi antenna technology has been conventionally used within one of two operational modes: either beamforming; a mode within which the multi antennas commonly shape a single directive beam toward the desired direction (the underline set of antennas are fed with complex weights but a single datastream). Unlike digital beamforming, the analogue beamforming approach uses a number of passive antennas (antennas terminated with passive adaptive loads rather than being connected to separate RF chains) coupled to a single active antenna (the one connected to the RF port). By controlling the passive antennas' loading, the response of the antenna system in the far-field is controlled. Analogue beamforming replaces the RF hardware required generally for up-converting and down-converting the baseband complex signals with a low-cost DC control circuitry.

The second major utilization of ST communication is MIMO; a mode within which the multi antennas transmit independent datastreams (spatial multiplexing) or redundant datastreams (ST codes). It is the topic of this dissertation to describe the concept of 'analogue MIMO' and address the following challenges:

- How to modulate multi signals while having a single radio and;
- How to transmit multi signals, again using a single radio.

## 1.2 Related Work

There is some work in the literature that is found related to the topic of this thesis, summarized as follows:

1. The original work in (KKCC06; KKP07; KKP08) forms the basis for this thesis. In (KKCC06) a $2 \times 2$ MIMO system with a single active element at the transmit side, implemented using switched parasitic arrays (SPA); however the scheme was restricted to ON-OFF keying modulation scheme which is not popular in mobile communications. In (KKP07; KKP08), the authors propose a beam-space MIMO (BS-MIMO) transmission scheme using 3- and 5-element ESPAR antennas. According to the BS-MIMO approach, two different symbols are simultaneously sent toward the channel virtual

angles (Say02). This is achieved by creating an ESPAR pattern in the far-field that is a linear combination of weakly correlated beams (cardioids). However, the scheme proposed in (KKCC06; KKP07; KKP08) can hardly be scaled to modulation schemes of higher orders. The main limitation comes from the difficulty of obtaining the desired linear combinations for the *chosen set of basis functions* (i.e. the cardioids). The current thesis generalizes the concept of BS-MIMO with a single radio to complex signaling formats as well as to arbitrary radiating elements.

2. In (PPS+06; SPM06) the authors propose hybrid array structures of active and passive antennas. The passive antennas will simply enhance the diversity performance (during the reception mode) by switching to one of the predetermined antenna states. The adaptive MIMO system is proposed for base-stations. The topic of the thesis is quite different in the sense that we only consider a single active antenna system intended for portable RF units.
3. In (Vau99), the author describes how low cost parasitic antenna elements can provide considerable diversity gains using compact antenna systems. The topic of this paper is about signals multiplexing with one radio rather than antenna diversity with one radio.
4. In (SW01), a MIMO-like realization using a single active element and a number of PEs was shown to provide comparable capacity to that of conventional MIMO, where the array far-field is changed on every symbol period. However, the authors in (SW01) did not describe how the suggested realization may transmit multi signals.
5. The work in (Mig06) describes how SISO sub-channels are created by expanding the electromagnetic field into a set of orthogonal functions (high order harmonics). In this thesis the far-field is expanded by decomposing the Euler functions used as spatial phase terms when expressing the array far-field. The spatial phase term is generally expressed as $\exp(j\kappa\widehat{\mathbf{r}}.\mathbf{r}_i)$ where $\kappa$ is the wavenumber, $\widehat{\mathbf{r}}$ is the unit radial vector from the coordinate origin in the observation direction $(\vartheta, \varphi)$, $\mathbf{r}_i$ is the position vector from the origin to the center of the $i$th antenna element.
6. The work in (BMK08) describes how compact ESPAR antennas may encode the combinations of data symbols to be transmitted onto different sets of beampatterns. For example, transmitting two QPSK signals requires according to that approach 16 different beampatterns, and at least 16 training symbols, thus making the scheme impractical. In our approach, we map the data symbols onto a predefined basis and simply train the receiver with such basis. For example, transmitting two QPSK signals according to our approach requires at least 2 training symbols for estimating the response of the two basis functions.
7. In (OHSM05) a transmission code of rate 1/2 was proposed using a single radio. In fact, a simple time-switched ST code (YV03) will outperform the

approach in (OHSM05) regarding both performance and complexity.

8. The transmission and reception techniques and the spatial basis proposed in (BEK10) is completely adopted from the work in (AKPK08)(APK+09).
9. In (ea08a), the authors propose an antenna system of two RF sources and four antenna elements. The proposed antenna system is capable of changing its polarization state (at the symbol rate), and thus transmitting the $4 \times 4$ Jafarkhani (quasi-orthogonal) code. This thesis only considers single RF chain MIMO transmitters.
10. In (AR09), the author describes how to construct a ST block code (STBC) by quickly switching a set of antennas. The work in (AR09) relates to pulse position modulation (PPM) with multi radios for ultra wideband (UWB) communications while the thesis considers constant envelope modulation for classical mobile communications.
11. In (HRB09), the authors alter the far-field of a parasitic array with thousands of switches, at a rate equal to the modulation rate. The work in (HRB09) is intended for secure information transmission by limiting the information bandwidth to a small angle. Our work is intended for MIMO transmission rather than secure communication.

## 1.3 Thesis Outline

The rest of the thesis is organized as follows:

- *Chapter 2*: This chapter first shows how two BPSK signals can be transmitted by switching two antennas at the modulation rate. The chapter then describes from a signal space approach the interactions when the two antennas are closely spaced and matched according to different matching techniques.
- *Chapter 3*: This chapter conveys the idea of antenna switching to beam switching where the RF excitation point becomes fixed. It shows how the BPSK signals are mapped onto a spatial basis obtained be decomposing the Euler functions comprising the array far-field. More importantly we show how the signal format is extended to high order complex modulations.
- *Chapter 4*: This chapter first generalizes the basis derivation from any a Mirror Image Pattern Pair (MIPP). Then it proposes a prototyping methodology for designing and optimizing an SPA of microstrip line for MIMO transmission.
- *Chapter 5*: This chapter experimentally validates the concept of MIMO transmission with a single radio.
- *Chapter 6*: Finally this chapter concludes the work.

## 1.4 Notation

We use the following notations: a bold small letter designates a vector and a bold big letter designates a matrix. The operators $()^*, ()^T, ()^H$ designate complex conjugate, transpose and complex conjugate transpose (Hermitian) operators, respectively. The notation $\mathbf{I}_N$ indicates an identity matrix of size $N \times N$. The operator $\mathrm{diag}(\mathbf{v})$ returns a square matrix with the elements of the vector $\mathbf{v}$ laid across the main diagonal of the matrix. The operators $\mathbb{E}\{.\}$, $\mathrm{Var}\{.\}$ and $\mathrm{tr}\{.\}$ return the expectation, the variance and the trace of the operand, respectively. Moreover, we use the following abbreviations:

**Table 1.1:** Abbreviations

| Acronym | Meaning |
|---|---|
| 2-D | 2-dimensional |
| AWGN | Additive White Gaussian Noise |
| DMN | Decoupling and Matching Network |
| ESPAR | Electronically Steerable Parasitic Array Radiator |
| i.i.d | independent and identically distributed |
| MIMO | Multiple-Input Multiple-Output |
| MISO | Multiple-Input Single-Output |
| PE | Parasitic Element |
| PDF | Probability Density Function |
| PIN | Positive Intrinsic Negative |
| SAS | Switched Antenna System |
| SIMO | Single-Input-Multi-Output |
| SINR | Signal to Interference and Noise Ratio |
| SISO | Signal-Input-Single-Output |
| SPA | Switched Parasitic Array |
| SNR | Signal to Noise Ratio |
| ZMCSCGRV | Zero Mean Circular Symmetric Complex Gaussian Random Variable |

# 2

# MIMO Transmission via Antenna Switching

In this chapter we show that two BPSK signals can be simultaneously transmitted using a single active antenna at a time, thus requiring a single RF source. The idea is to modulate one BPSK substream to one of two transmit antennas while mapping the second substream to the index of the active antenna (a SAS changes the excitation point (the RF port) at a rate equal to the modulation rate). This is practically possible using RF switches or by simply using PIN diodes[1].

## 2.1 A 2-Element SAS

Consider two BPSK symbols $x_1$ and $x_2$, transmitted over two antennas, and received using $\mathcal{K}_R$ antennas after propagating through a narrowband channel $\mathbf{H} \in \mathbb{C}^{\mathcal{K}_R \times 2}$. The narrowband received signal model can be written as

$$\mathbf{y} = \mathbf{H}\mathbf{x} + \mathbf{n}, \tag{2.1}$$

where $\mathbf{y} \in \mathbb{C}^{\mathcal{K}_R \times 1}$, $\mathbf{x} \in \mathbb{R}^{2 \times 1}$ defined as

$$\mathbf{x} := \begin{bmatrix} x_1 \\ x_2 \end{bmatrix} \tag{2.2}$$

,
and $\mathbf{n} \in \mathbb{C}^{\mathcal{K}_R \times 1}$ is a vector representing the additive white Gaussian noise (AWGN). The noise is assumed spatially white across the $\mathcal{K}_R$ receive antennas, with zero

[1] The PIN diode has a switching delay in the order of nanoseconds (Poz05; Pac), thus leading to a negligible transient delay with respect to the symbol period.

mean and variance $\sigma_n^2$, thus $\mathbb{E}\left\{\mathbf{n}\mathbf{n}^H\right\} = \mathbf{I}_{\mathcal{K}_R}\sigma_n^2$. By introducing an orthonormal $2 \times 2$ matrix $\mathbf{U}$ such that $\mathbf{U}\mathbf{U}^T = \mathbf{U}^T\mathbf{U} = \mathbf{I}$, the received signal model can be rewritten as

$$\begin{aligned} \mathbf{y} &= \mathbf{H}\mathbf{U}\mathbf{U}^T\mathbf{x} + \mathbf{n} \\ &= \widetilde{\mathbf{H}}\widetilde{\mathbf{x}} + \mathbf{n}, \end{aligned} \tag{2.3}$$

where $\widetilde{\mathbf{H}} = \mathbf{H}\mathbf{U}$ and $\widetilde{\mathbf{x}} = \mathbf{U}^T\mathbf{x}$ are unitary transformations of $\mathbf{H}$ and $\mathbf{x}$, respectively. Notice that (2.3) is equivalent to (2.1), since $\widetilde{\mathbf{H}}$ and $\widetilde{\mathbf{x}}$ are just rotations of $\mathbf{H}$ and $\mathbf{x}$, respectively. However, by setting $\mathbf{U} = \frac{1}{\sqrt{2}}\begin{bmatrix} 1 & 1 \\ 1 & -1 \end{bmatrix}$, the vector $\widetilde{\mathbf{x}}$ collapses to a scalar as $x_2$ is at one of the two possible states: $+x_1$ or $-x_2$ (BPSK signaling). The result is quite remarkable in the sense that a transmitter with a single RF frontend and two transmit antennas will be able to spatially multiplex two BPSK signals by transmitting a single scalar value to one of the two available antennas at a time. For example, an RF switch can be used as we describe later to swap the driven antenna (the RF excitation port) according to the location of the non-zero entry of $\widetilde{\mathbf{x}}$, at a rate equal to the modulation rate. On the other hand, the receiver recovers the received signal exactly as in classical MIMO decoders. The matrix $\mathbf{H}$ is obtained from $\widetilde{\mathbf{H}}$ (i.e., $\mathbf{H} = \widetilde{\mathbf{H}}\mathbf{U}^T$) which can be estimated by training the receiver using $\widetilde{\mathbf{x}}$.

According to this approach, the SAS may either open-circuit the antenna corresponding to the zero entry of $\mathbf{x}$, or short it through its matching impedance. In the first scenario, the passive antenna becomes invisible and the open-circuit correlation is the limiting factor that controls the diversity performance of the proposed transmission technique (i.e. there will be no MC between the two antennas). Assuming uncorrelated and distantly spaced receive antennas, the channel can be written according to the Kronecker model (ea00; KTCV02) as $\mathbf{H} = \mathbf{H}_w\mathbf{R}_T^{1/2}$, where $\mathbf{R}_T$ is the open-circuit correlation between the two antennas. In case of a uniform field distribution, the open-circuit correlation is simply given by the $J_0(\kappa d)$ where $J_0$ is the zero order Bessel function (Jak74), $\kappa$ is the wavenumber and $d$ is the spacing in units of wavelengths.

In the second scenario, the passive antenna parasitically disturbs the far-field due to the MC effect, which plays a role in the diversity performance of the proposed technique as detailed in the following

## 2.2 Case 1: Individual Port Matching

If we assume that each of the two antenna elements is matched by the impedance $\dot{Z}_M$ (balanced uncoupled matching (ea08c; LA06)), then the transmit coupling

matrix becomes

$$\mathbf{C}_T = \left( \underbrace{\begin{bmatrix} \dot{Z}_M & 0 \\ 0 & \dot{Z}_M \end{bmatrix}}_{\dot{\mathbf{Z}}_M} + \underbrace{\begin{bmatrix} Z_{11} & Z_{12} \\ Z_{12} & Z_{11} \end{bmatrix}}_{\mathbf{Z}_{TT}} \right)^{-1} = \begin{pmatrix} C_{11} & C_{12} \\ C_{12} & C_{11} \end{pmatrix}, \tag{2.4}$$

where $\dot{\mathbf{Z}}_M = \dot{Z}_M \mathbf{I}_2$. $Z_{ij} = Z_{ji}$ and $C_{ij} = C_{ji}$, $\{i, j\} \in \{1, 2\}$ are the elements of the mutual impedance matrix $\mathbf{Z}_{TT}$ and the elements of the transmit coupling matrix $\mathbf{C}_T$, respectively. The far-field can be written as $\mathcal{G}_T(\varphi) = \boldsymbol{\mathcal{G}}_{\text{iso}}(\varphi)\, \mathbf{C}_T \mathbf{x}$, where $\varphi$ is the observational angle in the azimuth plane. $\boldsymbol{\mathcal{G}}_{\text{iso}}(\varphi) = [\mathcal{G}_{\text{iso1}}(\varphi) \;\; \mathcal{G}_{\text{iso2}}(\varphi)]$ is the vector of the isolated element patterns (i.e. the pattern of each element when the others are open). $\mathbf{C}_T$ in (2.4) is a Toeplitz symmetric matrix, hence its eigenvectors are orthonormal. Let $\mathbf{U}_T$ be a matrix the columns of which are the eigenvectors of $\mathbf{C}_T$ and $\mathbf{\Lambda}_T$ be a diagonal matrix the elements of which are the eigenvalues of $\mathbf{C}_T$, then for the given $\mathbf{C}_T$ we get $\mathbf{U}_T = \frac{1}{\sqrt{2}} \begin{bmatrix} 1 & -1 \\ 1 & 1 \end{bmatrix}$ and $\mathbf{\Lambda}_T = \text{diag}([C_\Sigma \;\; C_\Delta])$ such that $C_\Sigma = C_{11} + C_{12}$ and $C_\Delta = C_{11} - C_{12}$. The array far-field can be decomposed into two basis functions as follows:

$$\begin{aligned} \mathcal{G}_T(\varphi) &= \boldsymbol{\mathcal{G}}_{\text{iso}}(\varphi)\, \mathbf{U}_T \mathbf{\Lambda}_T \mathbf{U}_T^T \mathbf{x}, \\ &= \boldsymbol{E}_T(\varphi)\, \mathbf{\Lambda}_T \mathbf{U}_T^T \mathbf{x}, \\ &= \boldsymbol{\mathcal{B}}_T(\varphi)\, \mathbf{U}_T^T \mathbf{x}, \\ &= \boldsymbol{\mathcal{B}}_T(\varphi)\, \widetilde{\mathbf{x}}, \end{aligned} \tag{2.5}$$

where

$$\boldsymbol{\mathcal{B}}_T(\varphi) = \boldsymbol{E}_T(\varphi)\, \mathbf{\Lambda}_T = [\mathcal{B}_\Sigma(\varphi) \;\; \mathcal{B}_\Delta(\varphi)], \tag{2.6a}$$

$$\boldsymbol{E}_T(\varphi) = \boldsymbol{\mathcal{G}}_{\text{iso}}(\varphi)\, \mathbf{U}_T = [\mathscr{E}_\Sigma(\varphi) \;\; \mathscr{E}_\Delta(\varphi)], \tag{2.6b}$$

where $\boldsymbol{E}(\varphi)$ is the vector of the eigenpatterns $\mathscr{E}_\ell(\varphi), \ell \in \{\Sigma, \Delta\}$ (WC04) such that

$$\frac{1}{2\pi} \oint_\varphi \mathscr{E}_\Sigma(\varphi) \mathscr{E}_\Delta^*(\varphi) \cdot d\varphi = 0. \tag{2.7}$$

Notice that (2.7) states that the two eigenpatterns are orthogonal either in the free-space or in a fully-scattered channel. Moreover, $\boldsymbol{\mathcal{B}}_T(\varphi)$ is the vector of the

basis functions $\mathcal{B}_\ell(\varphi), \ell \in \{\Sigma, \Delta\}$ defined as a scaled version of the $\ell^{th}$ eigenpattern (scaled by $C_\ell(\varphi), \ell \in \{\Sigma, \Delta\}$) as per (2.6a) as follows:

$$\begin{aligned}\mathcal{B}_\Sigma(\varphi) &= C_\Sigma \mathscr{E}_\Sigma(\varphi) = C_\Sigma \frac{\mathcal{G}_{\text{iso1}}(\varphi) + \mathcal{G}_{\text{iso2}}(\varphi)}{\sqrt{2}}, \\ \mathcal{B}_\Delta(\varphi) &= C_\Delta \mathscr{E}_\Delta(\varphi) = C_\Delta \frac{\mathcal{G}_{\text{iso1}}(\varphi) - \mathcal{G}_{\text{iso2}}(\varphi)}{\sqrt{2}}.\end{aligned} \tag{2.8}$$

### 2.2.1 Spatial Multiplexing of Two BPSK Signals

Till now we have shown that the far-field of the 2-element array is a linear combination of the two basis functions $\mathcal{B}_\Sigma(\varphi)$ and $\mathcal{B}_\Delta(\varphi)$, (see (2.5) and (2.6a)), onto which the two mode voltages $\widetilde{\mathbf{x}}$ are mapped. For a fixed $\mathbf{C}_T$ (fixed array topology and fixed $\dot{Z}_M$), the linear combination of the basis is controlled only by the set of the mode voltages $\widetilde{\mathbf{x}}$. Let the 2-element array be driven by a single feeding RF voltage signal. If we simply switch the input voltage vector $\mathbf{x}$ from $[x_1 \;\; 0]^T$ where the first element is driven and the second is parasitically excited by the field of the first to $[0 \;\; x_1]^T$ where the second element is driven and the first is parasitically excited by the field of the second element; the mode voltages switch consequently from $\widetilde{\mathbf{x}} = \frac{1}{\sqrt{2}}[x_1 \;\; x_1]^T$ to $\widetilde{\mathbf{x}} = \frac{1}{\sqrt{2}}[x_1 \;\; -x_1]^T$. According to the antenna elements' state $S \in \{0, 1\}$ where $S = 0$ refers to the state when the first antenna element is active and the second is passive (vise versa when $S = 1$), the far-field becomes function of $S$ as follows

$$\begin{aligned}\mathcal{G}_T(\varphi) &= \frac{1}{\sqrt{2}}\Big(x_1\mathcal{B}_\Sigma(\varphi) + x_1(-1)^S\mathcal{B}_\Delta(\varphi)\Big), \\ &= s_1\mathcal{B}_\Sigma(\varphi) + s_2\mathcal{B}_\Delta(\varphi),\end{aligned} \tag{2.9}$$

where two independent BPSK signals $\left(s_1 = \frac{x_1}{\sqrt{2}}\right)$ and $\left(s_2 = \frac{x_1}{\sqrt{2}}(-1)^S\right)$ are mapped onto the two basis functions. The result is welcome in the sense that a switched antenna system with a single RF-frontend can be used for mapping two BPSK signals onto the proposed basis. Fig. 2.1 shows a switched antenna system with two symmetrical antenna elements where the state $S$ is obtained by XOR-ing the bit streams ($b_1$ and $b_2$) in the binary domain i.e. $S := b_1 \oplus b_2$. The first bit stream is modulated to $s_1 = \frac{v_s}{\sqrt{2}}$ and up-converted while the output state $S$ controls the polarity of the DC source. When the DC source is positive ($S = 0$), the varactor diodes $D_1$ and $D_4$ are forward-biased and the varactor diodes $D_2$ and $D_3$ are reverse-biased. Consequently the first antenna element is driven by $s_1$ and the second is parasitically excited by the field of the first antenna element and the inverse scenario takes place when $S = 1$ (notice that both of the antenna elements are matched by $\dot{Z}_M = Z_M + Z_o$ irrespective of the diodes state $S$, where $Z_o$ is the characteristic impedance of the RF-DC cable).

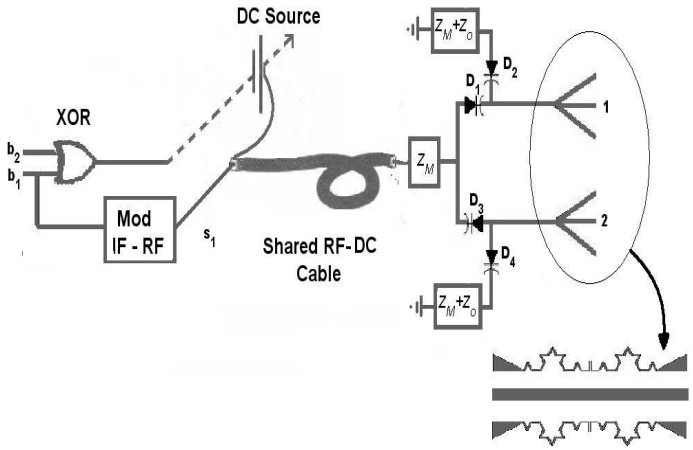


**Figure 2.1:** A switched antenna system with a single RF-frontend, a shared RF-DC feeding circuit and a shared RF-DC cable. An array of two fractal dipoles with a common reflector is proposed as an example of two closely-coupled antennas.

### 2.2.2 Mutual Information Analysis

A simple analytical model regarding the mutual information of the proposed scheme is introduced in this part. We consider a system where the transmitter is equipped with a switched antenna system as shown in Fig. 2.1 whereas the receiver is equipped with two distantly spaced antenna elements. The $2 \times 2$ spatial channel matrix $\mathbf{H}$ when taking the MC and the open-circuit correlation at the transmit end of the communication link may be expanded (JM05a) as $\mathbf{H} = \mathbf{H}_w \left(\eta_T \mathbf{R}_T\right)^{1/2} \mathbf{C}_T$ where $\mathbf{C}_T, \mathbf{R}_T$ are the transmitter coupling and open-circuit correlation matrices respectively and $\eta_T$ is the transmitter efficiency. $\mathbf{H}_w$ is a matrix the elements of which are zero mean circularly symmetric complex Gaussian variables (ZMCSCGV). The received signal vector $\mathbf{y}$ can be written as

$$\begin{aligned} \mathbf{y} &= \mathbf{H}_w \left(\eta_T \mathbf{R}_T\right)^{1/2} \mathbf{C}_T \mathbf{x} + \mathbf{n}, \\ &= \mathbf{H}_w \left(\eta_T \mathbf{R}_T\right)^{1/2} \mathbf{U}_T \mathbf{\Lambda}_T \mathbf{U}_T^H \mathbf{x} + \mathbf{n}, \\ &= \mathbf{H}_w \underbrace{\left(\eta_T \mathbf{R}_T\right)^{1/2} \mathbf{U}_T \mathbf{\Lambda}_T}_{\mathbf{\Psi}^{1/2}} \widetilde{\mathbf{x}} + \mathbf{n} \end{aligned} \tag{2.10}$$

where $\mathbf{n}$ is the noise vector assumed ZMCSCGV. By using the $\log_2 \det(\cdot)$ formula (GNP03), the upper bound that comes from the Jensen's inequality and the concavity of $\log_2 \det(\cdot)$[1], the average mutual information is found to be bounded from

[1]The $\log_2 \det(\cdot)$ is concave over positive semi-definite matrices (Hor96). Since $\mathbf{\Psi}$ is positive semi-definite, the term $\mathbf{I}_2 + \frac{\rho}{2}\mathbf{\Psi}$ is positive semi-definite too, as it is a one-to-one mapping of $\mathbf{\Psi}$, thus

above as

$$\Im_{av} \quad \leq \quad \log_2 \det \left( \mathbf{I}_2 + \frac{\rho}{2} \mathbf{\Psi} \right), \tag{2.11}$$

where the 2 in (2.11) is the number of the eigenmodes (the two basis functions or the two eigenpatterns); $\rho$ is the average received signal to noise ratio (SNR) per antenna.

### 2.2.3 Receiver Decoding

The two BPSK symbols can be simply decoded as in classical ST decoding techniques. However the receiver has to first estimate the receive antennas' responses to the proposed basis. This is done by first estimating the receive antenna responses to $\mathcal{G}_T(\varphi)$ over the different antenna states; then the response of the $k$th receive antenna to the basis $\mathcal{B}_\Sigma(\varphi)$ and $\mathcal{B}_\Delta(\varphi)$ is found from

$$h_k = s_1 h_{k,\Sigma} + s_2 h_{k,\Delta}. \tag{2.12}$$

where $h_{k,\Sigma}$ is the response of the $k$th receive antenna to $\mathcal{B}_\Sigma(\varphi)$ and $h_{k,\Delta}$ is the response of the $k$th receive antenna to $\mathcal{B}_\Delta(\varphi)$

*Proof:*

Without loss of generality we consider vertically polarized signals impinging onto a receiving array of omnidirectional antennas; the channel response of the $k$th omni receive antenna to the first transmitting antenna element is written from (WSW04) as

$$\begin{aligned} h_k &= \mathscr{C}_k \sum_{p=1}^{P} \beta_l \mathcal{G}_1(\varphi_p) \\ &= \mathscr{C}_k \sum_{p=1}^{P} \left( \beta_l s_1 \mathcal{B}_\Sigma(\varphi_p) + \beta_l s_2 \mathcal{B}_\Delta(\varphi_p) \right) \\ &= s_1 \mathscr{C}_k \sum_{p=1}^{P} \beta_l \mathcal{B}_\Sigma(\varphi_p) + s_2 \mathscr{C}_k \sum_{p=1}^{P} \beta_l \mathcal{B}_\Delta(\varphi_p) \\ &= s_1 h_{k,\Sigma} + s_2 h_{k,\Delta} \end{aligned} \tag{2.13}$$

where $\mathscr{C}_k = \sqrt{\frac{\Re(Z_{11}')}{\Re(Z_{11})}} \sqrt{G_{\mathrm{Rx}k} G_{\mathrm{Tx}1} \left(\frac{\lambda}{4\pi}\right)^2}$, $Z_{11}'$ is the self-impedance of the receiving

preserving the positive definiteness.

antenna subsystem, $P$ is the number of relevant paths, $G_{\mathrm{Tx}1}$, $G_{\mathrm{Rx}k}$ are the effective gains of transmit antenna 1 and the $k$th receive antenna, respectively (WSW04) and $\beta_l$ is the gain of the $l$th path.

### 2.2.4 Practical Example

In this example we consider a uniform field distribution which is a reasonable assumption when assuming many scatterers in the full angular spread. The transmitter is equipped with a switched antenna system of two fractal antenna elements as shown in Fig. 2.1 where a common reflector is intentionally inserted in the middle so that the two isolated element patterns $\mathcal{G}_{\mathrm{iso}1}(\varphi)$ and $\mathcal{G}_{\mathrm{iso}2}(\varphi)$ are decorrelated. Notice from 2.8 that the basis function $\mathcal{B}_{\Sigma}(\varphi)$ will eventually vanish if both $\mathcal{G}_{\mathrm{iso}1}(\varphi)$ and $\mathcal{G}_{\mathrm{iso}2}(\varphi)$ become highly correlated (WC04). The transmit antenna system is described by $Z_{11} = 4.986 - j0.7155\Omega$ and $Z_{12} = 1.147 - j17.07\Omega$. The *maximum* array spacing (as the inter-element spacing is not uniform) is about $0.2\lambda$, and the operating frequency is 4 GHz. The isolated element patterns are obtained using an accurate electromagnetic simulator (IE3) and the open-circuit correlation matrix under the given channel conditions is found to be $\mathbf{R}_T = \begin{bmatrix} 1 & 0.4618 - j0.1874 \\ 0.4618 + j0.1874 & 1 \end{bmatrix}$. The transmitter employs the proposed scheme for spatially multiplexing two BPSK signals, whereas the access point is assumed to have two largely spaced and optimally matched antenna elements and surrounded by many scatterers. The real part of the matching impedance $R_M$ was changed from $0\Omega$ up to $50\Omega$ with a step of $1\Omega$ and the imaginary part $X_M$ from $-50\Omega$ up to $50\Omega$ with a step $5\Omega$. At every loading, 10,000 channel realizations were taken and the 10% outage rate was found as shown in Fig. 2.2 at an SNR of 10 dB. The optimal matching impedance $Z_M^{opt}$ is chosen to be the one that maximizes the 10% outage rate as being a figure of merit when considering flat-fading or quasi-static MIMO channels (as in (APK+09)). For the given antenna system, $Z_M^{opt}$ is found to be $15 + j0\Omega$, at which the maximum outage rate is 3.95 b/s/Hz; the transmitter efficiency is 78% and the power imbalance between the basis is $-0.48$ dB

## 2.3 Case 2: Multiport Conjugate Matching

In this part we assume the two closely-spaced antennas decoupled and matched using a lossless DMN. Moreover, rather than spatial multiplexing, we describe how the SAS can transmit the Alamouti code of BPSK signals with a single RF source and compact array dimensions.

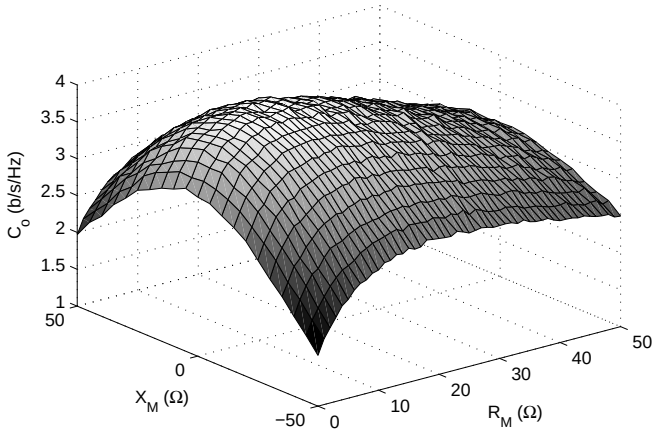


**Figure 2.2:** 10% outage rate assuming Gaussian signaling.

### 2.3.1 Decoupled and Matched Antenna System

A general antenna system of two identical antenna elements has the mutual impedance matrix $\mathbf{Z}_{TT}$ as shown in (2.4). $\mathbf{Z}_{TT}$ can be decomposed as follows

$$\begin{aligned} \mathbf{Z}_{TT} &= \mathbf{U}\mathbf{\Lambda}\mathbf{U}^T, \\ \mathbf{U} = \frac{1}{\sqrt{2}}\begin{bmatrix} 1 & 1 \\ -1 & 1 \end{bmatrix}, \mathbf{\Lambda} &= \operatorname{diag}\left(\begin{bmatrix} Z_\Sigma & Z_\Delta \end{bmatrix}\right), \\ Z_\Sigma &= \frac{1}{\sqrt{2}}\left(Z_{11} + Z_{12}\right) \\ Z_\Delta &= \frac{1}{\sqrt{2}}\left(Z_{11} - Z_{12}\right). \end{aligned} \tag{2.14}$$

Notice that $\mathbf{U}$ is an orthonormal matrix i.e. $\mathbf{U}\mathbf{U}^T = \mathbf{I}_2$. Having decomposed $Z_{TT}$, a DMN of a series reactive load $jX$ and a shunt admittance $jB$ (as shown in Fig. 2.3) can now be found so that the impedance of port 1 ($Z_{\text{Port 1}} = Z_\Sigma + jX$) equals the impedance of port 2 ($Z_{\text{Port 2}} = Z_\Delta - j/(2B)$). By equating the real and imaginary parts of $Z_{\text{Port 1}}$ and $Z_{\text{Port 2}}$, closed form expressions for $X$ and $B$ are obtained as in (YC08). Having the two ports decoupled, the ports can now be matched *individually* using e.g. L-section matching as described in (Poz05).

### 2.3.2 An Orthonormal Space

We define the port *beampattern* as the one obtained when exciting the port with a unit voltage signal while terminating the second with its matching impedance. To

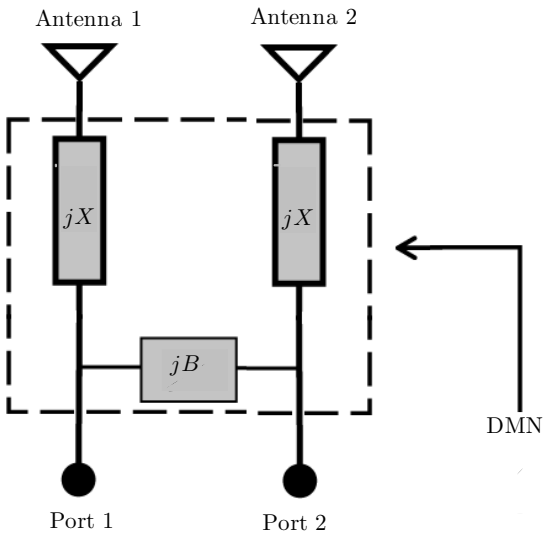


**Figure 2.3:** Antenna system of two identical antenna elements connected to a DMN.

do so, we write down the total far-field pattern of the decoupled antenna system as

$$\mathcal{G}_T(\varphi) = \left[1 \;\; e^{-j\kappa d\cos(\varphi)}\right](\mathbf{Y}_S + \mathbf{Y}_B)\begin{bmatrix} x_1 \\ x_2 \end{bmatrix},$$

and

$$\mathbf{Y}_S = \begin{bmatrix} Z_\Sigma + jX & 0 \\ 0 & Z_\Delta + jX \end{bmatrix}^{-1}, \mathbf{Y}_B = \begin{bmatrix} +jB & -jB \\ -jB & +jB \end{bmatrix}, \tag{2.15}$$

where $\varphi$ is the angle in the azimuth plane, $k = 2\pi/\lambda$ is the wavenumber, $\lambda$ is the carrier wavelength, $d$ is the inter-element spacing in wavelengths, $\mathbf{Y}_S$ is the series admittance matrix and $\mathbf{Y}_B$ is the shunt one. Consequently the beampatterns of RF ports 1 and 2 are defined as $\mathcal{G}_1(\varphi) := \mathcal{G}_T(\varphi)|_{x_1=1,\, x_2=0}$ and $\mathcal{G}_2(\varphi) := \mathcal{G}_T(\varphi)|_{x_1=0,\, x_2=1}$, respectively. Notice that the total far-field pattern can alternatively be written as linear combination of the port beampatterns onto which the input signals are mapped as follows

$$\mathcal{G}_T(\varphi) = \mathcal{G}_1(\varphi)\, x_1 + \mathcal{G}_2(\varphi)\, x_2. \tag{2.16}$$

The two beampatterns $\mathcal{G}_1(\varphi)$ and $\mathcal{G}_1(\varphi)$ form an orthonormal space by the

DMN effect i.e. $\frac{1}{2\pi}\int_{-\pi}^{+\pi}\mathcal{G}_1(\varphi)\,\mathcal{G}_2^*(\varphi)\cdot d\varphi = \frac{1}{2\pi}\int_{-\pi}^{+\pi}\mathcal{G}_2(\varphi)\,\mathcal{G}_1^*(\varphi)\cdot d\varphi = 0$ and $\frac{1}{2\pi}\int_{-\pi}^{+\pi}\mathcal{G}_1(\varphi)\,\mathcal{G}_1^*(\varphi)\cdot d\varphi = \frac{1}{2\pi}\int_{-\pi}^{+\pi}\mathcal{G}_2(\varphi)\,\mathcal{G}_2^*(\varphi)\cdot d\varphi = \eta_T = 1$ where $\eta_T$ is the transmit efficiency of the antenna system. Both effects of the DMN i.e. the full decorrelation of the port beampatterns and the full matching of the antenna system are already known in the literature

### 2.3.3 An Alternative Orthonormal Space

By defining two basis functions $\mathcal{B}_\Sigma(\varphi)$ and $\mathcal{B}_\Delta(\varphi)$ as

$$\begin{aligned}\mathcal{B}_\Sigma(\varphi) &:= \frac{1}{\sqrt{2}}\left(\mathcal{G}_1(\varphi)+\mathcal{G}_2(\varphi)\right)\\ \mathcal{B}_\Delta(\varphi) &:= \frac{1}{\sqrt{2}}\left(\mathcal{G}_1(\varphi)-\mathcal{G}_2(\varphi)\right),\end{aligned} \tag{2.17}$$

an orthonormal basis is obtained.

*Proof:*

Considering the azimuth plane, the cross-correlation between the basis is given by

$$\begin{aligned}\varrho_{12} &= \frac{1}{2\pi}\int_{-\pi}^{+\pi}\mathcal{B}_\Sigma(\varphi)\,\mathcal{B}_\Delta^*(\varphi)\cdot d\varphi\\ &= \frac{1}{4\pi}\int_{-\pi}^{+\pi}\left(\mathcal{G}_1(\varphi)+\mathcal{G}_2(\varphi)\right)\left(\mathcal{G}_1^*(\varphi)-\mathcal{G}_2^*(\varphi)\right)\cdot d\varphi\\ &= \frac{1}{4\pi}\int_{-\pi}^{+\pi}\mathcal{G}_1(\varphi)\,\mathcal{G}_1^*(\varphi)\cdot d\varphi + \frac{1}{4\pi}\int_{-\pi}^{+\pi}\mathcal{G}_1(\varphi)\,\mathcal{G}_2^*(\varphi)\cdot d\varphi\\ &- \frac{1}{4\pi}\int_{-\pi}^{+\pi}\mathcal{G}_2(\varphi)\,\mathcal{G}_1^*(\varphi)\cdot d\varphi - \frac{1}{4\pi}\int_{-\pi}^{+\pi}\mathcal{G}_2(\varphi)\,\mathcal{G}_2^*(\varphi)\cdot d\varphi\\ &= 1/2+0-0-1/2\\ &= 0\end{aligned} \tag{2.18}$$

The same applies to $\varrho_{21}$. Moreover,

$$\begin{aligned}
\varrho_{11} &= \frac{1}{2\pi}\int_{-\pi}^{+\pi} \mathcal{B}_{\Sigma}(\varphi)\,\mathcal{B}_{\Sigma}^{*}(\varphi)\cdot d\varphi \\
&= \frac{1}{4\pi}\int_{-\pi}^{+\pi} (\mathcal{G}_1(\varphi)+\mathcal{G}_2(\varphi))\,(\mathcal{G}_1^{*}(\varphi)+\mathcal{G}_2^{*}(\varphi))\cdot d\varphi \\
&= \frac{1}{4\pi}\int_{-\pi}^{+\pi} \mathcal{G}_1(\varphi)\,\mathcal{G}_1^{*}(\varphi)\cdot d\varphi + \frac{1}{4\pi}\int_{-\pi}^{+\pi} \mathcal{G}_1(\varphi)\,\mathcal{G}_2^{*}(\varphi)\cdot d\varphi \\
&- \frac{1}{4\pi}\int_{-\pi}^{+\pi} \mathcal{G}_2(\varphi)\,\mathcal{G}_1^{*}(\varphi)\cdot d\varphi - \frac{1}{4\pi}\int_{-\pi}^{+\pi} \mathcal{G}_2(\varphi)\,\mathcal{G}_2^{*}(\varphi)\cdot d\varphi \\
&= 1/2+0+0+1/2 \\
&= 1
\end{aligned} \tag{2.19}$$

The same applies to $\varrho_{22}$. *The two beampatterns form a linear mixture of orthonormal basis.*

### 2.3.4 Alamouti Transmit Diversity

In this part we show that a single RF source attached to a decoupled and a matched antenna system of two antenna elements and connected to an RF switch, is capable of transmitting the Alamouti code of two BPSK signals. This is done by first mapping the signals from the classical orthonormal space of the port beampatterns $\mathcal{G}_1(\varphi)$ and $\mathcal{G}_2(\varphi)$ of RF ports 1 and 2 respectively, formed by the DMN effect

In the classical Alamouti transmit diversity scheme (Ala98), a block of real signals $\begin{bmatrix} x_1/\sqrt{2} & -x_2/\sqrt{2} \\ x_2/\sqrt{2} & x_1/\sqrt{2} \end{bmatrix}$ is mapped onto two transmit antennas over two symbol periods. By applying this block to the antenna system shown in Fig. 2.3, the far-fields during the first and the second symbol periods become

$$\begin{aligned}
\mathcal{G}_{T1}(\varphi) &= \mathcal{G}_1(\varphi)\,x_1/\sqrt{2} + \mathcal{G}_2(\varphi)\,x_2/\sqrt{2} \\
&= x_1/\sqrt{2}\,[\mathcal{G}_1(\varphi) + x_2/x_1\mathcal{G}_2(\varphi)]
\end{aligned} \tag{2.20}$$

and

$$\begin{aligned}
\mathcal{G}_{T2}(\varphi) &= -\mathcal{G}_1(\varphi)\,x_2/\sqrt{2} + \mathcal{G}_2(\varphi)\,x_1/\sqrt{2} \\
&= -x_2/\sqrt{2}\,[\mathcal{G}_1(\varphi) - x_1/x_2\mathcal{G}_2(\varphi)]
\end{aligned} \tag{2.21}$$

respectively. Notice that the ratio $x_2/x_1 \in \{-1,1\}$ in (2.20) under BPSK signaling as well as the ratio $-x_1/x_2 \in \{1,-1\}$ in (2.21). Let the driving signal be $x_1$ during the first symbol period and $-x_2$ during the second. The antenna element to

be driven during the first symbol period is determined by the ratio $x_2/x_1$ and in the second symbol period by the ratio $-x_1/x_2 = -x_2/x_1$, which is simply the other antenna element. By this way, similar far-field expressions to those in (2.20) and (2.21) are obtained, however the BPSK symbols are mapped from the classical orthonormal space created by the DMN effect i.e. the space of $\mathcal{G}_1(\varphi)$ and $\mathcal{G}_2(\varphi)$ onto the orthonormal space of $\mathcal{B}_\Sigma(\varphi)$, $\mathcal{B}_\Delta(\varphi)$. This mapping enables the Alamouti functionality using a single driving RF source. The scheme is described in algorithmic manner as follows:

*During the first symbol period*

**if** $x_2/x_1 = 1$ **then**

$x_1 \rightarrow$ RF Port 1

$$\begin{aligned}\widetilde{\mathcal{G}}_{T1}(\varphi) &= \mathcal{G}_1(\varphi)\, x_1 \\ &= x_1/\sqrt{2}\,[\mathcal{B}_\Sigma(\varphi) + \mathcal{B}_\Delta(\varphi)]\end{aligned}$$

**else**

$x_1 \rightarrow$ RF Port 2

$$\begin{aligned}\widetilde{\mathcal{G}}_{T1}(\varphi) &= \mathcal{G}_2(\varphi)\, x_1 \\ &= x_1/\sqrt{2}\,[\mathcal{B}_\Sigma(\varphi) - \mathcal{B}_\Delta(\varphi)]\end{aligned}$$

**end if**

*During the second symbol period*

**if** $-x_1/x_2 = 1$ **then**

$-x_2 \rightarrow$ RF Port 1

$$\begin{aligned}\widetilde{\mathcal{G}}_{T2}(\varphi) &= -\mathcal{G}_1(\varphi)\, x_2 \\ &= -x_2/\sqrt{2}\,[\mathcal{B}_\Sigma(\varphi) + \mathcal{B}_\Delta(\varphi)]\end{aligned}$$

**else**

$-x_2 \rightarrow$ RF Port 2

$$\begin{aligned}\widetilde{\mathcal{G}}_{T2}(\varphi) &= -\mathcal{G}_2(\varphi)\, x_2 \\ &= -x_2/\sqrt{2}\,[\mathcal{B}_\Sigma(\varphi) - \mathcal{B}_\Delta(\varphi)]\end{aligned}$$

**end if**

Fig. 2.4 shows how a simple control circuit is used for switching the antenna elements, driving one of the RF ports and terminating the other with its matching impedance $Z_M$, simultaneously. The figure shows how the DC signals $H$ :=High and $L$ :=Low are used for switching the active RF port and to forward bias or reverse bias the diodes $D1$ and $D2$.

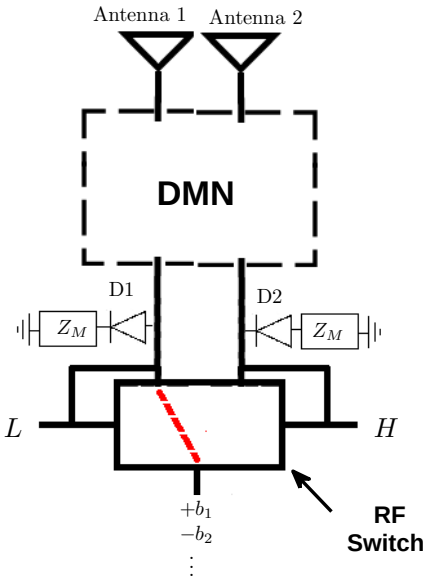


**Figure 2.4:** A schematic diagram of a control circuit for switching, driving and matching the antenna elements using attached to a single RF source.

### 2.3.5 Performance Evaluation

In this part we first describe an antenna system example of two closely-spaced dipoles. The antenna system is used later for evaluating the proposed space-time transmission technique in a geometrical channel model representing a realistic scattering environment.

#### 2.3.5.1 Antenna System Example

We consider two $\lambda/2$ thin electrical dipoles spaced by $\lambda/20$. The mutual impedance matrix of the antenna system is given by $\mathbf{Z}_{TT} = \begin{bmatrix} 73.1 + j43.0 & 71.6 + j24.3 \\ 71.6 + j24.3 & 73.1 + j43.0 \end{bmatrix}$. The DMN components are calculated from the closed-form expressions in (YC08) as $X = -33.75\ \Omega$ and $B = -0.0037\ \mho$. The orthonormal beampatterns $\mathcal{G}_k(\varphi), k \in \{1, 2\}$ are shown in Fig. 2.5 whereas the proposed basis is shown in Fig. 2.6. Notice that such an antenna system addresses the major limitations of mobile handheld terminals in the sense that

- The DMN enhances the energy efficiency by maximizing the transmit antenna efficiency and minimizing the cross-talk between the two RF ports.
- The signals are mapped onto an orthonormal basis derived from the original orthonormal space created by the DMN.

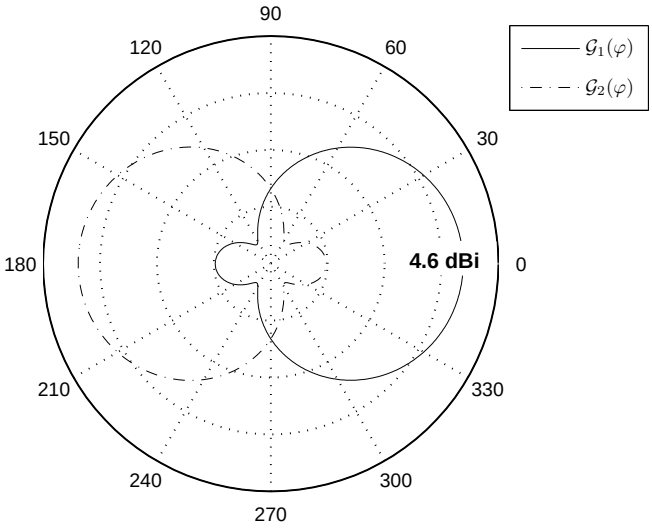


**Figure 2.5:** Port beampatterns of two decoupled dipoles spaced by $\lambda/20$ (classical orthonormal space).

- The RF hardware (PA, ADC, DAC) is reduced by using a single radio.
- The interference among the parallel RF chains which is found to have a negative impact on the system performance is avoided by using a single RF chain.

#### 2.3.5.2 Simulation Results

We evaluate the proposed transmit diversity technique by extensive Monte Carlo simulations. We consider a 2-D outdoor macro-cellular geometrically based circular single bounce channel model as in (ea98), with 10 scatterers surrounding the transmitter (uniformly distributed). Simpler channel models e.g. the independent and identically distributed (canonical) channel model, cannot be used here due to the non-uniform angular distribution of the power in the space. We assume that the transmitter is equipped with the suggested antenna system and implements the proposed Alamouti scheme using BPSK signaling (transmission over the proposed basis functions shown in Fig. 2.6). We also assume that the receiver is equipped with two antennas (spaced by $10\lambda$) and knows the channel and that we have a flat fading environment. Fig. 2.7 shows the performance results in terms of the error probability $P_b$ versus the bit signal to noise ratio $E_b/N_o$ of a communication system example, and compared to the performance of a system example that implements the classical Alamouti code (using a similar antenna system with two

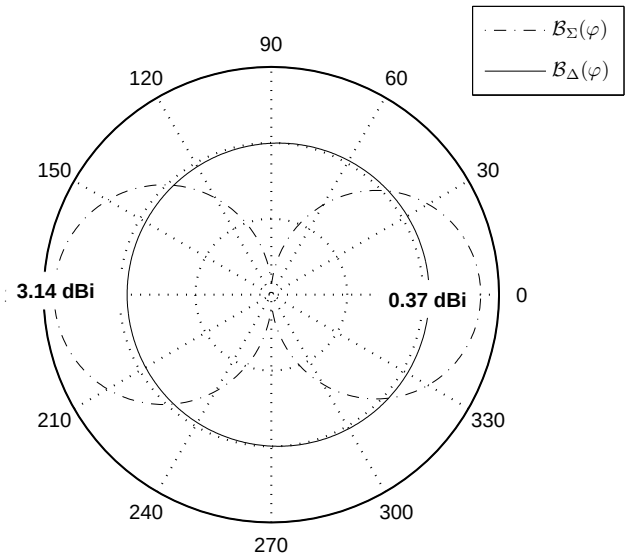


**Figure 2.6:** Basis functions derived from the port beampatterns shown in Fig. 2.5 (proposed orthonormal space).

driven RF ports), thus the communication is done over the beampatterns shown in Fig. 2.5. The figure shows that the performance of the proposed technique is comparable to its classical counterpart, however the proposed scheme requires a single radio. The figure also shows the classical BPSK performance of a $1 \times 1$ system example comprised of isotropic antennas at both ends of the communication system as a reference.

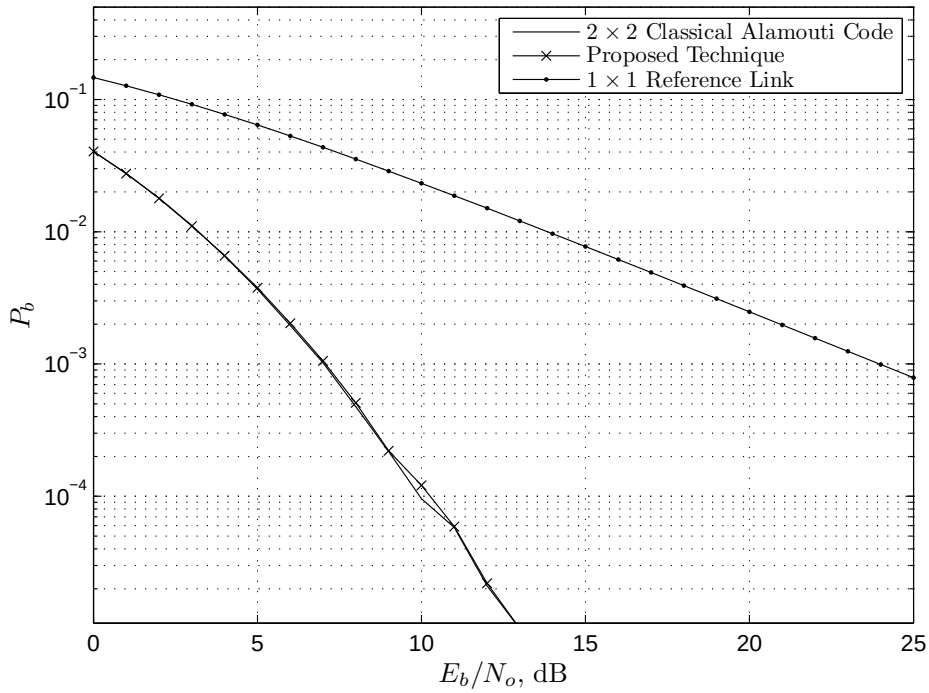


**Figure 2.7:** Performance evaluation of the proposed technique.

# 3

# MIMO Transmission via Reactance-Assisted Antenna Systems

In this chapter we implement reduced complexity MIMO transmission using reactance-assisted antenna systems. A switched parasitic array (SPA) of a single driven element (and thus a single RF frontend) surrounded by PEs (PE) loaded with variable reactive loads is proposed and described. The idea is to map the signals onto a set of angular functions comprising the SPA far-field. By this way, independent information streams are encoded over the angular variations of the far-field in the wavevector domain (TBP05), rather than spatial variations as usually happen in conventional MIMO systems. The array can spatially multiplex all the possible alphabets of the input vector of signals by creating all the desired linear combinations (of the basis functions) corresponding to the input. In the first part of this chapter, we propose a simple approach for transmitting two BPSK signals using a 3-element SPA. In the second part we propose a universal scheme for encoding multi high order PSK symbols onto the SPA beampattern. The desired combinations are obtained by projecting the ratio of the symbols to be spatially multiplexed on the ratio of the basis functions' weights (complex coefficients), which are functions of the antenna parameters as well as the variable SPA loading.

## 3.1 Parasitic Antenna Theory

In this work we mainly focus on the 3-element SPA antenna which is implemented using a single active antenna element and two PEs (PE) surrounding the active element at relative local angles of 0 and $\pi$ as shown in Fig. 3.1.

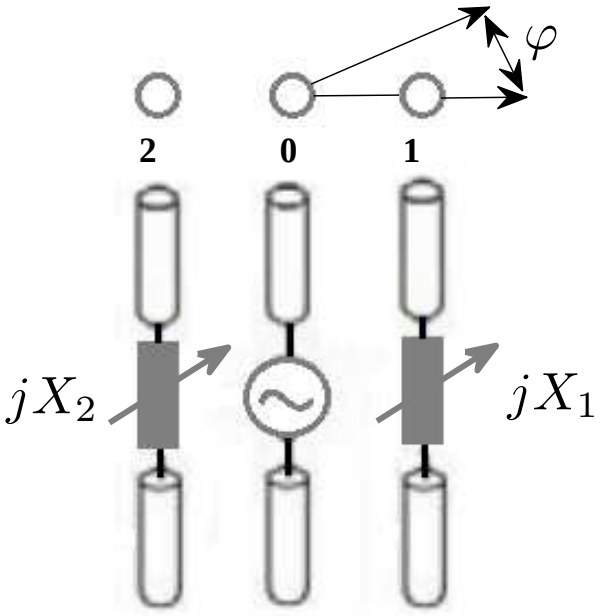


**Figure 3.1:** A 3-element SPA.

The PEs are loaded with variable reactors (varactors) that control the imaginary part of the PEs' input impedances. By adjusting the varactors' response, the radiation pattern of the SPA antenna system is controlled. The currents on the PE are induced by MC with the current on the central element according to the equation (OG00)

$$\mathbf{i} = \mathbf{w} v_s \tag{3.1}$$

where $v_s$ represents the transmitted voltage signal source with the amplitude and the phase from the driving RF port at the central element, $\mathbf{w} := [\mathbf{Z}_{TT} + \mathbf{X}]^{-1}\,\mathbf{u}$ is the "*equivalent weight vector*" (OG00) and $\mathbf{Z}_{TT}$ is the mutual impedance matrix given by

$$\mathbf{Z}_{TT} = \begin{pmatrix} Z_{00} & Z_{01} & Z_{01} \\ Z_{01} & Z_{11} & Z_{12} \\ Z_{01} & Z_{12} & Z_{11} \end{pmatrix} \tag{3.2}$$

where we assumed $Z_{ij} = Z_{ji}$, $\{i, j\} \in \{0, 1, 2\}$ by assuming that the antennas

are made of electrically reciprocal materials, $\mathbf{X}$ is a diagonal matrix defined as $\mathbf{X} := \text{diag}\left([Z_0 \;\; jX_1 \;\; jX_2]\right)$, where $Z_0$ is the characteristic impedance of $50\Omega$ (equal to the source impedance $Z_s$ at the central active port for matching purposes), while $jX_i$ is the loading of the $i^{th}$ PE, and finally $\mathbf{u}$ is a selection vector defined as $\mathbf{u} := [\; 1 \;\; 0 \;\; 0 \;]^T$

$$\boldsymbol{\alpha}(\varphi) := \left[\; 1 \quad \exp(-j\kappa d\cos(\varphi - 0)) \quad \exp(-j\kappa d\cos(\varphi - \pi)) \;\right]^T \tag{3.3}$$

where $\kappa = \frac{2\pi}{\lambda}$ is the wavenumber and $d$ is the SPA inter-element spacing.

The far-field and the circuit relations of the array are re-written according to (LDP06) and (MK02) as

$$\begin{aligned} \mathcal{G}_T(\varphi) &= \boldsymbol{\alpha}^T(\varphi)\mathbf{w}v_s \\ &= i_s\Big(1 + \gamma_1\exp(-j\kappa d\cos(\varphi)) + \gamma_2\exp(j\kappa d\cos(\varphi))\Big) \end{aligned} \tag{3.4}$$

where

$$i_s = v_s/Z_{in} \tag{3.5}$$

$$\gamma_1 = \frac{Z_{12}Z_{01} - Z_{01}\left(Z_{11} + jX_2\right)}{\left(Z_{11} + jX_1\right)\left(Z_{11} + jX_2\right) - Z_{12}^2} \tag{3.6}$$

$$\gamma_2 = \frac{Z_{12}Z_{01} - Z_{01}\left(Z_{11} + jX_1\right)}{\left(Z_{11} + jX_1\right)\left(Z_{11} + jX_2\right) - Z_{12}^2} \tag{3.7}$$

Finally, as the SPA is intended for portable radio units living on a limited battery, the SPA efficiency is an important factor to be maintained at a high value. The SPA efficiency $\eta$ is simply given by

$$\eta_T = 1 - |\Gamma_{\text{in}}|^2 \tag{3.8}$$

where $\Gamma_{\text{in}}$ is the input reflection coefficient such that

$$\Gamma_{\text{in}} = (Z_{\text{in}} + Z_o)^{-1}(Z_{\text{in}} - Z_o) \tag{3.9}$$

where $Z_{\text{in}}$ is the driving point impedance given by

$$Z_{\text{in}} = Z_{00} + \gamma_1 Z_{01} + \gamma_2 Z_{02} \tag{3.10}$$

## 3.2 BPSK-MIMO via an SPA

### 3.2.1 Transmission Technique

The far-field can be expressed as a linear combination of two basis functions by decomposing the Euler's functions in (3.4), as follows

$$\mathcal{G}_T(\varphi) = i_s\Big(\underbrace{1+(\gamma_1+\gamma_2)\cos(\kappa d\cos(\varphi))}_{\mathcal{B}_\Sigma(\varphi)}\underbrace{-j\,(\gamma_1-\gamma_2)\sin(\kappa d\cos(\varphi))}_{\mathcal{B}_\Delta(\varphi)}\Big) \tag{3.11}$$

Notice that in (3.11) $\mathcal{B}_\Sigma(\varphi)\perp\mathcal{B}_\Delta(\varphi)$ irrespective of $\gamma_1$ and $\gamma_2$. This is because the $\sin(\kappa d\cos(\varphi))$ beampattern is orthogonal to both the of the spatial omni pattern (the term 1) and to the spatial $\cos(\cos(\varphi))$ beampattern. By swapping the loads $X_1 \leftrightarrow X_2$, the complex coefficients swap as $\gamma_1 \leftrightarrow \gamma_2$, thus phase shifting $\mathcal{B}_\Delta(\varphi)$ by 180° without affecting $\mathcal{B}_\Sigma(\varphi)$ and without changing the driving point impedance seen by the central active antenna. According to the SPA loading state ($[jX_1\ jX_2]$ or $[jX_2\ jX_1]$), the far-field becomes

$$\begin{aligned}\mathcal{G}_T(\varphi) &= i_s\left(\mathcal{B}_\Sigma(\varphi)+(-1)^S\mathcal{B}_\Delta(\varphi)\right)\\ &= i_s\mathcal{B}_\Sigma(\varphi)+i_s(-1)^S\mathcal{B}_\Delta(\varphi)\\ &= x_1\mathcal{B}_\Sigma(\varphi)+x_2\mathcal{B}_\Delta(\varphi)\end{aligned} \tag{3.12}$$

Fig. 3.2 shows a simple control circuit for spatially multiplexing two BPSK signals using the 3-element SPA array. The first BPSK sub-stream ($x_1 = i_s$) is fed into the single active port after being modulated and up-converted. The second sub-stream ($x_2 = i_s(-1)^S$) is *XOR*-ed with the first in the binary domain ($b_1 \oplus b_2$) and the output control signal is used for binary switching between the two reactances $jX_1$ and $jX_2$ (i.e. selecting $[jX_1\ jX_2]$ when $b_1 \oplus b_2 = 0$ and $[jX_2\ jX_1]$ when $b_1 \oplus b_2 = 1$). Notice that $(\gamma_1 - \gamma_1)$ at $[jX_1\ jX_2]$ becomes $(\gamma_1 - \gamma_1)$ at $[jX_2\ jX_1]$.

### 3.2.2 Outage Rate Maximization

The reactive loads that control $\gamma_i$, $i \in \{0,1,2\}$ can be *jointly optimized* against some parameters e.g. the maximum radiated power or the maximum mutual information (BMK08). In this part we are interested in maximizing the outage capacity as being a figure of merit in slow fading MIMO communications. The open-loop capacity is intuitively maximized when the *power imbalance* between the two angular basis $\mathcal{B}_\Sigma(\varphi)$ and $\mathcal{B}_\Delta(\varphi)$ is made close to 0dB and the *matching efficiency* is made close to unity. The correlation between the signals is already

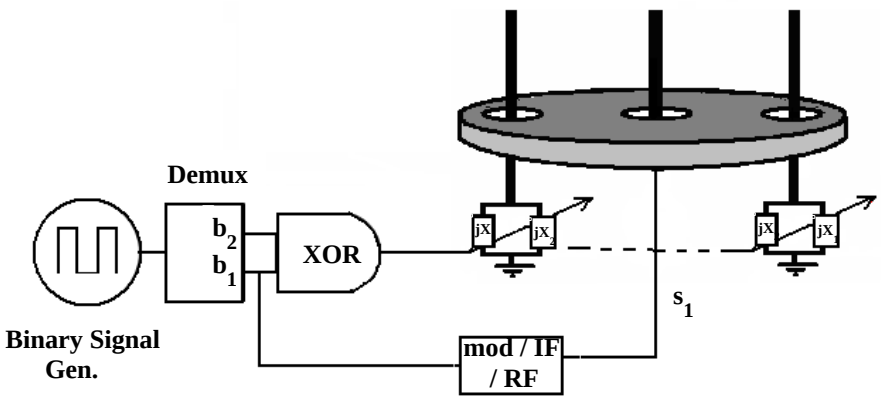


**Figure 3.2:** A simplified 3-element SPA control circuit.

nulled by the orthogonality of the basis (assuming uniform distribution of the field) and does not consequently affect the throughput potential. The effects of these parameters can be captured *using the exact SPA far-field* normalized with respect to a reference isotropic source.[1] The outage capacity is calculated using the log det formula (GF98) i.e assuming Gaussian signaling (the formula may serve as an upper-bound for the attainable rate under BPSK signaling). We use the same SPA antenna in (ea03b) at the transmit side, i.e. a 3-element SPA with $\lambda/10$ inter-element spacing, and a single omni receiver at the other side of the link. An exhaustive search was conducted through which the reactive loads were scanned from $-j100\Omega$ up to $j100\Omega$ with a step of $j\Omega$. The 10% outage capacity at SNR of 10dB was found at every loading within an indoor environment described by a 2-D geometrically based elliptical single bounce channel model as that described in (ea98). Fig. 3.3 shows the 10% outage capacity versus the PE loadings. A maximum 10% outage capacity of 1.9144 b/s/Hz is obtained at a loading of $[jX_1 \quad jX_2] = [-j4 \quad -j60]\,\Omega$. At such loading, a radiation efficiency of 95% and power imbalance between the angular basis of 0.4 dB are obtained.

[1] Notice that the MC is taken into account within the far-field calculation, where the currents are calculated from the mutual impedance matrix $\mathbf{Z}_{TT}$ and the SPA loading. The normalizing of the channel is done with respect to a reference SISO link with two isotropic sources at both ends of the communication link. The isotropic sources are obtained by loading the SPA PE's with 2k$\Omega$ each (ea03a).

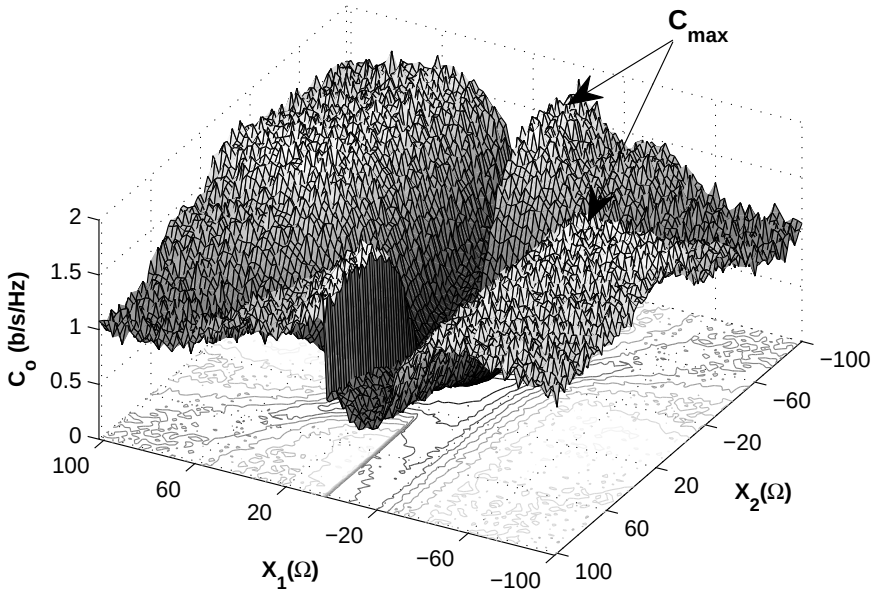


**Figure 3.3:** The 10% outage capacity at SNR of 10dB versus the two reactive loadings $jX_1$ and $jX_2$. The maximum outage capacity $C_{\max}$ is obtained at $[-j4 \quad -j60]\,\Omega$ and $[-j60 \quad -j4]\,\Omega$.

### 3.2.3 Some Receiver Techniques

The 3-element SPA could also function as a MIMO receiver for spatially demultiplexing the signals. A simple reception scheme is to demultiplex two real signals via IQ-separation i.e. the I-channel is separated from the Q-channel. This gives the receiver two independent equations to solve for the two unknown signals $x_1$ and $x_2$. The complex vector $\mathbf{h} = [h_1 \;\; h_2]$ is transformed after the IQ-separation into a real matrix

$$\mathbf{H} = \begin{bmatrix} \Re\{h_1\} & \Re\{h_2\} \\ \Im\{h_1\} & \Im\{h_2\} \end{bmatrix}$$

where the $\Re\{.\}$ operator returns the real part of the operand while the $\Im\{.\}$ operator returns the imaginary part of the operand and $h_i$ is the response of the receiver omni pattern to the $i^{th}$ transmit angular basis. Despite simplicity, the IQ-separation scheme suffers from some drawbacks, e.g the scheme is restricted to real signals, the transmit diversity order extracted by the receiver is reduced and the average SNR at the receiver is split between the two channels. An alternative demultiplexing scheme is to switch the receiver radiation pattern between two beams during each symbol period. Each beam samples different part of the space and collects consequently independent spatial samples of the received signal. Notice that the 3-element SPA can create at most three independent complex patterns (equal to the number of array elements) and consequently demultiplex up to three complex signals, or six real signals via extra IQ-separation (LL05). However, switching the beam patterns every half of the symbol period doubles the signal bandwidth (at the receiver side), which in turn doubles the Gaussian noise power at the receiver front-end. The signal model maybe described as

$$\mathbf{y} = \frac{1}{\sqrt{2}} \begin{bmatrix} h_{11} & h_{12} \\ h_{21} & h_{22} \end{bmatrix} \begin{bmatrix} x_1 \\ x_2 \end{bmatrix} + \sqrt{2} \begin{bmatrix} n_1 \\ n_2 \end{bmatrix}, \tag{3.13}$$

where $h_{ji}$ is the response of the $j^{th}$ receiving beam to the $i^{th}$ basis function, $n_j$ is the Gaussian noise collected within half of the symbol period by the $j^{th}$ receiving beam. The factor $\frac{1}{\sqrt{2}}$ is due to integrating each beam over half of the symbol period while the factor $\sqrt{2}$ is due to doubling the bandwidth. For design simplicity, the two optimal reactances for the transmission mode are also used for the reception mode i.e. $\mathcal{G}_1(\varphi) = \mathcal{B}_\Sigma(\varphi) + \mathcal{B}_\Delta(\varphi)$ and $\mathcal{G}_2(\varphi) = \mathcal{B}_\Sigma(\varphi) - \mathcal{B}_\Delta(\varphi)$. Notice that the two reactances are quite close to the optimal loads of $[0 \;\; -j60]\,\Omega$ used in (ea03b) for reception pattern diversity. This is verified in the scatter plot of the equivalent weight vector $\mathbf{w}_i$, $i \in \{0, 1, 2\}$ as shown in Fig. 3.4. The (thick) dot on $\mathbf{w}_0$ curve is the one corresponding to the optimal transmit loading, which is close to the optimal matching point $1 + j0$ (ea03b) while the dots on $\mathbf{w}_1$ and $\mathbf{w}_2$ curves are well apart so that both $\mathcal{G}_1(\varphi)$ and $\mathcal{G}_2(\varphi)$ are weakly correlated.

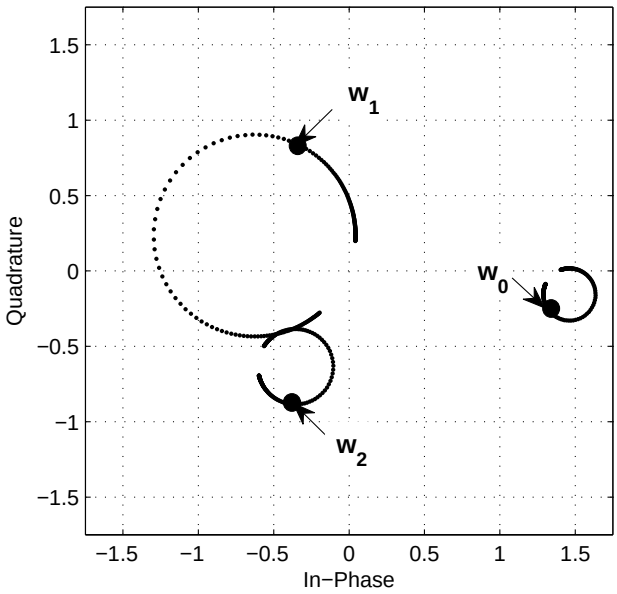


**Figure 3.4:** Equivalent weight vectors $\mathbf{w}_i$ at $jX_1 = -j4\Omega$.

### 3.2.4 Simulation Results

The same channel model is used for evaluating the performance of the transmission and reception schemes. Two nodes equipped with 3-element $\lambda/10$ SPA antennas are communicating within a peer-to-peer link at an operating frequency of 2.4 GHz. The two nodes are located at the foci of an ellipse with a 16m separation distance and 0.7 eccentricity and surrounded by twelve scatterers (ea98). The first node spatially multiplexes two BPSK signals and the second demultiplexes the signals using the proposed reception schemes using the optimal set of loads. Fig. 3.5 shows that the beam-switching reception technique outperforms its counterpart (IQ-Separation) at medium and high SNR regimes as it extracts a higher diversity order. At low SNR, IQ-Separation performs better as the performance is dominated by the noise level, reminding that the IQ-separation collects half the noise power of that collected by the beam-switching technique.

## 3.3 A Simple Example of Two Active Transmit Antennas

Before we show how to extend the previous findings to high order signaling we show how the far-field of a conventional MEA is composed of basis functions over

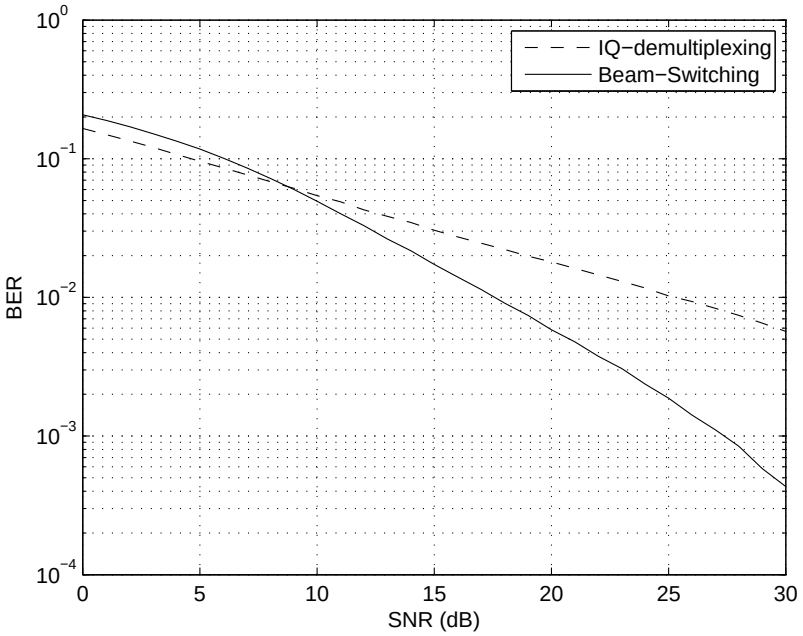


**Figure 3.5:** Performance of IQ-demultiplexing technique versus beam-switching demultiplexing technique using 3-element $\lambda/10$ SPA antennas at both ends of the communication link for spatially (de)multiplexing 2 BPSK signals.

which the signals are conveyed from the transmit to the receive side. We consider a conventional MEA where we focus our analysis on the transmitter which is the user handheld device (mobile, laptop, PDA, etc..). Assume that the transmitter is a horizontal linear array consisting of two identical co-polar antennas. The array far-field from (CO07) is written as

$$\mathcal{G}_T(\varphi) = \underbrace{[1 \quad \exp\left(-j\kappa d\cos(\varphi)\right)]}_{\boldsymbol{\alpha}^T(\varphi)} \underbrace{[\mathbf{Z}_M + \mathbf{Z}_{TT}]^{-1}}_{\mathbf{C}_T} \begin{bmatrix} s_1 \\ s_2 \end{bmatrix}, \tag{3.14}$$

where $\mathbf{Z}_M = Z_M\mathbf{I}_2$ (balanced uncoupled matching) and $s_i$ is the $i^{th}$ RF signal driving the $i^{th}$ element.

$$\mathcal{G}_T(\varphi) = s_1\mathcal{G}_1(\varphi) + s_2\mathcal{G}_2(\varphi) \tag{3.15}$$

where

$$\mathcal{G}_k(\varphi) = \boldsymbol{\alpha}^T(\varphi)\mathbf{C}_T\mathbf{u}_k, \tag{3.16}$$

are the *unit excitation active element responses* of antennas 1 and 2, respectively. The far-field *comprises a linear mixture of the active element patterns onto which the transmitted signals are mapped* i.e. the active element patterns form a *basis*[1].

### 3.3.1 Spatial Correlation

The basis onto which the signals are mapped can be directly used for calculating the transmit covariance matrix upon which the diversity performance of the system depends. By defining the vector $\boldsymbol{\mathcal{G}}(\varphi) = [\mathcal{G}_1(\varphi)\ \mathcal{G}_2(\varphi)]$, the transmit covariance matrix becomes

$$\mathbf{R}_T = \oint \mathcal{A}(\varphi)\ \boldsymbol{\mathcal{G}}^H(\varphi)\,\boldsymbol{\mathcal{G}}(\varphi)\cdot d\varphi, \tag{3.17}$$

where $\mathcal{A}(\varphi)$ is the power azimuth spectrum (PAS). In the special case when $\mathcal{A}(\varphi)$ is uniform in the 2-D, we get

[1]The term basis refers to a set of angular functions that comprise the whole space. The *basis is not necessarily to be orthogonal*!

$$\begin{aligned}\mathbf{R}_T &= \frac{1}{2\pi}\oint \boldsymbol{\mathcal{G}}^H(\varphi)\,\boldsymbol{\mathcal{G}}(\varphi)\cdot d\varphi,\\ &= c\mathbf{C}_T\mathbf{R}_{O.C.}^{1/2}\end{aligned} \tag{3.18}$$

where $c$ is a normalizing factor and

$$\mathbf{R}_{O.C.} = \begin{pmatrix} 1 & J_0(\kappa d) \\ J_0(\kappa d) & 1 \end{pmatrix} \tag{3.19}$$

is the open-circuit correlation matrix.

### 3.3.2 Far-Field Reformulation

The far-field can be further re-written as

$$\begin{aligned}\mathcal{G}_T(\varphi) &= s_1\left(\mathcal{G}_1(\varphi) + \frac{s_2}{s_1}\mathcal{G}_2(\varphi)\right)\\ &= s_1\underbrace{\left(\mathcal{G}_1(\varphi) + \mathcal{R}_s\mathcal{G}_2(\varphi)\right)}_{\widetilde{\mathcal{G}}_T(\varphi)}\end{aligned} \tag{3.20}$$

where $\widetilde{\mathcal{G}}_T(\varphi)$ is termed the 'effective radiation pattern' (CO07). The effective radiation pattern is a normalized version of the total far-field, which basically shows that the magnitude of the beampattern is controlled by the relative ratio of the two symbols $\mathcal{R}_s := \frac{s_2}{s_1}$. For example, the possible QPSK linear combinations of $\mathcal{G}_1(\varphi)$ and $\mathcal{G}_2(\varphi)$ are shown in TABLE I. The rest of the linear combinations give the same $\mathcal{R}_s$ and consequently the same effective radiation pattern, but with different phases due to a different $s_1$. For example, the linear combinations of the symbol pairs $(s_1, s_2) = \{(1,1), (-1,-1), (j,j), (-j,-j)\}$ give the same $\mathcal{R}_s = \{1,1,1,1\}$, and consequently the same $\widetilde{\mathcal{G}}_T(\varphi)$. The ratio $\mathcal{R}_s$ belongs to a unit circle for PSK modulation schemes as the two PSK signals have the same magnitude (constant envelope). The general notation of a complex symbol $s_m$ is $A_m e^{j(\omega t+\phi_m)}$ where $A_m, \omega_m, \phi_m$ are the signal amplitude, angular frequency and phase respectively. The notation of a baseband PSK symbol derived from a unity average power signal constellation can be written as $\exp(j\phi_m)$ where $A_m = 1$, $\phi_m = \frac{2\pi}{M}m, m \in \{0,\, 1,\, \ldots, M-1\}$ where $M$ is the order of the PSK signal constellation, while the angular component is dropped for simplicity. Consequently, the ratio of two baseband PSK symbols can be written as

$$\mathcal{R}_s := \frac{s_2}{s_1} = \exp\left(j\frac{2\pi}{M}m\right) \quad , m = \{0, 1, \ldots, M-1\}. \tag{3.21}$$

**Table 3.1:** Two QPSK Signals Combinations

| $[s_1 \;\; s_2]^T$ | $s_1$ | $\mathcal{R}_s$ | $\widetilde{\mathcal{G}}_T(\varphi) = \mathcal{G}_1(\varphi) + \mathcal{R}_s\mathcal{G}_2(\varphi)$ |
|---|---|---|---|
| $[1 \;\; 1]^T$ | 1 | $+1$ | $\mathcal{G}_1(\varphi) + \mathcal{G}_2(\varphi)$ |
| $[1 \;\; -1]^T$ | 1 | $-1$ | $\mathcal{G}_1(\varphi) - \mathcal{G}_2(\varphi)$ |
| $[1 \;\; j]^T$ | 1 | $+j$ | $\mathcal{G}_1(\varphi) + j\mathcal{G}_2(\varphi)$ |
| $[1 \;\; -j]^T$ | 1 | $-j$ | $\mathcal{G}_1(\varphi) - j\mathcal{G}_2(\varphi)$ |

The scatter plot of $\mathcal{R}_s$ has some important properties that are directly derived from the definition of $\mathcal{R}_s$:

- Rotating $\mathcal{R}_s$ by $\Delta\Phi$ is equivalent to rotating the signal constellation of the second stream by $\Delta\Phi$ with respect to the signal constellation of the first stream (the receiver has to reversely rotate the constellation of the second stream before decoding). However, rotating the signal constellation does not affect its properties.
- The relative average input power of the second stream to the first one equals the circle radius of $\mathcal{R}_s$ squared.

The radiation pattern in (3.15) has two degrees of freedom which are the two independent signals fed into the two antenna elements[1]. This representation is not useful for single feed arrays, since a single stream of symbols is fed into the active element at a time. On the other hand, a representation such as in (3.20) would be quite useful for single feed array where $s_1$ is equivalent to the signal fed into the active element (first degree of freedom), whereas the second degree of freedom can be determined by $\mathcal{R}_s$ which is controlled as we show in this work by the independent reactive loading of the PEs.

## 3.4 Any PSK-MIMO via SPA

### 3.4.1 Far-Field Approximation

The angular cosine term in (3.4) approaches the omni beampattern as the inter-element spacing decreases i.e. the angular dependence of the angular beampattern decreases by decreasing the spacing. This finding is exploited for approximating the far-field in (3.4) whenever the antenna system is compact as

[1] Assuming a non-reconfigurable array, consequently $d$ is fixed.

$$\begin{aligned}\mathcal{G}_T(\varphi) &= i_s\Big(\mathcal{B}_0(\varphi) + (\gamma_1+\gamma_2)\,\mathcal{B}_\Sigma(\varphi) - j\,(\gamma_1-\gamma_2)\,\mathcal{B}_\Delta(\varphi)\Big)\\ &\cong i_s\Big((1+(\gamma_1+\gamma_2)\,\tau)\mathcal{B}_0(\varphi) - j\,(\gamma_1-\gamma_2)\,\mathcal{B}_\Delta(\varphi)\Big)\end{aligned} \tag{3.22}$$

where $\mathcal{B}_0(\varphi)$ is the omnidirectional beam, $\mathcal{B}_\Sigma(\varphi) := \cos(\kappa d\cos(\varphi))$, $\mathcal{B}_\Delta(\varphi) := \sin(\kappa d\cos(\varphi))$, $\tau$ is an approximation (correction) factor for the magnitude of cosine term with respect to omni term (to be explained later). From 3.22, the relative ratio of the basis coefficients (out of which the effective pattern is determined) becomes

$$\mathcal{R}_x = j\frac{\gamma_1-\gamma_1}{1+(\gamma_1+\gamma_1)\,\tau}, \tag{3.23}$$

Finally (3.23) can be written as

$$\mathcal{G}_T(\varphi) = x_1\mathcal{B}_0(\varphi) + x_2\mathcal{B}_\Delta(\varphi) \tag{3.24}$$

where

$$\begin{aligned}x_1 &= i_s(1+(\gamma_1+\gamma_1)\tau)\\ x_2 &= i_s\exp(-j\pi/2)\,(\gamma_1-\gamma_1)\end{aligned} \tag{3.25}$$

### 3.4.2 Approximation Accuracy

The previous analysis was based on the finding that the spatial cosine term becomes highly correlated with the omni one, regarding both magnitude and phase. For example, the two spatial terms have a correlation factor $\varrho$ of 0.9996 at a spacing of $\lambda/16$. The cosine term can be approximated as $\tau\mathcal{B}_\Sigma(\varphi)$, where $\tau$ is a correction factor for the magnitude of cosine term with respect to the omni such that

$$\tau^2 = \frac{1}{2\pi}\oint|\cos(\kappa d\cos(\varphi))|^2\cdot d\varphi \tag{3.26}$$

from which $\tau$ is about 0.9623 for a linear array of thin dipoles spaced by $\lambda/16$.

Fig. 3.6 shows the polar magnitudes of the spatial terms cosine, sine and omni for the linear array of dipoles (spacing of $\lambda/16$), whereas Fig. 3.7 shows the channel

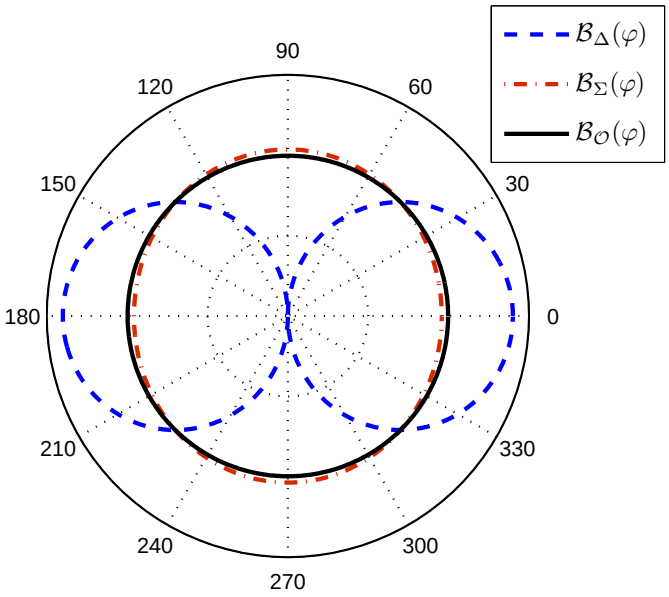


**Figure 3.6:** Magnitude of the basis functions at an inter-element spacing of $\lambda/16$.

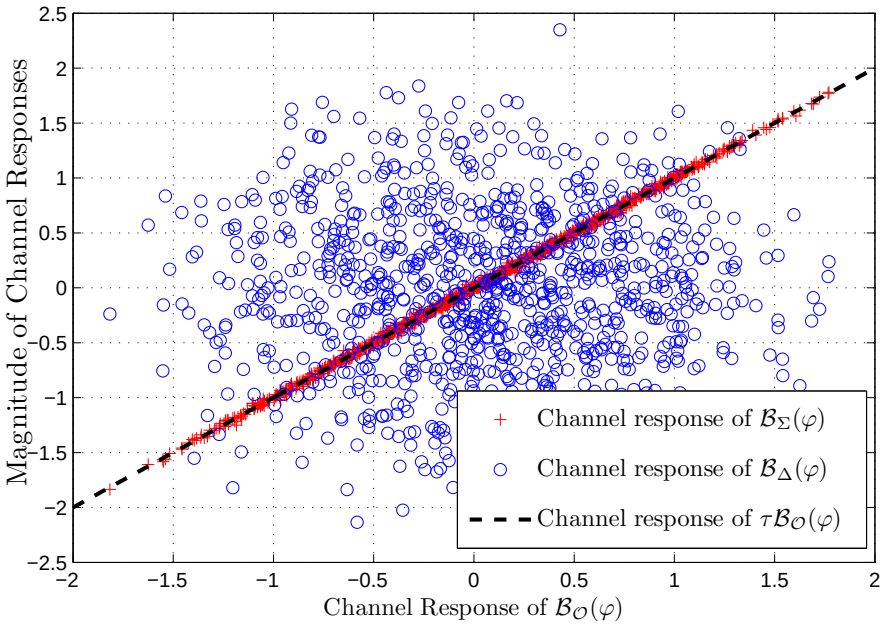


**Figure 3.7:** Magnitude of the channel responses of the basis functions.

responses[1] (over a thousand of channel realizations) of the sine, cosine and the scaled omni $\tau\mathcal{B}_\Sigma(\varphi)$ versus the channel responses of $\mathcal{B}_\Sigma(\varphi)$, where the channel is a 2-D geometrically based circular single bounce channel model as that in (ea98), with 20 scatterers surrounding the transmitter. The figure clearly shows that the wireless channel responses when triggered with a cosine are almost identical to those of $\tau\mathcal{B}_\Sigma(\varphi)$.

### 3.4.3 Spatial Multiplexing

For PSK signaling, the ratio $\mathcal{R}_x$ should have a locus of a circle. Assuming perfect channel state information (CSI) being available at the receiver but not at the transmitter, an optimal transmission policy is the one that isotropically distributes the power across the signals. However, since the proposed approach maps the signals onto a set of already imbalanced basis, the optimal circle radius in case of an uninformed transmitter, is the one that balances the relative average power of the two basis functions in (3.24). The power imbalance between the signals is given by

$$\Delta_P = \underbrace{\left(\frac{|\gamma_1-\gamma_2|^2}{|1+(\gamma_1+\gamma_2)\,\tau|^2}\right)}_{r^2=\frac{q_\Delta}{q_\Sigma}} \underbrace{\left(\frac{\frac{1}{2\pi}\oint|\mathcal{B}_\Delta(\varphi)|^2\cdot d\varphi}{\frac{1}{2\pi}\oint|\mathcal{B}_\Sigma(\varphi)|^2\cdot d\varphi}\right)}_{\Delta_B} \tag{3.27}$$

where $r$ denotes the scale of the basis and $\Delta_B$ denotes the power imbalance between the two basis functions in a uniform field. The optimal radius under open-loop transmission, denoted by $r_{OL}$, is the one that makes $\Delta_P = 1$. At an inter-element spacing of $\lambda/16$, $r_{OL}$ is found from (3.27) to be 3.67. Notice that *the circle is no more a unit circle* since the two basis functions are naturally imbalanced and consequently $r_{OL} \neq 1$. Fig. 3.8 shows the values of $\mathcal{R}_x$ in the complex plane that lie on a circle with the optimal radius (when the two reactive loadings change from $-j500\Omega$ to $j500\Omega$, step $j0.1\Omega$). $\mathcal{R}_x \cong r_{OL}\mathcal{R}_s \exp j\Delta\Phi_R$ where $r_{OL} = 3.67$ and $\Delta\Phi_R = 0.1$ rad. $\mathcal{R}_x$ is a scaled up version of $\mathcal{R}_s$ (so the two basis are equipowered), and slightly rotated so that each point of $\mathcal{R}_x$ has a corresponding loading. TABLE II shows the values of the reactive loadings required for obtaining the linear combinations of up to 16-PSK signal constellations. The values can be obtained using a variable reactor (varactor) as in the ESPAR antenna or lumped components as in the SPA. In the same table, $E_1$ is the absolute error in magnitude between $|\mathcal{R}_x|$ and $r_{OL}$, i.e. $E_1 = \left|\frac{|\mathcal{R}_x|-r_{OL}}{r_{OL}}\right|$, while $E_2$ is the absolute error in phase i.e. $E_2 = \left|\frac{\angle\mathcal{R}_x-\angle\mathcal{R}_s}{\angle\mathcal{R}_s}\right|$. It is clear that the *maximum absolute error* whether in phase or magnitude does not exceed 0.5% of the desired value. PSK

[1] Each channel response is single complex value and equals the summation of the multipath gains scaled by the complex far-field. Path loss and mobile terminal orientation are all taken into account.

transmission schemes with orders higher than sixteen cannot be projected on the circle of the optimal radius due to having two opposite gaps that can not be closed at any loading. These gaps are a consequence of the non-linear mapping (OT02) from the reactance space to equivalent wave-vector space. The result is that a limited number of PSK signal constellations can be optimally supported within the proposed scheme due to such gaps. $\mathcal{R}_x$ of *any* PSK signal constellation can be (sub-optimally) projected on a circle with a larger radius, e.g. $r_{MIN}$ in Fig. 3.8 is the radius of the first full circle beyond the gaps, where the basis functions suffer from a power imbalance $\Delta_P$ of 3.6 dB (although such projection is suboptimal, our simulations later on show that we have a marginal mutual information loss compared to the isotropic power allocation policy).

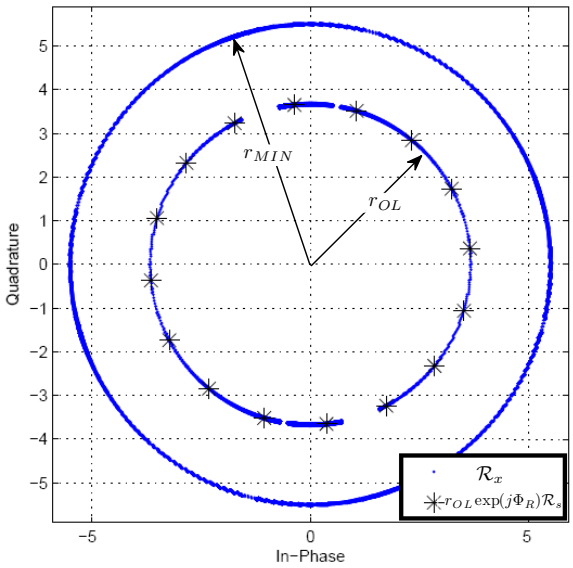


**Figure 3.8:** $\mathcal{R}_x$ values that lie on the optimal radius $r_{OL}$, over which a scaled up version of $\mathcal{R}_x$ regarding a 16-PSK signal constellation is projected, and the values of $\mathcal{R}_x$ that lie on the smallest radius $r_{MIN}$ of the first full-circle beyond the gaps.

### Dynamic Power Allocation

The power allocation *across the basis functions* can be optimized by maximizing the instantaneous mutual information over each channel realization as will be detailed later. Notice that this kind of power allocation is different from the optimal water-pouring (GNP03) precoding scheme, as the former only requires a single real number ($r$ or $q_\Delta$ or $q_\Sigma$ from (3.27)) to be fed back to the transmitter while the latter requires the whole channel matrix to be available at the transmitter for

**Table 3.2:** Corresponding Reactive Loadings for Different PSK Modulation Orders ($M$)

| $\mathcal{R}_x$ | $jX_1(\Omega)$ | $jX_2(\Omega)$ | $M$ | $E_1$ | $E_2$ |
|---|---|---|---|---|---|
| $e^{j0\frac{2\pi}{16}}$ | $j15.2$ | $j5.5$ | $2, 4, 8, 16$ | 0.42% | 0.39% |
| $e^{j1\frac{2\pi}{16}}$ | $j13.1$ | $j0.8$ | 16 | 0.05% | 0.1% |
| $e^{j2\frac{2\pi}{16}}$ | $j10.9$ | $-j9.5$ | $8, 16$ | 0.16% | 0.07% |
| $e^{j3\frac{2\pi}{16}}$ | $j7.7$ | $-j78$ | 16 | 0.13% | 0.12% |
| $e^{j4\frac{2\pi}{16}}$ | $-j10.5$ | $j53.7$ | $4, 8, 16$ | 0.01% | 0% |
| $e^{j5\frac{2\pi}{16}}$ | $j30$ | $j34.4$ | 16 | 0.01% | 0.03% |
| $e^{j6\frac{2\pi}{16}}$ | $j11.9$ | $j21.6$ | $8, 16$ | 0.35% | 0.09% |
| $e^{j7\frac{2\pi}{16}}$ | $j8.7$ | $j17.8$ | 16 | 0.15% | 0.17% |
| $e^{j8\frac{2\pi}{16}}$ | $j5.5$ | $j15.2$ | $2, 4, 8, 16$ | 0.42% | 0.39% |
| $e^{j9\frac{2\pi}{16}}$ | $j11.7$ | $j13.1$ | 16 | 0.05% | 0.1% |
| $e^{j10\frac{2\pi}{16}}$ | $j0.8$ | $j10.9$ | $8, 16$ | 0.16% | 0.07% |
| $e^{j11\frac{2\pi}{16}}$ | $-j78$ | $j7.7$ | 16 | 0.13% | 0.12% |
| $e^{j12\frac{2\pi}{16}}$ | $j53.7$ | $-j10.5$ | $4, 8, 16$ | 0.01% | 0% |
| $e^{j13\frac{2\pi}{16}}$ | $j34.4$ | $j30$ | 16 | 0.01% | 0.03% |
| $e^{j14\frac{2\pi}{16}}$ | $j21.6$ | $j11.9$ | $8, 16$ | 0.35% | 0.09% |
| $e^{j15\frac{2\pi}{16}}$ | $j17.8$ | $j8.7$ | 16 | 0.15% | 0.17% |

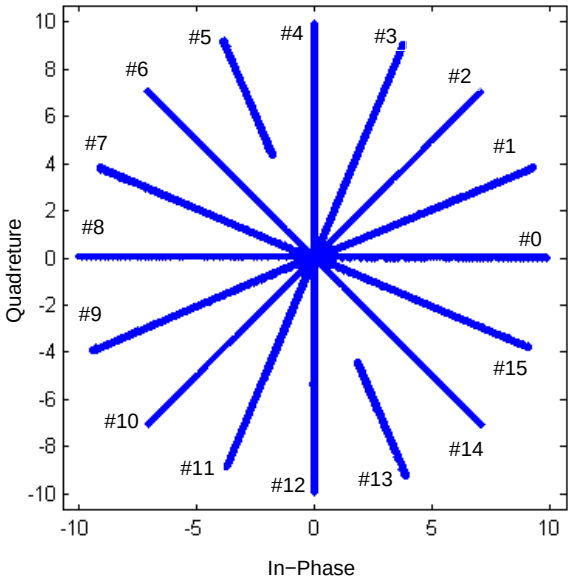


**Figure 3.9:** Scatter plot of $\mathcal{R}_x$ within a radius $r$ ranging from 0 up to 10 along the angles of $\mathcal{R}_x$ of a 16-PSK.

optimally allocating the power across the eigenvectors of the channel. The radius $r$ represents the relative scale of the two basis functions, thus the optimal $\mathcal{R}_x$ is the one of which $r_{CL}$ maximizes the instantaneous mutual information. In this case, the transmitter will have to use a look-up table, consequently the transmitter's control circuit selects the corresponding reactive loadings $[jX_1 \;\; jX_2]$ from the look-up table as follows

$$[jX_1 \;\; jX_2] = \arg\min_{\mathcal{R}_x} \left| r_{CL} \exp\left(j\Delta\Phi_R\right) \mathcal{R}_s - \mathcal{R}_x \right|, \tag{3.28}$$

which returns the corresponding loadings of the closest $\mathcal{R}_x$ to $\mathcal{R}_x^{opt}$. In (3.28) we used the minimum distance as a criterion for picking up the optimal (closest to the optimal) loadings, since some of $\mathcal{R}_x^{opt}$ will not have a corresponding loading, due to having the aforementioned opposite gaps as shown in Fig. 3.9. The figure clearly shows that BPSK (e.g. segments #0,#8), QPSK (e.g. segments #0,#4,#8,#12) and 8-PSK (e.g. segments (e.g. segments #0,#2,#4,#6,#8,#10,#12,#14) are supported within a closed loop transmission scheme, as the $\mathcal{R}_x$ segments are continuous up to a ratio of $r = 10$, which is equivalent to a power imbalance of 8.71

dB[1]. On the other hand, 16-PSK and higher order PSK modulation schemes will have some cases where optimal power allocation policy does not have a corresponding loading, and consequently the closest to the optimal loading will be selected as in (3.28). As an example, let's consider a uniform power allocation transmission scheme similar to that described in (KKP08). The scheme is done by feeding the driven element with the first PSK symbol from the two PSK symbols to be spatially multiplexed as shown in Fig. 3.10, after being modulated and converted to the IF/RF bands; at the same time, the control signal loads the PE with the two reactances $[jX_1 \;\; jX_2]$ (from TABLE II) according to the ratio of the two symbols $\mathcal{R}_x$. Loading the PE can be done using lumped reactances with PIN diodes as in SPAs, or simply by reverse-biasing a variable reactor (varactor) using a suitable voltage signal as in the ESPAR antennas (a one-to-one mapping exists between the reverse biasing voltage and the varactor reactance (OT02)). The ratio $\mathcal{R}_x$ is a scaled up version of the ratio of the two symbols to be spatially multiplexed $\mathcal{R}_s$ (with some possible rotations), so that the two SISO sub-channels have a specific power allocation policy. For example, transmitting the QPSK symbol pair $(j, -1)$ using a 3-element $\lambda/16$ SPA array is done as follows:

- Feed the active element with the first QPSK symbol.
- Simultaneously, the control circuit should change the loading of the PE according to the ratio $\mathcal{R}_s = \frac{-1}{j} = j \equiv \mathcal{R}_x = r_{OL}\mathcal{R}_s = r_{OL}\angle\frac{\pi}{2}$[2] (ignoring the rotation of $\mathcal{R}_x$ in this example). From TABLE II, $[jX_1 \;\; jX_2]$ should be $[-j10.5 \;\; j53.7]\Omega$.

The far-field according to this procedure may be written as $\mathcal{G}_T(\varphi)=j\mathcal{B}_0-(3.67)\mathcal{B}_\Delta(\varphi)$.

### 3.4.4 Throughput Analysis

In this part we consider the throughput potential of a flat-fading MIMO channel where the transmitter is equipped with a compact 3-element parasitic array, whereas the receiver is equipped with a conventional ULA of uncorrelated and uncoupled elements. We start first by rewriting down the channel matrix under the MC effect and the proposed far-field approximation. The far-field of the compact 3-element parasitic array can be written in the same form of (3.15)

$$\mathcal{G}_T(\varphi) = \boldsymbol{\mathcal{B}}(\varphi)\mathbf{x}^T \tag{3.29}$$

where

[1] $\Delta P(dB) = 10\log\left(r^2\Delta_B\right)$.
[2] The phasor notation $A\angle\phi$ means a complex quantity with magnitude $A$ and phase $\phi$.

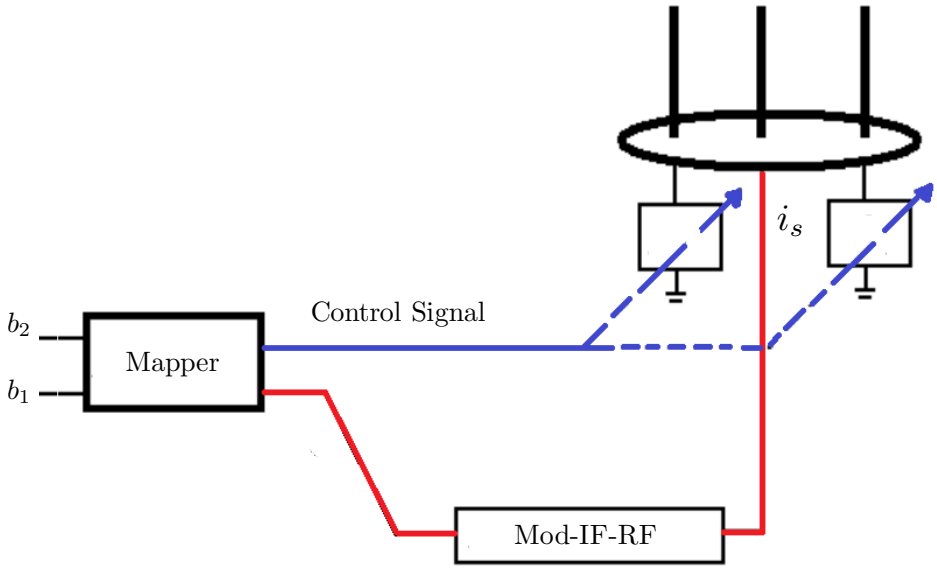


**Figure 3.10:** Simplified schematic diagram of 3-element SPA control circuit.

$$\begin{aligned} \boldsymbol{\mathcal{B}}(\varphi) &= [\mathcal{B}_\Sigma(\varphi)\ \mathcal{B}_\Delta(\varphi)] \\ \mathbf{x} &= [x_1\ x_2] \end{aligned} \tag{3.30}$$

The channel matrix can now be written as

$$\mathbf{H} = \mathbf{H}_w \mathbf{R}_T^{1/2} \tag{3.31}$$

where the transmit covariance matrix is given by

$$\mathbf{R}_T = \frac{1}{2\pi} \oint \boldsymbol{\mathcal{B}}^H(\varphi)\, \boldsymbol{\mathcal{B}}(\varphi) \cdot d\varphi \tag{3.32}$$

assuming a uniform field distribution. The receive covariance matrix is assumed to be equal to the identity matrix (i.e. uncorrelated distantly spaced antennas). Given the channel matrix, the general channel capacity formula for a Gaussian signaling is given from (GNP03) as

$$C = \max_{\text{trace}(\mathbf{R}_{xx})=\mathcal{K}_T} \log_2 \det \left( \mathbf{I}_{\mathcal{K}_R} + \frac{\rho}{\mathcal{K}_T} \mathbf{H} \mathbf{R}_{xx} \mathbf{H}^H \right), \tag{3.33}$$

where $\mathbf{R}_{xx} = \mathbb{E}\left\{\mathbf{x}^H\mathbf{x}\right\}$ is the covariance of the input. The capacity in (3.33) is achieved when the distribution of the input is Gaussian. Unlike conventional MIMO, $\mathbf{R}_{xx}$ in the proposed BS-MIMO system is controlled by controlling the reactive loads. Although this work is restricted to PSK signaling which does not achieve the capacity of a Gaussian signaling, the equation in (3.33) serves as an upper-bound for the spectral efficiency potential of the proposed encoding scheme and simplifies the analysis. In the simulation part we evaluate the upper-bound capacity assuming Gaussian signaling, however we estimate the capacity of different $M$-PSK transmission schemes using Monte-Carlo simulation. According to the CSI availability at the transmitter we have two different power allocation policies:

#### 3.4.4.1 No Feedback

From (3.32) and (3.33), the mutual information[1] is written as

$$\begin{aligned}\Im_{av} &= \mathbb{E}_{\mathbf{H}}\left[\log_2 \det\left(\mathbf{I}_2 + \frac{\rho}{2}\mathbf{R}_{xx}\mathbf{H}^H\mathbf{H}\right)\right] \\ &\leq \log_2 \det\left(\mathbf{I}_2 + \frac{\rho}{2}\mathbf{R}_{xx}\mathbb{E}_{\mathbf{H}}\left[\mathbf{H}^H\mathbf{H}\right]\right) \\ &= \log_2 \det\left(\mathbf{I}_2 + \frac{\rho}{2}\mathbf{R}_{xx}\mathbf{R}_T\right) \end{aligned} \tag{3.34}$$

which is maximized when the elements of the diagonal matrix $\mathbf{R}_{xx}\mathbf{R}_T$ are equal, i.e. when $\mathbf{R}_{xx} = a_n\mathbf{R}_T^{-1}$ ($a_n$ is a normalizing scalar) leading to a balanced basis. In fact, when the channel is not known to the transmitter but only to the receiver, an optimal power allocation policy in conventional MIMO communications is to divide the power equally across the transmit antennas (Tel99). In the proposed beamspace MIMO, power allocation is virtually implemented by picking the reactive loads that balance the average power across the *naturally imbalanced* basis functions.

#### 3.4.4.2 Limited Feedback

The instantaneous power allocation (rather than the average power allocation) across the basis functions can be optimized on every single channel realization. The allocation policy can be easily implemented by the receiver (which knows the channel). The receiver then feeds a single real value back to the transmitter. By expressing $\mathbf{R}_{xx}$ as diag $([q_\Sigma \; q_\Delta])$, $q_\Sigma$ can be quantized into $2^n$ levels between 0 and $\mathcal{K}_T = 2$) where $n$ is number of quantizing bits. The mutual information is found

[1] Some times the term open-loop capacity is used with some abuse of language.

on every level of $q_{\Sigma}^{l}$, and the maximum value is found by simple exhaustive search as

$$q_{\Sigma}^{opt} = \arg\max_{\mathbf{R}_{xx}^{(l)}} \left\{ \log_2 \det \left( \mathbf{I}_2 + \mathbf{R}_{xx}^{(l)} \mathbf{H}^H \mathbf{H} \right) \right\}, \tag{3.35}$$

In the simulation part, it is shown that two bits for quantizing $q_{\Sigma}$ are enough to give a mutual information gain marginally close to that with infinite resolution (analog feedback) (ea08b). In addition, the mutual information gain using such a scheme decreases as the signal-to-noise (SNR) ratio increases and asymptotically coincides with the uniform power allocation policy (see Fig. 3.11, the results are discussed in later).

### 3.4.5 Simulation Results

We consider an outdoor propagation scenario, described by a 2-D geometrically based circular single bounce channel model as that described in (ea98). We assume that all the signals are transmitted and received from a single location corresponding to the phase center of the transmitting and receiving arrays. The inter-element spacing between the transmitter elements equals $\lambda/16$, while the inter-element spacing between the receiving antenna elements equals $10\lambda$. The transmitter coupling matrix is already taken into consideration within the calculation of the far-fields before normalizing, whereas the receiver coupling matrix is assumed to be an identity matrix, due to the largely assumed inter-element spacing.

We start first by evaluating the mutual information upper bound using the log det formula (i.e. assuming Gaussian signaling). Fig. 3.11 shows the 10% outage capacities of communication system examples within a $2 \times 2$ MIMO setting, using a 3-element $\lambda/16$ SPA. The mutual information is compared to the theoretical one from (3.34) when the elements of the uncoupled matrix $\mathbf{H}$ are assumed to be i.i.d. and to the optimal waterfilling precoding scheme. The figure clearly shows that the simulation results practically coincide with the theoretical ones. The two fixed power allocation policies (i.e. when $\Delta P = 0$ or 3.6 dB as a result of mapping the symbols onto the circle of $r_{OL}$ and $r_{MIN}$ respectively) are shown to be almost identical. The figure also shows that the optimal power allocation using two bits for quantizing and feeding back $\delta_{\Sigma}$ gives almost the same mutual information when analog feedback is used. Last but not least, the two optimal power allocation policies (among the basis function) are shown to be inferior to the optimal waterfilling (WF) capacity, as the latter optimally allocates the power among the channel eigenvectors rather than the basis functions (A 10% capacity gain is achieved by the proposed power allocation scheme at SNR=0dB, while a 20% capacity gain is achieved by the theoretical WF scheme at the same SNR).

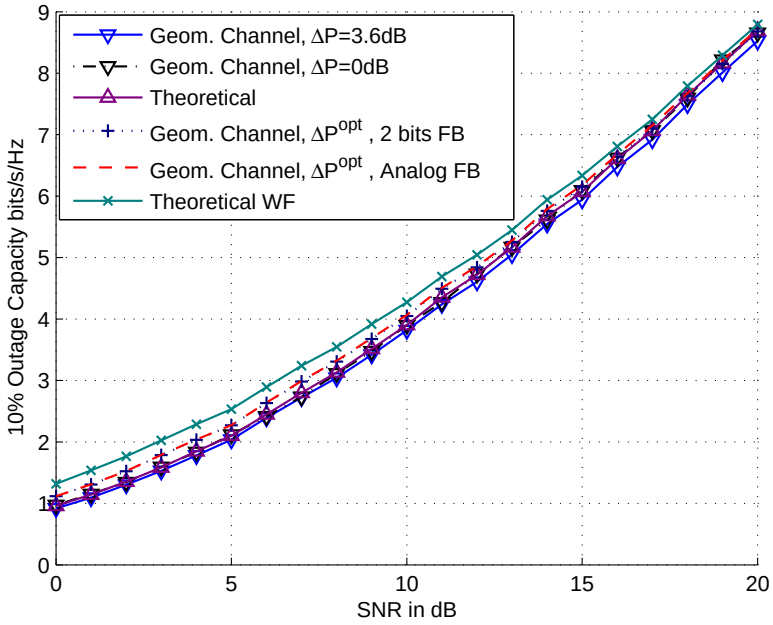


**Figure 3.11:** 10% outage capacities for $2 \times 2$ MIMO system examples (assuming Gaussian signaling) using different power allocation policies among the basis functions.

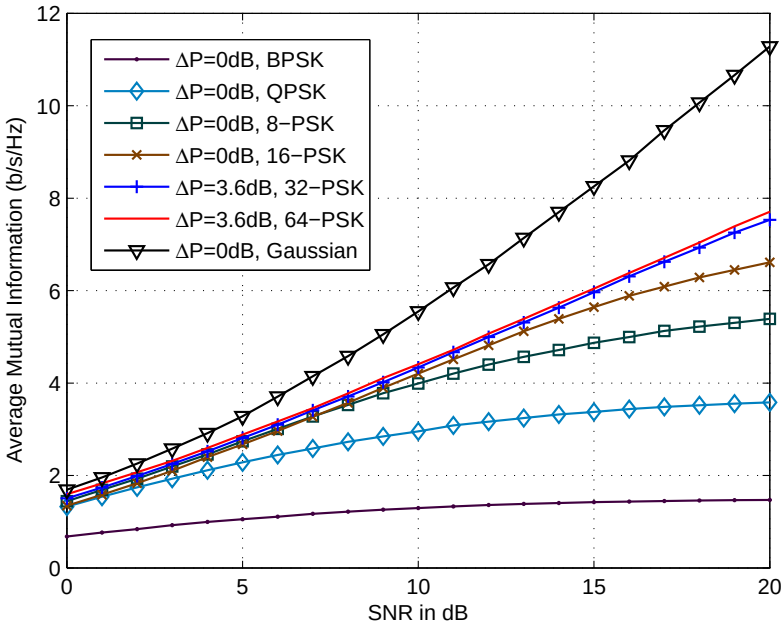


**Figure 3.12:** Average mutual information for $2 \times 2$ MIMO system examples using different PSK signaling schemes.

Fig. 3.12 shows the exact average mutual information of different PSK transmission schemes using the proposed encoding scheme within the geometrical channel. The average mutual information was obtained using a Monte-Carlo simulation (see (YMK06)) where $10,000$ channel realizations were used for estimating the conditional probability distribution of the output given all the possible input alphabets (the input is a 1000 uniformly distributed PSK symbols). The figure shows that the average mutual information of an $M$-PSK transmission scheme saturates at high SNR at $2\log_2 M$ (within a $2 \times 2$ MIMO) setting. The figure also shows that a QPSK transmission suffices at low SNR while a 64-PSK has no appreciable gain over a 32-PSK (at least at low and medium SNR regime). Fig. 3.13 shows the CDF of the instantaneous mutual information (using the log det formula of (3.34)) of some system examples at SNR$=$ 10 dB using a 3-element $\lambda/16$ SPA within a $2 \times 1$ Alamouti diversity scheme. The mutual information is compared to the theoretical one (assuming the elements of $\mathbf{H}$ are i.i.d. and uniform power distribution between the basis functions). The figure shows that the mutual information of the two fixed-power allocation schemes is quite comparable to the mutual information of the balanced i.i.d. channel model. Finally, as realistic radiation patterns will have some irregularities (e.g. due to using dirty RF components (KW06) or coupling with the neighboring objects), the angular functions will no more form a pure basis. Fig. 3.14 illustrates the mutual information sensitivity to different correlation coefficients between the angular functions. The figure clearly shows that a correlation factor up to $|\varrho| = 0.3$ can be an acceptable upper-bound.

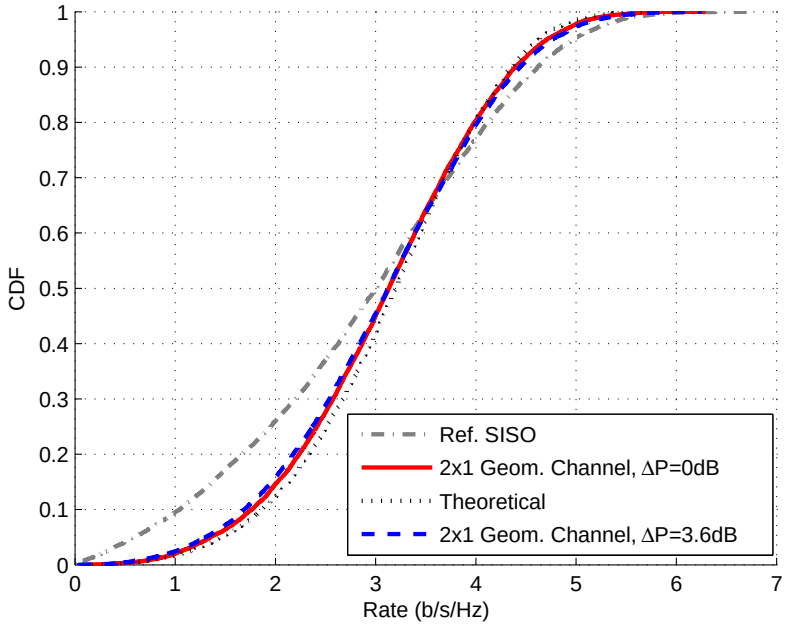


**Figure 3.13:** Empirical CDF of instantaneous channel mutual information at SNR= 10 dB for $2 \times 1$ system examples.

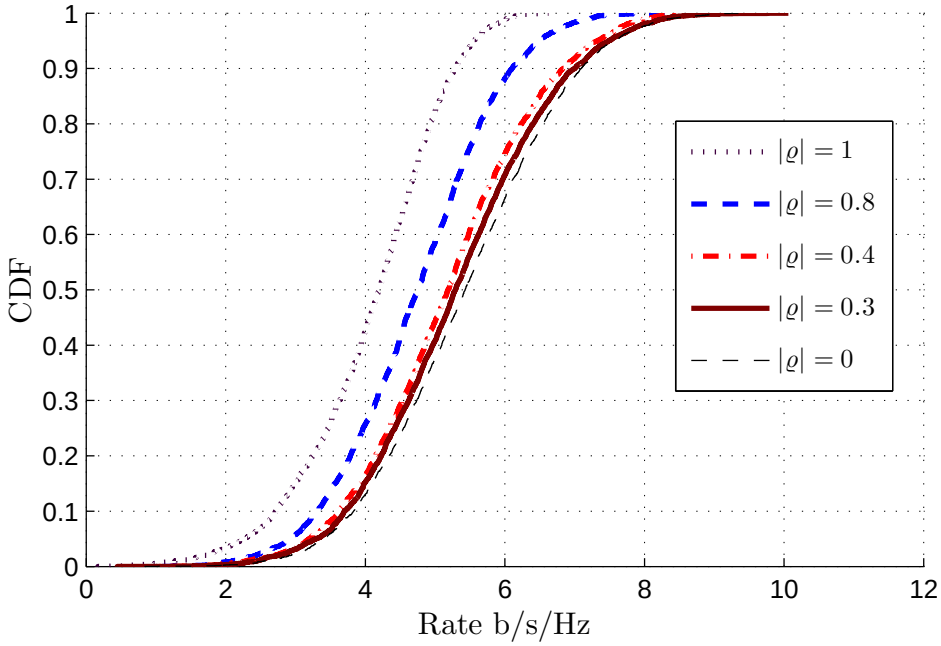


**Figure 3.14:** Effect of correlation between angular functions on system mutual information.

# 4

# Generalized Beamspace MIMO Model and Antenna Design

This chapter has the following contributions:

- Generalizing the derivation of the bases from Mirror Image Pattern Pairs (MIPPs) i.e. when one beampattern is a rotated version of the other, regardless of how the MIPPs are expressed.
- Extending previous proofs to a general *3D RF propagation with polarized waves*.
- Proposing a practical SPA example of printed dipoles. The SPA is modeled, optimized regarding the average rate of transmission, finally designed and demonstrated.

## 4.1 General MIMO Transmission with a Single RF Source

In this section we first prove the existence of an orthogonal basis whenever a MIPP can be formed. Based on this, a technique for transmitting two BPSK signals using arbitrary single radio based antenna system capable of forming a MIPP is described.

### 4.1.1 Orthogonal Bases Using MIPPs

The correlation between two arbitrary beampatterns $\mathcal{G}_1(\vartheta,\varphi)$ and $\mathcal{G}_2(\vartheta,\varphi)$ is given by

$$\varrho_{12} = \frac{1}{\sqrt{P_1 P_2}} \int_{\varphi} \int_{\vartheta} \mathcal{G}_1(\vartheta,\varphi)\, \mathcal{G}_2^*(\vartheta,\varphi) \sin(\vartheta) \cdot d\vartheta d\varphi \tag{4.1}$$

where

$$P_1 = \frac{1}{4\pi}\int_{\varphi}\int_{\vartheta} |\mathcal{G}_1(\vartheta,\varphi)|^2 \sin(\vartheta)\cdot d\vartheta d\varphi,$$
$$P_2 = \frac{1}{4\pi}\int_{\varphi}\int_{\vartheta} |\mathcal{G}_2(\vartheta,\varphi)|^2 \sin(\vartheta)\cdot d\vartheta d\varphi, \tag{4.2}$$

are the spatial integrations of the power beampatterns of $\mathcal{G}_1(\vartheta,\varphi)$ and $\mathcal{G}_2(\vartheta,\varphi)$ over the space, respectively. Whenever $P_1 = P_2$, the two beampatterns are called 'balanced'.

**Lemma.1:** For a MIPP $\mathcal{G}_1(\vartheta,\varphi)$ and $\mathcal{G}_2(\vartheta,\varphi)$, the set of the angular functions defined as

$$\mathcal{B}_{\Sigma}(\vartheta,\varphi) := \frac{1}{\sqrt{2}}\big(\mathcal{G}_2(\vartheta,\varphi) + \mathcal{G}_1(\vartheta,\varphi)\big),$$
$$\mathcal{B}_{\Delta}(\vartheta,\varphi) := \frac{1}{\sqrt{2}}\big(\mathcal{G}_2(\vartheta,\varphi) - \mathcal{G}_1(\vartheta,\varphi)\big), \tag{4.3}$$

form an orthogonal basis.

*Proof*: For two beampatterns that are circularly-symmetric, we have $P_1 = P_2$ since one beampattern is just a rotated version of the other. Moreover, the correlation between the two beams can be easily proved to be real (APCK10), and thus $\varrho_{12} = \varrho_{12}^*$. Based on these observations, the proof is straightforward and is given in (4.4).

$$\begin{aligned}
\varrho_{\Sigma\Delta} &= \frac{1}{4\pi\sqrt{P_{\Sigma}P_{\Delta}}}\int_{\varphi}\int_{\vartheta} \mathcal{B}_{\Sigma}(\vartheta,\varphi)\,\mathcal{B}_{\Delta}^{*}(\vartheta,\varphi)\sin(\vartheta)\cdot d\vartheta d\varphi \\
&= \frac{1}{8\pi\sqrt{P_{\Sigma}P_{\Delta}}}\int_{\varphi}\int_{\vartheta} \big(\mathcal{G}_2(\vartheta,\varphi) + \mathcal{G}_1(\vartheta,\varphi)\big)\,\big(\mathcal{G}_2^{*}(\vartheta,\varphi) - \mathcal{G}_1^{*}(\vartheta,\varphi)\big)\sin(\vartheta)\cdot d\vartheta d\varphi \\
&= \frac{1}{2\sqrt{P_{\Sigma}P_{\Delta}}}\Big(P_2 - \sqrt{P_1P_2}\varrho_{12}^{*} + \sqrt{P_1P_2}\varrho_{12} - P_1\Big) \\
&= \frac{1}{2\sqrt{P_{\Sigma}P_{\Delta}}}\left(P_1 - P_1\varrho_{12} + P_1\varrho_{12} - P_1\right) \\
&= 0
\end{aligned} \tag{4.4}$$

**Corollary.1:** A balanced basis is obtained by designing the two beampatterns $\mathcal{G}_1(\vartheta,\varphi)$ and $\mathcal{G}_2(\vartheta,\varphi)$ described in **Lemma** .1 to be orthogonal to each other.

*Proof*: Let $\mathcal{G}_1(\vartheta,\varphi) \perp \mathcal{G}_2(\vartheta,\varphi)$, the proof is straightforward as shown in (4.6) on top of page 3. In (4.6), $P_\Sigma$ and $P_\Delta$ are the spatial integration of the power beampatterns of $\mathcal{B}_\Sigma(\vartheta,\varphi)$ and $\mathcal{B}_\Delta(\vartheta,\varphi)$, over the space, given respectively by

$$\begin{aligned} P_\Sigma &= \frac{1}{4\pi}\int_\varphi\int_\vartheta |\mathcal{B}_\Sigma(\vartheta,\varphi)|^2 \sin(\vartheta)\cdot d\vartheta d\varphi, \\ P_\Delta &= \frac{1}{4\pi}\int_\varphi\int_\vartheta |\mathcal{B}_\Delta(\vartheta,\varphi)|^2 \sin(\vartheta)\cdot d\vartheta d\varphi. \end{aligned} \tag{4.5}$$

$$\begin{aligned} 0 &= \frac{1}{4\pi\sqrt{P_1P_2}}\int_\varphi\int_\vartheta \mathcal{G}_1(\vartheta,\varphi)\,\mathcal{G}_2^*(\vartheta,\varphi)\sin(\vartheta)\cdot d\vartheta d\varphi \\ 0 &= \frac{1}{8\pi\sqrt{P_1P_2}}\int_\varphi\int_\vartheta \left(\mathcal{B}_\Sigma(\vartheta,\varphi)-\mathcal{B}_\Delta(\vartheta,\varphi)\right)\left(\mathcal{B}_\Sigma^*(\vartheta,\varphi)+\mathcal{B}_\Delta^*(\vartheta,\varphi)\right)\sin(\vartheta)\cdot d\vartheta d\varphi \\ 0 &= \frac{1}{2\sqrt{P_1P_2}}\left(P_\Sigma+\varrho_{\Sigma\Delta}\sqrt{P_\Sigma P_\Delta}-\varrho_{\Sigma\Delta}^*\sqrt{P_\Sigma P_\Delta}-P_\Delta\right) \\ 0 &= \frac{1}{2\sqrt{P_1P_2}}\left(P_\Sigma-P_\Delta\right) \\ \Rightarrow\quad P_\Sigma &= P_\Delta \end{aligned} \tag{4.6}$$

### 4.1.2 Transmission Technique Description

In this part we show that an arbitrary antenna system having a single RF input but has the capability of creating a MIPP will be capable of transmitting two BPSK signals $s_1$ and $s_2$, simultaneously. The two BPSK signals are mapped onto an orthogonal set of basis functions, thus independent fading between the two signals is almost always guaranteed regardless of the transceiver compactness. Let the sole RF port be fed by the signal $s_1$, the antenna beampattern in the

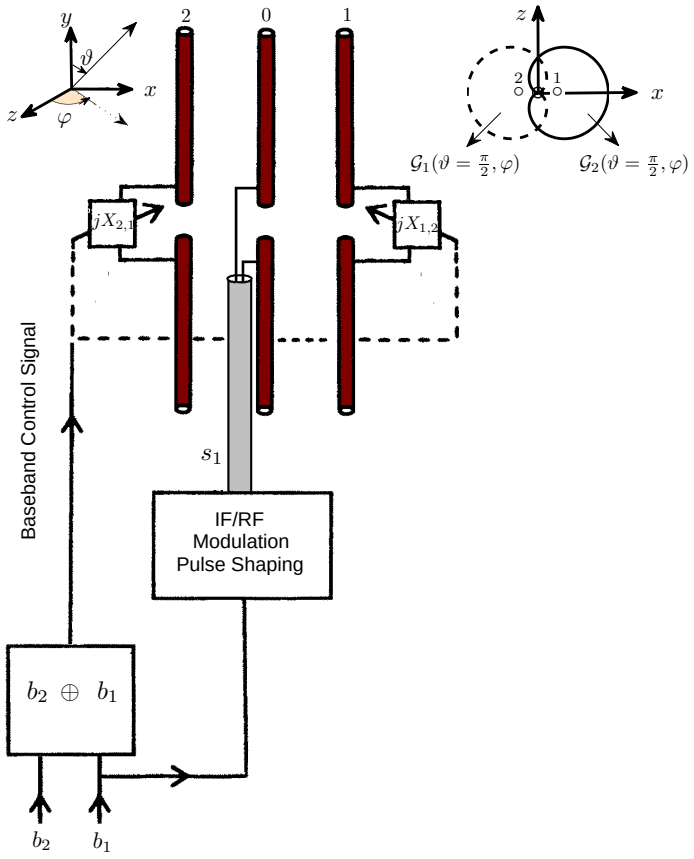


**Figure 4.1:** Schematic diagram of the proposed technique where the first bitstream is modulated, up converted and fed into the central active element whereas the second bitstream is XORed with the first one. The output control signal is used for swapping the loads of the PE.

far-field becomes either

$$
\begin{aligned}
& \textit{State 1} \\
\mathcal{G}_T(\vartheta,\varphi) &= \mathcal{G}_1(\vartheta,\varphi)\, s_1 \\
&= \frac{s_1}{\sqrt{2}}\left[\mathcal{B}_\Sigma(\vartheta,\varphi) - \mathcal{B}_\Delta(\vartheta,\varphi)\right] \\
& \text{or } \textit{State 2} \\
\mathcal{G}_T(\vartheta,\varphi) &= \mathcal{G}_2(\vartheta,\varphi)\, s_1 \\
&= \frac{s_1}{\sqrt{2}}\left[\mathcal{B}_\Sigma(\vartheta,\varphi) + \mathcal{B}_\Delta(\vartheta,\varphi)\right] \\
& \text{or generally as} \\
\mathcal{G}_T(\vartheta,\varphi) &= \frac{s_1}{\sqrt{2}}\left[\mathcal{B}_\Sigma(\vartheta,\varphi) + (-1)^S \mathcal{B}_\Delta(\vartheta,\varphi)\right] \qquad (4.7a) \\
&= \frac{1}{\sqrt{2}}\left[s_1\mathcal{B}_\Sigma(\vartheta,\varphi) + s_2\mathcal{B}_\Delta(\vartheta,\varphi)\right] \qquad (4.7b)
\end{aligned}
$$

where $S$ is the antenna system state such that $S := 1$ is *State 1* within which the antenna system transmits over $\mathcal{G}_1(\vartheta, \varphi)$ and $S := 2$ is *State 2* within which the antenna system transmits over $\mathcal{G}_2(\vartheta, \varphi)$. From (4.7b) it is obvious how the two BPSK signals: $s_1$ which is modulated in the baseband, up-converted and fed into the input RF port and $s_2 = (-1)^S s_1$ which is aerially modulated on the antenna far-field by controlling the antenna state $S$, are mapped onto the space of $\mathcal{B}_\Sigma(\vartheta, \varphi)$ and $\mathcal{B}_\Delta(\vartheta, \varphi)$, respectively. Table I shows the state $S$ required for transmitting $s_2$ according to the value of $s_1$ where $[b_1 \;\; b_2]^T$ is input vector of bits modulated into $[s_1 \;\; s_2]^T$. Fig. 4.1 shows a schematic diagram of the proposed technique, where the XORing of the two bitstreams gives the required $S$ i.e. $S = b_1 \oplus b_2$ giving 0 and 1 which correspond to $S := 1$ and $S := 2$, respectively.

**Table 4.1:** Two BPSK Signals Combinations

| $[b_1 \;\; b_2]^T$ | $[s_1 \;\; s_2]^T$ | $S$ |
|---|---|---|
| $[\,1 \quad 1\,]^T$ | $[\,1/\sqrt{2} \quad 1/\sqrt{2}\,]^T$ | 2 |
| $[\,1 \quad 0\,]^T$ | $[\,1/\sqrt{2} \quad -1/\sqrt{2}\,]^T$ | 1 |
| $[\,0 \quad 1\,]^T$ | $[-1/\sqrt{2} \quad 1/\sqrt{2}\,]^T$ | 1 |
| $[\,0 \quad 0\,]^T$ | $[-1/\sqrt{2} \quad -1/\sqrt{2}\,]^T$ | 2 |

### 4.1.3 System Training

The two BPSK signals that are transmitted in the beam-space domain and received using a classical uniform linear array of $\mathcal{K}_R$ antenna elements ($\mathcal{K}_R$-element ULA), can be decoded by first estimating the receive antenna responses to the proposed basis.

**Lemma.2:** A beampattern comprising a linear mixture of basis functions (at the transmitter side) creates a linear combination of the individual channel responses to the different basis functions (at the receiver side).

*Proof*: First we define $2 \times 1$ column vectors $\boldsymbol{\mathcal{G}}_{1,T}(\vartheta, \varphi)$, $\boldsymbol{\mathcal{G}}_{2,T}(\vartheta, \varphi)$, $\boldsymbol{\mathcal{B}}_{\Sigma,T}(\vartheta, \varphi)$ and $\boldsymbol{\mathcal{B}}_{\Delta,T}(\vartheta, \varphi)$, where the first and the second elements of every column vector represent the $\hat{\vartheta}$ and $\hat{\varphi}$ polarizations of the corresponding pattern, respectively. We also define $\boldsymbol{\mathcal{G}}_{k,R}(\vartheta, \varphi)$ as the vector of the polarization components of the $k$th receiver antenna pattern $\mathcal{G}_{k,R}(\vartheta, \varphi)$. As in (JM05a), we assume that the propagation channel between the transmitter and the receiver consists of a set of $L$ plane waves, with the $l$th wave characterized by a complex voltage gain $\beta_l$, angle of departure $(\vartheta_{l,T}, \varphi_{l,T})$, and angle of arrival $(\vartheta_{l,R}, \varphi_{l,R})$. We also assume that each plane wave undergoes a polarization transformation due to scattering

that can be expressed as the unitary matrix

$$\mathbf{O}_l = \begin{bmatrix} o_{l,\vartheta\vartheta} & o_{l,\vartheta\varphi} \\ o_{l,\varphi\vartheta} & o_{l,\varphi\varphi} \end{bmatrix}. \tag{4.8}$$

The response of the $k$th receive antenna ($1 \leq k \leq \mathcal{K}_R$) when illuminated by the beampattern $\mathcal{G}_1(\vartheta, \varphi)$ is the complex channel gain representing the ratio of the received voltage signal to the transmitted voltage signal, and may be written as shown in (4.9), where $\mathscr{C}_{k,1}$ is a constant that depends on the receiver and the transmitter active gains and impedances (WSW04), $h_{k,\Sigma}$ and $h_{k,\Delta}$ are the responses of the $k$th receive antenna to $\mathcal{B}_\Sigma(\vartheta, \varphi)$ and $\mathcal{B}_\Delta(\vartheta, \varphi)$, respectively. By applying the same analysis, the response of the $k$th receive antenna when illuminated by $\mathcal{G}_2(\vartheta, \varphi)$ becomes $h_{k2} = \frac{1}{\sqrt{2}}(h_{k,\Sigma} + h_{k,\Delta})$.

$$\begin{aligned}
h_{k1} &= \mathscr{C}_{k1} \sum_{l=1}^{L} \boldsymbol{\mathcal{G}}_{k,R}(\vartheta_{l,R}, \varphi_{l,R})\, \beta_l \mathbf{O}_l \boldsymbol{\mathcal{G}}_{1,T}(\vartheta_{l,T}, \varphi_{l,T}) \\
&= \mathscr{C}_{k1} \sum_{l=1}^{L} \boldsymbol{\mathcal{G}}_{k,R}(\vartheta_{l,R}, \varphi_{l,R})\, \beta_l \mathbf{O}_l \left(\boldsymbol{\mathcal{B}}_{\Sigma,T}(\vartheta_{l,T}, \varphi_{l,T}) - \boldsymbol{\mathcal{B}}_{\Delta,T}(\vartheta_{l,T}, \varphi_{l,T})\right) \\
&= \mathscr{C}_{k1} \sum_{l=1}^{L} \boldsymbol{\mathcal{G}}_{k,R}(\vartheta_{l,R}, \varphi_{l,R})\, \beta_l \mathbf{O}_l \boldsymbol{\mathcal{B}}_{\Sigma,T}(\vartheta_{l,T}, \varphi_{l,T}) \\
&\quad - \mathscr{C}_{k1} \sum_{l=1}^{L} \boldsymbol{\mathcal{G}}_{k,R}(\vartheta_{l,R}, \varphi_{l,R})\, \beta_l \mathbf{O}_l \boldsymbol{\mathcal{B}}_{\Delta,T}(\vartheta_{l,T}, \varphi_{l,T}) \\
&= \frac{1}{\sqrt{2}}(h_{k,\Sigma} - h_{k,\Delta})
\end{aligned} \tag{4.9}$$

Based on the proof of **Lemma.2:**, the receiver can decode the two BPSK signals by estimating the channel responses of the basis as

$$h_{k,\Sigma} = \frac{1}{\sqrt{2}}(h_{k,1} + h_{k,2}), \tag{4.10a}$$

$$h_{k,\Delta} = \frac{1}{\sqrt{2}}(h_{k,1} - h_{k,2}). \tag{4.10b}$$

By constructing the matrix of the receive antennas' responses, the receiver can zero-force the received signal by inverting the channel matrix (or using any other reception techniques) for decoding $s_1$ and $s_2$.

## 4.2 Antenna Model and Optimization

In this part we adopt the antenna topology proposed in (AKPP09), i.e. a symmetrical 3-element SPA, where the central element is the active one while the other two are

passive. The two PEs are loaded with pure imaginary loads $[jX_1 \;\; jX_2]$ as the real part of a complex load degrades the efficiency of the antenna system. Obviously the antenna system can create a MIPP that are mirror images of each other around the E-plane (the $yz$ plane in Fig. 4.1) by simply permuting the reactive loads of the PE as $[jX_1 \;\; jX_2] \leftrightarrow [jX_2 \;\; jX_1]$, based on the image theory. In other words, having the first beampattern $\mathcal{G}_1(\vartheta, \varphi)$ at $[jX_1 \;\; jX_2]$, the beampattern $\mathcal{G}_2(\vartheta, \varphi) = \mathcal{G}_1(\vartheta, -\varphi)$ is obtained at $[jX_2 \;\; jX_1]$. Consequently, by feeding the central active element with the first BPSK datastream and permuting the loads according to the second datastream, the two streams are simultaneously transmitted out of a single radio and mapped onto an orthogonal basis according to **Lemma.1**, irrespective of $X_1$ and $X_2$. Having the two loads $X_1$ and $X_2$ as a degree of freedom when considering BPSK signaling, we can optimize the loads according to a specific criterion as we show in Subsection III.C.

### 4.2.1 Basis Formulation

Although the beampattern of thin electrical dipoles (or monopoles) can be practically approximated by the superposition of the currents induced on the wire antenna elements, this is not true when considering arbitrary radiating elements e.g. flat or fractal dipoles, slot antennas etc. To overcome this problem, we implement full wave electromagnetic modeling based on the SPA scattering parameters (S-parameters) denoted by $S_{ij}, \{i, j\} \in \{0, 1, 2\}$, as well as the 3D complex active port patterns[1] of the antenna elements 0, 1 and 2 shown in Fig. 4.1, denoted by $E_0(\vartheta, \varphi)$, $E_1(\vartheta, \varphi)$ and $E_2(\vartheta, \varphi)$, respectively. An expression of the electric far-field beampattern of a 3-element SPA based on the aforementioned quantities and the variable antenna loading has been derived in (LDP06) using Mason's rule. From (LDP06) and after some manipulations, the two basis functions obtained when swapping the imaginary loads of the two PEs become

$$\begin{aligned}
\mathcal{B}_\Sigma(\vartheta, \varphi) &= \sqrt{2} E_0(\vartheta, \varphi) \\
&\quad + \frac{1}{\sqrt{2}} \left(\mathcal{L}_1^1 + \mathcal{L}_1^2\right) E_1(\vartheta, \varphi) + \left(\mathcal{L}_2^1 + \mathcal{L}_2^2\right) E_2(\vartheta, \varphi) \\
\mathcal{B}_\Delta(\vartheta, \varphi) &= \frac{1}{\sqrt{2}} \left(\mathcal{L}_1^1 - \mathcal{L}_1^2\right) E_1(\vartheta, \varphi) + \left(\mathcal{L}_2^1 - \mathcal{L}_2^2\right) E_2(\vartheta, \varphi)
\end{aligned} \tag{4.11}$$

where

[1] The active port pattern is defined as the beampattern obtained when driving the corresponding port (whether being active or passive) with a unit excitation voltage signal while terminating the other ports with reference impedances(Poz94).

$$\begin{aligned}
\mathcal{L}_1^1 &= \frac{\Gamma_1\mathcal{S}_{10}\left(1-\Gamma_2\mathcal{S}_{22}\right)+\Gamma_1\Gamma_2\mathcal{S}_{12}\mathcal{S}_{20}}{1-\Gamma_1\mathcal{S}_{11}-\Gamma_2\mathcal{S}_{22}+\Gamma_1\Gamma_2\mathcal{S}_{11}\mathcal{S}_{22}-\Gamma_1\Gamma_2\mathcal{S}_{12}\mathcal{S}_{21}} \\
\mathcal{L}_1^2 &= \frac{\Gamma_2\mathcal{S}_{10}\left(1-\Gamma_1\mathcal{S}_{22}\right)+\Gamma_1\Gamma_2\mathcal{S}_{12}\mathcal{S}_{20}}{1-\Gamma_2\mathcal{S}_{11}-\Gamma_1\mathcal{S}_{22}+\Gamma_1\Gamma_2\mathcal{S}_{11}\mathcal{S}_{22}-\Gamma_1\Gamma_2\mathcal{S}_{12}\mathcal{S}_{21}} \\
\mathcal{L}_2^1 &= \frac{\Gamma_1\mathcal{S}_{20}\left(1-\Gamma_2\mathcal{S}_{11}\right)+\Gamma_1\Gamma_2\mathcal{S}_{21}\mathcal{S}_{10}}{1-\Gamma_1\mathcal{S}_{11}-\Gamma_2\mathcal{S}_{22}+\Gamma_1\Gamma_2\mathcal{S}_{11}\mathcal{S}_{22}-\Gamma_1\Gamma_2\mathcal{S}_{12}\mathcal{S}_{21}} \\
\mathcal{L}_2^2 &= \frac{\Gamma_2\mathcal{S}_{20}\left(1-\Gamma_1\mathcal{S}_{11}\right)+\Gamma_1\Gamma_2\mathcal{S}_{21}\mathcal{S}_{10}}{1-\Gamma_2\mathcal{S}_{11}-\Gamma_1\mathcal{S}_{22}+\Gamma_1\Gamma_2\mathcal{S}_{11}\mathcal{S}_{22}-\Gamma_1\Gamma_2\mathcal{S}_{12}\mathcal{S}_{21}}
\end{aligned} \tag{4.12}$$

and $\mathcal{S}_{ij} \in \boldsymbol{\mathcal{S}}$ such that

$$\boldsymbol{\mathcal{S}} = \begin{bmatrix} \mathcal{S}_{00} & \mathcal{S}_{01} & \mathcal{S}_{02} \\ \mathcal{S}_{10} & \mathcal{S}_{11} & \mathcal{S}_{12} \\ \mathcal{S}_{20} & \mathcal{S}_{21} & \mathcal{S}_{22} \end{bmatrix}, \tag{4.13}$$

$$\Gamma_k = \left(jX_k + Z_0\right)^{-1}\left(jX_k - Z_0\right), \quad k \in \{1,2\}, \tag{4.14}$$

where we assumed $\Gamma_0 = 0$ by having the source impedance at the central driven port equal to the reference impedance $Z_0 = 50\,\Omega$. The basis coefficients in (4.12) are derived with respect to a general scattering matrix. Swapping the two reactive loads as $[\Gamma_1\ \Gamma_2] \leftrightarrow [\Gamma_2\ \Gamma_1]$, swaps the coefficients $\left(\mathcal{L}_k^1 - \mathcal{L}_k^2\right) \leftrightarrow \left(\mathcal{L}_k^2 - \mathcal{L}_k^1\right)$, $k \in \{1,2\}$ in (4.11), thus phase-shifting $\mathcal{B}_\Delta(\vartheta,\varphi)$ by 180° without affecting $\mathcal{B}_\Sigma(\vartheta,\varphi)$. By this way, the $(-1)^S$ factor is obtained. The two functions $\mathcal{B}_\Delta(\vartheta,\varphi)$ and $\mathcal{B}_\Sigma(\vartheta,\varphi)$ are the basis functions that are used to transmit two PSK signals of any modulation order

### 4.2.2 Received Signal Model

Considering a narrowband, flat-fading, point-to-point communication link where the two BPSK symbols are transmitted in the beam-space domain over two basis functions (equivalent to two uncorrelated virtual antennas) and received using an $\mathcal{K}_R$-element ULA of uncorrelated and uncoupled antenna elements. Assuming independent fading statistics at the transmitter and the receiver, the Kronecker product (ea00; KTCV02) can be assumed and thus the channel transfer function can be written as[1]

$$\mathbf{H}_{ch} = \mathbf{H}_w \mathbf{R}_T^{1/2}, \tag{4.15}$$

where the elements of the matrix $\mathbf{H}_w \in \mathbb{C}^{\mathcal{K}_R \times 2}$ are independent and identically distributed (i.i.d.) complex Gaussian random variables with zero mean and unit variance. The correlation at the receiver side is ignored from the aforementioned assumptions

[1] In (LA06), the correlation based channel model accounts for the MC by explicitly incorporating the coupling matrices. However in (4.15), the MC is implicitly taken into consideration within the calculation of the basis functions in (4.11).

regarding the receiving ULA. Defining the row vector $\boldsymbol{\mathcal{B}}(\vartheta,\varphi) = [\mathcal{B}_\Sigma(\vartheta,\varphi)\ \ \mathcal{B}_\Delta(\vartheta,\varphi)]$, the transmit covariance matrix[1] $\mathbf{R}_T$ is obtained as

$$\begin{aligned}\mathbf{R}_T &= \frac{1}{4\pi}\int_\varphi\int_\vartheta \boldsymbol{\mathcal{B}}^H(\vartheta,\varphi)\,\boldsymbol{\mathcal{B}}(\vartheta,\varphi)\sin(\vartheta)\cdot d\vartheta d\varphi,\\ &= \begin{bmatrix} P_\Sigma & \varrho_{\Sigma\Delta}\sqrt{P_\Sigma P_\Delta} \\ \varrho^*_{\Sigma\Delta}\sqrt{P_\Sigma P_\Delta} & P_\Delta \end{bmatrix},\\ &= \mathrm{diag}\left[P_\Sigma\ P_\Delta\right], \end{aligned} \tag{4.16}$$

which is simply the power distribution across the basis functions since $\varrho_{\Sigma\Delta} = 0$ according to **Lemma.1**. Notice that $P_\Sigma + P_\Delta = P_1 + P_2 = 2P_1 = P_t$, which is easily obtained from (4.2) and the basis definition in (4.3), where $P_t$ is the average transmit power. Defining the power imbalance ratio between the basis functions as $r = \frac{P_\Sigma}{P_\Delta}$, we can write $\mathbf{R}_T$ as $P_t\mathbf{Q}$ where $\mathbf{Q}$ is the normalized power distribution across the basis functions such that $\mathrm{trace}\{\mathbf{Q}\} = 1$. $\mathbf{Q}$ can be written as $\mathrm{diag}([q_1\ q_2])$ such that $q_1 = r/(1+r)$ and $q_2 = 1/(1+r)$. From the above, the received signal model becomes

$$\begin{aligned}\mathbf{y} &= \sqrt{P_t}\mathbf{H}_w\mathbf{Q}^{1/2}\mathbf{s} + \mathbf{n}\\ &= \sqrt{P_i\eta_T}\underbrace{\mathbf{H}_w\mathbf{Q}^{1/2}}_{\mathbf{H}}\mathbf{s} + \mathbf{n}\end{aligned} \tag{4.17}$$

where $P_i$ is the power into the transmitter (input power) and $0 \le \eta_T \le 1$ is the efficiency of the transmit antenna system being equal to $\eta_T = 1 - |\Gamma|^2$, where $\Gamma$ is the SPA return loss derived in (LDP06). Finally $\mathbf{s} = [s_1\ \ s_2]^T$ is the vector of the modulated BPSK signals (see TABLE I), and $\mathbf{n}$ is a vector representing the white Gaussian noise, with zero mean and $\sigma_n^2$ variance.

### 4.2.3 Optimization Criterion

In this work, we define the optimal SPA loads as the ones that maximize the average rate of transmission. However, in MIMO communications, average rate computation often demands tackling calculations of expectations with respect to random matrices rather than random scalar variables. For this reason, we derive an upperbound on the average rate and deploy it as an optimization criterion. We assume open-loop operation where the channel is known to the receiver but unknown to the transmitter. The ergodic capacity of a MIMO random channel, denoted by $\Im_{av}$, is the ensemble average of the information rate over the distribution of the elements of the channel matrix $\mathbf{H} = \mathbf{H}_w\mathbf{Q}^{1/2} \in \mathbb{C}^{\mathcal{K}_R\times 2}$. By using the $\log_2\det(\cdot)$ formula (GNP03), the upper

[1] Since the basis functions are imbalanced, the transmit covariance matrix rather than the transmit correlation matrix is considered.

bound that comes from the Jensen's inequality and the concavity of $\log_2 \det(\cdot)$[1], we get

$$\begin{aligned}\Im_{av} &= \mathbb{E}_{\mathbf{H}}\left[\log_2 \det\left(\mathbf{I}_2 + \frac{P_i\eta_T}{\sigma_n^2}\mathbf{H}^H\mathbf{H}\right)\right] \\ &\leq \log_2 \det\left(\mathbf{I}_2 + \frac{P_i\eta_T}{\sigma_n^2}\mathbb{E}_{\mathbf{H}}\left[\mathbf{H}^H\mathbf{H}\right]\right) \\ &= \log_2 \det\left(\mathbf{I}_2 + \frac{P_i\eta_T}{\sigma_n^2}\mathbf{Q}\right) \\ &= \log_2\left(1 + \frac{P_i\eta_T r}{\sigma_n^2(1+r)^2}\right). \end{aligned} \tag{4.18}$$

In (4.18), the average transmitted power is not divided by the number of the basis functions (the number of the virtual antennas), since the trace of $\mathbf{Q}$ is normalized to a unity rather than to the number of the basis functions (both forms are equivalent). The optimal loading is defined as the one that maximizes the average throughput upperbound in (4.18) i.e.

$$[X_1 \;\; X_2]_{opt} = \arg \max_{[X_1 \;\; X_2]} \left\{\log_2\left(1 + \frac{P_i\eta_T r}{\sigma_n^2(1+r)^2}\right)\right\}. \tag{4.19}$$

In (4.19), $\eta_T$ is made part of the optimization criterion by constraining $P_i$ rather than $P_t$ as the SPA efficiency is a key design parameter when considering portable RF units with limited storage batteries.

## 4.3 Antenna System Design

In this section we consider the 3-element SPA shown in Fig. 4.2, where the radiating elements are thin printed dipoles. The planar topology of the SPA makes it better fit in compactness-constrained mobile units as compared to the majority of the wire parasitic antennas already proposed in the literature. The current SPA was proposed earlier in (PCAK10), however in this work we complete the work by describing the implementation and the measurements of the prototype.

### 4.3.1 Design Parameters and Optimal Loading

The first design steps consist of making some initial choices on the antenna materials and the basic topology. We consider a 3-element SPA of flat dipoles as radiating elements as shown in Fig. 4.2, designed on an $h = 1.5$ mm thick substrate of relative permittivity $\varepsilon = 2.17$. The dipole lengths and spacing are 48.3 mm and 11 mm, respectively.

[1]The $\log_2 \det(\cdot)$ is concave over positive semi-definite matrices (Hor96). Since $\mathbf{Q}$ is positive semi-definite, the term $\mathbf{I}_2 + \frac{P_i\eta_T}{\sigma_n^2}\mathbf{Q}$ is positive semi-definite too, as it is a one-to-one mapping of $\mathbf{Q}$, thus preserving the positive definiteness.

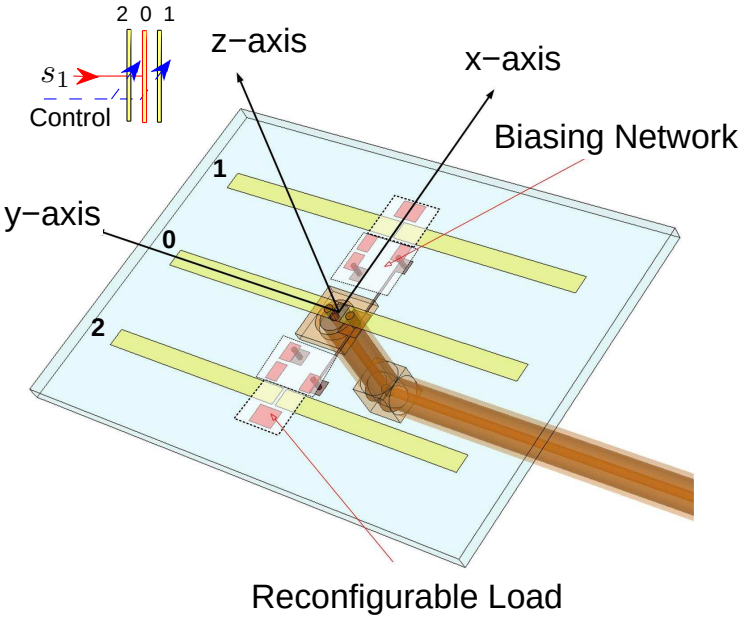


**Figure 4.2:** Schematic diagram of the SPA initially proposed in (PCAK10).

The spacing is $\sim 0.1\lambda$ at the desired operational frequency of 2.6 GHz. The SPA was simulated using HFSS®, with ports at the locations of the variable loads. The resulting 3-port S-parameters and the complex 3D active port patterns were exported to MATLAB®, where a computer routine scans the realizable range of the reactance space searching for $[X_1 \;\; X_2]_{opt}$. Fig. 4.3 shows an optimization contour plot of $\Im_{av}(X_1, X_2)$ at an input signal to noise ratio $P_i/\sigma_n^2$ of 10 dB. The figure shows that $\Im_{av}$ is maximized at $[X_1 \;\; X_2]_{opt} = [-100 \;\; +27]\ \Omega$. At such loading, the upperbound on $\Im_{av}$ is 5 b/s/Hz, the power imbalance between the two basis functions is 0.56 dB, and the SPA efficiency is 97%.

### 4.3.2 Reconfigurable Impedance Implementation

The design of the variable load, explained in more detail in the earlier partial work of (PCAK10), consists of the following steps: First, an adequate layout for the reconfigurable load area is selected ('Reconfigurable Load Area' in Fig. 4.4a, and the parasitic capacitance ($C_{P,a}$, $C_{P,b}$, and $C_{P,c}$) between the different pads are extracted from full-wave simulations. Here the inductive effect in the pads can be neglected in the design. Subsequently, the surface-mounted elements to implement $Z_{A,a}$ and $Z_{A,b}$ are deduced from the circuit of Fig. 4.4 so that the overall impedance in each state $Z_1$ and $Z_2$ (see Fig. 4.4b) match the target values deduced in the previous section, namely $Z_1 = jX_1 = j(+27)\,\Omega$ and $Z_2 = jX_2 = j(-100)\,\Omega$. Finally, a DC biasing network was designed using large RF-block inductors $L_{DC}$ and a resistor $R_{DC}$ to precisely control

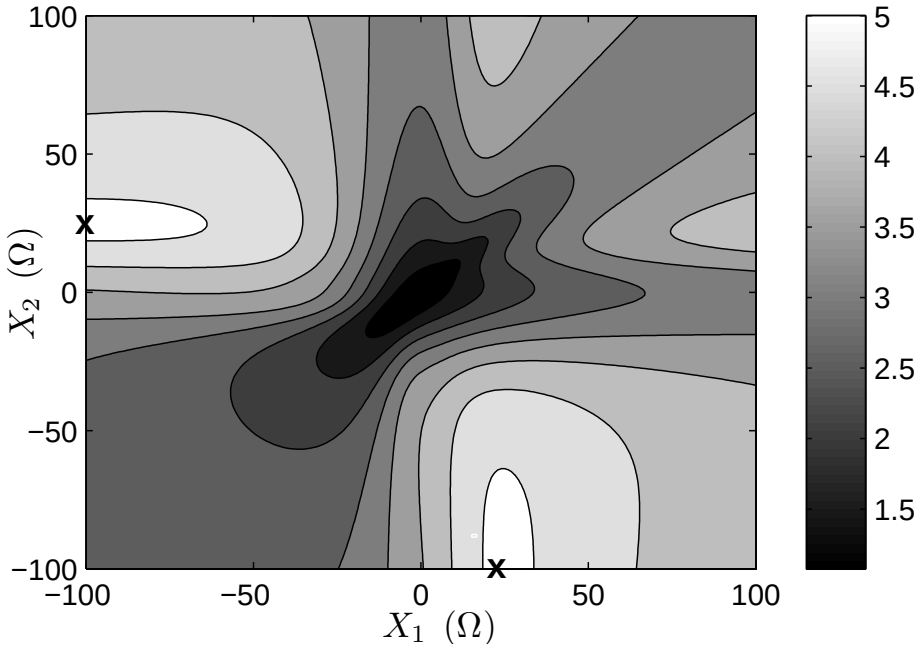


**Figure 4.3:** An optimization contour map regarding the upperbound on $\Im_{av}$ with respect to $X_1$ and $X_2$.

the diode biasing current. As can be seen in Fig. 4.7, the DC paths are then driven to the other side of the substrate by vias, where they can conveniently be connected to the DC voltage references in the antenna environment (see Section V). The PIN diode (Aeroflex Metelics MPN7310A-0805) serves as a low capacitance fast switch, with a negligible transient switching time (orders of nanoseconds) . $Z_{A,a}$ and $Z_{A,b}$ are capacitors of 0.5 pF and 0.8 pF, respectively. The biasing network elements are $L_{DC} = 22$ nH and $R_{DC} = 910\,\Omega$.

In order to experimentally validate the reconfigurable load design prior to its insertion in each of the SPA parasitic dipoles, it was fabricated and measured using a thru-reflect-line (TRL) calibration kit, which allows placing the measurement reference planes at the desired locations, as required here. It is then possible to extract the desired impedances $Z_1$ and $Z_2$ from the measured S-parameters and microstrip line impedance, as shown in Fig. 4.5 for each of the diode states. The imaginary parts of the measured impedance $Z_1$ and $Z_2$ at the design frequency of 2.6 GHz are $+38\,\Omega$ and $-108\,\Omega$ in the ON and the OFF states, respectively. These values are close to the target reactances of $+27\,\Omega$ and $-100\,\Omega$, considering the tolerances of the SMD elements and the impact of the biasing network. The real parts of $Z_1$ and $Z_2$ are not exactly zero due the diode and SMD components finite resistances, which were neglected in the design procedure (are only $+5\,\Omega$ and $+3\,\Omega$ in the OFF and the ON states, respectively). The target basis functions (at $[X_1\ X_2]_{opt} = [-100\ \ +27]\ \ \Omega$) and the achieved ones

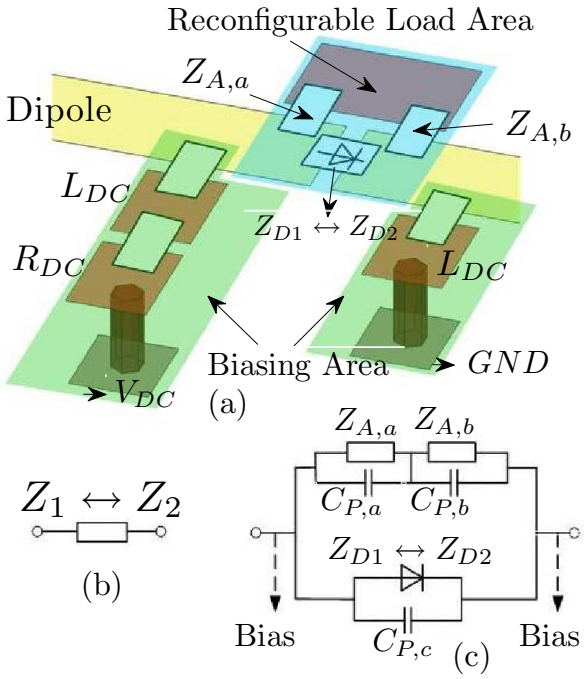


**Figure 4.4:** Reconfigurable dipole load impedance: (a) Layout and elements view, including biasing network, (b) target two-state variable impedance and (c) detailed implementation circuit, including layout parasitic capacitances.

($[X_1 \ X_2]_{opt} = [-108 \ \ +38] \ \Omega$) are compared in Fig. 4.6.

## 4.4 Simulation and Measurement Results

The current section presents the measurements of the different SPA parameters and compares them to the corresponding parameters obtained by computer simulations.

### 4.4.1 Antenna Demonstration

A photograph of the fully operational fabricated antenna is shown in Fig. 4.7. It was observed that a good balanced excitation of the active dipole is simply obtained by connecting the central and the outer conductors of a coaxial connector to each of the dipole arms. The variable load designed and characterized in Section IV.B was introduced in each parasitic dipole of the SPA, including the DC biasing network. The DC ground pad of each variable load on the backside of the substrate is connected by a printed line to the coaxial connector outer conductor (which thus serves as a DC ground), whereas each actuation pad (shown as '$V_{DC}$' in Fig. 4.4) is connected by a thin wire to the bias voltages for controlling the states of the diodes. In order to improve the antenna performance and provide pure measured patterns, the DC wires are driven along the coaxial feed, which is oriented toward the minimum radiation of the SPA (i.e. parallel to the

dipoles, see Fig. 4.7). A standard 9V battery is used as a DC source in the radiation pattern measurements. The battery is placed behind a piece of an absorber (located in the direction of minimum radiated power density), as can be seen in Fig. 4.8. Therefore the antenna states were simply selected by connecting each of the two DC wires to the 0V or 9V references. The impact of the biasing voltages on the antenna performance was investigated, showing similar responses for −10V to 0V as the OFF (or 'reverse-biased') state, while +3V to +10V are acceptable for the ON (or 'forward-biased') state.

### 4.4.2 Return Loss

Fig. 4.9 shows the simulated and measured return loss of the SPA around the design frequency of 2.6 GHz. The graph only shows the response in the operational states of the antenna, namely when it is loaded by the reactance load pairs $[jX_1\ jX_2]$ and $[jX_2\ jX_1]$. As explained earlier in Section IV, the return loss is the same for both states due to the SPA symmetry, which is confirmed here by the similarity between the two measured curves in Fig. 4.9. The SPA was found to have poor matching in the two (unused) states $[jX_1\ jX_1]$ and $[jX_2\ jX_2]$), which are not shown here.

The agreement between simulations and the measurements is moderate, since the measured bandwidth is larger than the one obtained by simulation and is not exactly centered around the design frequency of 2.6 GHz. Nevertheless the measurements show good return loss at 2.6 GHz. The −10dB measured bandwidth is 5.6% and 7.1% for a reference of −10 dB, for $S := 1$ and $S := 2$, respectively .

### 4.4.3 Radiation Patterns

Fig. 4.10 shows the H-plane co- and cross- polarized far fields of the beampattern $\mathcal{G}_1(\vartheta, \varphi)$ in the H-plane i.e. $\mathcal{G}_1(\vartheta = \frac{\pi}{2}, \varphi)$, in the first operational antenna state ($S := 1$). Note that the maximum of the co-polarized beampattern, located at $\varphi = +90°$, corresponds to the direction of the load in the OFF state. The co-polarized pattern reassembles the ideal cardioids decomposable into an orthogonal basis. The simulated and measured co- and cross- polarized beampatterns are in good agreement, as shown in Fig 4.10. Because of the SPA symmetrical structure and the reactance pair antisymmetry, the other antenna beampattern should simply be a mirror image of the first beampattern around the $\varphi = 0° - 180°$ axis, which is well verified by the measured prototype as can be seen in Fig. 4.11. Notice that $\mathcal{G}_1(\vartheta = \frac{\pi}{2}, \varphi) = \mathcal{G}_2(\vartheta = \frac{\pi}{2}, -\varphi)$, resulting in a MIPP.

Finally, the proposed antenna prototype has been successfully used for spatially multiplexing two BPSK datastrams *over the air* with a total bit rate of 800kbps at 2.6 GHz. The experiments constitute to the best of the authors' knowledge the first MIMO transmission with a single RF source yet to be proposed. A simple zero-forcing decoding was implemented by the receiver which was equipped with two distantly spaced monopoles. The receiver first estimates the receive antennas' responses to the two beampatterns $\mathcal{G}_1(\varphi, \vartheta)$ and $\mathcal{G}_2(\varphi, \vartheta)$ using classical training. Then it calculates the responses to the basis functions from (4.10b). Finally the $2 \times 2$ complex channel matrix

is inverted and used for equalizing the received signal. The experiments' setup are explained in the next chapter, as the current chapter is intended to highlight the theory and the SPA design behind such a new concept in wireless communications.

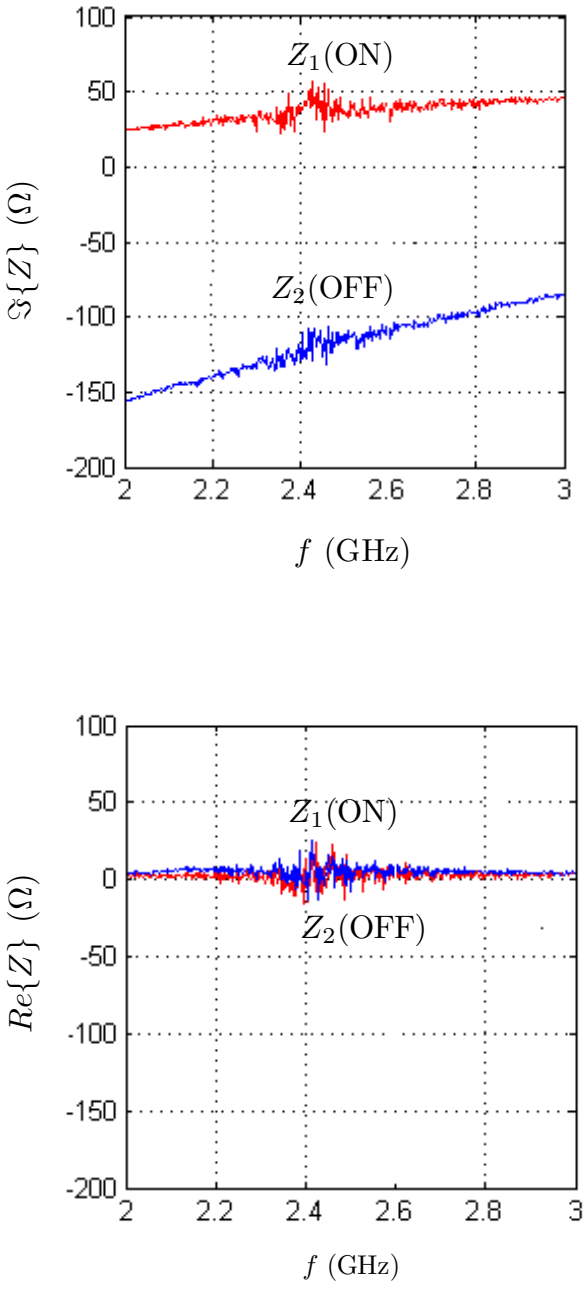


**Figure 4.5:** Measured load impedance in each diode state of the PIN diode, extracted from the S-parameter measurements on a dedicated microstrip TRL calibration kit, from (PCAK10). The OFF and ON diode states correspond to a reversed ($V_{DC} = 0V$) and forward ($I = 9$mA) bias, respectively.

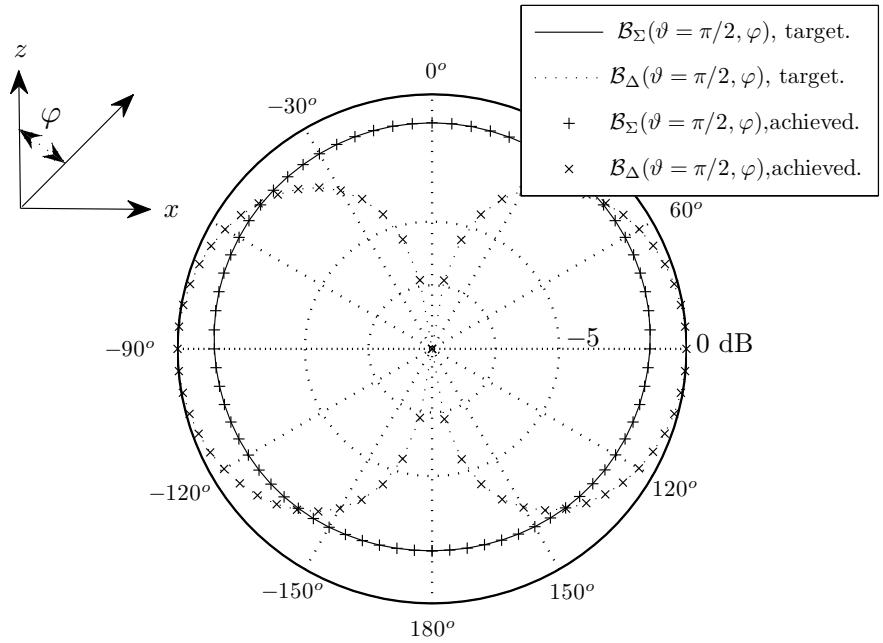


**Figure 4.6:** The magnitude of the H-plane co- polarized basis functions at the target loads of $[+27 \;\; -100]\,\Omega$ and at the practically achieved loads of $[+38 \;\; -108]\;\Omega$. The two basis functions resemble the omni and the angular sine functions, which are orthogonal to each other.

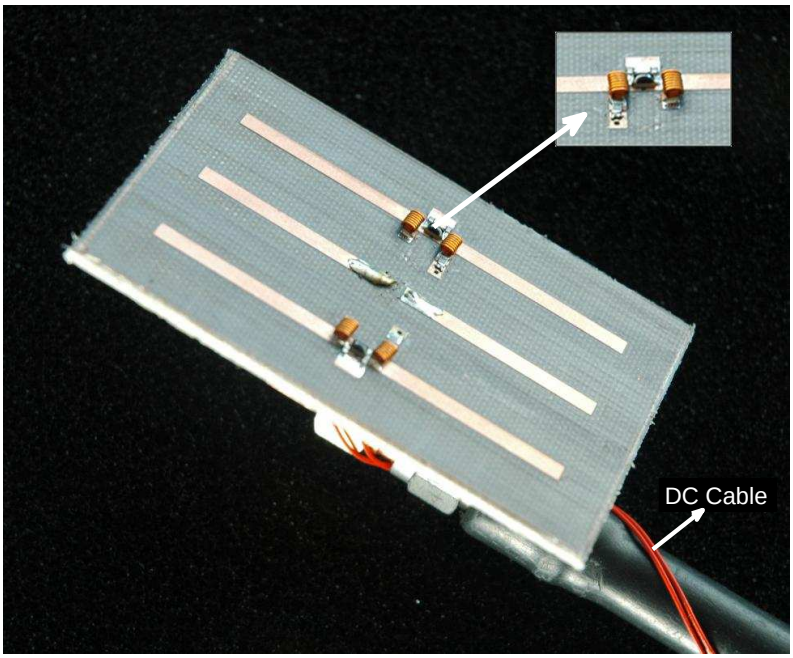


**Figure 4.7:** Photograph of the fully operational SPA, optimized for the proposed aerial MIMO approach.

**Figure 4.8:** Set-up of the antenna for reconfigurable radiation pattern measurements, with a 9V battery placed behind the absorber cone in a direction of the low field intensity.

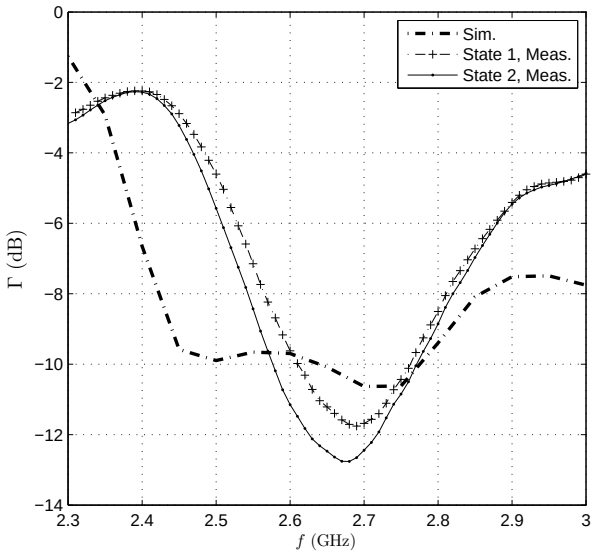


**Figure 4.9:** Return Loss (dB) of the SPA for both loading states i.e. $S := 1$ and $S := 2$.

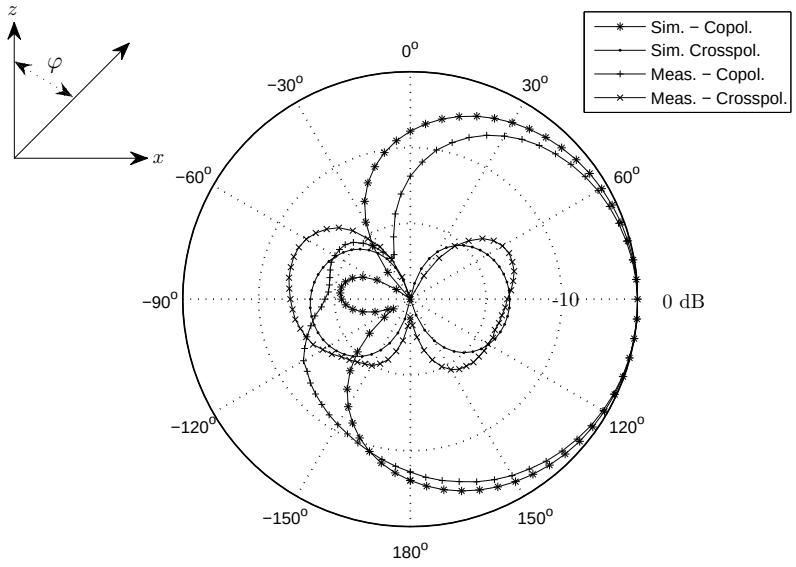


**Figure 4.10:** Simulated and measured co- and cross- polarization components at $f = 2.6$ GHz.

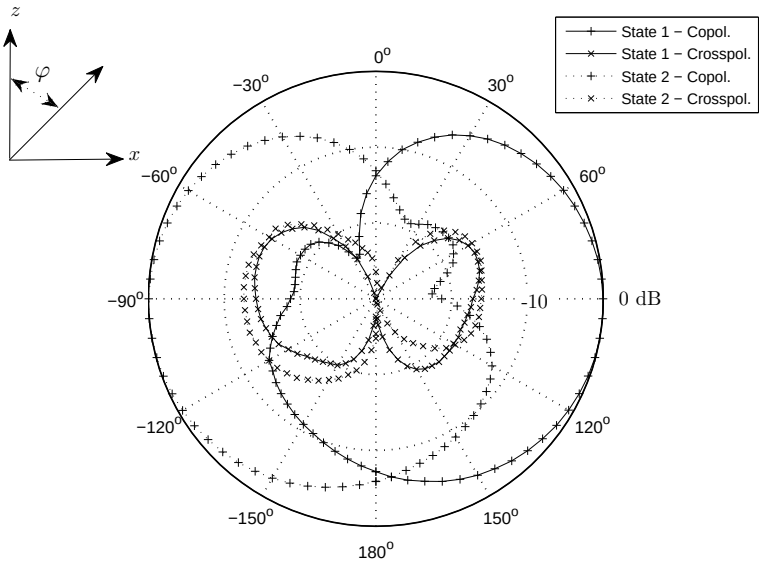


**Figure 4.11:** Measured co- and cross- polarization components at $f = 2.6$ GHz.

# 5

# Proof-of-Concept Experiments

This chapter validates a previously reported concept regarding the capability of transmitting multiple signals using one RF chain and a compact switched parasitic array (SPA). The experiments were conducted in an indoor environment using a 2.6 GHz prototype made of a single active printed dipole coupled to two passive ones. To the best of our knowledge, this is the first over-the-air experiment of spatial multiplexing with a single RF frontend yet to be demonstrated.

## 5.1 Transmit and Receive Subsystems

The experiments were conducted using a 2.6 GHz SPA prototype shown in Fig. 5.1, which has been fully modeled and optimized in (APCK10). The SPA consists of three printed dipoles (central active surrounded by two parasites) where the planar topology makes it better fit for handheld terminals. The dipoles' spacing is 11mm and the dipoles' lengths are 42mm. The SPA is optimized for BPSK signaling (PCAK10), regarding the average rate of communication at a target frequency of 2.6 GHz. The antenna system maintains a transmit efficiency above 95% while switching its loading state (the loads are switched using the Aeroflex Metelics MPN7310A-0805 PIN diode). The choice of the operating frequency was determined by the MMDS band ($2.5 - 2.7$ GHz) at which the available MIMO testbed operates. The testbed consists of a transmit subsystem unit shown in Fig. 5.2 and a receive subsystem unit shown in Fig. 5.3, supporting up to two and three RF modules, respectively (however in this experiment only one RF module is used at the transmit side and two at the receive side). The synchronization of the MIMO testbed is made through a GPS synchronization unit.

Fig. 5.4 shows a simplified schematic diagram of the signal flow at the transmit side. A digital baseband signal generated by the SBC62 stand alone DSP card is converted to analog using the DAC40 omnibus module (both the DSP and the DAC are from Innovative Integration (INN)). The SBC62 DSP stand alone card is based around the Texas Instrument TMS320C6201 processor whereas the DAC40 is a four channel analog output module. Each channel is independent and capable of generating 40MHz waveform via 14-bit converters. The four DAC channels are used to generate In-phase

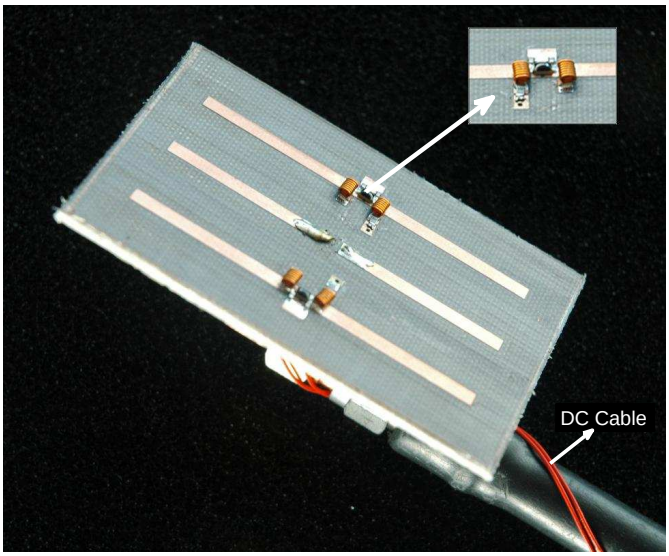


**Figure 5.1:** SPA of printed microstrip dipoles.

and Quadrature-phase baseband inputs to every RF module. The analog baseband is up-converted to the desired frequency in the MMDS band and transmitted through the antennas after passing through a bandpass RF filter. In the next section we describe how a baseband control signal is used to mimic a second stream of data at the transmit side.

On the other hand, the signals are captured by two omnidirectional antennas spaced by 23cm or $2\lambda$ as shown in Fig. 5.5. The received signal passes through the RF filters to the RF modules where it is down-converted to the analog baseband and digitized using the A4D1 omnibus module. The omnibus module is a 10 MHz 14-bit ADC of four channels from Innovative Integration.

## 5.2 Experiment Description

### 5.2.1 Signal Processing Before Transmission

Two binary trains of pulses was generated at a bit rate of 410kbps each. The first train was modulated into a BPSK symbol stream (using a raised-cosine waveform with 0.3 roll-off factor) and up-converted to 2.6 GHz. The high frequency modulated signal is used to drive the active antenna element (the central element of the SPA shown in Fig. 5.1). The second binary train was XORed with the first binary train in the baseband domain and the output baseband control signal was amplified and used for switching the

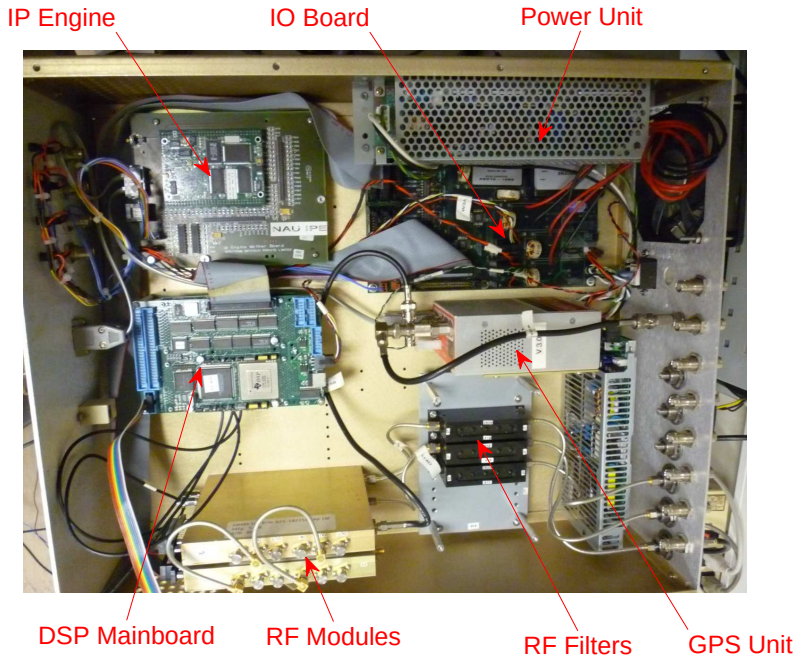


**Figure 5.2:** Transmit subsystem unit.

SPA loads ($jX_1 \leftrightharpoons jX_2$). The amplification of the baseband control signal is necessary as the switching diodes of the parasitic antenna elements need a minimum range of ±6V in order to operate, whereas the output of the DAC ranges between $\pm 2V$. Fig. 5.6 shows the comparator circuit that was used to magnify the voltage level of the control signal, using the LM6171 high-speed low-power low-distortion feedback amplifier from National Semiconductors (NAT). The sources $Vcc1 = +9.7V$ and $Vcc2 = +8.9V$ are taken from an external DC power supply giving an output of $\pm 9V$ with a negligible transient delay compared to the symbol period. The amplifier offers a high slew rate of 3600V/$\mu s$ and a unity-gain bandwidth of 100 MHz and is capable of amplifying the input signal with a switching frequency of 500 KHz and an amplitude ranging between $\pm 2V$. Fig. 5.7 shows input and output control signals i.e. the control signals before and after amplifications, as well as the switching transients (it can be observed that the transient delay is indeed negligible compared to the symbol period).

### 5.2.2 Signal Processing After Reception

As the data symbols are carried over two spatial functions over the air, the receiver needs to estimate its antenna responses to the two basis functions using a predefined training sequence (a training sequence of 8 BPSK symbols was used for every BPSK substream). The SPA far-field $\mathcal{G}(\varphi)$ is at one of two states: either $\mathcal{G}_1(\varphi) = \mathcal{B}_1(\varphi) + \mathcal{B}_2(\varphi)$ or $\mathcal{G}_2(\varphi) = \mathcal{B}_1(\varphi) - \mathcal{B}_2(\varphi)$ (APCK10). The receiver constructs the equivalent channel matrix representing the receive antenna responses to the spatial basis functions. The

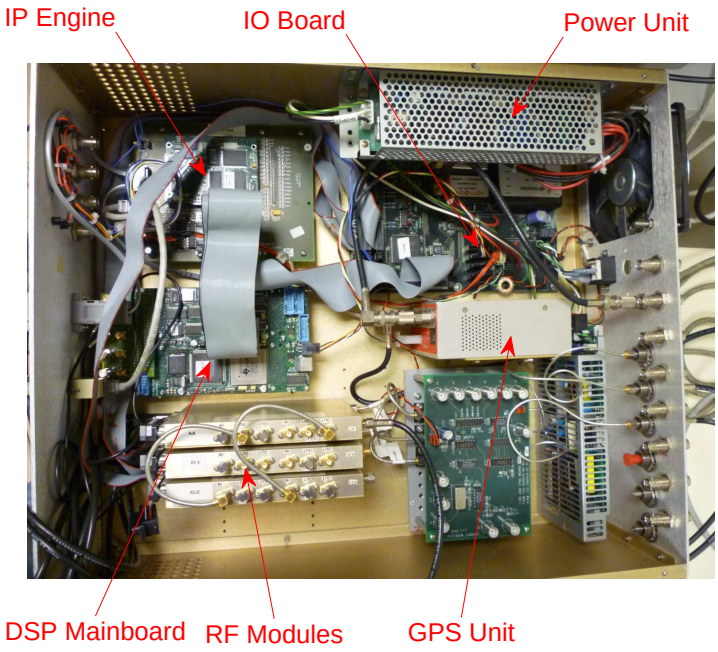


**Figure 5.3:** Receive subsystem unit.

equivalent matrix is used for equalizing the received signal and decoupling the two BPSK symbol streams. We have adopted the linear zero-forcing as a simple decoding technique, thus the estimated transmitted signal becomes

$$\begin{aligned} \widehat{\mathbf{x}} &= \mathbf{H}^{-1}\mathbf{y} \\ &= \mathbf{x} + \mathbf{H}^{-1}\mathbf{n} \end{aligned} \tag{5.1}$$

where $\mathbf{H}$ is a $2 \times 2$ matrix given by

$$\mathbf{H} = \frac{1}{\sqrt{2}} \begin{pmatrix} h_{11} + h_{12} & h_{11} - h_{12} \\ h_{21} + h_{22} & h_{21} - h_{22} \end{pmatrix}, \tag{5.2}$$

such that $\mathbf{H}_{ij}$, $\{i, j\} \in \{1, 2\}$ is the response of the $j$th receive antenna to $\mathcal{B}_i(\varphi)$, whereas $h_{ij}$, $\{i, j\} \in \{1, 2\}$ is the response of the $j$th receive antenna to $\mathcal{G}_i(\varphi)$, according to the relations between $\mathcal{G}_i(\varphi)$ and $\mathcal{B}_i(\varphi)$, $i \in 1, 2$ (APCK10); the operator $(.)^{-1}$ inverts the matrix operand and finally $\mathbf{n}$ is a vector representing the additive white Gaussian noise with zero mean and $N_o$ variance. Every demodulated signal comprises of two noisy clouds such that $\widehat{\mathbf{x}}_1 = \mathbf{c}_1 \cup \mathbf{c}_2$ and $\widehat{\mathbf{x}}_2 = \mathbf{c}_3 \cup \mathbf{c}_4$ as shown in Fig. 5.10. The signal-to-noise ratio (SNR) of the $i$th cloud is calculated as

$$\mathrm{SNR}_i = \frac{\mathbb{E}\left\{\mathbf{c}_i^H \mathbf{c}_i\right\} - \mathrm{Var}\left\{\mathbf{c}_i\right\}}{\mathrm{Var}\left\{\mathbf{c}_i\right\}} \tag{5.3}$$

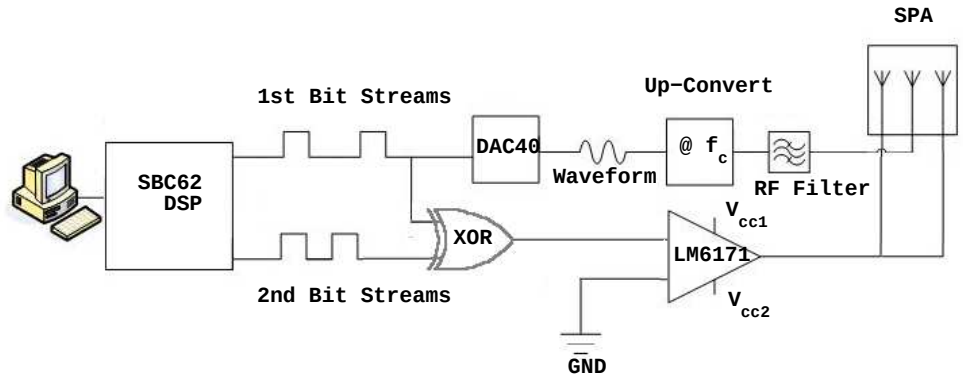


**Figure 5.4:** A simplified schematic diagram of the signal flow at the transmit side.

where $\mathbb{E}\{.\}$ returns the sample mean of the operand and $\mathrm{Var}\{.\}$ returns the sample variance of the operand. The four clouds have almost the same SNR and the mean of the four SNRs is finally considered. The bit SNR referred to as $E_b/N_o$, is calculated by adding $\log_{10}(0.5\mathcal{S})$ to the average SNR (in dB), where $\mathcal{S}$ is the number of samples per one symbol whereas the 0.5 factor is due to using real signaling. In this experiment, $\mathcal{S}$ was set to 5 samples per symbol such that each transmission has 410 symbols or equivalently 2048 samples.

## 5.3 Experimental Results

Fig. 5.9 shows the received signal constellations before equalization and Fig. 5.9 shows the received signal constellations after equalization (spatial separation), onto which the transmitted signals (red dots) are also projected, for comparison reasons. The figure shows that the two BPSK signals have been indeed decoupled at the receiver side thus validating the theory of MIMO with a single RF source. On the other hand, Fig. 5.11 shows the bit probability of error ($P_b$) versus $E_b/N_o$ obtained by measurements as well as the performance of a $2\times2$ BPSK-MIMO with a Rayleigh channel of independent and identically distributed coefficients, and zero-forcing decoding[1]. The figure shows that the performance of the beamspace MIMO is comparable to the conventional one, thus validating the importance of such a new approach for realizing single radio compact-sized MIMO transceivers.

[1]Theoretically, $P_b$ of a $2\times2$ BPSK-MIMO under Rayleigh fading and a zero-forcing receiver is unsurprisingly identical to the performance of $1\times1$ BPSK-SISO i.e $P_b = 0.5\left(1-\sqrt{\frac{E_b/No}{E_b/No+1}}\right)$.


**Figure 5.5:** A setup showing the two receiving antennas (the two white hemispheres on the left side of the figure).

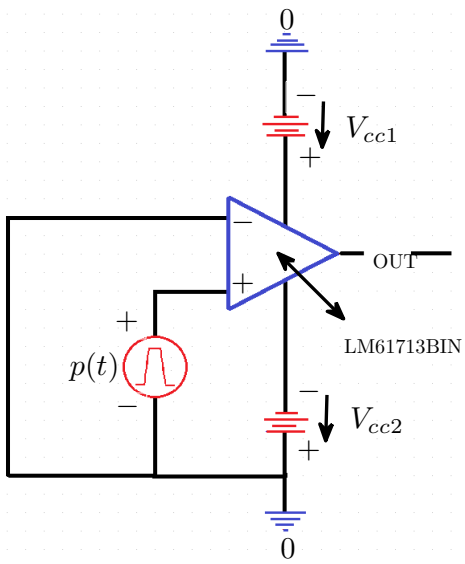


**Figure 5.6:** Schematic diagram of the amplifier circuit used for magnifying the baseband control signal.

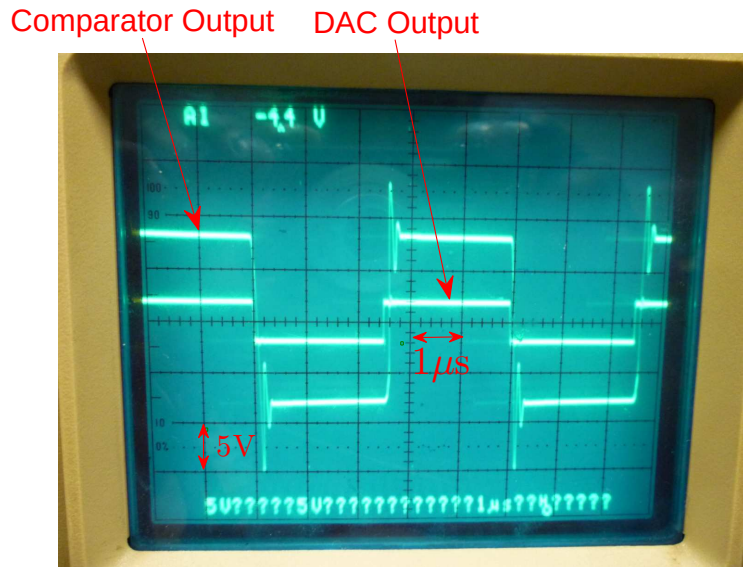


**Figure 5.7:** Baseband control signal before and after amplification.

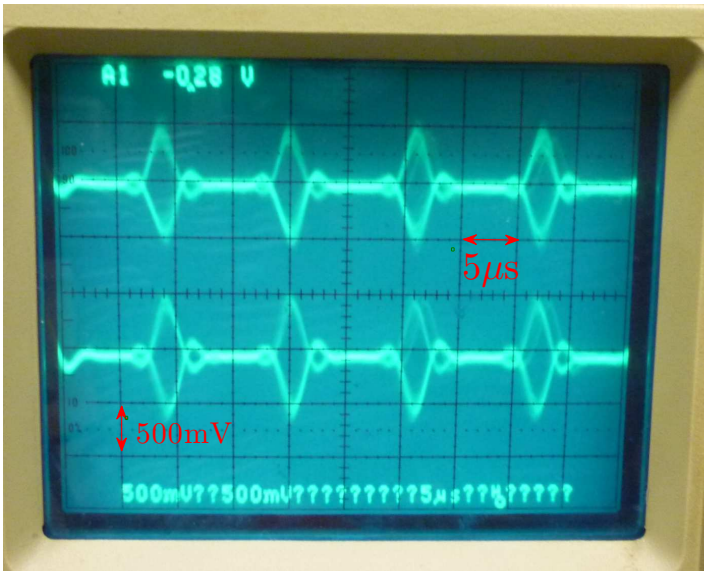


**Figure 5.8:** Baseband received signal.

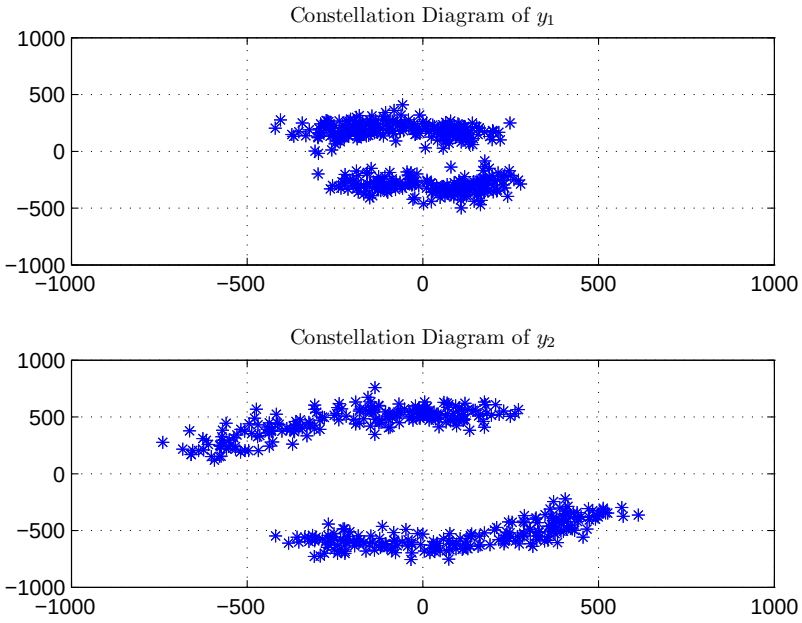


**Figure 5.9:** Scatter plot of received signal constellation before equalization.

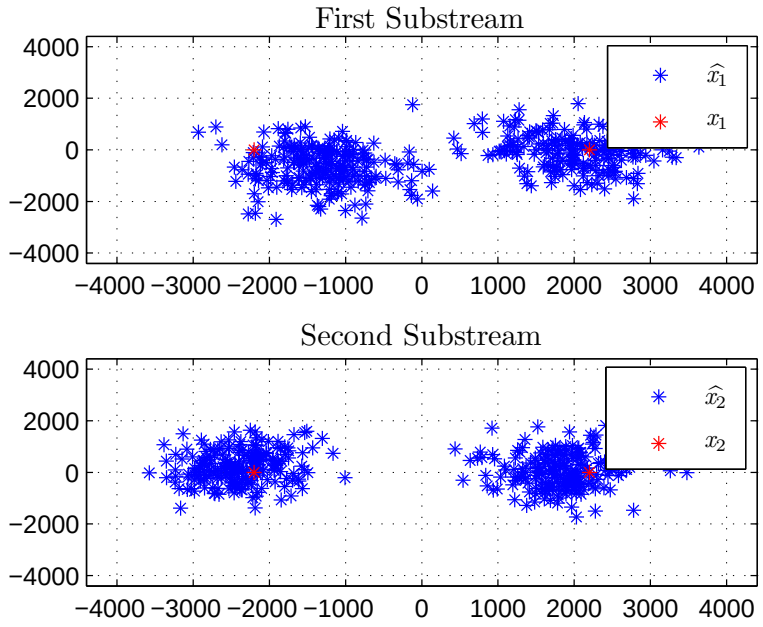


**Figure 5.10:** Scatter plot of received signal constellation after equalization.

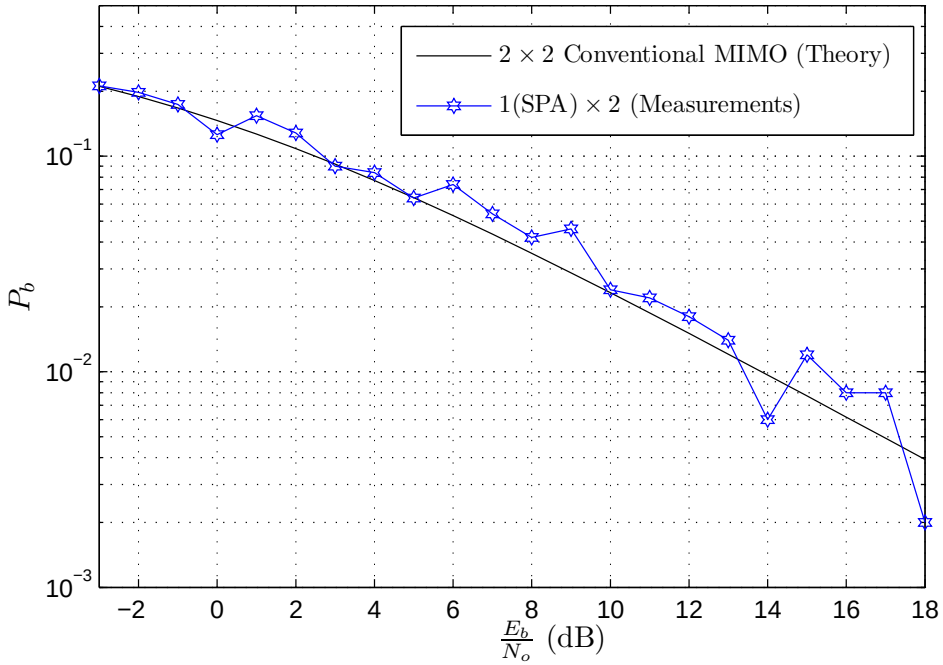


**Figure 5.11:** Probability of error versus the transmit signal to noise ratio (per bit).

# 6

# Conclusion

This dissertation has investigated the possibility of emulating conventional MIMO transmission with a single RF source, using a switched antenna system (SAS) or a reactance-assisted antenna system. It was demonstrated by both simulations and measurements that the proposed approach achieves performance comparable to classical MIMO systems at a reduced RF hardware complexity. The contribution of this work is summarized as follows:

- *Chapter 2* : In this chapter a spatial multiplexing scheme based on antenna switching was proposed. The outage performance of a compact switched-antenna system with a single RF chain is evaluated and shown to be comparable to a system equipped with two active antennas, yet the proposed scheme is limited to BPSK signaling. Moreover, a technique that constitutes to our best knowledge the most compact implementation yet to be proposed for Alamouti code with a single RF source has been proposed using two closely-spaced antennas, decoupled and matched using a decoupling and a matching network. Again, the complex-signaling format that exploits the quadrature degree of freedom is not supported.
- *Chapter 3* : This chapter started by extending the previous finding to beam switching rather than antenna switching. The approach has been successfully extended to any PSK modulation scheme where spatial multiplexing rate of 2 PSK symbols/s has been achieved using a 3-element ë/16 parasitic array. Different power allocation schemes among the basis have been proposed with limited feedback. Transmit diversity using Alamouti scheme was also implemented using a single front-end, making it a viable option for the uplink via lower cost terminal devices.
- *Chapter 4* : The chapter generalized the previously proposed approach to arbitrary radiating elements. The idea was to obtain an orthogonal or orthonormal basis out of MIPPs. The chapter also provided design steps for an example of a 3-element SPA, capable of forming a MIPP that are mirror images of each other. The SPA was optimized for BPSK signaling by deriving a criterion that maximizes the SPA efficiency and minimizes the power imbalance between the basis functions, simultaneously. A reconfigurable impedance was designed and a fully operational

SPA for single radio MIMO transmission was demonstrated. The measured SPA parameters are in good agreement with the target values, regarding the SPA return loss and the radiation patterns in the different SPA states.

- *Chapter 5* : The chapter demonstrated a successful MIMO transmission at a total rate of 820kbps has been conducted over the air, using a single RF source. The experiments took place in an indoor office environment using a fast-switching 2.6 GHz prototype. The experiments constitute to the best of the authorsŠ knowledge the first successful MIMO transmission with a single RF source.

# Bibliography


[AG05] J. B. Andersen and B. N. Getu. The MIMO cube - a compact MIMO antenna. *IEEE Transactions on Wireless Communications*, 2005.

[AKPK08] O. N. Alrabadi, A. Kalis, C. B. Papadias, and A. G. Kanatas. Spatial multiplexing by decomposing the far-field of a compact ESPAR antenna. *IEEE International Symposium on Personal, Indoor and Mobile Radio Communications*, 2008.

[AKPP09] O. N. Alrabadi, A. Kalis, C. B. Papadias, and R. Prasad. A universal encoding scheme for MIMO transmission using a single active element for PSK modulation schemes. *IEEE Transactions on Wireless Communications*, 2009.

[Ala98] S. Alamouti. A simple transmit diversity technique for wireless communications. *IEEE JSAC*, 1998.

[APCK10] O. N. Alrabadi, J. Perruisseau-Carrier, and A. Kalis. MIMO transmission using a single RF source: Theory and antenna design. *submitted to: IEEE Transactions on Antennas and Wireless Propagation*, 2010.

[APK+09] O. N. Alrabadi, C. B. Papadias, A. Kalis, N. Marchetti, and R. Prasad. MIMO transmission and reception techniques using three-element ESPAR antennas. *IEEE Communications Letters*, 2009.

[AR09] C. Abou-Rjeily. Pulse antenna permutation and pulse antenna modulation: Two novel diversity schemes for achieving very high data-rates with unipolar MIMO-UWB communications. *IEEE Journal on Selected Areas in Communications*, 2009.

[AV03] J. B. Andersen and R. Vaughan. *Channels, Propagation and Antennas for Mobile Communication.* 2003.

[BEK10] V. Barousis, G. Efthymoglou, and A. G. Kanatas. A complete MIMO system built on a single RF communication ends. *PIERS ONLINE*, 2010.

[BMK08] R. Bains, R. Muller, and A. Kalis. On the link performance of a proposed compact antenna system. *IEEE Communications Letters*, 2008.

## BIBLIOGRAPHY


[CGK09] P. Constantinou, P. Gika, and C. G. Kakoyiannis. Compact antennas with reduced mutual coupling for wireless sensor networks. *High Frequency Electronics*, 2009.

[CO07] B. Clerckx and C. Oestges. *MIMO Wireless Communication, From Real-World Propagation to Space-Time Code Design*. 2007.

[CR98] J. M. CiofiňĄ and G. G. Raleigh. Spatio temporal coding for wireless communication. *IEEE Trans. Commun.*, 1998.

[CWC08] S. Chung, Y. Wang, and S. Chen. A decoupling technique for increasing the port isolation between two strongly coupled antennas. *IEEE Transactions on Antennas and Propagation*, 2008.

[ea98] J. Fuhl et al. Unified channel model for mobile radio systems with smart antennas. *Ins. Elect. Eng. - Radar Sonar Navigation*, 1998.

[ea00] D. S. Shiu et al. Fading correlation and its effect on the capacity of multi-element antenna systems. *IEEE Trans. Commun.*, 2000.

[ea03a] J. Cheng et al. Electronically steerable parasitic array radiator antenna for omni- and sector pattern forming applications to wireless ad hoc networks. *IEE Proc.-Microw. Antennas Propag.*, 2003.

[ea03b] M. Taromaru et al. Reactance diversity: a novel and ultimate-low-cost antifading reception scheme with a binary-controlled 3-element ESPAR antenna. *Proc. Asia-Pacific Microwave Conf.*, 2003.

[ea05] B. K. Lau et al. Capacity analysis for compact MIMO systems. *Vehicular Technology Conference*, 2005.

[ea06] M. Yamamoto et al. Performance of angle switch diversity using ESPAR antenna for mobile reception of terrestrial digital TV. *Vehicular Technology Conference*, 2006.

[ea08a] F. Fazel et al. Space-time block coded reconïňĄgurable MIMO communication system using ORIOL antennas. *IEEE Wireless Communications and Networking Conference*, 2008.

[ea08b] V. Barousis et al. A limited feedback technique for beamspace mimo systems with single rf front-end. *IEEE International Symposium on Personal, Indoor and Mobile Radio Communications*, 2008.

[ea08c] Y. Fei et al. Optimal single-port matching impedance for capacity maximization in compact MIMO arrays. *IEEE Trans. Antennas and Propagation*, 2008.

[EK05] H. Eul and O. Klemp. Analytical approach for MIMO performance and electromagnetic coupling in linear dipole arrays. *International Symposium on Wireless Communication Systems*, 2005.

[EK07] H. Eul and O. Klemp. Diversity efiňĄciency of multimode antennas impacted by finite pattern correlation and branch power imbalances. *IEEE ISWCS*, 2007.

[EK08] H. Eul and O. Klemp. Diversity performance of multimode antennas in directive angle of arrival scenarios. *Wireless Press. Comm.*, 2008.

[GF98] M. J. Gans and G. J. Foschini. Limits of wireless communication in a fading environment when using multiple antennas. *Wireless Personal Communications*, 1998.

[GNP03] D. Gore, R. Nabar, and A. Paulraj. *Introduction to Space-Time Wireless Communications*. 2003.

[GO00] K. Gyoda and T. Ohira. Electronically steerable passive array radiator antennas for low-cost analog adaptive beamforming. *IEEE Int. Conf. Phased Array Syst. and Tech.*, 2000.

[HM99] B. M. Hochwald and T. L. Marzetta. Capacity of a mobile multiple antenna communication link in rayleigh ïňĆat fading. *IEEE Trans. Inform.Theory*, 1999.

[Hor96] R. A. Horn. *Matrix analysis*. 1996.

[HRB09] A. Hajimiri, D. B. Rutledge, and A. Babakhani. Near-field direct antenna modulation. *IEEE Microwave Magazine*, 2009.

[HSB+06] M. A. Hein, R. Stephan, K. Blau, C. Volmer, and J. Weber. Miniaturized antenna arrays using decoupling networks with realistic elements. *IEEE Trans. Microwave Theory Tech.*, 2006.

[IE3] Electromagnetic simulation and electronic design simulation, http://www.zealand.com.

[INN] http://www.innovatve-dsp.com.

[IWF02] T. Itoh, Y. Wang, and J. D. Fredrick. A smart antenna receiver array using a single RF channel and digital beamforming. *IEEE Transactions on Microwave Theory and Techniques*, 2002.

[Jak74] W. C. Jakes. *Microwave Mobile Communications*. 1974.

[JM05a] A. Jensen and M. L. Morris. Network model for MIMO systems with coupled antennas and noisy amplifiers. *IEEE Transactions on Antennas and Propagation*, 2005.

[JM05b] M. A. Jensen and M. L. Morris. Modeling front-end signal coupling in MIMO systems. *IEEE Wireless Communications and Applied Computational Electromagnetics*, 2005.

[JW04] M. A. Jensen and J. W. Wallace. Termination-dependent diversity performance of coupled antennas: Network theory analysis. *IEEE Trans. Antennas and Propagation*, 2004.

[KKCC06] A. Kalis, A. G. Kanatas, M. Carras, and A. G. Constantinides. On the performance of MIMO systems in the wavevector domain. *IST Mobile and Wireless Communications Summit*, 2006.

[KKP07] A. Kalis, A. G. Kanatas, and C. Papadias. An ESPAR antenna for beamspace-MIMO systems using PSK modulation schemes. *IEEE International Conference on Communications 2007*, 2007.

[KKP08] A. Kalis, A. G. Kanatas, and C. Papadias. A novel approach to MIMO transmission using a single rf front end. *IEEE Journal on Selected Areas in Communications*, 2008.

[Kle09] O. Klempl. Performance considerations for UWB-MIMO antennas with multimode pattern diversity. *European Conference on Antennas and Propagation*, 2009.

[KTCV02] J. M. Kahn, D. Tse, C. Chuah, and R. A. Valenzuela. Capacity scaling in MIMO wireless systems under correlated fading. *IEEE Transactions on info. theory*, 2002.

[KW06] C. Kuhnert and W. Wiesbeck. *Antenna Engineering Handbook*. 2006.

[L1] Overview of 3gpp release 8.

[L2] LTE: MIMO Techniques in 3GPP-LTE. *Freescale Semiconductor*.

[LA06] B. K. Lau and J. B. Andersen. On closely coupled dipoles with load matching in a random field. *IEEE PIMRC*, 2006.

[LDP06] J. Laheurte, L. Dussopt, and L. Petit. MEMS-switched parasitic-antenna array for radiation pattern diversity. *IEEE Transactions on Antennas and Propagation*, 2006.

[LL05] P. Liu and W. Li. Blind separation of BPSK sources by electrically steerable parasitic array radiator. *Int. Workshop VLSl Design and Video Tech.*, 2005.

[LOT96] Jun W. Lu, S. O'Keefe, and D. V. Thiel. Electronic beam steering in wire and patch antenna systems using switched parasitic elements. *Antennas and Propagation Society International Symposium, AP-S Digest*, 1996.

[LPL06] D. Livezey, A. Pham, and C. Lu. On the feasibility of CMOS multi-band phase shifters for multiple-antenna transmitters. *IEEE Microwave and Wireless Components Letters*, 2006.

[Mig06] M. D. Migliore. An intuitive electromagnetic approach to MIMO communication systems. *IEEE antennas and propagation magazines*, 2006.

[MK02] R. J. Marhefka and J. D. Kraus. *Antennas, For All Applications*. 2002.

[MKAL06] A. F. Molisch, G. Kristensson, J. B. Andersen, and B. K. Lau. Impact of matching network on bandwidth of compact antenna arrays. *IEEE Transactions on Antennas and Propagation*, 2006.

[NAT] http://www.national.com/analog.com.

[NS04] A. Nosratinia and S. Sanaye. Antenna selection in MIMO systems. *IEEE Communications Mgazine*, 2004.

[OG00] T. Ohira and K. Gyoda. Design of electronically steerable passive array radiator (ESPAR) antennas. *IEEE Antennas and Propagation Society International Symposium*, 2000.

[OHSM05] M. Okoniewski, S. V. Hum, A. Sutinjo, and G. G. Messier. A spaceâĂŞtime coding scheme utilizing phase shifting antennas at RF frequencies. *IEEE Antennas and Wireless Propagation Lett.*, 2005.

[OT02] T. Ohira and M. Taromaru. A study on the mapping from the reactance space to equivalent weight vector space in ESPAR antenna. *Technical Report of IEICE, RCS*, 2002.

[OTIS04] T. Ohira, M. Taromaru, K. Iigusa, and T. Sawaya. Reactance diversity: proof-of-concept experiments in an indoor multipath-fading environment with a 5-ghz prototype planar ESPAR antenna. *Consumer Communications and Networking Conference*, 2004.

[Pac] H. Packard. *Fast switching PIN diodes*.

[PCAK10] J. Perruisseau-Carrier, O. N. Alrabadi, and A. Kalis. Implementation of a reconfigurable parasitic antenna for beam-space BPSK transmissions. *2010 European Microwave Conference (EuMA)*, 2010. vi, 62, 63, 68, 73

[Poz94] D. M. Pozar. The active element pattern. *IEEE Trans. on Antennas and Propagation*, 1994.

[Poz05] D. M. Pozar. *Microwave Engineering*. 2005.

[PPS+06] D. Pinchera, V. Patriarca, F. Schettino, M. D. Migliore, and M. Di Zazzo. A novel parasitic-MIMO antenna. *Antennas and Propagation Society international Symposium*, 2006.

## BIBLIOGRAPHY


[RBD05] J. Romeu, S. Blanch, and S. Dossche. Three different ways to decorrelate two closely spaced monopoles for MIMO applications. *IEEE/ACES International Conference on Wireless Communications and Applied Computational Electromagnetics*, 2005.

[Say02] A. M. Sayeed. Deconstructing multiantenna fading channels. *IEEE Trans. Signal Processing*, 2002.

[SPM06] F. Schettino, D. Pinchera, and M. D. Migliore. Improving channel capacity using adaptive MIMO antennas. *Antennas and Propagation Society international Symposium*, 2006.

[SW01] T. Svantesson and M. Wennstrom. An antenna solution for MIMO channels: the switched parasitic antenna. *IEEE 12th Int. Symp. Personal, Indoor and Mobile Radio Communications*, 2001.

[TAPP10] E. P. Tsakalaki, O. N. Alrabadi, C. B. Papadias, and R. Prasad. An adaptive reactance-assisted antenna system for the MIMO uplink. *IEEE International Conference on Electronics, Circuits, and Systems*, 2010.

[TBP05] D. N. C. Tse, R. W. Brodersen, and A. S. Y. Poon. Degrees of freedom in multiple-antenna channels: a signal space approach. *IEEE Trans. on Information Theory*, 2005.

[Tel99] I. E. Telatar. Capacity of multi-antenna gaussian channels. *Wireless Personal Communications*, 1999.

[Vau99] R. Vaughan. Switched parasitic elements for antenna diversity. *IEEE Trans. on Antennas and Propagation*, 1999.

[VLT05] S. Verdu, A. Lozano, and A. M. Tulino. Impact of antenna correlation on the capacity of multi-antenna channels. *IEEE Trans. on Information Theory*, 2005.

[WC04] X. Wang and H. J. Chaloupka. On the properties of small arrays with closely spaced antenna elements. *IEEE Antennas and Propagation Society International Symposium*, 2004.

[WIK04] Y. Wang, T. Itoh, and S. Kim. A compact realization of antenna arrays for mobile communications. *IEEE Vehicular Technology Conference*, 2004.

[Win87] J. H. Winters. On the capacity of radio communication systems with diversity in a rayleigh fading environment. *IEEE J. Select Areas in Commun.*, 1987.

[WSW04] C. Waldschmidt, S. Schulteis, and W. Wiesbeck. Complete RF system model for analysis of compact MIMO arrays. *IEEE Trans. on Veh. Tech.*, 2004.

[YC08] Y. Yu and J. C. Coetzee. Closed-form design equations for decoupling networks of small arrays. *IEE Elec. Lett.*, 2008.

[YMK06] R. D. Yates, I. Maric, and G. Kramer. *Cooperative Communications*. 2006.

[YTE91] Y. Yamada, T. Takahash, and Y. Ebine. Study of vertical space diversity for land mobile radio. *Electronics and Communications in Japan*, 1991.

[YV03] J. Yuan and B. Vucetic. *Space-Time Coding*. 2003.

# A Universal Encoding Scheme for MIMO Transmission Using a Single Active Element for PSK Modulation Schemes

Osama N. Alrabadi, *Student Member, IEEE*, Constantinos B. Papadias, *Senior Member, IEEE*, Antonis Kalis, *Member, IEEE*, and Ramjee Prasad, *Fellow, IEEE*

***Abstract*—A universal scheme for encoding multiple symbol streams using a single driven element (and consequently a single radio frequency (RF) frontend) surrounded by parasitic elements (PE) loaded with variable reactive loads, is proposed in this paper. The proposed scheme is based on creating a MIMO system by expanding the far-field of a compact parasitic array into an orthogonal set of angular functions (basis). Independent information streams are encoded by means of angular variations of the far-field in the wavevector domain, rather than spatial variations as usually happens in conventional MIMO systems. The array can spatially multiplex the input streams by creating all the desired linear combinations (for a given modulation scheme) of the basis functions. The desired combinations are obtained by projecting the ratio of the symbols to be spatially multiplexed on the ratio of the basis functions' weights (complex coefficients), which is a function of the currents induced on the PE within the antenna domain, and controlled by the independent reactive loadings.**

***Index Terms*—Adaptive antennas, space-time coding, MIMO, switched parasitic array, ESPAR.**

## I. Introduction

MIMO array processing has been established as an effective means to achieve remarkable spectral efficiency. The capacity of such space-time wireless channels has been shown to increase almost linearly with the number of transmit-receive antennas [1] [2]. However, the current vision for future applications of space-time signal processing is mostly restricted to implementations of multiple-input, single-output (MISO) or single-input, multiple-output (SIMO) systems, as the base stations can afford the complexity of multiple antennas and multiple frontends, whereas mobile (handheld) platforms still use mostly single antennas (specially in the transmission mode), due to size, power and cost constraints. Unfortunately, the capacity of such systems is much lower than the capacity achievable by MIMO systems. Namely, the capacity of the simplest $2 \times 2$ MIMO system supersedes the capacity of theoretical open-loop $\infty \times 1$ MISO system [3], let alone the capacity of practical MISO systems as currently implemented in communication systems. Moreover, the high costs and the complexity underlying the integration of MIMO techniques in wireless communications systems prevent the use of arrays larger than $4 \times 4$ even in the most recent wireless protocols (e.g. IEEE 802.16, LTE). In [4] [5], the authors use parasitic elements side to side with a number of active elements for enhancing the capacity of the MIMO channel. The idea of using more than one active element is still unattractive for wireless devices due to the aforementioned constraints, and the need for a complex decoupling network [6] to compensate for the strong mutual coupling among the co-polar active elements. In [7], a MIMO-like realization using a single active element and a number of parasitic elements was shown to provide comparable capacity to that of conventional MIMO, where the array far-field is changed on every symbol period. However, the authors in [7] did not propose any transmission schemes using the suggested realization. In [8] [9] [10], the authors show that a parasitic array with a single active element has comparable performance to a $2 \times 2$ MIMO system, in a rich scattering environment. That was based on exploiting the wavevector domain [11] for increasing the capacity of a space-time wireless channel. For example, in [8] a $2 \times 2$ MIMO system with a single active element was implemented using switched parasitic arrays (SPA); however the scheme was restricted to ON-OFF keying modulation scheme which is not popular in mobile communications. In [9] [10], the authors propose a beam-space MIMO (BS-MIMO) transmission scheme using three or five elements of an electronically steerable parasitic array radiator (ESPAR) antenna[1]. According to the BS-MIMO approach, two different symbols are simultaneously sent toward the channel virtual angles [15]. This is achieved by creating an ESPAR pattern in the far-field that is a linear combination of weakly correlated beams (cardioids). However, the scheme proposed in [8] [9] [10] can hardly be scaled to PSK modulation orders higher than QPSK[2]. The main drawback of the BS-MIMO is the

Manuscript received June 24, 2008; revised January 16, 2009 and March 13, 2009; accepted April 28, 2009. The associate editor coordinating the review of this paper and approving it for publication was L. Deneire.

O. N. Alrabadi is with the Broadband Wireless and Sensor Networks Group (BWiSE), Athens Information Technology (AIT), GR-19002, Athens, Greece, and with the Center for TeleInFrastructure (CTiF), Aalborg University (AAU), 9220, Aalborg East, Denmark (e-mail: osal@ait.edu.gr).

C. B. Papadias and A. KalisBroadband are with the Wireless and Sensor Networks Group (BWiSE), Athens Information Technology (AIT), GR-19002, Athens, Greece (e-mail: {papadias, akal}@ait.edu.gr).

R. Prasad is with the Center for TeleInFrastructure (CTiF), Aalborg University (AAU), 9220, Aalborg East, Denmark (e-mail: prasad@es.aau.dk).

Digital Object Identifier 10.1109/TWC.2009.080824

[1]The ESPAR is a smart antenna system that was developed in 2000 at ATR labs in Japan [12]. An $(N+1)$-element ESPAR consists of a single active element surrounded by $N$ parasitic elements (PE) loaded with variable reactive loads. The ESPAR was successfully used for beam and null steering [13], and for reactance diversity [14].

[2]We remind the reader that even QPSK according to the BS-MIMO approach was obtained using a 5-element ESPAR array rather than a 3-element one [9].

difficulty of obtaining the desired linear combinations for the chosen set of basis functions (i.e. the cardioids). It is the objective of this paper to describe a *universal transmission scheme using parasitic arrays with a single active element for all phase shift keying (PSK) modulation schemes*. This work is complementary to the novel approach in [16] [17], where two and three SISO sub-channels were created by decomposing the far-field of a compact ESPAR antenna. The approach in [16] [17] confirms the conclusions in [18] about creating SISO sub-channels by expanding the electromagnetic field into a set of orthogonal functions. However, the approach in [16] [17] was implemented using simple symmetrical load switching and consequently, only BPSK modulation scheme could be supported. In this paper, we scale up the scheme of expanding the electromagnetic far-field into a set of basis functions to *all PSK modulation schemes*. We show how different power allocation schemes can be implemented. We also describe the implementation of Alamouti transmit diversity within the proposed scheme, where the two conventional transmit antennas are replaced by two orthogonal functions. The rest of this paper is divided as follows: In section II we show that a conventional multi-element array (MEA) can be viewed as a mapping device that maps the input symbols vector onto a set of basis functions. In section III we show how to emulate a conventional MEA using a compact-sized 3-element SPA, for both spatial multiplexing and transmit diversity. Section IV investigates different MIMO transmission schemes while section V extends the analysis to arrays with planar topologies. In section VI we develop a simple channel model and derive some mutual information formulas. Section VII compares the throughput potential of some system examples using the proposed emulation schemes within an outdoor geometrical based channel model, to our theoretical results. Finally the paper concludes with our results.

## II. A Simple Example of a Conventional MEA

We consider a conventional MEA where we focus our analysis on the transmitter which is the user handheld device (mobile, laptop, PDA, etc..). Assume that the transmitter is a horizontal linear array consisting of two identical co-polar antennas. The array far-field from [19] is written as

$$G(\theta) = g_{isol}(\theta)\begin{bmatrix}1 & e^{-jkd\cos(\theta)}\end{bmatrix}\underbrace{[\mathbf{Z}_L+\mathbf{Z}]^{-1}}_{\mathbf{M}_t}\begin{bmatrix}V_{01}\\ V_{02}\end{bmatrix}, \quad (1)$$

where $g_{isol}(\theta)$ is the pattern of each antenna element when isolated, $k = 2\pi/\lambda$ is the wavenumber, $\lambda$ is the carrier wavelength, $d$ is the inter-element spacing, $\theta$ is the direction of departure (DoD). $\mathbf{Z}_L = \begin{bmatrix} Z_{L1} & 0 \\ 0 & Z_{L2}\end{bmatrix}$, where $Z_{Li}$ is the terminal impedance of the $i^{th}$ antenna element, $\mathbf{Z}$ is the impedance matrix due to mutual coupling, $\mathbf{M}_t$ is the transmitter coupling matrix and $V_{0i}$ is the $i^{th}$ source voltage driving the $i^{th}$ element. Assuming the two antennas are uncoupled ($\mathbf{M}_t = \mathbf{I}_2$ where $\mathbf{I}_k$ is a $k \times k$ identity matrix) and replacing the two source voltages by the two symbols $s_0$ and $s_1$ to be sent from the first and second antennas respectively, we can rewrite the pattern in Eq. (1) as follows [3]

$$G(\theta) = s_0 + s_1 e^{-jkd\cos(\theta)}, \quad (2)$$

which can be rewritten as

$$\begin{aligned} G(\theta) &= s_0\underbrace{\left(1+\frac{s_1}{s_0}e^{-jkd\cos(\theta)}\right)}_{\widetilde{G}(\theta)} \\ &= s_0\left(B_0(\theta)+\Re_s B_1(\theta)\right), \end{aligned} \quad (3)$$

where $\widetilde{G}(\theta)$ is termed the 'effective pattern' [19]. The effective pattern can be seen as a *linear combination of two basis*[4] *functions*: $B_0(\theta) = 1$, and $B_1(\theta) = e^{-jkd\cos(\theta)}$, and their linear combination is controlled by the ratio of the two symbols $\Re_s := \frac{s_1}{s_0}$. For example, the possible QPSK linear combinations of $B_0(\theta)$ and $B_1(\theta)$ are shown in TABLE I. The rest of the linear combinations give the same $\Re_s$ and consequently the same effective pattern $\widetilde{G}(\theta)$, but with different phases due to different $s_0$. For example, the linear combinations of the symbol pairs $(s_0, s_1) = \{(1,1),(-1,-1),(j,j),(-j,-j)\}$ give the same $\Re_s = \{1,1,1,1\}$, and consequently the same $\widetilde{G}(\theta)$, but different $s_0$. The ratio $\Re_s$ belongs to a unit circle for PSK modulation schemes as the two PSK signals have the same magnitude (constant envelope) as do the two basis functions $B_0(\theta)$ and $B_1(\theta)$. The general notation of a complex symbol $s_m$ is $A_m e^{j(\omega t+\phi_m)}$ where $A_m, \omega_m, \phi_m$ are the signal amplitude, angular frequency and phase respectively. The notation of a baseband PSK symbol derived from a unity average power signal constellation can be written as $e^{j\phi_m}$ where $A_m = 1$, $\phi_m = \frac{2\pi}{M}m, m \in \{0,\ 1,\ \ldots, M-1\}$ where $M$ is the order of the PSK signal constellation, while the angular component is dropped. Consequently, the ratio of two baseband PSK symbols can be written as

$$\Re_s := \frac{s_1}{s_0} = e^{j\frac{2\pi}{M}m}\ ,\ m = \{0,1,\ldots,M-1\}. \quad (4)$$

TABLE I
TWO QPSK SIGNALS COMBINATIONS

| $[s_0\ \ s_1]^T$ | $s_0$ | $\Re_s$ | $\widetilde{G}(\theta) = B_0(\theta)+\Re_s B_1(\theta)$ |
|---|---|---|---|
| $[1\quad 1]^T$ | 1 | 1 | $B_0(\theta)+B_1(\theta)$ |
| $[1\ -1]^T$ | 1 | $-1$ | $B_0(\theta)-B_1(\theta)$ |
| $[1\quad j]^T$ | 1 | $j$ | $B_0(\theta)+jB_1(\theta)$ |
| $[1\ -j]^T$ | 1 | $-j$ | $B_0(\theta)-jB_1(\theta)$ |

The scatter plot of $\Re_s$ has some important properties that are directly derived from the definition of $\Re_s$:

- Rotating $\Re_s$ by $\Delta\Phi$ is equivalent to rotating the signal constellation of the second stream by $\Delta\Phi$ with respect to the signal constellation of the first stream (the receiver

[3]The isolated element pattern is omitted intentionally for simplicity while we assume that each antenna element has an omnidirectionnal radiation pattern in its H-plane.

[4]The term basis is used in this paper whenever the set of the angular functions are orthogonal or approximately orthogonal.

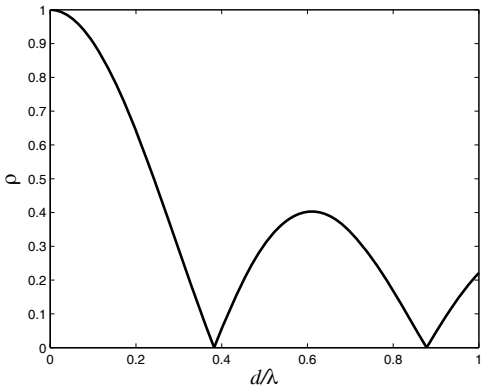


Fig. 1. Correlation factor $\rho_{01}$ between $B_0(\theta) = 1$ and $B_1(\theta) = e^{-j2\pi\frac{d}{\lambda}\cos(\theta)}$ at different $d/\lambda$.

has to reversely rotate the constellation of the second stream before decoding). However, rotating the signal constellation does not affect its properties.

- The average power of $\Re_s$ (which is the square of the circle radius) equals the relative average power of the second stream to the first one.

The ratio $\Re_s$ controls the magnitude of the effective pattern, whereas the first symbol ($s_0$) controls the phase (when $\Re_s$ is fixed). The pattern in Eq. (2) has two degrees of freedom which are the two independent signals fed into the two uncorrelated antenna elements[5]. This representation is not useful for parasitic arrays with a single driven element, since a single stream of symbols is fed into the active element at a time. On the other hand, a representation such as in Eq. (3) would be quite useful for parasitic arrays where $s_0$ is equivalent to the signal fed into the active element (first degree of freedom), whereas the second degree of freedom can be determined by the independent loadings of the parasitic elements as we show later. Fig.1 shows the correlation factor between the two basis functions (neglecting the mutual coupling effect), reminding that the correlation factor of two patterns (or two components of a given pattern e.g. $B_0(\theta)$ and $B_1(\theta)$) in the $\theta-$domain is defined (see [20]) as

$$\rho_{01} = \frac{\left|\int_0^{2\pi} B_0(\theta)B_1^*(\theta)\cdot d\theta\right|}{\sqrt{\int_0^{2\pi} B_0(\theta)B_0^*(\theta)\cdot d\theta \;.\; \int_0^{2\pi} B_1(\theta)B_1^*(\theta)\cdot d\theta}}, \quad (5)$$

where $()^*$ is the complex conjugate operator. The figure clearly shows that *the two angular functions $B_0(\theta)$ and $B_1(\theta)$ are not suitable for compact array design as they require some sufficient spacing to be uncorrelated.*

## III. Parasitic Array with a Single Active Element and Two Passive Ones

It was shown in [16] that parasitic arrays with symmetric topologies (with respect to the central active element) can emulate conventional MEA for the BPSK modulation scheme, where a simple load-switching can create the desired linear combinations of the two signals. In this section we show that the far-field (or equivalently the array factor - $AF$) of a compact-sized 3-element SPA (or ESPAR) can be approximated into a linear combination of two basis functions, where the linear combination is controlled by the array reactive loadings. We start first by analyzing the 3-element SPA, composed of a central active element surrounded by two parasitic elements (at relative angles of $0^\circ$ and $180^\circ$ with respect to the central element). The far-field and the circuit relations of the array are written according to [21] and [22] as

$$\begin{aligned} G(\theta) &= g_{isol}(\theta)\times AF \\ &= V_0\frac{\eta e^{\omega t-kr}}{2\pi r}\times\left[1\;\; e^{-jkd\cos(\theta)}\;\; e^{jkd\cos(\theta)}\right]\overbrace{[\mathbf{Z}+\mathbf{X}]^{-1}}^{\mathbf{M}_t}\begin{bmatrix}1\\0\\0\end{bmatrix} \\ &= I_{in}\frac{\eta e^{\omega t-kr}}{2\pi r}\times\left[1\;\; e^{-jkd\cos(\theta)}\;\; e^{jkd\cos(\theta)}\right]\begin{bmatrix}1\\ I_1/I_0\\ I_2/I_0\end{bmatrix}, \quad (6)\end{aligned}$$

where

$$\mathbf{Z} = \begin{bmatrix} Z_{00} & Z_{01} & Z_{02}\\ Z_{10} & Z_{11} & Z_{12}\\ Z_{20} & Z_{21} & Z_{22}\end{bmatrix},$$
$$\mathbf{X} = \begin{bmatrix} Z_s & 0 & 0\\ 0 & jX_{L1} & 0\\ 0 & 0 & jX_{L2}\end{bmatrix}. \quad (7)$$

where $V_0$ is the terminal voltage whereas $I_0$, $I_1$ and $I_2$ are the currents induced on the active and the two parasitic elements respectively by mutual coupling. $Z_{ii}$, $i\in\{0,1,2\}$ is the self-impedance of the antenna elements, whereas $Z_{ij}$ is the mutual impedance (due to mutual coupling) between element $i$ and element $j$, such that $Z_{ij}=Z_{ji}$. $Z_s$ is the source impedance assumed $50\Omega$, $X_{Li}$, $i\in\{1,2\}$ is the reactance of the $i^{th}$ parasitic element. $\eta=120\pi$ is the free-space impedance, $I_{in}$ is the input signal to be fed into the active element (equivalent to the reference signal $s_0$ in Eq. (3)), $r$ is the distance, $\omega=2\pi f$ where $f$ is the frequency in Hz. The $AF$ can be decomposed using Euler's formula as follows:

$$\begin{aligned} AF &= 1+\left(\frac{I_1}{I_0}\right)e^{-jkd\cos(\theta)}+\left(\frac{I_2}{I_0}\right)e^{jkd\cos(\theta)} \\ &= 1+\left(\frac{I_2+I_1}{I_0}\right)\cos(kd\cos(\theta))+\left(-j\frac{I_2-I_1}{I_0}\right)\sin(kd\cos(\theta)) \\ &= B_0(\theta)+\left(\frac{I_2+I_1}{I_0}\right)B_1(\theta)+\left(-j\frac{I_2-I_1}{I_0}\right)B_2(\theta). \quad (8)\end{aligned}$$

The $AF$ depends on the relative ratios of the currents induced on the array elements (as well as the relative locations of the elements), rather than the currents themselves. It is clear that the $AF$ is similar to the effective pattern $\widetilde{G}(\theta)(\theta)$ in a conventional MEA. All the parasitic arrays considered in this paper are assumed to be loaded with purely reactive loads so they are equivalent to either reactive SPA or ESPAR antennas (see [23] for the comparison between SPA and ESPAR antennas). This is mainly because the resistive part (of arbitrary impedance) reduces the antenna efficiency. When

[5]Assuming a non-reconfigurable array, consequently $d$ is fixed.

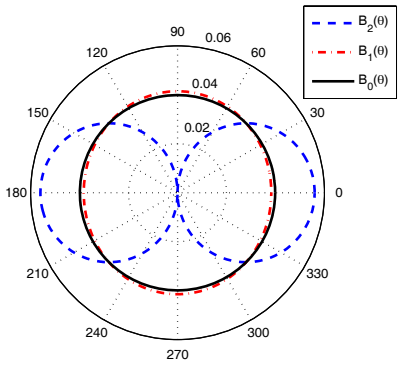


Fig. 2. Magnitude of $B_{2,1,0}(\theta)$ at an inter-element spacing of $\lambda/16$.

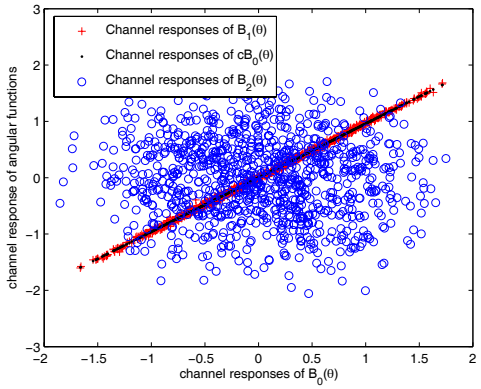


Fig. 3. Channel responses of $B_2(\theta), B_1(\theta)$ and $cB_0(\theta)$ versus the channel responses of $B_0(\theta)$.

the inter-element spacing is small enough (e.g. $\lambda/16$ or less[6]), the angular function $B_1(\theta)$ becomes highly correlated with the omni one $B_0(\theta)$, regarding both magnitude and phase. For example, the two angular functions have a correlation factor $\rho_{01}$ of 0.9996 at a spacing of $\lambda/16$. The function $B_1(\theta)$ can be approximated as $cB_0(\theta)$, where $c$ is a correction factor for the magnitude of $B_1(\theta)$ with respect to $B_0(\theta)$ and is given for a spacing of $\lambda/16$ (see [16]) as:

$$c = \sqrt{\frac{\int_0^{2\pi} B_1(\theta)B_1^*(\theta)\cdot d\theta}{\int_0^{2\pi} B_0(\theta)B_0^*(\theta)\cdot d\theta}} = (0.96213)\,. \tag{9}$$

Fig.2 shows the magnitude of the angular functions $B_0(\theta), B_1(\theta)$ and $B_2(\theta)$ at a spacing of $\lambda/16$, whereas Fig.3 shows the channel responses[7] (over a thousand of channel realizations) of $B_2(\theta), B_1(\theta)$ and $cB_0(\theta)$ versus the channel responses of $B_0(\theta)$, where the channel is a 2-D geometrically based circular single bounce channel model as that in [25], with 20 scatterers surrounding the transmitter. The figure clearly shows that the wireless channel responses when triggered with $B_1(\theta)$ are almost identical to those of $cB_0(\theta)$. Consequently, the angular function $B_1(\theta)$ can be well approximated as the angular function $cB_0(\theta)$ (i.e. $B_1(\theta) \cong cB_0(\theta)$) at such spacing. From Eq. (8) we can write[8]

$$\begin{aligned} G(\theta) &\cong I_{in}\left(B_0(\theta) + \frac{I_2+I_1}{I_0}cB_0(\theta) + j\frac{I_2-I_1}{I_0}B_2(\theta)\right) \\ &= \grave{I}_{in}\left(B_0(\theta) + j\frac{I_2-I_1}{I_0+(I_2+I_1)\,c}B_2(\theta)\right) \\ &= s_0\left(B_0(\theta) + \Re_I B_2(\theta)\right), \end{aligned} \tag{10}$$

such that

$$\begin{aligned} \Re_I &= j\frac{I_2-I_1}{I_0+(I_2+I_1)\,c} \\ &= j\frac{\alpha_{20}-\alpha_{10}}{1+(\alpha_{20}+\alpha_{10})\,c}, \end{aligned} \tag{11}$$

where $\alpha_{20}$ and $\alpha_{10}$ are calculated as in [21] to be

$$\begin{aligned} \alpha_{10} &= \left(\frac{I_1}{I_0}\right) = \frac{Z_{12}Z_{02} - Z_{01}\left(Z_{22}+jX_{L2}\right)}{\left(Z_{11}+jX_{L1}\right)\left(Z_{22}+jX_{L2}\right) - Z_{12}^2} \\ \alpha_{20} &= \left(\frac{I_2}{I_0}\right) = \frac{Z_{12}Z_{02} - Z_{02}\left(Z_{11}+jX_{L1}\right)}{\left(Z_{11}+jX_{L1}\right)\left(Z_{22}+jX_{L2}\right) - Z_{12}^2}. \end{aligned} \tag{12}$$

From Eq. (8) and Eq. (10), the set of angular functions $B_0(\theta), B_1(\theta)$, and $B_2(\theta)$ can be approximately reduced into the set of $B_0(\theta)$ and $B_2(\theta)$. The ratio $\Re_I$ is symmetric around the origin (in the complex plane) and consequently the ratio of the two symbols to be spatially multiplexed (i.e. $\Re_s$ which is a circle for PSK signal constellations) is projected over the scatter plot of $\Re_I$. On the other hand, *the two basis functions $B_0(\theta)$ and $B_2(\theta)$ are orthogonal regardless of the strong mutual coupling*, i.e. $\rho_{02} = 0$. Consequently, two symbol streams can be fully decorrelated (at the transmitter side) by mapping them directly onto $B_0(\theta)$ and $B_2(\theta)$. It is worth mentioning that the inter-element spacing has a lower bound controlled by the ability of matching the driving point impedance, which for a 3-element parasitic array is written from [21] [26] as

$$Z_{in} = Z_{00} + \alpha_{10}Z_{01} + \alpha_{20}Z_{02}, \tag{13}$$

bearing in mind that matching a single active element does not require any decoupling network [6]. On the other hand, the upper bound of the inter-element spacing is determined by the acceptable approximation in Eq. (10). The active element can be perfectly matched by knowing the patterns (i.e. by knowing the required PE loadings) before hand. The matching in our case is done *dynamically*, for example whenever the control circuit changes the PE loadings, it matches the single active element according to Eq. (13), which is possible by knowing the required loadings for a given $\Re_s$ in advance (as both $\alpha_{01}$ and $\alpha_{02}$ are calculated by knowing $[jX_{L1}\ jX_{L2}]$ according to Eq. (12)).

[6]It is worth mentioning that a 3-element ESPAR antenna with an inter-element spacing of $\lambda/20$ was successfully implemented in [24] for mobile reception of terrestrial digital TV.

[7]Each channel response is single complex value and equals the summation of the multipath gains scaled by the complex far-field. Path loss and mobile terminal orientation are all taken into account.

[8]The term $\frac{\eta}{2\pi r}e^{\omega t - kr}$ is intentionally omitted for simplicity.

## IV. MIMO Transmission Techniques

### A. Spatial Multiplexing

The ratio $\Re_I$ should have a locus of a circle for PSK mapping. Assuming the channel state information (CSI) is only available at the receiver, an optimal circle radius ($r_{optimal} = \left|\Re_I^{opt}\right|$) is the one that balances the power between the two basis functions (i.e. an *orthonormal* rather than orthogonal set of angular functions can be obtained). The power imbalance can be defined as

$$\Delta P = \frac{\int_0^{2\pi} B_0(\theta)B_0^*(\theta)\cdot d\theta}{\int_0^{2\pi}\left(\Re_I B_2(\theta)\right)\left(\Re_I B_2(\theta)\right)^*\cdot d\theta} = \frac{\int_0^{2\pi} B_0(\theta)B_0^*(\theta)\cdot d\theta}{r^2\int_0^{2\pi} B_2(\theta)B_2^*(\theta)\cdot d\theta}. \quad (14)$$

The optimal radius $r_{optimal}$ is obtained when $\Delta P = 1$. At an inter-element spacing of $\lambda/16$, $r_{optimal}$ is found from Eq. (14) to be 3.67. Notice that *the circle is no more a unit circle* since the two basis functions are naturally imbalanced and consequently $r_{optimal} \neq 1$. Fig.4 shows the values of $\Re_I$ in the complex plane that lie on a circle with the optimal radius (when the two reactive loadings change from $-j500\Omega$ to $j500\Omega$, step $j0.1\Omega$). $\Re_I \cong r_{optimal}\Re_s e^{j\Delta\Phi_R}$ where $r_{optimal} = 3.67$ and $\Delta\Phi_R = 0.1$ rad. $\Re_I$ is a scaled up version of $\Re_s$ (so the two basis are equipowered), and slightly rotated so that each point of $\Re_I$ has a corresponding loading. TABLE II shows the values of the reactive loadings required for obtaining the linear combinations of up to 16-PSK signal constellations. The values are quite practical, and can be simply obtained using a variable reactor (varactor) as in ESPAR antennas or a lumped reactance as in a SPA (if the varactor does not support a switching rate comparable to the symbol rate). In the same table, $E_1$ is the absolute error in magnitude between $|\Re_I|$ and $r_{optimal}$, i.e. $E_1 = \left|\frac{|\Re_I| - r_{optimal}}{r_{optimal}}\right|$, while $E_2$ is the absolute error in phase i.e. $E_2 = \left|\frac{\angle\Re_I - \angle\Re_s}{\angle\Re_s}\right|$. It is clear that the *maximum absolute error* whether in phase or magnitude does not exceed $0.5\%$ of the desired value. PSK transmission schemes with orders higher than sixteen cannot be projected on the circle of the optimal radius due to having two opposite gaps that can not be closed at any loading. These gaps are a consequence of the non-linear mapping [27] from the reactance space to equivalent wave-vector space. The result is that a limited number of PSK signal constellations can be optimally supported within the proposed scheme due to such gaps. $\Re_s$ of *any* PSK signal constellation can be (sub-optimally) projected on a circle with a larger radius, e.g. $r_{min}$ in Fig.4 is the radius of the first full circle without gaps, where the basis functions suffer from a power imbalance $\Delta P$ of 3.6 dB (although such projection is suboptimal, our simulations later on show that we have a marginal mutual information loss compared to the ideal scheme with uniform power allocation policy-this result is not surprising as a similar marginal mutual information loss occurs in conventional MIMO under the same power imbalance conditions).

*Optimal Power Allocation:* The power allocation *across the basis functions* can be optimized by maximizing the instantaneous mutual information over each channel realization (see section VI). Notice that this kind of power allocation

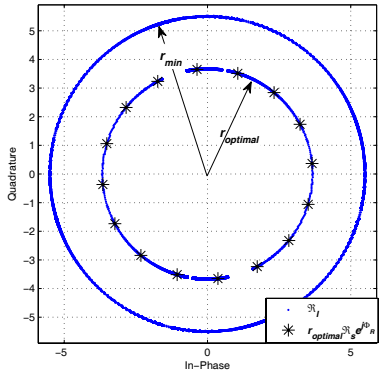


Fig. 4. $\Re_I$ values that lie on the optimal radius $r_{optimal}$, over which a scaled up version of $\Re_s$ of a 16-PSK signal constellation is projected, and the values of $\Re_I$ that lie on the smallest radius of the first full-circle beyond the gaps $r_{min}$.

TABLE II
CORRESPONDING REACTIVE LOADINGS FOR DIFFERENT PSK MODULATION ORDERS ($M$)

| $\Re_s$ | $jX_{L1}(\Omega)$ | $jX_{L2}(\Omega)$ | $M$ | $E_1$ | $E_2$ |
|---|---|---|---|---|---|
| $e^{j0\frac{2\pi}{16}}$ | $j15.2$ | $j5.5$ | $2,4,8,16$ | $0.42\%$ | $0.39\%$ |
| $e^{j1\frac{2\pi}{16}}$ | $j13.1$ | $j0.8$ | $16$ | $0.05\%$ | $0.1\%$ |
| $e^{j2\frac{2\pi}{16}}$ | $j10.9$ | $-j9.5$ | $8,16$ | $0.16\%$ | $0.07\%$ |
| $e^{j3\frac{2\pi}{16}}$ | $j7.7$ | $-j78$ | $16$ | $0.13\%$ | $0.12\%$ |
| $e^{j4\frac{2\pi}{16}}$ | $-j10.5$ | $j53.7$ | $4,8,16$ | $0.01\%$ | $0\%$ |
| $e^{j5\frac{2\pi}{16}}$ | $j30$ | $j34.4$ | $16$ | $0.01\%$ | $0.03\%$ |
| $e^{j6\frac{2\pi}{16}}$ | $j11.9$ | $j21.6$ | $8,16$ | $0.35\%$ | $0.09\%$ |
| $e^{j7\frac{2\pi}{16}}$ | $j8.7$ | $j17.8$ | $16$ | $0.15\%$ | $0.17\%$ |
| $e^{j8\frac{2\pi}{16}}$ | $j5.5$ | $j15.2$ | $2,4,8,16$ | $0.42\%$ | $0.39\%$ |
| $e^{j9\frac{2\pi}{16}}$ | $j11.7$ | $j13.1$ | $16$ | $0.05\%$ | $0.1\%$ |
| $e^{j10\frac{2\pi}{16}}$ | $j0.8$ | $j10.9$ | $8,16$ | $0.16\%$ | $0.07\%$ |
| $e^{j11\frac{2\pi}{16}}$ | $-j78$ | $j7.7$ | $16$ | $0.13\%$ | $0.12\%$ |
| $e^{j12\frac{2\pi}{16}}$ | $j53.7$ | $-j10.5$ | $4,8,16$ | $0.01\%$ | $0\%$ |
| $e^{j13\frac{2\pi}{16}}$ | $j34.4$ | $j30$ | $16$ | $0.01\%$ | $0.03\%$ |
| $e^{j14\frac{2\pi}{16}}$ | $j21.6$ | $j11.9$ | $8,16$ | $0.35\%$ | $0.09\%$ |
| $e^{j15\frac{2\pi}{16}}$ | $j17.8$ | $j8.7$ | $16$ | $0.15\%$ | $0.17\%$ |

is different from the optimal water-pouring [28] precoding scheme, as the former only requires a single real number (e.g. $\Delta P$ or $\Delta_0$ or $\Delta_1$) to be fed back to the transmitter while the latter requires the whole channel matrix to be available at the transmitter for optimally allocating the power across the eigenvectors of the channel. Having calculated the optimal power allocation variables $\Delta_0^{opt}$ and $\Delta_1^{opt}$, an optimal $\Re_I$ becomes

$$\Re_I^{opt} = \sqrt{\frac{\Delta_1^{opt}}{\Delta_0^{opt}}}\frac{s_1}{s_0} = \sqrt{\frac{\Delta_1^{opt}}{\Delta_0^{opt}}}\Re_s. \quad (15)$$

In this case, the transmitter will have to use a look-up table rather than a scatter plot, consequently the transmitter control circuit selects the corresponding reactive loadings $[jX_{L1}\ jX_{L2}]$ from the look-up table as follows

$$[jX_{L1}\ jX_{L2}] = \arg\min_{\Re_I}\left|\Re_I^{opt} - \Re_I\right|, \quad (16)$$

which returns the corresponding loadings of the closest $\Re_I$ to

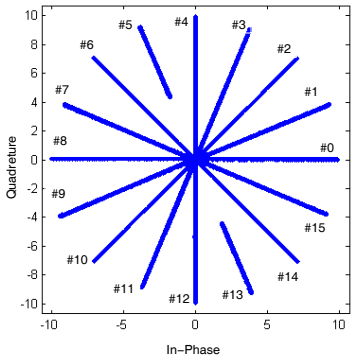


Fig. 5. Scatter plot of $\Re_I$ within a radius $\sqrt{\frac{\Delta_1}{\Delta_0}}$ ranging from 0 up to 10 along the angles of $\Re_s$ of a 16-PSK.

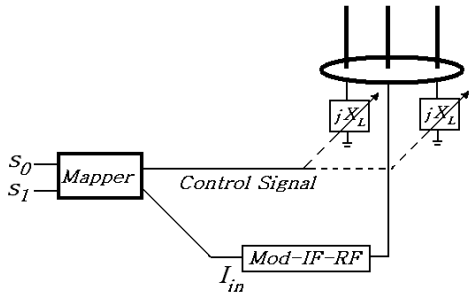


Fig. 6. Simplified schematic diagram of 3-element SPA control circuit.

$\Re_I^{opt}$. In Eq. (16) we used the minimum distance as a criterion for picking up the optimal (closest to the optimal) loadings, since some of $\Re_I^{opt}$ will not have a corresponding loading, due to having the aforementioned opposite gaps as shown in Fig.5. The figure clearly shows that BPSK (e.g. segments $\#0, \#8$), QPSK (e.g. segments $\#0, \#4, \#8, \#12$) and 8-PSK (e.g. segments (e.g. segments $\#0, \#2, \#4, \#6, \#8, \#10, \#12, \#14$) are supported within a closed loop transmission scheme, as the $\Re_I$ segments are continuous up to a ratio of $\sqrt{\frac{\Delta_1}{\Delta_0}} = 10$, which is equivalent to a power imbalance of $8.71$ dB[9] between the two basis functions. On the other hand, 16-PSK and higher order PSK modulation schemes will have some cases where optimal power allocation policy does not have a corresponding loading, and consequently the closest to the optimal loading will be selected as in Eq. (16). As an example, let's consider a uniform power allocation transmission scheme similar to that described in [10]. The scheme is done by feeding the driven element with the first PSK symbol from the two PSK symbols to be spatially multiplexed as shown in Fig.(6), after being modulated and converted to the intermediate frequency (IF) and the radio frequency (RF) bands; at the same time, the control signal loads the PE with the two reactances $[jX_{L1} \;\; jX_{L2}]$ (from TABLE II) according to the ratio of the two symbols $\Re_s$. Loading the PE can be done using lumped reactances and PIN diodes as in SPA antennas, or simply by reverse-biasing a variable reactor (varactor) using a suitable voltage signal as in ESPAR antennas (a one-to-one mapping exists between the reverse biasing voltage and the varactor reactance [27]). The ratio $\Re_I$ is a scaled up version of the ratio of the two symbols to be spatially multiplexed $\Re_s$ (with some possible rotations), so that the two SISO sub-channels have a specific power allocation policy. For example, transmitting the QPSK symbol pair $(j, -1)$ using a 3-element $\lambda/16$ SPA array is done as follows:

- Feed the active element with the first QPSK symbol.
- Simultaneously, the control circuit should change the loading of the PE according to the ratio $\Re_s = \frac{-1}{j} = j \equiv \Re_I = r_{_{optimal}}\Re_s = r_{_{optimal}}\angle\frac{\pi}{2}$[10] (forget the rotation of $\Re_s$ in this example). From TABLE II, $[jX_{L1} \;\; jX_{L2}]$ should be $[-j10.5 \;\; j53.7]\Omega$.

The far-field according to this procedure may be written as $G = I_{in}AF = s_0\widetilde{G}(\theta)$, from which $G = j\left\{1 + j3.67\sin(kd\cos(\theta))\right\} = \underbrace{j}_{s_0} B_0 \underbrace{-1}_{s_1}\dot{B}_2$, where $B_0 = 1$ and $\dot{B}_2 = 3.67B_2 = 3.67\sin(kd\cos(\theta))$ are equi-powered.

### B. Transmit Diversity

Space-time coding schemes are used to increase the robustness of the wireless channels rather than increasing the spatial multiplexing rate. We consider one of the most successful transmit diversity schemes that increases the link robustness using an uninformed transmitter, being introduced by Alamouti in [30]. Unlike the conventional Alamouti scheme which is implemented using two transmit antennas, we propose a transmission scheme based on the Alamouti code that uses only one active element. This is done by reconsidering the far-field in Eq. (2). The far-fields according to the Alamouti code within the first and the second symbol periods are $G_{T_1}(\theta) = s_0 + s_1 e^{-jkd\cos(\theta)}$ and $G_{T_2}(\theta) = -s_1^* + s_0^* e^{-jkd\cos(\theta)}$. Consequently, a parasitic array can emulate Alamouti far-fields as long as $\Re_I$ has the corresponding values of $\Re_s = \left\{\frac{s_1}{s_0}, \frac{-s_0^*}{s_1^*}\right\}$. The proposed scheme is done as follows: In the first symbol period, the symbol $s_0$ is fed into the active element while the control circuit loads the PE with corresponding loading of $\Re_s = s_1/s_0$. In the second symbol period, the symbol $-s_1^*$ is fed into the active element while the control circuit loads the PE with corresponding loading of $-1/\Re_s^* = -s_0^*/s_1^*$. The feasible characteristics of the proposed scheme are:

- $-1/\Re_s^* = -\Re_s$ for all PSK schemes (see Eq. (4)), consequently no extra reactive loading values will be required.
- The single receive antenna responses to the two basis functions fade independently due to the uncorrelation between the basis functions, consequently a diversity order of two (full diversity) is extracted by the single receive antenna.

[9] $\Delta P(dB) = 10\log\left(\frac{\Delta_1}{\Delta_0}\frac{\int_0^{2\pi} B_2 B_2^* . d\theta}{\int_0^{2\pi} B_0 B_0^* . d\theta}\right)$.

[10] The phasor notation $A\angle\phi$ means a complex quantity with magnitude $A$ and phase $\phi$.

## V. Planar Arrays

A planar array that makes use of another dimension can be used for increasing the number of the degrees of freedom. For example, a compact planar parasitic array where the central active element is surrounded by four parasitic elements at relative angles of $0°, 90°, 180°$ and $270°$ was used in [16] for expanding the far-field into three basis functions, and consequently supporting three SISO sub-channels [18]. However the simple load switching in [16] was restricted to the BPSK modulation scheme. The same approach followed in this paper is applied to the planar array (SPA or ESPAR of [16]). The far-field of the array can be written as

$$\begin{aligned} G(\theta) &= I_{in} \times (AF) \\ &\cong I_{in}\left(B_0(\theta) + \Re_I^1 B_2(\theta) + \Re_I^2 B_2^{`}(\theta)\right) \\ &\cong s_0\left(B_0(\theta) + \Re_I^1 B_2(\theta) + \Re_I^2 B_2^{`}(\theta)\right), \end{aligned} \quad (17)$$

where

$$\Re_I^1 = j\frac{I_2 - I_1}{(I_4 + I_3 + I_2 + I_1)\,c + I_0},$$
$$\Re_I^2 = j\frac{I_4 - I_3}{(I_4 + I_3 + I_2 + I_1)\,c + I_0},$$

where $B_2(\theta) = \sin(kd\cos(\theta))$ and $B_2^{`}(\theta) = \sin(kd\sin(\theta))$ such that $B_1(\theta) \perp B_2(\theta) \perp B_2^{`}(\theta)$. Both $\Re_I^1$ and $\Re_I^2$ are found to be circles with either $r_{optimal}$ for BPSK, QPSK, 8-PSK and 16-PSK, or $r_{min}$ for any PSK scheme, as in the 3-element SPA. However, the two ratios $\Re_I^1$ and $\Re_I^2$ should be non-redundant, as the corresponding $\Re_s^1$ and $\Re_s^2$ are independent, so that three independent streams can be simultaneously encoded. Taking QPSK transmission scheme as an example: $\Re_I^1$ and $\Re_I^2$ can independently have *any* of the values $\{1, -1, j, -j\}$; consequently sixteen different loadings (i.e. $\mathbf{X}_k$, $k \in \{1, 2, \ldots, 16\}$) are required for spatially multiplexing three QPSK signals. An exhaustive search for creating the scatter plots of both $\Re_I^1$ and $\Re_I^2$ by changing the reactive loads of the four parasitic elements simultaneously from $-j100\Omega$ up to $j100\Omega$ with a step of $j\Omega$ was followed. Larger loading ranges or fine tuning could not be implemented due to the limited computational power. The main result is that the 5-element $\lambda/16$ SPA satisfies the stated condition.

## VI. Throughput Analysis

In this section we consider the throughput potential of a flat-fading MIMO channel where the transmitter is equipped with a compact 3-element parasitic array (the same analysis applies to the 5-element planar parasitic array), whereas the receiver is equipped with conventional ULA with uncorrelated and uncoupled elements. We start first by rewriting down the channel matrix under the mutual coupling effect and the proposed far-field approximation. The far-field of the compact 3-element parasitic array can be written in the same form of Eq.(6) as

$$G(\theta,\phi) = \frac{\eta I_{in}}{2\pi r} e^{\omega t - kr} \underbrace{\begin{bmatrix} 1 & \sin(kd\cos(\theta)) \end{bmatrix}}_{\widetilde{\mathbf{a}}_T(\theta)} \underbrace{\begin{bmatrix} 1 & \Re_I \\ \Re_I & 1 \end{bmatrix}}_{\mathbf{M}_t} \begin{bmatrix} 1 \\ 0 \end{bmatrix}, \quad (18)$$

where the transmitter coupling matrix is always normalized so that $\mathbf{M}_t = \mathbf{I}_2$ in the absence of coupling, $\widetilde{\mathbf{a}}_T(\theta)$ is the steering vector after the proposed approximation. The coupling matrix can be rewritten using the impedance notations as

$$\mathbf{M}_t = \begin{bmatrix} 1 & j\frac{\alpha_{10}-\alpha_{20}}{1+\alpha_{10}+\alpha_{20}} \\ j\frac{\alpha_{10}-\alpha_{20}}{1+\alpha_{10}+\alpha_{20}} & 1 \end{bmatrix}. \quad (19)$$

The channel matrix when taking the mutual coupling into account can be written as [19]:

$$\begin{aligned} \widetilde{\mathbf{H}} &= \mathbf{M}_r \mathbf{H} \mathbf{M}_t \\ &= \mathbf{I}_{M_R} \mathbf{H} \mathbf{M}_t, \end{aligned} \quad (20)$$

where $\widetilde{\mathbf{H}}$ is the channel matrix when taking the mutual coupling into account, $\mathbf{M}_r$ is the receiver coupling matrix assumed identity (i.e. $\mathbf{M}_r = \mathbf{I}_{M_R}$) according to our assumption about the receiving ULA elements, $\mathbf{H}$ is the channel matrix under no coupling. In order to evaluate the performance of MIMO systems in the beamspace domain a parametric physical model that considers the geometry of the scattering environment is required. Such models have been extensively studied in the literature [25]. In these models, each path $i$ connecting the area of the transmitter with the area of the receiver has a single angle-of-departure (AoD) $\theta_{T,i}$ and a single angle-of-arrival (AoA) $\theta_{R,i}$, and a path gain $b_i$. If $K$ such paths exist, then assuming $\mathbf{a}_R(\theta_{R,i})$ the steering vector of the receiving array, the uncoupled channel response can be written as

$$\begin{aligned} \mathbf{H} &= \sum_{i=1}^{K} b_i \mathbf{a}_R(\theta_{R,i}) \widetilde{\mathbf{a}}_T^H(\theta_{T,i}) \\ &= \mathbf{A}_R(\Theta_R) \mathbf{H}_b \widetilde{\mathbf{A}}_T^H(\Theta_T), \end{aligned} \quad (21)$$

where $\Theta_R$, $\Theta_T$ are the direction vectors of the AoA and AoD respectively, $\mathbf{A}_R(\Theta_R)$, $\widetilde{\mathbf{A}}_T(\Theta_T)$ are the $M_{R,T} \times K$ receive and transmit steering matrices, and $\mathbf{H}_b$ is a diagonal $K \times K$ matrix whose entries represent the complex gain of each path. Given the channel matrix $\widetilde{\mathbf{H}}$, the general channel capacity formula for a Gaussian signaling is given from [28] as

$$C = \max_{Tr(R_{ss})=M_T} \log_2 \det\left(\mathbf{I}_{M_R} + \frac{\rho}{M_T} \widetilde{\mathbf{H}} \mathbf{R}_{ss} \widetilde{\mathbf{H}}^{\dagger}\right), \quad (22)$$

where $\mathbf{R}_{ss}$ is the covariance of the input which amounts to the power distribution among the basis functions $B_0(\theta)$ and $B_2(\theta)$. The capacity in Eq. (22) is achieved when the distribution of the input is Gaussian. Although the paper is restricted to PSK signaling which does not achieve the capacity of a Gaussian signaling, the closed-form equation in (22) serves as an upper-bound for the spectral efficiency potential of the proposed encoding scheme and simplifies the analysis. In the simulation part of this paper we evaluate the upper-bound capacity assuming Gaussian signaling and we

also estimate the capacity of different $M$-PSK transmission schemes using Monte-Carlo simulation. According to the CSI availability at the transmitter we have two different power allocation policies:

### A. Fixed Power Allocation

When the channel is not known to the transmitter but only to the receiver, a natural power allocation policy is to divide the power equally among the basis functions [2] (by mapping on the circle of radius $r_{optimal}$). In this case $\mathbf{R}_{ss} = \frac{P_T}{M_T}\mathbf{I}_{M_T}$. From Eq.(20) and Eq.(22) the mutual information[11] is written as

$$\begin{aligned}\Im(\widetilde{\mathbf{H}}) &= \log_2 \det\left(\mathbf{I}_{M_T} + \frac{\rho}{M_T}\widetilde{\mathbf{H}}^{\dagger}\widetilde{\mathbf{H}}\right)\\ &= \log_2 \det\left(\mathbf{I}_{M_T} + \frac{\rho}{M_T}\mathbf{M}_t^{\dagger}\mathbf{H}^{\dagger}\mathbf{H}\mathbf{M}_t\right)\\ &= \sum_{i=1}^{r}\log_2\left(\mathbf{I}_{M_T} + \frac{\rho}{M_T}\lambda_i\left(\mathbf{M}_t^{\dagger}\mathbf{H}^{\dagger}\mathbf{H}\mathbf{M}_t\right)\right)\\ &\le \sum_{i=1}^{r}\log_2\left(\mathbf{I}_{M_T} + \frac{\rho}{M_T}\lambda_i\left(\mathbf{H}^{\dagger}\mathbf{H}\right)\right), \end{aligned} \tag{23}$$

where $\lambda_i()$ is the $i^{th}$ non-zero eigenvalue of the operand. The last equation comes from the Poincare separation theorem with equality occurring when the columns of $\mathbf{M}_t$ are the $M_R$ dominant singular vectors of $\mathbf{H}$. Therefore, the mutual information upper bound of the MIMO channel under mutual coupling corresponds to the standard open loop mutual information expression of a MIMO channel under no coupling. The "ergodic capacity", which is the average of the instantaneous mutual information in Eq.(23) over a large number of channel realizations, can be practically achieved using an MMSE-VBLAST successive interference cancellation (SIC) receiver when feeding back *all* the SNR values of the substreams at the receiver (or an MMSE D-BLAST and feeding back the average SNR of the substreams at the receiver [28]), i.e.

$$\begin{aligned}\overline{C}_{\text{MMSE-SIC}} &= \sum_{q=1}^{\min\{M_T,M_R\}}\log_2\left(1+\rho_q\right),\\ &= \log_2\det\left(\mathbf{I}_{M_R} + \frac{\rho}{M_T}\widetilde{\mathbf{H}}\widetilde{\mathbf{H}}\right), \end{aligned} \tag{24}$$

where $\rho_q$ denotes the SNR of the substream $q$. Having received different $\rho_q$'s via a low rate feedback channel, the transmitting parasitic array can adapt its transmission rate accordingly. This can be done through an *adaptive modulation* scheme where a linear combination of different PSK signal constellations is created. The order of the signal constellation is determined by the value of the SNR of its substream (the higher $\rho_q$, the higher the modulation order $M$ that can be supported). *The ratio $\Re_s$ of two different PSK signal constellations of orders $M_1$ and $M_2$ is the ratio $\Re_s$ of the higher order PSK signal constellation* (this comes directly from the definition of $\Re_s$). Consequently there is no need to search the reactance space for other loading values. On the other hand, mapping the signals on the full circle of $r_{min}$ so as to obtain the linear combination of higher order PSK signal constellations ($M > 16$), creates a power imbalance of 3.6 dB between the basis functions. Consequently

$$\begin{aligned}\mathbf{R}_{ss} &= \begin{bmatrix}\Delta_0 & 0\\ 0 & \Delta_1\end{bmatrix}\\ \text{s.t.}\quad &\Delta_0+\Delta_1 = M_T\end{aligned} \tag{25}$$

where $M_T$ is the number of the basis functions. From Eq. (25), we get $\Delta_0 = 0.608$ and $\Delta_1 = 1.3921$.

### B. Optimal Power Allocation

The power allocation among the basis functions can be optimized on every single channel realization. The optimal power allocation policy can be easily implemented by the receiver (which knows the channel), and which then feeds a single real value back to the transmitter. The mutual information under a variable power allocation scheme can be written from Eq. (22) as

$$\begin{aligned}\Im\left(\Delta_0,\Delta_1\right) &= \max_{\Delta_0+\Delta_1=M_T}\log_2\det\left(\mathbf{I}_{M_T}+\frac{\rho}{M_T}\mathbf{D}\right),\\ \mathbf{D} &= \begin{bmatrix}\Delta_0 & 0\\ 0 & \Delta_1\end{bmatrix}\widetilde{\mathbf{H}}^{\dagger}\widetilde{\mathbf{H}}, \end{aligned} \tag{26}$$

where Eq. (26) is maximized over the variables $\Delta_0$ and $\Delta_1$. The mutual information in Eq. (26) can be numerically found using an exhaustive search. In the case of two basis functions, a low complexity search is easily implemented by quantizing $\Delta_0$ into $2^n$ levels where $n$ is number of quantizing bits. The mutual information from Eq. (26) is found on every level of $\Delta_0^l$, and the maximum value is found as

$$\begin{aligned}\Delta_0^{opt} &= \arg\max\left\{\log_2\det\left(\mathbf{I}_{M_T}+\mathbf{D}^l\right)\right\},\\ \mathbf{D}^l &= \frac{\rho}{M_T}\begin{bmatrix}\Delta_0^l & 0\\ 0 & M_T-\Delta_0^l\end{bmatrix}\widetilde{\mathbf{H}}^{\dagger}\widetilde{\mathbf{H}}. \end{aligned} \tag{27}$$

In the simulation part of this paper, it is shown that two bits for quantizing $\Delta_0$ are enough to give a mutual information gain marginally close to that with infinite resolution (analog feedback) [29]. In addition, the mutual information gain using such a scheme decreases as the signal-to-noise (SNR) ratio increases and asymptotically coincides with the uniform power allocation policy (see Fig.7, the results are discussed in Section VII). This can be easily proved by approximating the mutual information from Eq. (26) at high SNR as [28]

$$C \approx \log_2\det\left(\begin{bmatrix}\Delta_0 & 0\\ 0 & \Delta_1\end{bmatrix}\right) + \log_2\det\left(\frac{\rho}{M_T}\widetilde{\mathbf{H}}^{\dagger}\widetilde{\mathbf{H}}\right), \tag{28}$$

which is maximized by maximizing $\log_2\left(\Delta_0\Delta_1\right)$ or equivalently by maximizing $\Delta_0\Delta_1$ subject to $\Delta_0+\Delta_1 = M_T = 2$, from which the product is maximized when $\Delta_0 = \Delta_1 = M_T/2$.

[11] Some times the term open-loop capacity is used with some abuse of language.

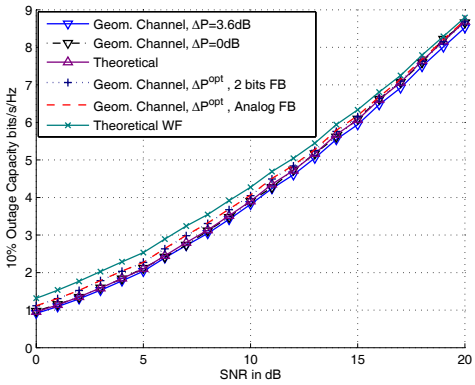


Fig. 7. 10% outage capacities for $2 \times 2$ MIMO system examples (assuming Gaussian signaling) using different power allocation policies among the basis functions.

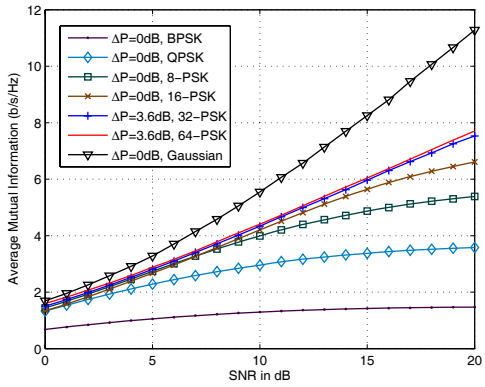


Fig. 8. Average mutual information for $2 \times 2$ MIMO system examples using different PSK signaling schemes.

## VII. Results

We consider an outdoor propagation scenario, described by a 2-D geometrically based circular single bounce channel model as that described in [25]. We assume that all the signals are transmitted and received from a single location corresponding to the phase center of the transmitting and receiving arrays. The inter-element spacing between the transmitter elements equals $\lambda/16$, while the inter-element spacing between the receiving antenna elements equals $10\lambda$. The transmitter coupling matrix is already taken into consideration within the calculation of the far-fields before normalizing, whereas the receiver coupling matrix is assumed to be an identity matrix, due to the largely assumed inter-element spacing. We start first by evaluating the mutual information upper bound using the $\log\det$ formula (i.e. assuming Gaussian signaling). Fig.7 shows the $10\%$ outage capacities of communication system examples within a $2\times2$ MIMO setting, using a 3-element $\lambda/16$ SPA. The mutual information is compared to the theoretical one from Eq. (23) when the elements of the uncoupled matrix $\mathbf{H}$ are assumed to be i.i.d. and to the optimal waterfilling precoding scheme. The figure clearly shows that the simulation results practically coincide with the theoretical ones. The two fixed power allocation policies (i.e. when $\Delta P = 0$ or 3.6 dB as a result of mapping the symbols onto the circle of $r_{optimal}$ and $r_{min}$ respectively) are shown to be almost identical. The figure also shows that the optimal power allocation using two bits for quantizing and feeding back $\Delta_0$ gives almost the same mutual information when analog feedback is used. Last but not lest, the two optimal power allocation policies (among the basis function) are shown to be inferior to the optimal waterfilling (WF) capacity, as the latter optimally allocates the power among the channel eigenvectors rather than the basis functions (A $10\%$ capacity gain is achieved by the proposed power allocation scheme at SNR=0dB, while a $20\%$ capacity gain is achieved by the theoretical WF scheme at the same SNR). Fig.8 shows the exact average mutual information of different PSK transmission schemes using the proposed encoding scheme within the geometrical channel. The average mutual information was obtained using a Monte-Carlo simulation (see [31]) where $10,000$ channel realizations were used for estimating the conditional probability distribution of the output given all the possible input alphabets (the input is a $1000$ uniformly distributed PSK symbols). The figure shows that the average mutual information of an $M$-PSK transmission scheme saturates at high SNR at $2\log_2 M$ (within a $2 \times 2$ MIMO) setting. The figure also shows that a QPSK transmission suffices at low SNR while a 64-PSK has no appreciable gain over a 32-PSK (at least at low and medium SNR regime). Fig.9 shows the CDF of the instantaneous mutual information (using the log det formula of Eq.(23)) of some system examples at SNR= 10 dB using a 3-element $\lambda/16$ SPA within a $2 \times 1$ Alamouti diversity scheme. The mutual information is compared to the theoretical one (assuming the elements of $\mathbf{H}$ are i.i.d. and uniform power distribution between the basis functions). The figure shows that the mutual information of the two fixed-power allocation schemes is quite comparable to the mutual information of the balanced i.i.d. channel model. Finally, as realistic radiation patterns will have some irregularities (e.g. due to using dirty RF components [32] or coupling with the neighboring objects), the angular functions will no more form a pure basis. Fig.10 illustrates the mutual information sensitivity to different correlation coefficients between the angular functions. The figure clearly shows that a correlation factor up to $\rho = 0.3$ can be an acceptable upper-bound.

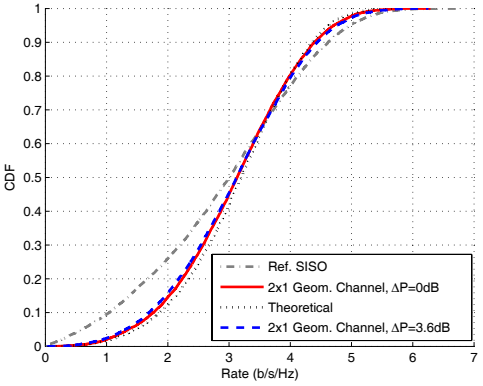


Fig. 9. Empirical CDF of instantaneous channel mutual information at SNR= 10 dB for $2 \times 1$ system examples.

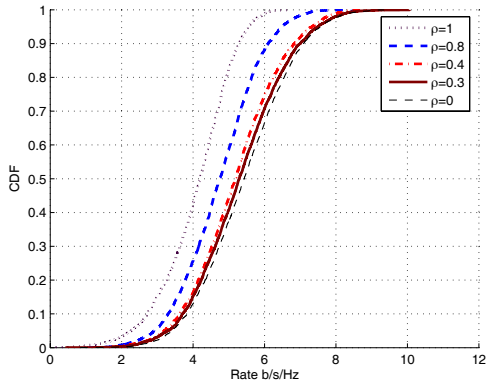


Fig. 10. Effect of correlation between angular functions on system mutual information.

## VIII. Conclusion

A novel emulation of MIMO transmission using parasitic arrays has been proposed and applied successfully to any PSK modulation scheme using compact-sized parasitic arrays. A spatial multiplexing rate of 2 and 3 PSK symbols/s has been achieved using a 3-element and 5-element $\lambda/16$ SPA antenna respectively. Different power allocation schemes among the basis have been proposed with limited feedback. Transmit diversity using Alamouti scheme was also implemented using a single front-end, making it a viable option for the uplink via lower cost terminal devices. A wideband encoding scheme where the optimal reactive loads are changed according to the carrier frequency will be the subject of future work.

## IX. Acknowledgment

This research work has been performed in the context of collaboration between AAU / CTiF and AIT for the joint offering of a Doctoral Program.

## References

[1] G. J. Foschini and M. J. Gans, "Limits of wireless communication in a fading environment when using multiple antennas," *Wireless Personal Commun.*, vol. 6, pp. 311-335, 1998.

[2] I. E. Telatar, "Capacity of multi-antenna Gaussian channels," *European Trans. Telecommun.*, pp. 585-595, Nov. 1999.

[3] C. B. Papadias, "On the spectral efficiency of space-time spreading schemes for multiple antenna CDMA systems," in *Proc. Thirty-Third Asilomar Conference on Signals, Systems, and Computers*, vol. 1, Oct. 1999.

[4] M. Di Zazzo, M. D. Migliore, F. Schettino, V. Patriarca, and D. Pinchera, "A novel parasitic-MIMO antenna," in *Proc. Antennas and Propagation Society International Symposium*, pp. 4474-4450, July 2006.

[5] M. D. Migliore, D. Pinchera, and F. Schettino, "Improving channel capacity using adaptive MIMO antennas," *IEEE Trans. Antennas Propagation*, vol. 54, no. 11, Nov. 2006.

[6] J. Weber, C. Volmer, K. Blau, R. Stephan, and M. A. Hein, "Miniaturized antenna arrays using decoupling networks with realistic elements," *IEEE Trans. Microwave Theory Tech.*, vol. 54, no. 6, pp. 2733-2740, June 2006.

[7] M. Wennstrom and T. Svantesson, "An antenna solution for MIMO channels: the switched parasitic antenna," in *Proc. IEEE 12th Int. Symp. Personal, Indoor and Mobile Radio Communications*, Sept. 2001, vol. 1, pp. A-159-A-163.

[8] A. Kalis, A. G. Kanatas, M. Carras, and A. G. Constantinides, "On the performance of MIMO systems in the wavevector domain," *IST Mobile & Wireless Communications Summit*, June 2006, Mykonos, Greece.

[9] A. Kalis, A. G. Kanatas, and C. Papadias, "An ESPAR antenna for beamspace-MIMO systems using PSK modulation schemes," *IEEE International Conference on Communications 2007*, Glasgow, UK, June 2007.

[10] A. Kalis, A. G. Kanatas, and C. B. Papadias, "A novel approach to MIMO transmission using a single RF front end," *IEEE J. Select. Areas Commun.*, vol. 26, no. 6, Aug. 2008.

[11] A. S. Y. Poon, R. W. Brodersen, and D. N. C. Tse, "Degrees of freedom in multiple-antenna channels: a signal space approach," *IEEE Trans. Inform. Theory*, vol. 51, no. 2, pp. 523-536, Feb. 2005.

[12] K. Gyoda and T. Ohira, "Design of electronically steerable passive array radiator (ESPAR) antennas," in *Proc. IEEE Antennas and Propagation Society International Symposium*, vol. 2, July 2000, pp. 922-925.

[13] D. V. Thiel, S. O'Keefe, J. W. Lu, "Electronic beam steering in wire and patch antenna systems using switched parasitic elements," in *Proc. Antennas and Propagation Society International Symposium, AP-S Digest* vol. 1, pp 534-537, 1996.

[14] T. Sawaya, K. Iigusa, M. Taromaru, and T. Ohira, "Reactance diversity: proof-of-concept experiments in an indoor multipath-fading environment with a 5-GHz prototype planar ESPAR antenna," in *Proc. Consumer Communications and Networking Conference*, Jan. 2004, pp. 678-680.

[15] A. M. Sayeed, "Deconstructing multiantenna fading channels," *IEEE Trans. Signal Processing*, vol. 50, pp. 2563-2579, Oct. 2002.

[16] O. N. Alrabadi, A. Kalis, C. Papadias, and A. Kanatas, "Spatial multiplexing by decomposing the far-field of a compact ESPAR antenna," *IEEE International Symposium on Personal, Indoor and Mobile Radio Communications (PIMRC)*, Sept. 2008.

[17] O. N. Alrabadi, C. B. Papadias, A. Kalis, N. Marchetti, and R. Prasad, "MIMO transmission and reception techniques using three-element ESPAR antennas," *IEEE Commun. Lett.*, vol. 13, no. 4, pp, 236-238, Apr. 2009.

[18] M. D. Migliore, "An intuitive electromagnetic approach to MIMO communication systems," *IEEE Antennas and Propagation Mag.*, vol. 48, no. 3, June 2006.

[19] C. Oestges and B. Clerckx, *MIMO Wireless Communication, From Real-World Propagation to Space-Time Code Design*, pp. 227-230, 1st ed., 2007.

[20] R. Vaughan and J. B. Andersen, "Antenna diversity in mobile communications," *IEEE Trans. Veh. Technol.*, vol. 36, no. 4, pp. 149-172, Nov. 1987.

[21] L. Petit, L. Dussopt, and J. Laheurte, "MEMS-switched parasitic-antenna array for radiation pattern diversity," *IEEE Trans. Antennas Propagation*, vol. 54, no. 9, Sept. 2006.

[22] J. D. Kraus and R. J. Marhefka, *Antennas, for All Applications*, pages 242-246, 3rd ed., 2002.

[23] D. V. Thiel, "Switched parasitic antennas and controlled reactance parasitic antennas: a systems comparison," in *Proc. IEEE 2004 Antennas and Propagation Society International Symposium*, pp. 3211-3214, vol. 3, June 2004.

[24] M. Yamamoto, M. Taromaru, H. Sadamichi, and A. Shimizu, "Performance of angle switch diversity using ESPAR antenna for mobile reception of terrestrial digital TV," *Vehicular Technology Conference*, Fall 2006.

[25] J. Fuhl, A. F. Molisch, and E. Bonek, "Unified channel model for mobile radio systems with smart antennas," *Ins. Elect. Eng. - Radar Sonar Navigation*, vol. 145, pp. 32-34, Feb. 1998.

[26] R. Vaughan, "Switched parasitic elements for antenna diversity," *IEEE Trans. Antennas Propagations*, vol. 47, no. 2, Feb. 1999.

[27] M. Taromaru and T. Ohira, "A study on the mapping from the reactance space to equivalent weight vector space in ESPAR antenna," technical report of IEICE, RCS2002-179, pp. 43-48, Oct. 2002.

[28] A. Paulraj, R. Nabar, and D. Gore, *Introduction to Space-Time Wireless Communications*. Cambridge, U.K.: Cambridge Univ. Press, 2003.

[29] V. Barousis, A. G. Kanatas, A. Kalis, and C. Papadias, "A limited feedback technique for beamspace MIMO systems with single RF front-end," *IEEE International Symposium on Personal, Indoor and Mobile Radio Communications (PIMRC)*, Sept. 2008.

[30] S. Alamouti, "A simple transmit diversity technique for wireless communications," *IEEE J. Select. Areas Commun.*, vol. 16, pp. 1451-1458, Oct. 1998.

[31] G. Kramer, I. Maric, and R. D. Yates, *Cooperative Communications*. Now Publishers Inc., pp. 13-14.

[32] W. Wiesbeck and C. Kuhnert, *Antenna Engineering Handbook*. University of Karlsruhe, ch. 57, p. 16.

**Osama N. Alrabadi** is currently working toward his PhD at both the Center for TeleInFrastruktur (CTiF) / Aalborg University in Denmark and Athens Information Technology (AIT) in Athens, Greece. He was born in 1979 in Jordan, where he received the Diploma of Electrical Engineering from the University of Jordan (JU) in 2002. He received his Masters degree in Information and Telecommunications (MSITT) from Athens Information Technology (AIT) - Greece in 2007 with the highest honor. In 2001 he joined Orange for undergraduate training in the microwave and GSM network maintenance department. From 2002 till 2007, he has been working as a telecommunication engineer at the National Electrical Power Company (NEPCO) and the Jordan Electrical Power Company (JEPCO) in remote metering and communications. His research interests include (but not limited to) MIMO and Cognitive radio techniques, design and modeling of compact MIMO transceivers, parasitic reconfigurable arrays and smart antennas. Mr. Alrabadi is an IEEE student member and a member of the Jordan Engineering Association since 2002.

**Constantinos B. Papadias** was born in Athens, Greece, in 1969. He received the Diploma of Electrical Engineering from the National Technical University of Athens (NTUA) in 1991 and the Doctorate degree in Signal Processing (highest honors) from the Ecole Nationale Suprieure des Tlcommunications (ENST), Paris, France, in 1995. From 1992 to 1995, he was Teaching and Research Assistant at the Mobile Communications Department, Eurcom, France. In 1995, he joined the Information Systems Laboratory, Stanford University, Stanford, CA, as Post-Doctoral Researcher, working in the Smart Antennas Research Group. In November 1997 he joined the Wireless Research Laboratory of Bell Labs, Lucent Technologies, Holmdel, NJ, as Member of Technical Staff and was later promoted to Technical Manager. From 2004 to 2005 he was an adjunct Associate Professor at Columbia University. In 2006 he joined Athens Information Technology (AIT) in Athens Greece, as an Associate Professor and was later promoted to Professor. He is also currently an Adjunct Professor at Carnegie Mellon University's Information Networking Institute (INI), as well as AIT's Doctoral Program Coordinator. His research interests range from baseband wireless communications and smart antenna systems to scheduling and system-level optimization of wireless systems to cognitive radio and multihop wireless sensor networks. He has authored over 100 papers and book chapters on these topics. His distinctions include the 2002 Bell Labs President's Award, the 2003 IEEE Signal Processing Society's Young Author Best Paper Award and ESI's "most cited paper of the decade" citation in the area of wireless networks in 2006. He has also made standards contributions (most notably as the co-inventor of the Space-Time Spreading (STS) technique that was adopted by the cdma2000 wireless standard for voice transmission) and holds 9 patents. He has participated in several EU projects and is currently the Technical Coordinator of the FP7 FET project CROWN, which is in the area of cognitive radio networks. He served on the steering board of the Wireless World Research Forum (WWRF) from 2002-2006. He was a Member of the IEEE Signal Processing for Communications Technical Committee from 2002-2008, acting as its Industrial Liaison, and is currently an Associate Editor of the IEEE TRANSACTIONS ON WIRELESS COMMUNICATIONS and the JOURNAL OF COMMUNICATIONS AND NETWORKS. From 2007-2009 he was a National Representative of Greece in the FP7 program "IDEAS." Dr. Papadias is a Senior Member of the IEEE and a member of the Technical Chamber of Greece.

**Antonis Kalis** is an associate professor of AIT and an adjunct professor of Carnegie Mellon University. He received his Electrical Engineering Diploma degree in 1997 from the EE Department of the University of Patras, Greece, and joined the Lab of Electromagnetics at the University of Patras, participating in various R&D projects for the Greek Government and the European Union, as research staff. In 2000 he worked as a Research Engineer and an Assistant Research Unit Manager the Computer Technology Institute. He received his Ph.D. with honors from the University of Patras, in June 2002. His research interests are in the areas of radio communications, antenna design and wireless networks. He has numerous journal and conference publications, a US patent, and the 2000 Chester Sall award of the Consumer Electronics Society in the above areas. Antonis Kalis is a member of the Technical Chamber of Greece, and the IEEE.

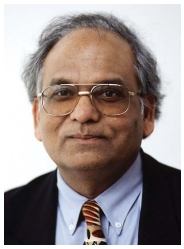

**Ramjee Prasad** is currently the Director of Center for Teleinfrastruktur (CTIF), and holds the chair of wireless information and multimedia communications. He is the project leader of several international, industrially and European Commission funded projects. He has published over 700 technical papers, contributed to several books, and has authored, coauthored, and edited thirty books. His latest book is "Introduction to Ultra Wideband for Wireless Communications".

Prof. Prasad has served as a member of the advisory and program committees of several IEEE international conferences. He has also presented keynote speeches, and delivered papers and tutorials on WPMC at various universities, technical institutions, and IEEE conferences. He was also a member of the European cooperation in the scientific and technical research (COST-231) project dealing with the evolution of land mobile radio (including personal) communications as an expert for The Netherlands, and he was a member of the COST-259 project. He was the founder and chairman of the IEEE Vehicular Technology/Communications Society Joint Chapter, Benelux Section, and is now the honorary chairman. In addition, Prof. Prasad is the founder of the IEEE Symposium on Communications and Vehicular Technology (SCVT) in the Benelux, and he was the symposium chairman of SCVT'93. Presently, he is the Chairman of IEEE Vehicular Technology/Communications/Information Theory/Aerospace and Electronics Systems/Society Joint Chapter, Denmark Section.

In addition, Prof. Prasad is the coordinating editor and editor-in-chief of the Springer International Journal on Wireless Personal Communications. He was the technical program chairman of the PIMRC'94 International Symposium held in The Hague, The Netherlands, from September 19-23, 1994 and also of the Third Communication Theory Mini-Conference in Conjunction with GLOBECOM'94, held in San Francisco, California, from November 27-30, 1994. He was the conference chairman of the fiftieth IEEE Vehicular Technology Conference and the steering committee chairman of the second International Symposium WPMC, both held in Amsterdam, The Netherlands, from September 19-23, 1999. He was the general chairman of WPMC'01 which was held in Aalborg, Denmark, from September 9-12, 2001, and of the first International Wireless Summit (IWS 2005) held also in Aalborg, Denmark on September 17-22, 2005. He is the General Chair of the First International Conference on Wireless Communication, Vehicular Technology, Information Theory and Aerospace & Electronic Systems Technology (Wireless VITAE) to be held on May 17-20, 2009 in Aalborg.

Prof. Prasad was also the founding chairman of the European Center of Excellence in Telecommunications, known as HERMES and now he is the honorary chairman. He is a fellow of IEEE, a fellow of IETE, a fellow of IEE, a member of The Netherlands Electronics and Radio Society (NERG), and a member of IDA (Engineering Society in Denmark). Prof. Prasad is advisor to several multinational companies. He has received several international awards, including the "Telenor Nordic 2005 Research Prize" (website: http://www.telenor.no/om/).

# MIMO Transmission and Reception Techniques Using Three-Element ESPAR Antennas

Osama N. Alrabadi, *Student Member, IEEE*, Constantinos B. Papadias, *Senior Member, IEEE*, Antonis Kalis, *Member, IEEE*, Nicola Marchetti, *Member, IEEE*, and Ramjee Prasad, *Fellow, IEEE*

***Abstract*—A novel scheme for spatially multiplexing two BPSK signals using a 3-element ESPAR (electronically steerable parasitic array radiator) antenna was reported in [3]. In this paper we first optimize the set of loads controlling the parasitic elements within the transmission mode by maximizing the outage capacity. We also propose different reception techniques for spatially demultiplexing real and complex signals (using the same set of loads). The proposed transmission and reception schemes are evaluated in an indoor peer-to-peer mobile ad-hoc channel via simulations, where each ad-hoc node is equipped with a 3-element ESPAR terminal.**

***Index Terms*—Ad-hoc, ESPAR, spatial (de)multiplexing.**

## I. Introduction

MIMO transmission schemes using parasitic arrays with a single RF port have recently been proposed in [1-3]. In [1], a MIMO-like realization using a single active element and a number of parasitic elements was shown to provide comparable capacity to that of conventional MIMO where the array far-field is changed on every symbol period. In [2], a novel scheme for *spatially multiplexing* two BPSK signals was introduced using a 3-element $\lambda/16$ ESPAR antenna. The scheme in [2] was further improved in [3] regarding the expansion of the ESPAR far-field into an orthonormal basis without approximation. In addition, the proposed spatial multiplexing scheme in [3] which is based on symmetrical load switching *does not* change the driving point impedance ($Z_{in}$) seen by the single active port (i.e. the matching is done only once at the design stage). The main idea in [2-3] is to map the signals directly onto an orthonormal basis within the wave-vector domain. Consequently a single analog RF front-end is required besides a simple control circuit (see Fig.1) for switching the reactances. In this paper, we first review the theory of the 3-element ESPAR in section II. Spatial multiplexing by expanding the ESPAR far-field is reviewed in section III. In section IV we optimize the set of loads for maximum outage capacity. In section V we propose different receiver techniques for *spatially demultiplexing* the signals. The transmission and reception schemes are evaluated in section VI in an indoor mobile ad-hoc channel.

Manuscript received December 23, 2008. The associate editor coordinating the review of this letter and approving it for publication was B. Chen.

O. N. Alrabadi is with the Broadband Wireless and Sensor Networks Group (BWiSE), Athens Information Technology (AIT), GR-19002, Athens, Greece (e-mail: osal@ait.edu.gr). He is also with the Center for TeleInFrastructure (CTiF), Aalborg University (AAU), 9220, Aalborg East, Denmark.

C. B. Papadias and A. Kalis are with the Broadband Wireless and Sensor Networks Group (BWiSE), Athens Information Technology (AIT), GR-19002, Athens, Greece (e-mail: {papadias, akal}@ait.edu.gr).

N. Marchetti and R. Prasad are with the Center for TeleInFrastructure (CTiF), Aalborg University (AAU), 9220, Aalborg East, Denmark (e-mail: {nm, prasad}@es.aau.dk).

Digital Object Identifier 10.1109/LCOMM.2009.082190

## II. Three-Element ESPAR Theory

The 3-element ESPAR antenna is implemented using a single active antenna element and two parasitic elements (PE) surrounding the active element at relative local angles of $0$ and $\pi$ as shown in Fig.1. The parasitic elements are short-circuited and loaded with variable reactors (varactors) that control the imaginary part of the parasitic elements' input impedances. By adjusting the varactors' response, the radiation pattern of the ESPAR antenna system is controlled. The currents on the monopoles are induced by mutual coupling with the current on the central element according to the equation $\mathbf{i} = \frac{v_s}{2Z_s}\mathbf{w}$ [4] where $v_s$ represents the transmitted voltage signal source with the amplitude and the phase from the driving RF port at the central element, $Z_s$ is the source impedance, $\mathbf{w} := [\mathbf{Z}+\mathbf{X}]^{-1}\mathbf{u}_0$ is the "*equivalent weight vector*" [4] and $\mathbf{Z}$ is the mutual impedance matrix given by

$$\mathbf{Z} = \begin{pmatrix} Z_{00} & Z_{01} & Z_{01} \\ Z_{01} & Z_{11} & Z_{12} \\ Z_{01} & Z_{12} & Z_{11} \end{pmatrix}$$

where we assumed $Z_{ij} = Z_{ji}$, $\{i,j\} \in \{0,1,2\}$ due to the structure symmetry. $\mathbf{X}$ is a diagonal matrix defined as $\mathbf{X} := diag([Z_0 \; jX_{L1} \; jX_{L2}])$, where $Z_0$ is the characteristic impedance of $50\Omega$ (equal to the source impedance $Z_s$ at the central active port for matching purposes), while $jX_{Li}$ is the loading of the $i^{th}$ parasitic element, and finally $\mathbf{u}_0$ is a selection vector defined as $\mathbf{u}_0 := [\; 1 \;\; 0 \;\; 0 \;]^T$ [4]. The far-field current signal in the azimuthal direction $\theta$ with its amplitude and the phase is represented as $G(\theta) = \mathbf{i}^T a(\theta)$. The steering vector $a(\theta)$ is defined based on the array geometry (see Fig.1) as $a(\theta) := \left[\; 1 \;\; e^{-jkd\cos(\theta-0)} \;\; e^{-jkd\cos(\theta-\pi)} \;\right]^T$, where $k = \frac{2\pi}{\lambda}$ is the wavenumber and $d$ is the the ESPAR inter-element spacing.

## III. Spatial Multiplexing of BPSK Signals

The embedded element patterns of the 3-element ESPAR antenna can be combined so that the array factor is expanded into an orthogonal *basis*. We first write the array factor ($AF$) of the three-element ESPAR antenna as [5]:

$$AF = I_{in}\left(1 + \alpha_{10}e^{-jkd\cos(\theta-0)} + \alpha_{20}e^{-jkd\cos(\theta-\pi)}\right), \tag{1}$$

where $I_{in}$ is the input signal to be fed into the active element (driven monopole). The $AF$ depends on the relative ratios of

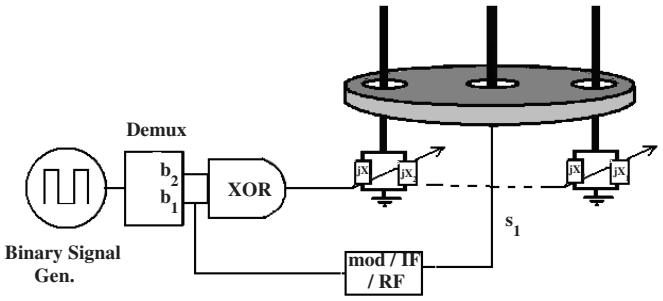


Fig. 1. Simplified 3-element ESPAR control circuit.

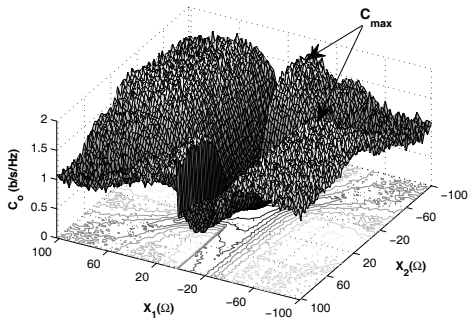


Fig. 2. The 10% outage capacity at SNR of 10dB versus the two reactive loadings $jX_{L1}$ and $jX_{L2}$. The maximum outage capacity $C_{\max}$ is shown at $[-j4 \quad -j60]\,\Omega$ and $[-j60 \quad -j4]\,\Omega$.

the currents induced on the monopoles rather than the currents themselves. The coefficients $\alpha_{10}$ and $\alpha_{20}$ are calculated as in [5] to be

$$\alpha_{10} = \left(\frac{I_1}{I_0}\right) = \frac{Z_{12}Z_{01} - Z_{01}\left(Z_{11} + jX_{L2}\right)}{\left(Z_{11} + jX_{L1}\right)\left(Z_{11} + jX_{L2}\right) - Z_{12}^2},$$
$$\alpha_{20} = \left(\frac{I_2}{I_0}\right) = \frac{Z_{12}Z_{01} - Z_{01}\left(Z_{11} + jX_{L1}\right)}{\left(Z_{11} + jX_{L1}\right)\left(Z_{11} + jX_{L2}\right) - Z_{12}^2}.$$

By expanding the $AF$ in Eq.(1) using Euler's formula we get

$$AF = I_{in}\underbrace{\left(1 + (\alpha_{10} + \alpha_{20})\cos(kd\cos(\theta))\right)}_{B_1(\theta)} - \underbrace{j\,(\alpha_{10} - \alpha_{20})\sin(kd\cos(\theta))}_{B_2(\theta)}. \quad (2)$$

Notice that in Eq.(2) $B_1(\theta) \perp B_2(\theta)$ irrespective of $\alpha_{10}$ and $\alpha_{20}$. This is because the $\sin(kd\cos(\theta))$ pattern is orthogonal to both the omni pattern (the term 1) and to the $\cos(kd\cos(\theta))$ pattern. Mapping two BPSK signals $s_1$ and $s_2$ onto the basis is done as follows:

$$\begin{aligned} AF &= s_1 B_1(\theta) + s_2 B_2(\theta) \\ &= s_1\left(B_1(\theta) + \frac{s_2}{s_1}B_2(\theta)\right) \\ &= I_{in}\left(B_1(\theta) + ((-1)^{b_1 \oplus b_2} B_2(\theta)\right). \end{aligned} \quad (3)$$

Fig.1 shows a simple control circuit for spatially multiplexing two BPSK signals using the 3-element ESPAR array. The first BPSK sub-stream ($s_1 = I_{in}$) is fed into the single active port after being modulated and up-converted. The second sub-stream ($s_2$) is *XOR*-ed with the first in the binary domain ($b_1 \oplus b_2$) and the output control signal is used for binary switching between the two reactances $jX_{L1}$ and $jX_{L2}$ (i.e. selecting $[jX_{L1} \;\; jX_{L2}]$ when $b_1 \oplus b_2 = 0$ and $[jX_{L2} \;\; jX_{L1}]$ when $b_1 \oplus b_2 = 1$). Notice that $(\alpha_{10} - \alpha_{20})$ at $[jX_{L1} \;\; jX_{L2}]$ becomes $(\alpha_{20} - \alpha_{10})$ at $[jX_{L2} \;\; jX_{L1}]$.

## IV. Load Optimization

The reactive loads that control $\alpha_{10}$ and $\alpha_{20}$ can be *jointly optimized* with respect to some parameters e.g. the maximum radiated power or the maximum mutual information [6]. In this paper we are interested in maximizing the outage capacity as being a figure of merit in slow fading MIMO communications. Notice that the open-loop capacity is maximized when the *power imbalance* between the two angular basis $B_1(\theta)$ and $B_2(\theta)$ is made close to 0dB and the *matching efficiency* is made close to unity. The correlation between the signals is already nulled due to the orthogonality of the basis and does not consequently affect the capacity. The effects of these parameters can be considered all together *by using the exact ESPAR far-field pattern* normalized with respect to a reference isotropic source.[1] The outage capacity is calculated using the well-known $\log\det$ formula [7] for open loop transmission which is a Gaussian signaling capacity expression. In this paper we assume that a strong long code, that makes the distribution of the input BPSK signaling look Gaussian, is used for attaining the theoretical upper-bound. We use the same ESPAR antenna as in [8] at the transmitter side, i.e. a 3-element ESPAR with $\lambda/10$ inter-element spacing, and a single omni receiver at the other side of the link. An exhaustive search was conducted through which the reactive loads were scanned from $-j100\Omega$ up to $j100\Omega$ with a step of $j\Omega$. The $10\%$ outage capacity at SNR of 10dB was found at every loading within an indoor environment described by a 2-D geometrically based elliptical single bounce channel model as that described in [10]. Fig.2 shows the $10\%$ outage capacity versus the PE loadings. A maximum $10\%$ outage capacity of $1.9144$ b/s/Hz is obtained at a loading of $[jX_{L1} \;\; jX_{L2}] = [-j4 \;\; -j60]\,\Omega$. At such loading, a matching efficiency of $95\%$ and a power imbalance between the angular basis of $0.4$ dB are obtained.

## V. Receiver Techniques

The 3-element ESPAR could also function as a MIMO receiver for spatially demultiplexing the signals. A simple reception scheme is to demultiplex two real signals via IQ-separation i.e. the I-channel is separated from the Q-channel. This gives at the receiver two independent equations to solve for the two unknown signals $s_1$ and $s_2$. The complex vector $\mathbf{h} = [h_1 \;\; h_2]$ is transformed after the IQ-separation into a real matrix $\mathbf{H} = \begin{bmatrix} \Re\{h_1\} & \Re\{h_2\} \\ \Im\{h_1\} & \Im\{h_2\} \end{bmatrix}$, where the $\Re\{.\}$ operator returns the real part of the operand while the $\Im\{.\}$ operator returns the imaginary part of the operand and $h_i$ is

[1]Notice that the mutual coupling is taken into account within the far-field pattern before normalizing, where the currents are calculated from the mutual impedance matrix $\mathbf{Z}$. The normalization is done with respect to a reference SISO link with two isotropic sources at both ends of the communication link. The isotropic sources are obtained by loading the ESPAR PE's with 2k$\Omega$ each [9].

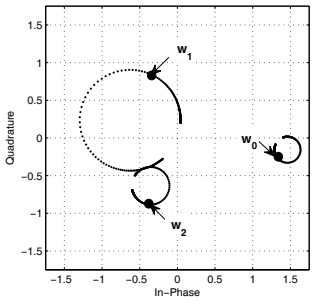


Fig. 3. Equivalent weight vectors $\mathbf{w}_i$ at $jX_1 = -j4\Omega$.

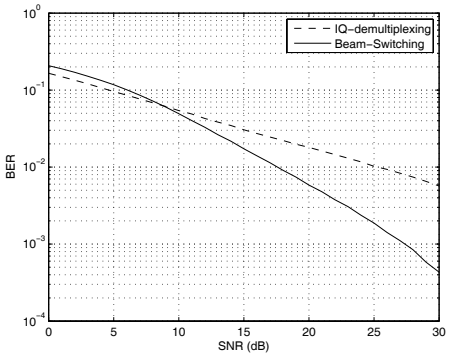


Fig. 4. Performance of IQ-demultiplexing technique versus beam-switching demultiplexing technique using 3-element $\lambda/10$ ESPAR antennas at both ends of the communication link for spatially (de)multiplexing 2 BPSK signals.

the response of the receiver omni pattern to the $i^{th}$ transmit angular basis. Despite simplicity, the IQ-separation scheme suffers from some drawbacks, e.g the scheme is restricted to real signals; the transmit diversity order extracted by the receiver is reduced; and the average signal to noise ratio (SNR) at the receiver is split between the two channels. An alternative demultiplexing scheme is to switch the receiver radiation pattern between two beams during each symbol period. Each beam samples different part of the space and collects consequently independent spatial samples of the received signal. Notice that the 3-element ESPAR can create at most three independent complex patterns (equal to the number of array elements) and consequently demultiplex up to three complex signals, or six real signals via extra IQ-separation [11]. However, switching the beam patterns every half of the symbol period doubles the signal bandwidth (at the receiver side), which in turn doubles the Gaussian noise power at the receiver front-end. The signal model may be described as

$$\mathbf{y} = \frac{1}{\sqrt{2}} \begin{bmatrix} h_{G_1B_1} & h_{G_1B_2} \\ h_{G_2B_1} & h_{G_2B_2} \end{bmatrix} \begin{bmatrix} s_1 \\ s_2 \end{bmatrix} + \sqrt{2} \begin{bmatrix} n_1 \\ n_2 \end{bmatrix}, \quad (4)$$

where $h_{G_iB_j}$ is the response of the $i^{th}$ receiving beam $G_i$ to the $j^{th}$ basis function $B_j$, and $n_i$ is the Gaussian noise collected within half of the symbol period. The factor $\frac{1}{\sqrt{2}}$ is due to integrating each beam over half of the symbol period while the factor $\sqrt{2}$ is due to the doubling of the bandwidth. For design simplicity, the two optimal reactances for the transmission mode are also used for the reception mode i.e. $G_1(\theta) = B_1(\theta) + B_2(\theta)$ and $G_2(\theta) = B_1(\theta) - B_2(\theta)$, where each beam has a gain of $4.3$ dBi. Notice that the two reactances are quite close to the optimal loads of $[0\ -j60]\,\Omega$ used in [8] for reception pattern diversity. This is verified in the scatter plot of the equivalent weight vector $\mathbf{w}_i, i \in \{0, 1, 2\}$ as shown in Fig.3. The black dot on the $\mathbf{w}_0$ curve is the one corresponding to the optimal transmit loading, which is close to the optimal matching point $1 + j0$ [8] while the black dots on the $\mathbf{w}_1$ and $\mathbf{w}_2$ curves are well apart so that both $G_1$ and $G_2$ are weakly correlated.

## VI. Results

The same channel model as in section IV is used for evaluating the performance of the transmission and reception schemes. Two nodes equipped with 3-element $\lambda/10$ ESPAR antennas are communicating within a peer-to-peer link at an operating frequency of $2.4$ GHz. The two nodes are located at the foci of an ellipse with a $16$m separation distance and $0.7$ eccentricity and surrounded by twelve scatterers [10]. The first node spatially multiplexes two BPSK signals and the second demultiplexes the signals using the proposed reception schemes with the optimal set of loads. Fig.4 shows that the beam-switching reception technique outperforms its counterpart (IQ-Separation) at medium and high SNR regimes as it extracts a higher diversity gain. At low SNR, IQ-Separation performs better as the performance is dominated by the noise level. Indeed, the IQ-separation collects only half the noise power collected by the beam-switching technique.

## References

[1] M. Wennstrom and T. Svantesson, "An antenna solution for MIMO channels: the switched parasitic antenna," in *Proc. IEEE 12th Int. Symp. Personal, Indoor and Mobile Radio Communications*, Sept. 2001, vol. 1, pp. A-159-A-163.

[2] A. Kalis, A. G. Kanatas, and C. B. Papadias, "A novel approach to MIMO transmission using a single RF front end," *IEEE J. Select. Areas Commun.*, vol. 26, no. 6, Aug. 2008.

[3] O. N. Alrabadi, A. Kalis, C. Papadias, and A. Kanatas, "Spatial multiplexing by decomposing the far-field of a compact ESPAR antenna," in *Proc. IEEE International Symposium on Personal, Indoor and Mobile Radio Communications (PIMRC)*, Sept. 2008.

[4] K. Gyoda and T. Ohira, "Design of electronically steerable passive array radiator (ESPAR) antennas," in *Proc. IEEE Antennas and Propagation Society International Symposium*, vol. 2, July 2000, pp. 922-925.

[5] L. Petit, L. Dussopt, and J. Laheurte, "MEMS-switched parasitic-antenna array for radiation pattern diversity," *IEEE Trans. Antennas and Propag.*, vol. 54, no. 9, Sept. 2006.

[6] R. Bains, A. Kalis, and R. Muller, "On the link performance of a proposed compact antenna system," *IEEE Commun. Lett.*, vol. 12, no. 10, Oct 2008.

[7] G. J. Foschini and M. J. Gans,"Limits of wireless communication in a fading environment when using multiple antennas," *Wireless Personal Commun.*, vol. 6, pp. 311-335, 1998.

[8] M. Taromaru, T. Ohira, K. Iigusa, and K. Kato, "Reactance diversity: a novel and ultimate-low-cost antifading reception scheme with a binary-controlled 3-element ESPAR antenna," in *Proc. Asia-Pacific Microwave Conf.*, FB7-3, pp. 1660-1663, Seoul, Nov. 2003.

[9] J. Cheng, M. Hashiguchi, K. Iigusa, and T. Ohira, "Electronically steerable parasitic array radiator antenna for omni- and sector pattern forming applications to wireless ad hoc networks", *IEE Proc.-Microw. Antennas Propag.* vol. 150, no. 4, Aug. 2003.

[10] J. Fuhl, A. F. Molisch, and E. Bonek, "Unified channel model for mobile radio systems with smart antennas," *Ins. Elect. Eng. - Radar Sonar Navigation*, vol. 145, pp. 32-4, Feb. 1998.

[11] W. Li and P. Liu "Blind separation of BPSK sources by electrically steerable parasitic array radiator," in *Proc. IEEE Int. Workshop VLSI Design & Video Tech.*, Suzhou, China, May 2005.

# Spatial Multiplexing via Antenna Switching

Osama N. Alrabadi, *Student Member, IEEE*, Constantinos B. Papadias, *Senior Member, IEEE*, Antonis Kalis, *Member, IEEE*, Nicola Marchetti, *Member, IEEE*, and Ramjee Prasad, *Fellow, IEEE*

***Abstract*—A simple scheme for spatially multiplexing two BPSK signals using a switched antenna system with a single RF chain, a shared RF-DC cable and a shared RF-DC feeding circuit is proposed. The idea is to modulate the first BPSK substream to one of the two array elements while exciting the second element parasitically by the field of the first one. The second substream is encoded in such a way to control which of the two elements will be driven. Decorrelating the two BPSK signals at the transmitter side is achieved by mapping the signals onto a set of orthogonal functions while the matching impedance of the two antenna elements is optimized for the maximum outage rate by maximizing the matching efficiency and minimizing the power imbalance between the basis functions, simultaneously.**

***Index Terms*—Antenna switching, spatial multiplexing, shared RF-DC.**

## I. Introduction

MIMO transmission and reception techniques using compact parasitic arrays have recently been reported in [1-3], where the array far-field is changed according to the input set of signals. In [1-2] a simple spatial multiplexing scheme using a compact 3-element symmetrical ESPAR antenna was implemented by decomposing the ESPAR far-field into two basis functions. The main idea is to feed the first substream into the single active port while encoding the second substream with respect to the first substream and using the output control signal for swapping the reactive loads of the parasitic elements, say between $[jX_1\, jX_2]$ and $[jX_2\, jX_1]$. The scheme in [1-2] is superior to that in [3] in the sense that the array matching efficiency *does not* change when swapping the two loads (hence the matching efficiency is optimized only once at the design stage). Although the scheme in [1-2] could address the main limitations regarding the integration of a second active antenna in the user equipment (UE) (e.g. the cost of multiple RF chains, the limited array area, the high signal correlation and the degraded matching efficiency), the scheme suffers from some caveats as *three* antenna elements (one active and two passive) are required for transmitting *two* BPSK signals and the need for a separate DC feeding circuit and a separate DC cable for swapping the loads. On the other hand, a parasitic array of two elements (one active and one passive) was shown to have two degrees of freedom (DoF) [4] in terms of the number of the basis functions composing its far-field [1]. However, the scheme in [1] was unable to access the two DoF of the 2-element parasitic array as detuning the single parasitic element (so as to create the desired linear combination of the basis functions) *distorts* the basis onto which the symbols are mapped! In this paper we propose a novel scheme for mapping two BPSK signals onto a set of two basis functions using the 2-element array. The idea is to use the first BPSK substream for modulating one of the two array elements and exciting the other element parasitically by the field of the active one. The second substream is encoded in such a way to control which of the two elements will be driven. The aforementioned functionality is supported by a novel shared RF-DC feeding network architecture and a shared RF-DC cable as in the ShRiquen antenna [5], for driving and switching the two antenna elements. Throughout the paper, a small letter designates a scalar; a bold small letter designates a vector; a bold big letter designates a matrix; an Euler-font letter designates a complex 3D pattern and a bold Euler-font letter designates a vector of 3D complex patterns. The operators $()^*, ()^T, ()^H$ designate complex conjugate, transpose and complex conjugate transpose (Hermitian) operators, respectively. The rest of the paper is organized as follows: in section II the theory of the 2-element array is introduced. Section III proposes a simple spatial multiplexing scheme using a single RF-frontend and a shared RF-DC feeding circuit. An analysis regarding the mutual information of the proposed scheme is addressed in section IV and finally a practical numerical example using an accurate electromagnetic simulator is given in section V. Finally the paper concludes with our results.

## II. Theory of a Two-Element Parasitic Array

In this paper we consider an arbitrary array of two antenna elements that can be dipoles, printed dipoles, fractal antennas, slot antennas, etc. If we assume that each of the two antenna elements is matched by the impedance $\dot{Z}_M$ (balanced uncoupled matching), then the array admittance matrix when taking the matching loads into account is written as

$$\mathbf{Y}_T = \left( \underbrace{\begin{bmatrix} \dot{Z}_M & 0 \\ 0 & \dot{Z}_M \end{bmatrix}}_{\dot{\mathbf{Z}}_M} + \underbrace{\begin{bmatrix} Z_{11} & Z_{12} \\ Z_{12} & Z_{11} \end{bmatrix}}_{\mathbf{Z}} \right)^{-1} = \begin{pmatrix} Y_{11} & Y_{12} \\ Y_{12} & Y_{11} \end{pmatrix}, \tag{1}$$

Manuscript received April 27, 2009. The associate editor coordinating the review of this letter and approving it for publication was F. Jondral.

O. N. Alrabadi is with the Broadband Wireless and Sensor Networks Group (BWiSE), Athens Information Technology (AIT), GR-19002, Athens, Greece (e-mail: osal@ait.edu.gr). He is also with the Center for TeleInFrastructure (CTiF), Aalborg University (AAU), 9220, Aalborg East, Denmark (e-mail: ona@es.aau.dk).

C. B. Papadias and A. Kalis are with the Broadband Wireless and Sensor Networks Group (BWiSE), Athens Information Technology (AIT), GR-19002, Athens, Greece (e-mail: {papadias, akal}@ait.edu.gr).

N. Marchetti and R. Prasad are with the Center for TeleInFrastructure (CTiF), Aalborg University (AAU), 9220, Aalborg East, Denmark (e-mail: {nm, prasad}@es.aau.dk).

Digital Object Identifier 10.1109/LCOMM.2009.090971

where $\dot{\mathbf{Z}}_M = \dot{Z}_M \mathbf{I}_2$ ($\mathbf{I}_2$ is the $2\times 2$ identity matrix). $Z_{ij} = Z_{ji}$ and $Y_{ij} = Y_{ji}$, $\{i,j\} \in \{1,2\}$ are the elements of the mutual impedance matrix $\mathbf{Z}$ and the elements of the admittance matrix $\mathbf{Y}_T$, respectively. The far-field can be written as $\mathcal{G}_T(\theta,\phi) = \boldsymbol{G}_{\text{iso}}(\theta,\phi)\,\mathbf{Y}_T\mathbf{v}_s$, where $\theta$ and $\phi$ are the observation angles in the elevation and azimuth planes, respectively. $\boldsymbol{G}_{\text{iso}}(\theta,\phi) = [\mathcal{G}_{\text{iso1}}(\theta,\phi)\ \ \mathcal{G}_{\text{iso2}}(\theta,\phi)]$ is the vector of the isolated element patterns (i.e. the pattern of each element when the others are open) and $\mathbf{v}_s$ is the vector of the RF voltage signals. $\mathbf{Y}_T$ in Eq.(1) is a Toeplitz symmetric matrix, hence its eigenvectors are orthonormal. Let $\mathbf{U}_T$ be a matrix the columns of which are the eigenvectors of $\mathbf{Y}_T$ and $\mathbf{\Lambda}_T$ be a diagonal matrix the elements of which are the eigenvalues of $\mathbf{Y}_T$; then for the given $\mathbf{Y}_T$ we get $\mathbf{U}_T = \frac{1}{\sqrt{2}}\begin{bmatrix} 1 & 1 \\ -1 & 1 \end{bmatrix}$ and $\mathbf{\Lambda}_T = \text{diag}([Y_1\ Y_2])$ such that $Y_1 = Y_{11} + Y_{12}$ and $Y_2 = Y_{11} - Y_{12}$. The array far-field can be decomposed into two basis functions as follows:

$$\begin{aligned}\mathcal{G}_T(\theta,\phi) &= \boldsymbol{G}_{\text{iso}}(\theta,\phi)\,\mathbf{U}_T\mathbf{\Lambda}_T\mathbf{U}_T^H\mathbf{v}_s,\\ &= \boldsymbol{E}_T(\theta,\phi)\,\mathbf{\Lambda}_T\mathbf{U}_T^H\mathbf{v}_s,\\ &= \boldsymbol{B}_T(\theta,\phi)\,\mathbf{U}_T^H\mathbf{v}_s,\\ &= \boldsymbol{B}_T(\theta,\phi)\,\mathbf{v}_m, \end{aligned} \tag{2}$$

where

$$\boldsymbol{B}_T(\theta,\phi) = \boldsymbol{E}_T(\theta,\phi)\,\mathbf{\Lambda}_T = [\mathcal{B}_1(\theta,\phi)\ \ \mathcal{B}_2(\theta,\phi)], \tag{3a}$$

$$\boldsymbol{E}_T(\theta,\phi) = \boldsymbol{G}_{\text{iso}}(\theta,\phi)\,\mathbf{U}_T = [\mathcal{E}_1(\theta,\phi)\ \ \mathcal{E}_2(\theta,\phi)], \tag{3b}$$

$$\mathbf{v}_m = \mathbf{U}_T^H\mathbf{v}_s = [v_1\ \ v_2]^T, \tag{3c}$$

where $\mathbf{v}_m$ is the vector of the mode voltages $v_k, k \in \{1,2\}$. $\boldsymbol{E}(\theta,\phi)$ is the vector of the eigenpatterns $\mathcal{E}_k(\theta,\phi), k \in \{1,2\}$ [6] such that

$$\oint_\Omega \mathcal{E}_1(\Omega)\mathcal{E}_2^*(\Omega) f(\Omega)\cdot d\Omega = 0, \ \text{ s.t. } \ f(\Omega) = 1/4\pi, \tag{4}$$

where $f(\Omega)$ is the 3D angular power spectra (APS) of the channel, whereas $\Omega$ is the solid angle. Eq.(4) states that the two eigenpatterns are orthogonal either in the free-space or in a fully-scattered channel. Finally $\boldsymbol{B}_T(\theta,\phi)$ is the vector of the basis functions $\mathcal{B}_k(\theta,\phi), k \in \{1,2\}$ defined as a scaled version of the $k^{th}$ eigenpattern (scaled by $Y_k$) as per Eq.(3a) as follows:

$$\begin{aligned}\mathcal{B}_1(\theta,\phi) &= Y_1\mathcal{E}_1(\theta,\phi) = Y_1\frac{\mathcal{G}_{\text{iso1}}(\theta,\phi) - \mathcal{G}_{\text{iso2}}(\theta,\phi)}{\sqrt{2}},\\ \mathcal{B}_2(\theta,\phi) &= Y_2\mathcal{E}_2(\theta,\phi) = Y_2\frac{\mathcal{G}_{\text{iso1}}(\theta,\phi) + \mathcal{G}_{\text{iso2}}(\theta,\phi)}{\sqrt{2}}. \end{aligned} \tag{5}$$

## III. Spatial Multiplexing of Two BPSK Signals

Till now we have shown that the far-field of the 2-element array is a linear combination of the two basis functions $\mathcal{B}_1(\theta,\phi)$ and $\mathcal{B}_2(\theta,\phi)$, (see Eq.(2) and Eq.(3a)), onto which the two mode voltages $v_k, k \in \{1,2\}$ are mapped. For a fixed $\mathbf{Y}_T$ (fixed array topology and fixed $\dot{Z}_M$), the linear combination of the basis is controlled only by the set of the mode voltages $\mathbf{v}_m$. Let the 2-element array be driven by a single feeding RF voltage signal. If we simply switch the input voltage vector $\mathbf{v}_s$ from $[v_s\ 0]^T$ where the first element is driven and the second is parasitically excited by the field of the first to $[0\ v_s]^T$ where the second element is driven and the first is parasitically excited by the field of the second element; the mode voltages switch consequently from $\mathbf{v}_m = \left[v_s/\sqrt{2}\ \ v_s/\sqrt{2}\right]^T$ to $\mathbf{v}_m = \left[v_s/\sqrt{2}\ \ -v_s/\sqrt{2}\right]^T$ as per Eq.(3c). According to the antenna elements' state $S \in \{0,1\}$ ($S = 0$ refers to the state when the first antenna element is active and the second is passive; the inverse for $S = 1$), the far-field becomes function of the antenna state as follows

$$\begin{aligned}\mathcal{G}_T(\theta,\phi) &= v_1\mathcal{B}_1(\theta,\phi) + v_2\mathcal{B}_2(\theta,\phi),\\ &= \frac{1}{\sqrt{2}}v_s\left(\mathcal{B}_1(\theta,\phi) + (-1)^S\mathcal{B}_2(\theta,\phi)\right),\\ &= s_1\mathcal{B}_1(\theta,\phi) + s_2\mathcal{B}_2(\theta,\phi), \end{aligned} \tag{6}$$

where two independent BPSK signals $\left(s_1 = \frac{v_s}{\sqrt{2}}\right)$ and $\left(s_2 = \frac{v_s}{\sqrt{2}}(-1)^S\right)$ are mapped onto the two basis functions. The result is welcome in the sense that a switched antenna system with a single RF-frontend can be used for mapping two BPSK signals onto the proposed basis. Fig. 1 shows a switched antenna system with two symmetrical antenna elements where the state $S$ is obtained by XOR-ing the bit streams ($b_1$ and $b_2$) in the binary domain i.e. $S := b_1 \oplus b_2$. The first bit stream is modulated to $s_1 = \frac{v_s}{\sqrt{2}}$ and up-converted while the output state $S$ controls the polarity of the DC source. When the DC source is positive ($S = 0$), the varactor diodes $D_1$ and $D_4$ are forward-biased and the varactor diodes $D_2$ and $D_3$ are reverse-biased. Consequently the first antenna element is driven by $s_1$ and the second is parasitically excited by the field of the first antenna element and the inverse scenario takes place when $S = 1$ (notice that both of the antenna elements are matched by $\dot{Z}_M = Z_M + Z_o$ irrespective of the diodes state $S$, where $Z_o$ is the characteristic impedance of the RF-DC cable).

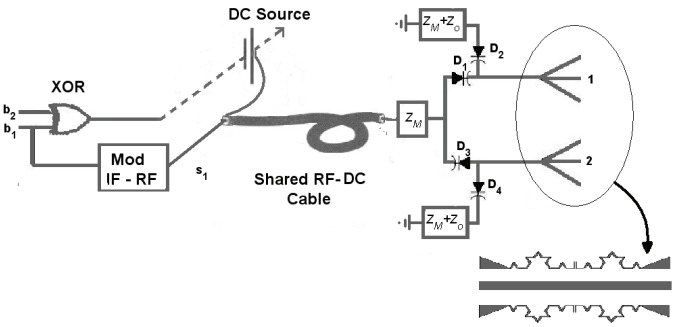


Fig. 1. A switched antenna system with a single RF-frontend, a shared RF-DC feeding circuit and a shared RF-DC cable. An array of two fractal dipoles with a common reflector is proposed as an example of two closely-coupled antennas (see section V).

## IV. Mutual Information Analysis

A simple analytical model regarding the mutual information of the proposed scheme is introduced in this section. We consider a system where the transmitter is equipped with a switched antenna system as shown in Fig. 1 whereas the receiver is equipped with two (active) antenna elements. The $2 \times 2$ spatial channel matrix $\mathbf{H}$ when taking the mutual coupling and the open-circuit correlation at both sides of the communication link may be expanded [7] as $\mathbf{H} =$

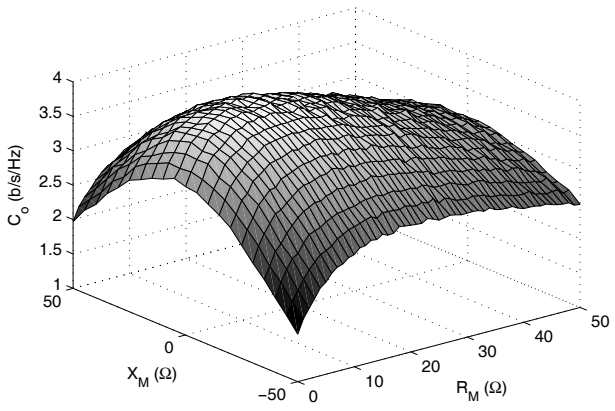


Fig. 2. $10\%$ outage rate assuming Gaussian signaling.

$\mathbf{M}_R \left(\eta_R \mathbf{R}_R\right)^{1/2} \mathbf{H}_w \left(\eta_T \mathbf{R}_T\right)^{1/2} \mathbf{M}_T$, where $\mathbf{M}_R, \mathbf{R}_R$ are the receiver coupling and open-circuit correlation matrices respectively and $\eta_R$ is the receiver efficiency. $\mathbf{M}_T, \mathbf{R}_T$ are the transmitter coupling and open-circuit correlation matrices respectively and $\eta_T$ is the transmitter efficiency. The transmitter coupling matrix is given by $\mathbf{M}_T = 2Z_o \mathbf{Y}_T$ and finally $\mathbf{H}_w$ is a matrix the elements of which are zero mean circularly symmetric complex Gaussian variables (ZMCSCGV). The received signal vector $\mathbf{y}$ can be written as

$$\begin{aligned}
\mathbf{y} &= \mathbf{M}_R \left(\eta_R \mathbf{R}_R\right)^{1/2} \mathbf{H}_w \left(\eta_T \mathbf{R}_T\right)^{1/2} \mathbf{M}_T \mathbf{v}_s + \mathbf{n}, \\
&= 2Z_o \mathbf{M}_R \left(\eta_R \mathbf{R}_R\right)^{1/2} \mathbf{H}_w \left(\eta_T \mathbf{R}_T\right)^{1/2} \mathbf{Y}_T \mathbf{v}_s + \mathbf{n}, \\
&= 2Z_o \mathbf{M}_R \left(\eta_R \mathbf{R}_R\right)^{1/2} \mathbf{H}_w \left(\eta_T \mathbf{R}_T\right)^{1/2} \mathbf{U}_T \mathbf{\Lambda}_T \mathbf{U}_T^H \mathbf{v}_s + \mathbf{n}, \\
&= 2Z_o \mathbf{M}_R \left(\eta_R \mathbf{R}_R\right)^{1/2} \mathbf{H}_w \left(\eta_T \mathbf{R}_T\right)^{1/2} \mathbf{U}_T \mathbf{\Lambda}_T \mathbf{v}_m + \mathbf{n}, \\
&= \mathbf{H}_T \mathbf{v}_m + \mathbf{n}, \qquad (7)
\end{aligned}$$

where $\mathbf{n}$ is the noise vector assumed ZMCSCGV, and $\mathbf{H}_T := 2Z_o \mathbf{M}_R \left(\eta_R \mathbf{R}_R\right)^{1/2} \mathbf{H}_w \left(\eta_T \mathbf{R}_T\right)^{1/2} \mathbf{U}_T \mathbf{\Lambda}_T$. The mutual information when no channel state information (CSI) is available at the transmitter is upper bounded [8] as [1]

$$\mathcal{I} \;\leq\; \log_2 \det \left( \mathbf{I}_2 + \frac{\rho}{N_T} \mathbf{H}_T \mathbf{Q} \mathbf{H}_T^H \right), \qquad (8)$$

where $N_T$ is the number of the eigenmodes (the two basis functions or the two eigenpattens); and $\rho$ is the average received signal to noise ratio (SNR) per antenna. $\mathbf{Q}$ is the power distribution across the two modes, hence $\mathbf{Q} = \mathbf{I}_2$ as per Eq.(3c) i.e. the power is uniformly distributed across the two basis functions.

## V. Practical Example

In this example we consider a uniform 3D-APS which is a reasonable assumption when assuming many scatterers in a full angular spread. The transmitter is equipped with a switched antenna system composed of two fractal antenna elements as shown in Fig. 1, where a common reflector is intentionally inserted in the middle so that the two isolated element patterns $\mathcal{G}_{\text{iso1}}(\theta, \phi)$ and $\mathcal{G}_{\text{iso2}}(\theta, \phi)$ are decorrelated. Notice from Eq.(5) that the basis function $\mathcal{B}_1(\theta, \phi)$ will eventually vanish if both $\mathcal{G}_{\text{iso1}}(\theta, \phi)$ and $\mathcal{G}_{\text{iso2}}(\theta, \phi)$ become highly correlated [6]. The transmit antenna system is characterized by $Z_{11} = 4.986 - j0.7155\Omega$ and $Z_{12} = 1.147 - j17.07\Omega$. The *maximum* array length (as the inter-element spacing is not uniform) is about $0.2\lambda$, and the operating frequency is $4$ GHz. The isolated element patterns are obtained using an accurate electromagnetic simulator [9] and the transmit open-circuit correlation matrix under the given channel conditions is found to be $\mathbf{R}_T = \begin{bmatrix} 1 & 0.4618 - j0.1874 \\ 0.4618 + j0.1874 & 1 \end{bmatrix}$. The transmitter employs the proposed scheme for spatially multiplexing two BPSK signals, whereas the access point is assumed to have two largely spaced and optimally matched antenna elements (hence $\mathbf{M}_R = \mathbf{I}_2$ and $\eta_R = 100\%$) and surrounded by many scatterers (hence $\mathbf{R}_R = \mathbf{I}_2$ too). The real part of the matching impedance $R_M$ was changed from $0\Omega$ up to $50\Omega$ with a step of $1\Omega$ and the imaginary part $X_M$ from $-50\Omega$ up to $50\Omega$ with a step $5\Omega$. At every loading, 10,000 channel realizations were taken and the $10\%$ outage rate was found as shown in Fig. 2 at an SNR of $10$ dB. The optimal matching impedance $Z_M^{opt}$ is considered to be the one that maximizes the $10\%$ outage rate as being a figure of merit when considering flat-fading or quasi-static MIMO channels (as in [2]). For the given antenna system, $Z_M^{opt}$ is found to be $15 + j0\Omega$, at which the maximum outage rate is $3.95$ b/s/Hz; the transmitter efficiency is $78\%$ and the power imbalance between the basis is $-0.48$ dB

## VI. Conclusion

A novel spatial multiplexing scheme based on antenna switching was proposed. The outage performance of a compact switched-antenna system with a single RF chain is evaluated and shown to be comparable to a system equipped with two active antennas, yet the proposed scheme is limited to BPSK signaling.

[1] The upper bound is achieved when the distribution of the input is Gaussian [8].

## References


[1] O. N. Alrabadi, A. Kalis, C. B. Papadias, and A. Kanatas, "Spatial multiplexing by decomposing the far-field of a compact ESPAR antenna," in *Proc. IEEE International Symposium on Personal, Indoor and Mobile Radio Communications (PIMRC)*, Sept. 2008, pp, 1-5.

[2] O. N. Alrabadi, C. B. Papadias, A. Kalis, N. Marchetti, and R. Prasad "MIMO transmission and reception techniques using three-element ESPAR antennas," *IEEE Commun. Lett.*, vol. 13, no. 4, pp. 236-238, Apr. 2009.

[3] A. Kalis, A. G. Kanatas, and C. B. Papadias, "A novel approach to MIMO transmission using a single RF front end," *IEEE J. Select. Areas Commun.*, vol. 26, no. 6, Aug. 2008.

[4] M. D. Migliore, "An intuitive electromagnetic approach to MIMO communication systems," *IEEE Antennas and Propagation Mag.*, vol. 48, no. 3, June 2006.

[5] K. Iigusa, M. Yamamoto, T. Sawaya, K. Kato, M. Taromaru, and T. Ohira, "RF- and DC-line share ring frequency controllable antenna," *IEEE Antennas and Propagation Society International Symposium*, 2005.

[6] H. J. Chalaupka and X. Wang, "On the properties of small arrays with closely spaced antenna elements," *IEEE Antennas and Propagation Society International Symposium*, 2004.

[7] M. L. Morris and A. Jensen, "Network model for MIMO systems with coupled antennas and noisy amplifiers," *IEEE Trans. Antennas and Propagation*, vol. 53, no. 1, Jan. 2005.

[8] I. E. Telatar, "Capacity of multi-antenna Gaussian channels," *European Trans. Telecommun.*, pp. 585-595, Nov. 1999.

[9] Electromagnetic Simulation and Electronic Design Simulation, http://www.zealand.com.

# Spatial Multiplexing with a Single Radio: Proof-of-Concept Experiments in an Indoor Environment with a 2.6-GHz Prototype

Osama N. Alrabadi, Chamath Divarathne, Philippos Tragas, Antonis Kalis, Nicola Marchetti, Constantinos B. Papadias, and Ramjee Prasad

***Abstract*—This letter validates a previously reported concept regarding the capability of transmitting multiple signals using one RF chain and a compact switched parasitic array (SPA). The experiments were conducted in an indoor environment using a 2.6 GHz prototype made of a single active printed dipole coupled to two passive ones. To the best of our knowledge, this is the first over-the-air experiment of spatial multiplexing with a single RF frontend yet to be demonstrated.**

***Index Terms*—Spatial multiplexing, , SPA, basis functions.**

## I. Introduction

ANALOGUE SPATIAL MULTIPLEXING techniques using compact parasitic antennas with a single RF chain have recently been reported [1-5]. The main idea of using an SPA for emulating a MIMO terminal is to smartly encode the signals onto the beampattern variations by parasitically controlling the driving antenna. This is done by mapping the independent datastreams onto a predefined basis that composes the SPA far-field.

*Background*: In [1], the authors proposed the idea of mapping the signals onto a set of predefined cardioids in the SPA far-field. By defining the spatial basis functions as $\mathcal{B}_1(\varphi)$ and $\mathcal{B}_2(\varphi)$, the desired beampattern in the far-field becomes $x_1\mathcal{B}_1(\varphi) + x_2\mathcal{B}_2(\varphi)$, where $x_1$ and $x_2$ are the signals to be spatially multiplexed. The reactive loads of the SPA were optimized for creating the (most accurate) linear combinations of the basis functions, under BPSK signaling. The work has been enhanced in [2] as an orthogonal spatial basis was obtained by decomposing the Euler functions comprising the SPA far-field. The approach in [2] maintains the SPA efficiency in case of BPSK signaling and preserves the SPA loadings as a degree of freedom to be optimized regarding a given criterion. The criterion was chosen to be the outage rate in [3] and finally the technique has been scaled to any PSK signaling dimension in [4].

*Current Contribution*: The current letter validates the concept of analogue MIMO transmission over the air in an indoor office environment. The experiments took place in the Broadband Wireless and Sensor Networks (B-WiSE) lab of Athens Information Technology. The target is to transmit two BPSK datastreams over the air via a single RF source at the transmit side as detailed later. The rest of the paper is organized as follows: Section II describes the transmit and receive subsystems. Section III describes the experiment setup whereas Section IV highlights the experiment results. Finally the paper concludes with its results.

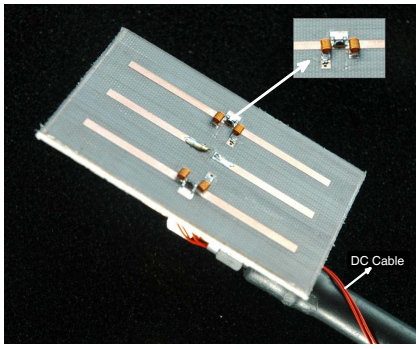


Fig. 1. SPA of printed microstrip dipoles.

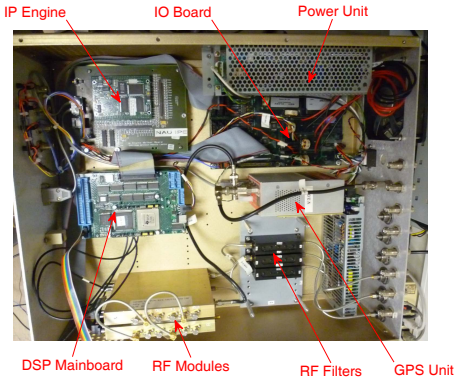


Fig. 2. Transmit subsystem unit.

## II. Transmit and Receive Subsystems

The experiments were conducted using a 2.6 GHz SPA prototype shown in Fig. 1, which has been fully modeled and optimized in [5]. The SPA consists of three printed dipoles (central active surrounded by two parasites) where the planar topology makes it better fit for handheld terminals. The dipoles' spacing is 11mm and the dipoles' lengths are 42mm. The SPA is optimized for BPSK signaling [6], regarding the average rate of communication at a target frequency of 2.6 GHz. The antenna system maintains a transmit efficiency above 95% while switching its loading state (the loads are switched using the Aeroflex Metelics MPN7310A-0805 PIN

Manuscript received November 3, 2010. The associate editor coordinating the review of this letter and approving it for publication was K. K. Wong.

O. N. Alrabadi is with the Broadband Wireless and Sensor Networks Group (BWiSE), Athens Information Technology (AIT), GR-19002, Athens, Greece, and with the Center for TeleInFrastructure (CTiF), Aalborg University (AAU), 9220, Aalborg East, Denmark (e-mail: osal@ait.edu.gr, ona@es.aau.dk).

C. Divarathne, P. Tragas, A. Kalis, and C. B. Papadias are with the Broadband Wireless and Sensor Networks Group (BWiSE), Athens Information Technology (AIT), GR-19002, Athens, Greece (e-mail: {cdiv, ptra, akal, papadias}@ait.edu.gr).

N. Marchetti and R. Prasad are with the Center for TeleInFrastructure (CTiF), Aalborg University (AAU), 9220, Aalborg East, Denmark (e-mail: {nm, prasad}@es.aau.dk).

Digital Object Identifier 10.1109/LCOMM.2011.121310.102119

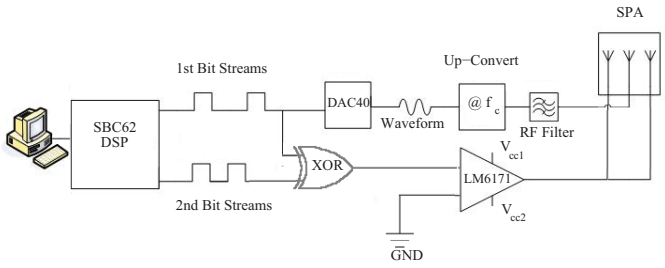


Fig. 3. A simplified schematic diagram of the signal flow at the transmit side.

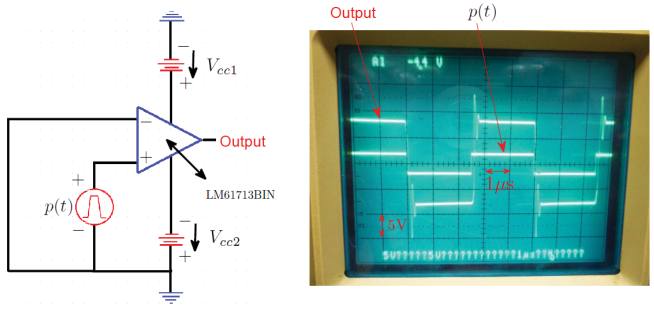


Fig. 4. Schematic diagram of the amplifier circuit used for magnifying the baseband control signal as well as a display of the baseband control signal before and after amplification.

diode). The choice of the operating frequency was determined by the MMDS band ($2.5 - 2.7$ GHz) at which the available MIMO testbed operates. The testbed consists of a transmit subsystem unit shown in Fig. 2 (the receive subsystem unit is not shown for the lack of space) supporting up to two RF modules (however in this experiment only one RF module is used at the transmit side and two at the receive side). The synchronization of the MIMO testbed is made through a GPS synchronization unit.

Fig. 3 shows a simplified schematic diagram of the signal flow at the transmit side. A digital baseband signal generated by the SBC62 stand alone DSP card is converted to analog using the DAC40 omnibus module (both the DSP and the DAC are from Innovative Integration [7]). The SBC62 DSP stand alone card is based around the Texas Instrument TMS320C6201 processor whereas the DAC40 is a four channel analog output module. Each channel is independent and capable of generating 40MHz waveform via 14-bit converters. The four DAC channels are used to generate In-phase and Quadrature-phase baseband inputs to every RF module. The analog baseband is up-converted to the desired frequency in the MMDS band and transmitted through the antennas after passing through a bandpass RF filter. In the next section we describe how a baseband control signal is used to mimic a second stream of data at the transmit side.

On the other hand, the signals are captured by two omnidirectional antennas spaced by 23cm or $2\lambda$. The received signal passes through the RF filters to the RF modules where it is down-converted to the analog baseband and digitized using the A4D1 omnibus module. The omnibus module is a 10 MHz 14-bit ADC of four channels from Innovative Integration.

## III. Experiment Description

### A. Signal Processing Before Transmission

Two binary trains of pulses was generated at a bit rate of 410kbps each. The first train was modulated into a BPSK symbol stream (using a raised-cosine waveform with 0.3 roll-off factor) and up-converted to 2.6 GHz. The high frequency modulated signal is used to drive the active antenna element (the central element of the SPA shown in Fig. 1). The second binary train was XORed with the first binary train in the baseband domain and the output baseband control signal was amplified and used for switching the SPA loads ($jX_1 \leftrightharpoons jX_2$). The amplification of the baseband control signal is necessary as the switching diodes of the parasitic antenna elements need a minimum range of $\pm$6V in order to operate, whereas the output of the DAC ranges between $\pm 2V$. Fig. 4 shows the comparator circuit that was used to magnify the voltage level of the control signal, using the LM6171 high-speed low-power low-distortion feedback amplifier from National Semiconductors [8]. The sources $Vcc1 = +9.7V$ and $Vcc2 = +8.9V$ are taken from an external DC power supply giving an output of $\pm 9V$ with a negligible transient delay compared to the symbol period. The amplifier offers a high slew rate of $3600\text{V}/\mu s$ and a unity-gain bandwidth of 100 MHz and is capable of amplifying the input signal with a switching frequency of 500 KHz and an amplitude ranging between $\pm 2V$. Fig. 4 shows also the input and output control signals i.e. the control signals before and after amplification, as well as the switching transients (it can be observed that the transient delay is indeed negligible compared to the symbol period).

### B. Signal Processing After Reception

As the data symbols are carried over two spatial functions over the air, the receiver needs to estimate its antenna responses to the two basis functions using a predefined training sequence (a training sequence of 8 BPSK symbols was used for every BPSK substream). The SPA far-field $\mathcal{G}(\varphi)$ is at one of two states: either $\mathcal{G}_1(\varphi) = \mathcal{B}_1(\varphi) + \mathcal{B}_2(\varphi)$ or $\mathcal{G}_2(\varphi) = \mathcal{B}_1(\varphi) - \mathcal{B}_2(\varphi)$ [5]. The receiver constructs the equivalent channel matrix representing the receive antenna responses to the spatial basis functions. The equivalent matrix is used for equalizing the received signal and decoupling the two BPSK symbol streams. We have adopted the linear zero-forcing as a simple decoding technique, thus the estimated transmitted signal becomes

$$\begin{aligned} \widehat{\mathbf{x}} &= \mathbf{H}^{-1}\mathbf{y} \\ &= \mathbf{x} + \mathbf{H}^{-1}\mathbf{n} \end{aligned} \tag{1}$$

where $\mathbf{H}$ is a $2 \times 2$ matrix given by

$$\mathbf{H} = \frac{1}{\sqrt{2}} \begin{pmatrix} h_{11} + h_{12} & h_{11} - h_{12} \\ h_{21} + h_{22} & h_{21} - h_{22} \end{pmatrix}, \tag{2}$$

such that $\mathbf{H}_{ij}$, $\{i,j\} \in \{1,2\}$ is the response of the $j$th receive antenna to $\mathcal{B}_i(\varphi)$, whereas $h_{ij}$, $\{i,j\} \in \{1,2\}$ is the response of the $j$th receive antenna to $\mathcal{G}_i(\varphi)$, according to the relations between $\mathcal{G}_i(\varphi)$ and $\mathcal{B}_i(\varphi)$, $i \in 1,2$ [5]; the operator $(.)^{-1}$

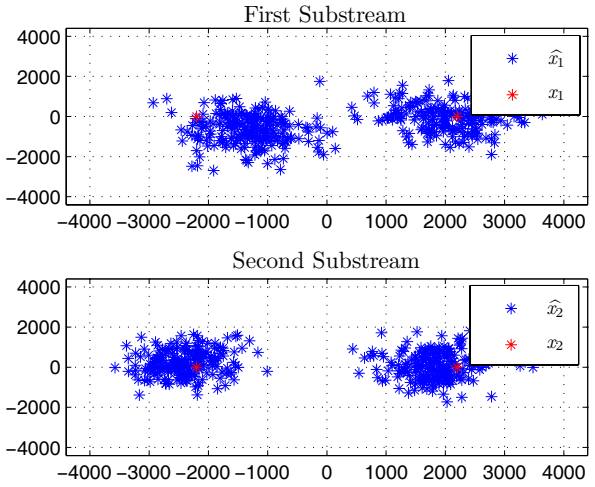


Fig. 5. Scatter plot of received signal constellation after equalization.

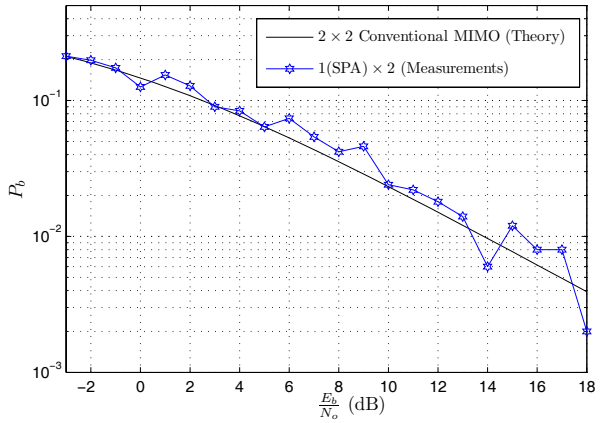


Fig. 6. Probability of error versus the transmit signal to noise ratio (per bit).

inverts the matrix operand and finally $\mathbf{n}$ is a vector representing the additive white Gaussian noise with zero mean and $N_o$ variance. Every demodulated signal comprises of two noisy clouds such that $\widehat{\mathbf{x}}_1 = \mathbf{c}_1 \cup \mathbf{c}_2$ and $\widehat{\mathbf{x}}_2 = \mathbf{c}_3 \cup \mathbf{c}_4$ as shown in Fig. 5. The signal-to-noise ratio (SNR) of the $i$th cloud is calculated as

$$\mathrm{SNR}_i = \frac{\mathbb{E}\left\{\mathbf{c}_i^H \mathbf{c}_i\right\} - \mathrm{Var}\left\{\mathbf{c}_i\right\}}{\mathrm{Var}\left\{\mathbf{c}_i\right\}} \tag{3}$$

where $\mathbb{E}\{.\}$ returns the sample mean of the operand and $\mathrm{Var}\{.\}$ returns the sample variance of the operand. The four clouds have almost the same SNR and the mean of the four SNRs is finally considered. The bit SNR referred to as $E_b/N_o$, is calculated by adding $\log_{10}(0.5\mathcal{S})$ to the average SNR (in dB), where $\mathcal{S}$ is the number of samples per one symbol whereas the $0.5$ factor is due to using real signaling. In this experiment, $\mathcal{S}$ was set to $5$ samples per symbol such that each transmission has $410$ symbols or equivalently $2048$ samples.

## IV. Experimental Results

Fig. 5 shows the received signal constellations after equalization (spatial separation), onto which the transmitted signals (red dots) are also projected, for comparison reasons. The figure shows that the two BPSK signals have been indeed decoupled at the receiver side thus validating the theory of MIMO with a single RF source. On the other hand, Fig. 6 shows the bit probability of error ($P_b$) versus $E_b/N_o$ obtained by measurements as well as the performance of a $2\times 2$ BPSK-MIMO with a Rayleigh channel of independent and identically distributed coefficients, and zero-forcing decoding[1]. The figure shows that the performance of the beamspace MIMO is comparable to the conventional one, thus validating the importance of such a new approach for realizing single radio compact-sized MIMO transceivers.

## V. Conclusion

A successful MIMO transmission at a total rate of $820$kbps has been conducted over the air, using a single RF source. The experiments took place in an indoor office environment using a fast-switching 2.6 GHz prototype. The experiments constitute to the best of the authors knowledge the first successful MIMO transmission with a single RF source.

## Acknowledgment

The authors acknowledge Julien Perruisseau-Carrier from the Centre Tecnologic de Telecomunicacions de Catalunya for his help on designing the transmit antenna prototype. The authors would also like to acknowledge Stanford University for donating to AIT's B-WiSE lab the MIMO testbed over which the experiments took place. Finally this work was partially supported by the Future and Emerging Technologies (FET) Programme within the Seventh Framework Programme for Research of the European Commission, under FET-Open grant CROWN-233843.

## References

[1] A. Kalis, A. G. Kanatas, and C. B. Papadias, "A novel approach to MIMO transmission using a single RF front end," *IEEE J. Sel. Areas Commun.*, vol. 26, no. 6, Aug. 2008.

[2] O. N. Alrabadi, A. Kalis, C. B. Papadias, and A. Kanatas, "Spatial multiplexing by decomposing the far-field of a compact ESPAR antenna," in *Proc. IEEE International Symposium on Personal, Indoor and Mobile Radio Communications (PIMRC)*, Sep. 2008, pp. 1-5.

[3] O. N. Alrabadi, C. B. Papadias, A. Kalis, N. Marchetti, and R. Prasad, "MIMO transmission and reception techniques using three-element ESPAR antennas," *IEEE Commun. Lett.*, vol. 13, no. 4, pp. 236-238, Apr. 2009.

[4] O. N. Alrabadi, C. B. Papadias, A. Kalis, and R. Prasad, "A universal encoding scheme for MIMO transmission using a single active element for PSK modulation schemes," *IEEE Trans. Wireless Commun.*, vol. 8, no. 9, Sep. 2009.

[5] O. N. Alrabadi, J. Perruisseau-Carrier, and A. Kalis, "MIMO transmission using a single RF source: theory and antenna design," minor revision at *IEEE Trans. Antennas and Wireless Propag.*, 2010.

[6] J. Perruisseau-Carrier, O. N. Alrabadi, and A. Kalis, "Implementation of a reconfigurable parasitic antenna for beam-space BPSK transmissions," in *Proc. European Microwave Conference (EuMC)*, 2010, pp. 644-647.

[7] http://www.innovative-dsp.com

[8] http://www.national.com/analog.com

[9] D. Tse and P. Viswanath, *Fundamentals of Wireless Communication*. Cambridge University Press, 2005.

[1]Theoretically, $P_b$ of a $2 \times 2$ BPSK-MIMO under Rayleigh fading and a zero-forcing receiver is unsurprisingly identical to the performance of $1 \times 1$ BPSK-SISO i.e $P_b = 0.5\left(1 - \sqrt{\frac{E_b/No}{E_b/No+1}}\right)$ [9].

# MIMO Transmission Using a Single RF Source: Theory and Antenna Design

Osama N. Alrabadi, Julien Perruisseau-Carrier and Antonis Kalis
*Members, IEEE*

***Abstract*— An approach for transmitting multiple signals using a single switched parasitic antenna (SPA) has been recently reported. The idea there is to map the signals to be transmitted onto a set of basis functions that serve as 'virtual antennas' in the beamspace (i.e. wavevector) domain. In this work, we generalize the derivation of the antenna pattern basis functions regarding a 3-element SPA of arbitrary radiating elements, within a symmetric array topology, for multiplexing signals in the wavevector domain (using different beampatterns) rather than in the hardware antenna domain with multiple feeding ports. A fully operational antenna system example is modeled, optimized regarding its return loss and the power imbalance between the basis functions, and finally realized. The measurements of the SPA show good agreement with the simulated target values, revealing an accurate design approach to be adopted as a fast SPA prototyping methodology. The SPA has been successfully employed for multiplexing two BPSK datastreams over-the-air, thus paving the way for practically compact and highly efficient MIMO transceiver designs.**

***Index Terms*— MIMO, Switched Parasitic Antenna, Basis functions, Reconfigurable Antenna.**

## I. Introduction

MULTI-INPUT MULTI-OUTPUT (MIMO) communication has gained lots of attention over the last decade as it enhances the spectral efficiency by exploiting the precious spatial resource dimension [1] [2]. Since the emergence of this technology, the classical approach has been assuming a transmitter with a number of transmit RF chains in order to independently map a set of signals onto a corresponding set of antennas. The receiver on the other hand performs some complex signal processing so as to decode the linear mixture of the signals and extract the useful data. However, having multiple RF chains at the user mobile terminal is rather costly. For example, the LTE - Release 8 standard supports a single antenna for the uplink transmission and two antennas for the downlink reception [3] [4]. The asymmetry in the number of antennas is mainly intended for avoiding the costly power amplifiers in the transmit RF chains. Although antenna selection is a terminal option, it requires instantaneous channel state information from the receiver back to the transmitter, which is a burden on the wireless communication system. Consequently, classical MIMO transmission especially in uplink scenarios may not be supported due to the practical limitations of the portable RF units.

To overcome these challenges, the authors in [5] describe how a half rate space-time (ST) code is transmitted with a single radio. In fact, a simple time-switched ST code [6] will outperform the approach in [5] regarding both performance and complexity. In [7], the authors propose an antenna system of two RF sources and four antenna elements. The proposed antenna system is capable of changing its polarization state (at the modulation rate), and thus transmitting the $4\times4$ Jafarkhani code. However, having two transmit RF chains may still be costly for low-end terminals.

On the other hand, the authors in [8] proposed a MIMO-like system using a switched parasitic antenna (SPA) with a single RF source. The SPA was shown to have a throughput potential comparable to that of conventional MIMO systems by switching the SPA far-field at the modulation rate, however no specific multiplexing techniques were proposed. In fact, parasitic antenna systems have been proposed over the past as a promising solution for addressing the problems associated with the difficulty of integrating multiple RF chains in compact portable units [9]. Such antenna systems comprise a single RF branch and multiple antenna elements loaded by variable reactive impedances. By controlling the reactance via a DC control, basic antenna properties, like the beampattern, can be reconfigured. Parasitic antennas have been widely used for providing receive angular (or pattern) diversity (examples are given in [10] [11]) and have recently been proposed for analogue beam and null steering [12].

The use of a compact-sized SPA for emulating open-loop MIMO transmission has been first proposed in the work of Kalis *et al* in [13] followed by work of Alrabadi *et al* [14]. The idea of using an SPA as a MIMO terminal is to drive the central active antenna with a high frequency RF signal modulated by the first datastream, while simultaneously driving a set of parasitic elements (PE) strongly coupled to the active one with a baseband (low frequency) control signal as shown in Fig. 1. The baseband control signal has information about the other datastreams to be transmitted over the air. By this way, it has been shown that the input datastreams are mapped onto an orthogonal set of basis functions in the wavevector domain via a single radio and compact array dimensions.

In this paper we focus on BPSK signaling format (the extension to all PSK is straightforward by following the approach in [14]) where we first *generalize* the derivation

Osama N. Alrabadi is with the Antennas, Propagation and Radio Networking (APNet) group, Department of Electronic Systems, Aalborg University, DK-9220 Aalborg, Denmark. (e-mail: ona@es.aau.dk).

Julien Perruisseau-Carrier is with the group for Adaptive MicroNano Wave Systems, LEMA/Nanolab, Ecole Polytechnique Fdrale de Lausanne (EPFL), Lausanne CH-1015, Switzerland. email: (julien.perruisseau-carrier@epfl.ch).

Antonis Kalis is with the Broadband Wireless and Sensor Networks (BWiSE) Group, Athens Information Technology (AIT), GR-19002, Athens, Greece. email: (akal@ait.edu.gr).

of the bases from mirror image pattern pairs (MIPPs) i.e. when one beampattern is a mirrored version of the other, regardless of how the MIPPs are expressed. We therefore extend previous findings by decoupling the wavevector domain [15] from the antenna domain and thus enabling MIMO functionality through any antenna system capable of creating MIPPs. At the receiver side, we prove that the receive antenna response to a beampattern that is a linear mixture of basis functions, is nothing more than the linear combination of the receive antenna responses to the different basis functions. By this way, the receiver decodes the transmitted data symbols by estimating the basis responses using classical training techniques.

A practical antenna system example of printed dipoles is proposed, modeled, optimized regarding the average rate of transmission, finally designed and demonstrated. The measured return loss and radiation patterns are in good agreement with the target parameters, revealing a fast and accurate designing methodology.

Throughout the paper a bold small letter designates a vector and a bold big letter designates a matrix. The operators $()^*, ()^T, ()^H$ designate complex conjugate, transpose and complex conjugate transpose (Hermitian) operators, respectively. The notation $\mathbf{I}_N$ indicates an identity matrix of size $N \times N$. The operator $\mathrm{diag}(\mathbf{v})$ returns a square matrix with the elements of the vector $\mathbf{v}$ laid across the main diagonal of the matrix. Moreover, we consider a classical uniform three-dimensional angular power spectrum seen by the transmitter (the mobile terminal), which is approximately the case when the mobile unit is surrounded by many scatterers.

The rest of the paper is organized as follows: in Section II we describe a technique for transmitting two BPSK signals simultaneously via a single RF frontend. Section III expresses the basis functions of a 3-element SPA based on full-wave electromagnetic modeling, and optimizes the SPA for BPSK signaling regarding the average rate of transmission. Section IV describes an SPA example of printed dipoles and explains its design implementation. Section V shows both simulation and measurement results and finally Section VI concludes the paper.

## II. MIMO Transmission with a Single RF Source

In this section we first prove the existence of an orthogonal basis whenever a MIPP can be formed. Based on this, a technique for transmitting two BPSK signals using arbitrary single radio based antenna system capable of forming a MIPP is described.

### A. Orthogonal Bases Using a MIPP

The correlation between two arbitrary beampatterns $\mathcal{G}_1(\vartheta,\varphi)$ and $\mathcal{G}_2(\vartheta,\varphi)$ is given by

$$\varrho_{12} = \frac{1}{\sqrt{P_1 P_2}} \int_{\varphi}\int_{\vartheta} \mathcal{G}_1(\vartheta,\varphi)\,\mathcal{G}_2^*(\vartheta,\varphi)\sin(\vartheta)\cdot d\vartheta d\varphi \quad (1)$$

where

$$P_1 = \frac{1}{4\pi}\int_{\varphi}\int_{\vartheta} |\mathcal{G}_1(\vartheta,\varphi)|^2 \sin(\vartheta)\cdot d\vartheta d\varphi,$$
$$P_2 = \frac{1}{4\pi}\int_{\varphi}\int_{\vartheta} |\mathcal{G}_2(\vartheta,\varphi)|^2 \sin(\vartheta)\cdot d\vartheta d\varphi, \quad (2)$$

are the spatial integration of the power beampatterns of $\mathcal{G}_1(\vartheta,\varphi)$ and $\mathcal{G}_2(\vartheta,\varphi)$ over the space, respectively. Whenever $P_1 = P_2$, the two beampatterns are called 'balanced'.

**Lemma.1:** For a MIPP $\mathcal{G}_1(\vartheta,\varphi)$ and $\mathcal{G}_2(\vartheta,\varphi)$, the set of the angular functions defined as

$$\mathcal{B}_\Sigma(\vartheta,\varphi) := \frac{1}{\sqrt{2}}\big(\mathcal{G}_2(\vartheta,\varphi) + \mathcal{G}_1(\vartheta,\varphi)\big),$$
$$\mathcal{B}_\Delta(\vartheta,\varphi) := \frac{1}{\sqrt{2}}\big(\mathcal{G}_2(\vartheta,\varphi) - \mathcal{G}_1(\vartheta,\varphi)\big), \quad (3)$$

form an orthogonal basis.

*Proof:* For two beampatterns that form a MIPP, we have $P_1 = P_2$ since one beampattern is just a mirrored version of the other. Moreover, the correlation between the two beams is *real* (see the proof at Appendix), and thus $\varrho_{12} = \varrho_{12}^*$. Based on these observations, the proof is straightforward and is given in (4) on top of page 3. ■

**Corollary.1:** A balanced basis is obtained by designing the two beampatterns $\mathcal{G}_1(\vartheta,\varphi)$ and $\mathcal{G}_2(\vartheta,\varphi)$ described in **Lemma** .1 to be orthogonal to each other i.e. if $\mathcal{G}_1(\vartheta,\varphi)$ and $\mathcal{G}_2(\vartheta,\varphi)$ are orthonormal, $\mathcal{B}_\Sigma(\vartheta,\varphi)$ and $\mathcal{B}_\Delta(\vartheta,\varphi)$ are orthonormal too[1].

*Proof:* Let $\mathcal{G}_1(\vartheta,\varphi) \perp \mathcal{G}_2(\vartheta,\varphi)$, the proof is straightforward as shown in (6) on top of page 3. In (6), $P_\Sigma$ and $P_\Delta$ are the spatial integration of the power beampatterns of $\mathcal{B}_\Sigma(\vartheta,\varphi)$ and $\mathcal{B}_\Delta(\vartheta,\varphi)$, over the space, given respectively by

$$P_\Sigma = \frac{1}{4\pi}\int_{\varphi}\int_{\vartheta} |\mathcal{B}_\Sigma(\vartheta,\varphi)|^2 \sin(\vartheta)\cdot d\vartheta d\varphi,$$
$$P_\Delta = \frac{1}{4\pi}\int_{\varphi}\int_{\vartheta} |\mathcal{B}_\Delta(\vartheta,\varphi)|^2 \sin(\vartheta)\cdot d\vartheta d\varphi. \quad (5)$$

■

### B. Transmission Technique Description

In this part we show that an arbitrary antenna system having a single RF input but has the capability of creating a MIPP will be capable of transmitting two BPSK signals $s_1$ and $s_2$, simultaneously. The two BPSK signals are mapped onto an orthogonal set of basis functions, thus independent fading between the two signals is almost always guaranteed regardless of the transceiver compactness. Let the sole RF port be fed by the signal $s_1$, the antenna beampattern in the far-field becomes either

[1]The reason we acquire an orthonormal basis $\mathcal{B}_\Sigma(\vartheta,\varphi)$ and $\mathcal{B}_\Delta(\vartheta,\varphi)$ from a MIPP, is that the MIPP by itself represents a linear combination (desired multiplexing relation) of the basis onto which the signals are mapped. The diversity action of the system directly depends on the transmit covariance of the basis (proportional to the identity matrix when the basis is orthonormal).

$$\begin{aligned}\varrho_{\Sigma\Delta} &= \frac{1}{4\pi\sqrt{P_\Sigma P_\Delta}}\int_\varphi\int_\vartheta \mathcal{B}_\Sigma(\vartheta,\varphi)\,\mathcal{B}^*_\Delta(\vartheta,\varphi)\sin(\vartheta)\cdot d\vartheta d\varphi \\ &= \frac{1}{8\pi\sqrt{P_\Sigma P_\Delta}}\int_\varphi\int_\vartheta \left(\mathcal{G}_2(\vartheta,\varphi)+\mathcal{G}_1(\vartheta,\varphi)\right)\left(\mathcal{G}^*_2(\vartheta,\varphi)-\mathcal{G}^*_1(\vartheta,\varphi)\right)\sin(\vartheta)\cdot d\vartheta d\varphi \\ &= \frac{1}{2\sqrt{P_\Sigma P_\Delta}}\left(P_2-\sqrt{P_1P_2}\varrho^*_{12}+\sqrt{P_1P_2}\varrho_{12}-P_1\right) \\ &= \frac{1}{2\sqrt{P_\Sigma P_\Delta}}\left(P_1-P_1\varrho_{12}+P_1\varrho_{12}-P_1\right) \\ &= 0 \end{aligned} \tag{4}$$

$$\begin{aligned} 0 &= \frac{1}{4\pi\sqrt{P_1P_2}}\int_\varphi\int_\vartheta \mathcal{G}_1(\vartheta,\varphi)\,\mathcal{G}^*_2(\vartheta,\varphi)\sin(\vartheta)\cdot d\vartheta d\varphi \\ 0 &= \frac{1}{8\pi\sqrt{P_1P_2}}\int_\varphi\int_\vartheta \left(\mathcal{B}_\Sigma(\vartheta,\varphi)-\mathcal{B}_\Delta(\vartheta,\varphi)\right)\left(\mathcal{B}^*_\Sigma(\vartheta,\varphi)+\mathcal{B}^*_\Delta(\vartheta,\varphi)\right)\sin(\vartheta)\cdot d\vartheta d\varphi \\ 0 &= \frac{1}{2\sqrt{P_1P_2}}\left(P_\Sigma+\varrho_{\Sigma\Delta}\sqrt{P_\Sigma P_\Delta}-\varrho^*_{\Sigma\Delta}\sqrt{P_\Sigma P_\Delta}-P_\Delta\right) \\ 0 &= \frac{1}{2\sqrt{P_1P_2}}\left(P_\Sigma-P_\Delta\right) \\ \Rightarrow\quad P_\Sigma &= P_\Delta \end{aligned} \tag{6}$$

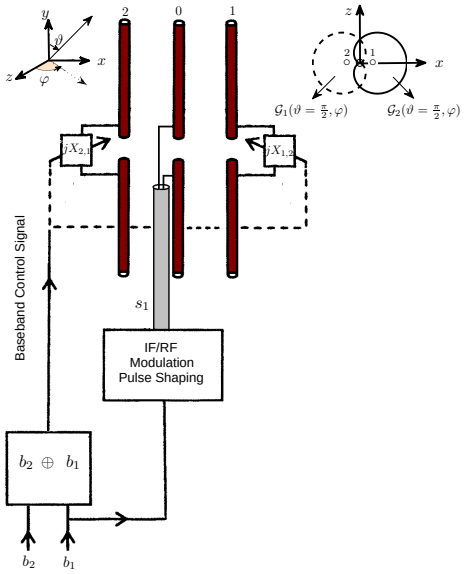


Fig. 1. Schematic diagram of the proposed technique where the first bitstream is modulated, up converted and fed into the central active element whereas the second bitstream is XORed with the first one. The output control signal is used for swapping the loads of the PE.

*State 1*

$$\begin{aligned}\mathcal{G}_T(\vartheta,\varphi) &= \mathcal{G}_1(\vartheta,\varphi)\,s_1 \\ &= \frac{s_1}{\sqrt{2}}\left[\mathcal{B}_\Sigma(\vartheta,\varphi)-\mathcal{B}_\Delta(\vartheta,\varphi)\right]\end{aligned}$$

or *State 2*

$$\begin{aligned}\mathcal{G}_T(\vartheta,\varphi) &= \mathcal{G}_2(\vartheta,\varphi)\,s_1 \\ &= \frac{s_1}{\sqrt{2}}\left[\mathcal{B}_\Sigma(\vartheta,\varphi)+\mathcal{B}_\Delta(\vartheta,\varphi)\right]\end{aligned}$$

or generally as

$$\mathcal{G}_T(\vartheta,\varphi) = \frac{s_1}{\sqrt{2}}\left[\mathcal{B}_\Sigma(\vartheta,\varphi)+(-1)^S\mathcal{B}_\Delta(\vartheta,\varphi)\right] \tag{7a}$$

$$= \frac{1}{\sqrt{2}}\left[s_1\mathcal{B}_\Sigma(\vartheta,\varphi)+s_2\mathcal{B}_\Delta(\vartheta,\varphi)\right] \tag{7b}$$

where $S$ is the antenna system state such that $S := 1$ is *State 1* within which the antenna system transmits over $\mathcal{G}_1(\vartheta,\varphi)$ and $S := 2$ is *State 2* within which the antenna system transmits over $\mathcal{G}_2(\vartheta,\varphi)$. From (7b) it is obvious how the two BPSK signals: $s_1$ which is modulated in the baseband, up-converted and fed into the input RF port and $s_2 = (-1)^S s_1$ which is spatially modulated on the antenna far-field by controlling the antenna state $S$, are mapped onto the space of $\mathcal{B}_\Sigma(\vartheta,\varphi)$ and $\mathcal{B}_\Delta(\vartheta,\varphi)$, respectively. In general, for any PSK modulation of order $N$, $s_2$ is a set of $N$ complex numbers evenly distributed over the unit circle, as discussed in Section IV of [12]. Table I shows the state $S$ required for transmitting $s_2$ according to the value of $s_1$ where $[b_1\ b_2]^T$ is input vector of bits modulated into $[s_1\ s_2]^T$. Fig. 1 shows a schematic diagram of the proposed technique, where the XORing of the two bitstreams gives the required $S$ i.e. $S = b_1 \oplus b_2$ giving 0 and 1 which correspond to $S := 1$ and $S := 2$, respectively.

TABLE I
TWO BPSK SIGNALS COMBINATIONS

| $[b_1\ b_2]^T$ | $[s_1\ s_2]^T$ | $S$ |
|---|---|---|
| $[\ 1\ \ 1\ ]^T$ | $[\ 1\ \ 1\ ]^T$ | 2 |
| $[\ 1\ \ 0\ ]^T$ | $[\ 1\ -1\ ]^T$ | 1 |
| $[\ 0\ \ 1\ ]^T$ | $[-1\ \ 1\ ]^T$ | 1 |
| $[\ 0\ \ 0\ ]^T$ | $[-1\ -1\ ]^T$ | 2 |

### C. System Training

The two BPSK signals that are transmitted in the beam-space domain and received using a classical uniform linear array of $n_R$ antenna elements ($n_R$-element ULA), can be

decoded by first estimating the receive antenna responses to the proposed basis.

**Proposition.1:** A beampattern comprising a linear mixture of basis functions (at the transmitter side) triggers a linear combination of the individual channel responses to the different basis functions (at the receiver side).

*Proof:* This directly stems from the principle of superposition in linear systems. To have a deeper insight, we first define $2 \times 1$ column vectors $\boldsymbol{\mathcal{G}}_{1,T}(\vartheta,\varphi)$, $\boldsymbol{\mathcal{G}}_{2,T}(\vartheta,\varphi)$, $\boldsymbol{\mathcal{B}}_{\Sigma,T}(\vartheta,\varphi)$ and $\boldsymbol{\mathcal{B}}_{\Delta,T}(\vartheta,\varphi)$, where the first and the second elements of every column vector represent the $\hat{\vartheta}$ and $\hat{\varphi}$ polarizations of the corresponding pattern, respectively. We also define $\boldsymbol{\mathcal{G}}_{k,R}(\vartheta,\varphi)$ as the vector of the polarization components of the $k$th receiver antenna pattern $\mathcal{G}_{k,R}(\vartheta,\varphi)$. As in [16], we assume that the propagation channel between the transmitter and the receiver consists of a set of $L$ plane waves, with the $l$th wave characterized by a complex voltage gain $\beta_l$, angle of departure $(\vartheta_{l,T},\varphi_{l,T})$, and angle of arrival $(\vartheta_{l,R},\varphi_{l,R})$. We also assume that each plane wave undergoes a polarization transformation due to scattering that can be expressed as the unitary matrix

$$\mathbf{O}_l = \begin{bmatrix} o_{l,\vartheta\vartheta} & o_{l,\vartheta\varphi} \\ o_{l,\varphi\vartheta} & o_{l,\varphi\varphi} \end{bmatrix}. \tag{8}$$

The response of the $k$th receive antenna ($1 \leq k \leq n_R$) when illuminated by the beampattern $\mathcal{G}_1(\vartheta,\varphi)$ is the complex channel gain representing the ratio of the received voltage signal to the transmitted voltage signal, and may be written as shown in (9), where $C_{k,1}$ is a constant that depends on the receiver and the transmitter active gains and impedances [17], $h_{k,\Sigma}$ and $h_{k,\Delta}$ are the responses of the $k$th receive antenna to $\mathcal{B}_\Sigma(\vartheta,\varphi)$ and $\mathcal{B}_\Delta(\vartheta,\varphi)$, respectively. By applying the same analysis, the response of the $k$th receive antenna when illuminated by $\mathcal{G}_2(\vartheta,\varphi)$ becomes $h_{k2} = \frac{1}{\sqrt{2}}(h_{k,\Sigma} + h_{k,\Delta})$. ■

Based on this, the receiver can decode the two BPSK signals by estimating the channel responses of the basis as

$$h_{k,\Sigma} = \frac{1}{\sqrt{2}}(h_{k,1} + h_{k,2}), \tag{10a}$$

$$h_{k,\Delta} = \frac{1}{\sqrt{2}}(h_{k,1} - h_{k,2}). \tag{10b}$$

By constructing the matrix of the receive antennas' responses, the receiver can zero-force the received signal by inverting the channel matrix (or using any other reception techniques) for decoding $s_1$ and $s_2$.

## III. Antenna Model and Optimization

In this paper we adopt the antenna topology proposed in [14], i.e. a symmetrical 3-element SPA, where the central element is the active one while the other two are passive. The two parasitic elements are loaded with pure imaginary loads $[jX_1 \;\; jX_2]$ as the real part of a complex load degrades the efficiency of the antenna system. Obviously the antenna system can create a MIPP around the E-plane (the $yz$ plane in Fig. 1) by simply permuting the reactive loads of the PE as $[jX_1 \;\; jX_2] \leftrightarrow [jX_2 \;\; jX_1]$, based on image theory. In other words, having the first beampattern $\mathcal{G}_1(\vartheta,\varphi)$ at $[jX_1 \;\; jX_2]$, the beampattern $\mathcal{G}_2(\vartheta,\varphi) = \mathcal{G}_1(\vartheta,-\varphi)$ is obtained at $[jX_2 \;\; jX_1]$. Consequently, by feeding the central active element with the first BPSK datastream and permuting the loads according to the second datastream, the two streams are simultaneously transmitted out of a single radio and mapped onto an orthogonal basis according to **Lemma.1**, irrespective of $X_1$ and $X_2$. Having the two loads $X_1$ and $X_2$ as a degree of freedom when considering BPSK signaling, we can optimize the loads according to a specific criterion as shown in Subsection III.C.

### A. Generalized Derivation of Antenna Basis Functions

Although the beampattern of thin electrical dipoles (or monopoles) can be practically approximated as an array factor by the superposition of the retarded currents induced on the wire antenna elements such as in Eq. (6) in [14], this is not true when considering general[2] radiating elements e.g. flat or fractal dipoles, slot antennas etc. To overcome this problem, we implement full wave electromagnetic modeling based on the SPA scattering parameters (S-parameters) denoted by $\mathcal{S}_{ij}, \{i,j\} \in \{0,1,2\}$, as well as the 3D complex active port patterns[3] of the antenna elements 0, 1 and 2 shown in Fig. 1, denoted by $E_0(\vartheta,\varphi)$, $E_1(\vartheta,\varphi)$ and $E_2(\vartheta,\varphi)$, respectively. An expression of the electric far-field beampattern of a 3-element SPA based on the aforementioned quantities and the variable antenna loading has been derived in [19] using Mason's rule. From [19] and after correcting the equations to properly adhere to Masons Rule, the two basis functions obtained when swapping the imaginary loads of the two parasitic elements become

$$\begin{aligned} \mathcal{B}_\Sigma(\vartheta,\varphi) &= \sqrt{2}E_0(\vartheta,\varphi) \\ &\quad + \frac{1}{\sqrt{2}}\left(\mathcal{L}_1^1 + \mathcal{L}_1^2\right)E_1(\vartheta,\varphi) + \left(\mathcal{L}_2^1 + \mathcal{L}_2^2\right)E_2(\vartheta,\varphi) \\ \mathcal{B}_\Delta(\vartheta,\varphi) &= \frac{1}{\sqrt{2}}\left(\mathcal{L}_1^1 - \mathcal{L}_1^2\right)E_1(\vartheta,\varphi) + \left(\mathcal{L}_2^1 - \mathcal{L}_2^2\right)E_2(\vartheta,\varphi) \end{aligned} \tag{11}$$

where

$$\begin{aligned} \mathcal{L}_1^1 &= \frac{\Gamma_1\mathcal{S}_{10}(1-\Gamma_2\mathcal{S}_{22}) + \Gamma_1\Gamma_2\mathcal{S}_{12}\mathcal{S}_{20}}{1-\Gamma_1\mathcal{S}_{11}-\Gamma_2\mathcal{S}_{22}+\Gamma_1\Gamma_2\mathcal{S}_{11}\mathcal{S}_{22}-\Gamma_1\Gamma_2\mathcal{S}_{12}\mathcal{S}_{21}} \\ \mathcal{L}_1^2 &= \frac{\Gamma_2\mathcal{S}_{10}(1-\Gamma_1\mathcal{S}_{22}) + \Gamma_1\Gamma_2\mathcal{S}_{12}\mathcal{S}_{20}}{1-\Gamma_2\mathcal{S}_{11}-\Gamma_1\mathcal{S}_{22}+\Gamma_1\Gamma_2\mathcal{S}_{11}\mathcal{S}_{22}-\Gamma_1\Gamma_2\mathcal{S}_{12}\mathcal{S}_{21}} \\ \mathcal{L}_2^1 &= \frac{\Gamma_1\mathcal{S}_{20}(1-\Gamma_2\mathcal{S}_{11}) + \Gamma_1\Gamma_2\mathcal{S}_{21}\mathcal{S}_{10}}{1-\Gamma_1\mathcal{S}_{11}-\Gamma_2\mathcal{S}_{22}+\Gamma_1\Gamma_2\mathcal{S}_{11}\mathcal{S}_{22}-\Gamma_1\Gamma_2\mathcal{S}_{12}\mathcal{S}_{21}} \\ \mathcal{L}_2^2 &= \frac{\Gamma_2\mathcal{S}_{20}(1-\Gamma_1\mathcal{S}_{11}) + \Gamma_1\Gamma_2\mathcal{S}_{21}\mathcal{S}_{10}}{1-\Gamma_2\mathcal{S}_{11}-\Gamma_1\mathcal{S}_{22}+\Gamma_1\Gamma_2\mathcal{S}_{11}\mathcal{S}_{22}-\Gamma_1\Gamma_2\mathcal{S}_{12}\mathcal{S}_{21}} \end{aligned} \tag{12}$$

[2]Again we emphasize that the arbitrariness of the elements is limited to the center element being a self mirror image, and the outer two being respective mirror images of each other, both about a vertical plane that divides the left and right sides of the SPA structure

[3]The active port pattern is defined as the beampattern obtained when driving the corresponding port (whether being active or passive) with a unit excitation voltage signal while terminating the other ports with reference impedances [18].

$$
\begin{aligned}
h_{k1} &= C_{k1}\sum_{l=1}^{L}\boldsymbol{\mathcal{G}}_{k,R}\left(\vartheta_{l,R},\varphi_{l,R}\right)\beta_l\mathbf{O}_l\boldsymbol{\mathcal{G}}_{1,T}\left(\vartheta_{l,T},\varphi_{l,T}\right)\\
&= C_{k1}\sum_{l=1}^{L}\boldsymbol{\mathcal{G}}_{k,R}\left(\vartheta_{l,R},\varphi_{l,R}\right)\beta_l\mathbf{O}_l\left(\boldsymbol{\mathcal{B}}_{\Sigma,T}\left(\vartheta_{l,T},\varphi_{l,T}\right)-\boldsymbol{\mathcal{B}}_{\Delta,T}\left(\vartheta_{l,T},\varphi_{l,T}\right)\right)\\
&= C_{k1}\sum_{l=1}^{L}\boldsymbol{\mathcal{G}}_{k,R}\left(\vartheta_{l,R},\varphi_{l,R}\right)\beta_l\mathbf{O}_l\boldsymbol{\mathcal{B}}_{\Sigma,T}\left(\vartheta_{l,T},\varphi_{l,T}\right)-C_{k1}\sum_{l=1}^{L}\boldsymbol{\mathcal{G}}_{k,R}\left(\vartheta_{l,R},\varphi_{l,R}\right)\beta_l\mathbf{O}_l\boldsymbol{\mathcal{B}}_{\Delta,T}\left(\vartheta_{l,T},\varphi_{l,T}\right)\\
&= \frac{1}{\sqrt{2}}\left(h_{k,\Sigma}-h_{k,\Delta}\right) \qquad (9)
\end{aligned}
$$

and $\mathcal{S}_{ij}\in\boldsymbol{\mathcal{S}}$ such that

$$
\boldsymbol{\mathcal{S}}=\begin{bmatrix}\mathcal{S}_{00} & \mathcal{S}_{01} & \mathcal{S}_{02}\\ \mathcal{S}_{10} & \mathcal{S}_{11} & \mathcal{S}_{12}\\ \mathcal{S}_{20} & \mathcal{S}_{21} & \mathcal{S}_{22}\end{bmatrix}, \qquad (13)
$$

$$
\Gamma_k=\left(jX_k+Z_0\right)^{-1}\left(jX_k-Z_0\right),\ \ k\in\{1,2\}, \qquad (14)
$$

where we assumed $\Gamma_0=0$ by having the source impedance at the central driven port equal to the reference impedance $Z_0=50\,\Omega$. The basis coefficients in (12) are derived with respect to a general scattering matrix. Swapping the two reactive loads as $[\Gamma_1\ \Gamma_2]\leftrightarrow[\Gamma_2\ \Gamma_1]$, swaps the coefficients $\left(\mathcal{L}_k^1-\mathcal{L}_k^2\right)\leftrightarrow\left(\mathcal{L}_k^2-\mathcal{L}_k^1\right),\ k\in\{1,2\}$ in (11), thus phase-shifting $\mathcal{B}_\Delta\left(\vartheta,\varphi\right)$ by $180^\circ$ without affecting $\mathcal{B}_\Sigma\left(\vartheta,\varphi\right)$. By this way, the $(-1)^S$ factor in (7a) is obtained. The two functions $\mathcal{B}_\Delta\left(\vartheta,\varphi\right)$ and $\mathcal{B}_\Sigma\left(\vartheta,\varphi\right)$ are the basis functions that are used to transmit two PSK signals of any modulation order [14].

### *B. Received Signal Model*

Considering a narrowband, flat-fading, point-to-point communication link where the two BPSK symbols are transmitted in the beam-space domain over two basis functions (equivalent to two uncorrelated virtual antennas) and received using an $n_R$-element ULA of uncorrelated and uncoupled antenna elements. Assuming independent fading statistics at the transmitter and the receiver, the Kronecker product [20] can be assumed and thus the channel transfer function can be written as[4]

$$
\mathbf{H}_{ch}=\mathbf{H}_w\mathbf{R}_T^{1/2}, \qquad (15)
$$

where the elements of the matrix $\mathbf{H}_w\in\mathbb{C}^{n_R\times 2}$ are independent and identically distributed (i.i.d.) complex Gaussian random variables with zero mean and unit variance. The correlation at the receiver side is ignored by the aforementioned assumptions regarding the receiving ULA. Defining the row vector $\boldsymbol{\mathcal{B}}\left(\vartheta,\varphi\right)=[\mathcal{B}_\Sigma\left(\vartheta,\varphi\right)\ \ \mathcal{B}_\Delta\left(\vartheta,\varphi\right)]$, the transmit covariance matrix[5] $\mathbf{R}_T$ is obtained as

$$
\begin{aligned}
\mathbf{R}_T &= \frac{1}{4\pi}\int_\varphi\int_\vartheta \boldsymbol{\mathcal{B}}^H\left(\vartheta,\varphi\right)\boldsymbol{\mathcal{B}}\left(\vartheta,\varphi\right)\sin\left(\vartheta\right)\cdot d\vartheta d\varphi,\\
&= \begin{bmatrix} P_\Sigma & \varrho_{\Sigma\Delta}\sqrt{P_\Sigma P_\Delta}\\ \varrho_{\Sigma\Delta}^*\sqrt{P_\Sigma P_\Delta} & P_\Delta\end{bmatrix},\\
&= \mathrm{diag}\left[P_\Sigma\ P_\Delta\right], \qquad (16)
\end{aligned}
$$

which is simply the power distribution across the basis functions since $\varrho_{\Sigma\Delta}=0$ according to **Lemma.1**. Notice that $P_\Sigma+P_\Delta=P_1+P_2=2P_1=P_t$, which is easily obtained from (2) and the basis definition in (3), where $P_t$ is the average transmit power. Defining the power imbalance ratio between the basis functions as $r=\frac{P_\Sigma}{P_\Delta}$, we can write $\mathbf{R}_T$ as $P_t\mathbf{Q}$ where $\mathbf{Q}$ is the normalized power distribution across the basis functions such that $\mathrm{trace}\{\mathbf{Q}\}=1$. $\mathbf{Q}$ can be written as $\mathrm{diag}([q_1\ q_2])$ such that $q_1=r/(1+r)$ and $q_2=1/(1+r)$. From the above, the received signal model becomes

$$
\begin{aligned}
\mathbf{y} &= \sqrt{P_t}\mathbf{H}_w\mathbf{Q}^{1/2}\mathbf{s}+\mathbf{n}\\
&= \sqrt{P_i\Delta_T}\underbrace{\mathbf{H}_w\mathbf{Q}^{1/2}}_{\mathbf{H}}\mathbf{s}+\mathbf{n} \qquad (17)
\end{aligned}
$$

where $P_i$ is the power into the transmitter (input power) and $0\le\Delta_T\le 1$ is the efficiency of the transmit antenna system being equal to $\Delta_T=1-|\Gamma|^2$, where $\Gamma$ is the SPA return loss derived in [19]. Finally $\mathbf{s}=[s_1\ \ s_2]^T$ is the vector of the modulated BPSK signals (see TABLE I), and $\mathbf{n}$ is a vector representing the white Gaussian noise, with zero mean and $\sigma_n^2$ variance.

### *C. Optimization Criterion*

In this work, we define the optimal SPA loads as the ones that maximize the average rate of transmission. However, in MIMO communications, average rate computation often demands tackling calculations of expectations with respect to random matrices rather than random scalar variables. For this reason, we derive an upperbound on the average rate and deploy it as an optimization criterion. We assume open-loop operation where the channel is known to the receiver but unknown to the transmitter. The ergodic capacity of a MIMO

[4]In [21], the correlation based channel model accounts for the mutual coupling by explicitly incorporating the coupling matrices. However in (15), the mutual coupling is implicitly taken into consideration within the calculation of the basis functions in (11).

[5]Since the basis functions are imbalanced, the transmit covariance matrix rather than the transmit correlation matrix is considered.

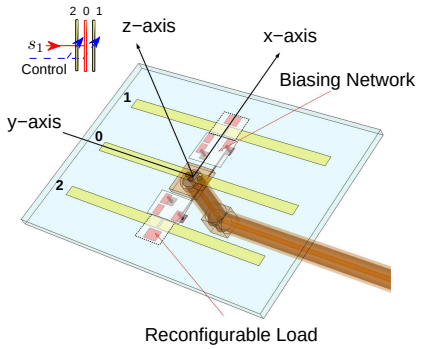


Fig. 2. Schematic diagram of the SPA initially proposed in [24].

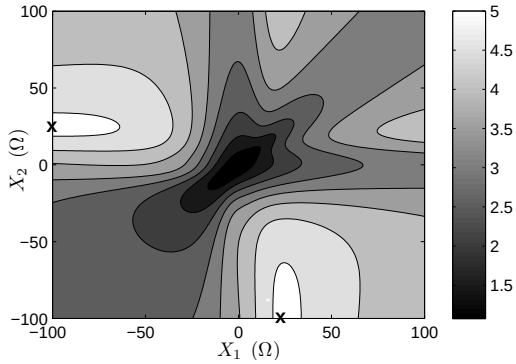


Fig. 3. An optimization contour map regarding the upperbound on $\Im_{av}$ with respect to $X_1$ and $X_2$.

random channel, denoted by $\Im_{av}$, is the ensemble average of the information rate over the distribution of the elements of the channel matrix $\mathbf{H} = \mathbf{H}_w\mathbf{Q}^{1/2} \in \mathbb{C}^{n_R\times 2}$. By using the $\log_2\det(\cdot)$ formula [22], the upper bound that comes from the Jensen's inequality and the concavity of $\log_2\det(\cdot)$[6], we get

$$\begin{aligned}\Im_{av} &= \mathbb{E}_{\mathbf{H}}\left[\log_2\det\left(\mathbf{I}_2+\frac{P_i\Delta_T}{\sigma_n^2}\mathbf{H}^H\mathbf{H}\right)\right]\\ &\le \log_2\det\left(\mathbf{I}_2+\frac{P_i\Delta_T}{\sigma_n^2}\mathbb{E}_{\mathbf{H}}\left[\mathbf{H}^H\mathbf{H}\right]\right)\\ &= \log_2\det\left(\mathbf{I}_2+\frac{P_i\Delta_T}{\sigma_n^2}\mathbf{Q}\right)\\ &= \log_2\left(1+\frac{P_i\Delta_T r}{\sigma_n^2(1+r)^2}\right). \end{aligned} \quad (18)$$

In (18), the average transmitted power is not divided by the number of the basis functions (the number of the virtual antennas), since the trace of $\mathbf{Q}$ is normalized to a unity rather than to the number of the basis functions (both forms are equivalent). The optimal loading is defined as the one that maximizes the average throughput upperbound in (18) i.e.

$$[X_1\ \ X_2]_{opt} = \arg\max_{[X_1\ \ X_2]}\left\{\log_2\left(1+\frac{P_i\Delta_T r}{\sigma_n^2(1+r)^2}\right)\right\}. \quad (19)$$

In (19), $\Delta_T$ is made part of the optimization criterion by constraining $P_i$ rather than $P_t$ as the SPA efficiency is a key design parameter when considering portable RF units with limited storage batteries.

## IV. Antenna System Design

In this section we consider the 3-element SPA shown in Fig. 2, where the radiating elements are thin printed dipoles. The planar topology of the SPA makes it better fit in compactness-constrained mobile units as compared to the majority of the wire parasitic antennas already proposed in the literature. The current SPA was proposed earlier in [24], however in this paper we complete the work by describing the implementation and the measurements of the prototype.

[6]The $\log_2\det(\cdot)$ is concave over positive semi-definite matrices [23]. Since $\mathbf{Q}$ is positive semi-definite, the term $\mathbf{I}_2+\frac{P_i\Delta_T}{\sigma_n^2}\mathbf{Q}$ is positive semi-definite too, as it is a one-to-one mapping of $\mathbf{Q}$, thus preserving the positive definiteness.

### A. Design Parameters and Optimal Loading

The first design steps consist of making some initial choices on the antenna materials and the basic topology. We consider a 3-element SPA of flat dipoles as radiating elements as shown in Fig. 2, designed on an $h = 1.5$ mm thick substrate of relative permittivity $\varepsilon = 2.17$. The dipole lengths and spacing are $48.3$ mm and $11$ mm, respectively. The spacing is $\sim 0.1\lambda$ at the desired operational frequency of $2.6$ GHz. The SPA was simulated using HFSS®, with ports at the locations of the variable loads. The resulting scattering matrix is given by

$$\boldsymbol{\mathcal{S}} = \begin{bmatrix} -0.43+\jmath 0.09 & 0.51-\jmath 0.09 & 0.51-\jmath 0.09\\ 0.51-\jmath 0.09 & -0.26+\jmath 0.14 & 0.22-\jmath 0.23\\ 0.51-\jmath 0.09 & 0.22-\jmath 0.23 & -0.26+\jmath 0.14\end{bmatrix}, \quad (20)$$

where the matrix is symmetric by the reciprocity theorem i.e. by the usual assumption of employing antennas with electrically reciprocal materials, thus $\mathcal{S}_{ij} = \mathcal{S}_{ji}$. Moreover, the symmetric topology of the SPA shown in Fig. 1 ensures that $\mathcal{S}_{02} = \mathcal{S}_{01}$ and $\mathcal{S}_{22} = \mathcal{S}_{11}$. The antenna system is lossy as $\boldsymbol{\mathcal{S}}^H\boldsymbol{\mathcal{S}} \neq \mathbf{I}_3$ when compared to the lossless 4-port network (expressed by $\boldsymbol{\mathcal{S}}_{\text{EQ}}$) in [19] as $\boldsymbol{\mathcal{S}}_{\text{EQ}}^H\boldsymbol{\mathcal{S}}_{\text{EQ}} = \mathbf{I}_4$ by the energy conservation principle when including the radiated beams in the network structure. Further, the diagonal elements of $\boldsymbol{\mathcal{S}}$ are non-vanishing as we aim at diminishing the return loss of the central active element rather than $\mathcal{S}_{ii}$. The resulting 3-port S-parameters and the complex 3D active port patterns were exported to MATLAB®, where a computer routine scans the realizable range of the reactance space searching for $[X_1\ \ X_2]_{opt}$ given by (19). Fig. 3 shows an optimization contour plot of $\Im_{av}(X_1, X_2)$ at a transmit signal to noise ratio[7] (SNR) $P_i/\sigma_n^2 = 10$ dB. The figure shows that $\Im_{av}$ is maximized at $[X_1\ \ X_2]_{opt} = [-100\ \ +27]\,\Omega$. At such loading, the upperbound on $\Im_{av}$ is $5$ b/s/Hz, the power imbalance between the two basis functions is $0.56$ dB, and the SPA

[7]In fact, the transmit SNR $P_t/\sigma_n^2$ is commonly used in the literature when evaluating the system performance. However, as the SPA loading will affect the transmit SNR through the matching efficiency, it seems more reasonable to use $P_i/\sigma_n^2$ which is simply the transmit SNR before the mismatch effect represented by $\Delta_T$. On the other hand, the way of calculating the receive SNR is different and is shown later in Eq. (20).

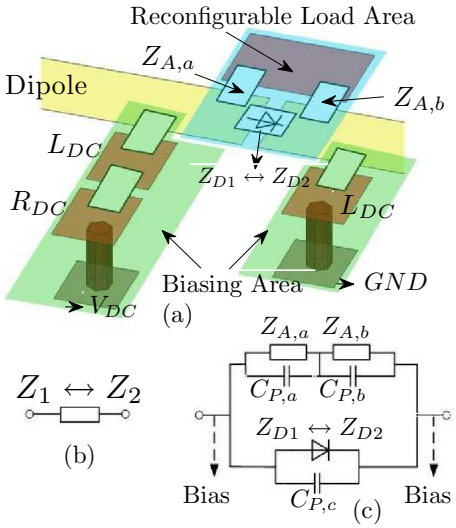


Fig. 4. Reconfigurable dipole load impedance: (a) Layout and elements view, including biasing network, (b) target two-state variable impedance and (c) detailed implementation circuit, including layout parasitic capacitances.

efficiency is 97%.

### B. Reconfigurable Impedance Implementation

The design of the variable load, explained in more detail in the earlier partial work of [24], consists of the following steps: First, an adequate layout for the reconfigurable load area, to be controlled using a PIN diode, is selected ('Reconfigurable Load Area' in Fig. 4a). The parasitic capacitance ($C_{P,a}$, $C_{P,b}$, and $C_{P,c}$) between the different pads are extracted from full-wave simulations. Here the inductive effect in the pads can be neglected in the design. Subsequently, the surface-mounted elements to implement $Z_{A,a}$ and $Z_{A,b}$ are deduced from the circuit of Fig. 4 so that the overall impedance in each state $Z_1$ and $Z_2$ (see Fig. 4b) match the target values deduced in the previous section, namely $Z_1 = jX_1 = j(+27)\ \Omega$ and $Z_2 = jX_2 = j(-100)\ \Omega$. Finally, a DC biasing network was designed using large RF-block inductors $L_{DC}$ and a resistor $R_{DC}$ to precisely control the diode biasing current. As can be seen in Fig. 6, the DC paths are then driven to the other side of the substrate by vias, where they can conveniently be connected to the DC voltage references in the antenna environment (see Section V). The PIN diode (Aeroflex Metelics MPN7310A-0805) serves as a low capacitance fast switch, with a negligible transient switching time (orders of nanoseconds) . $Z_{A,a}$ and $Z_{A,b}$ are capacitors of 0.5 pF and 0.8 pF, respectively. The biasing network elements are $L_{DC}$ = 22 nH and $R_{DC} = 910\,\Omega$.

In order to experimentally validate the reconfigurable load design prior to its insertion in each of the SPA parasitic dipoles, it was fabricated and measured using a thru-reflect-line (TRL) calibration kit, which allows placing the measurement reference planes at the desired locations, as required here. It is then possible to extract the desired impedances $Z_1$ and $Z_2$ from the measured S-parameters and microstrip line impedance, as shown in Fig. 5 for each of the diode states. The imaginary parts of the measured impedance $Z_1$

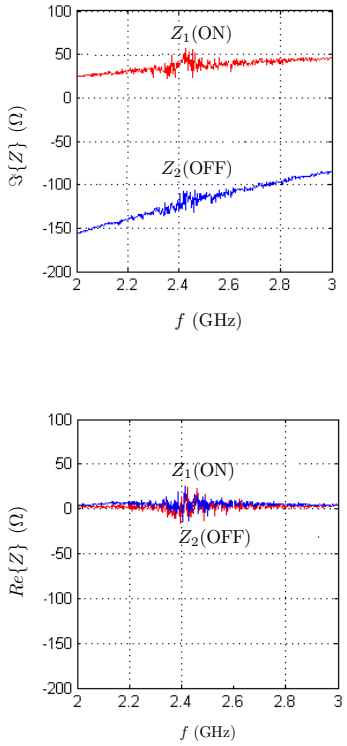


Fig. 5. Measured load impedance in each diode state of the PIN diode, extracted from the S-parameter measurements on a dedicated microstrip TRL calibration kit, from [24]. The OFF and ON diode states correspond to a reversed ($V_{DC} = 0V$) and forward ($I = 9$mA) bias, respectively.

and $Z_2$ at the design frequency of 2.6 GHz are $+38\,\Omega$ and $-108\,\Omega$ in the ON and the OFF states, respectively. These values are close to the target reactances of $+27\,\Omega$ and $-100\,\Omega$, considering the tolerances of the SMD elements and the impact of the biasing network. The real parts of $Z_1$ and $Z_2$ are not exactly zero due the diode and SMD components finite resistances, which were neglected in the design procedure (their measured average values are only $+5\,\Omega$ and $+3\,\Omega$ in the OFF and the ON states, respectively). The target basis functions (at $[X_1\ \ X_2]_{opt} = [-100\ \ +27]\ \Omega$) and the achieved ones ($[X_1\ \ X_2]_{opt} = [-108\ \ +38]\ \Omega$) are compared in Fig. 7, showing very good agreement.

## V. Simulation and Measurement Results

The current section presents the measurements of the different SPA parameters and compares them to the corresponding parameters obtained by computer simulations.

### A. Antenna Demonstration

A photograph of the fully operational fabricated antenna is shown in Fig. 6. It was observed that a good balanced excitation of the active dipole is simply obtained by connecting the central and the outer conductors of a coaxial connector to each of the dipole arms. The variable load designed and characterized in Section IV.B was introduced in each parasitic

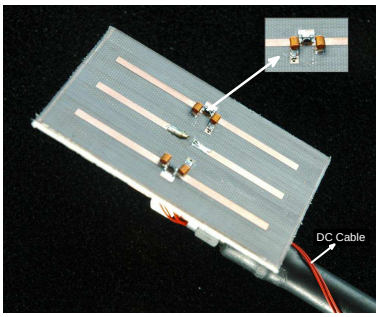


Fig. 6. Photograph of the fully operational SPA, optimized for the proposed aerial MIMO approach.

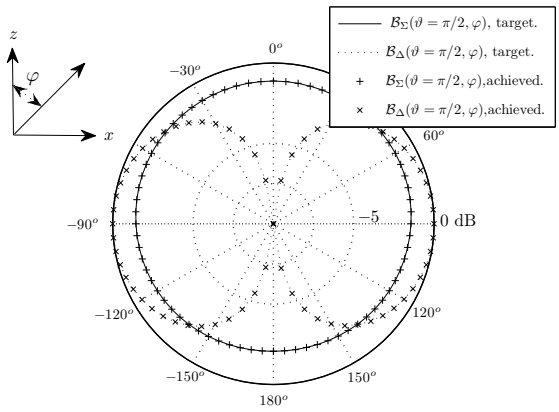


Fig. 7. The magnitude of the H-plane co- polarized basis functions at the target loads of $[+27\ \ -100]\,\Omega$ and at the practically achieved loads of $[+38\ \ -108]\ \Omega$. The two basis functions resemble the omni and the angular sine functions, which are orthogonal to each other.

dipole of the SPA, including the DC biasing network. The DC ground pad of each variable load on the backside of the substrate is connected by a printed line to the coaxial connector outer conductor (which thus serves as a DC ground), whereas each actuation pad (shown as '$V_{DC}$' in Fig. 4) is connected by a thin wire to the bias voltages for controlling the states of the diodes. In order to improve the antenna performance and provide pure measured patterns, the DC wires are driven along the coaxial feed, which is oriented toward the minimum radiation of the SPA (i.e. parallel to the dipoles, see Fig. 6). A standard $9$V battery is used as a DC source in the radiation pattern measurements. The battery is placed behind a piece of an absorber (located in the direction of minimum radiated power density), as can be seen in Fig. 8. Therefore the antenna states were simply selected by connecting each of the two DC wires to the $0$V or $9$V references. The impact of the biasing voltages on the antenna performance was investigated, showing similar responses for $-10$V to $0$V as the OFF (or 'reverse-biased') state, while $+3$V to $+10$V are acceptable for the ON (or 'forward-biased') state.

### B. Return Loss

Fig. 9 shows the simulated and measured return loss of the SPA around the design frequency of $2.6$ GHz. The graph

Fig. 8. Set-up of the antenna for reconfigurable radiation pattern measurements, with a $9$V battery places behind the absorber cone in a direction of the low field intensity.

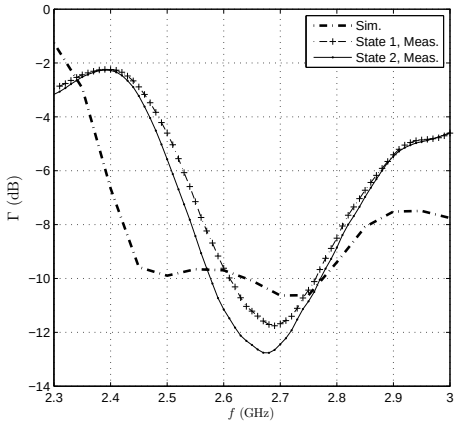


Fig. 9. Return Loss (dB) of the SPA for both loading states i.e. $S := 1$ and $S := 2$.

only shows the response in the operational states of the antenna, namely when it is loaded by the reactance load pairs $[jX_1\ jX_2]$ and $[jX_2\ jX_1]$. As explained earlier in Section IV, the return loss is the same for both states due to the SPA symmetry, which is confirmed here by the similarity between the two measured curves in Fig. 9. The SPA was found to have poor matching in the two (unused) states $[jX_1\ jX_1]$ and $[jX_2\ jX_2]$), which are not shown here.

The agreement between simulations and the measurements is moderate, since the measured bandwidth is larger than the one obtained by simulation and is not exactly centered around the design frequency of $2.6$ GHz. Nevertheless the measurements show good return loss at $2.6$ GHz. The $-10$dB measured bandwidth is $5.6\%$ and $7.1\%$ for a reference of $-10$ dB, for $S := 1$ and $S := 2$, respectively .

### C. Radiation Patterns

Fig. 10 shows the H-plane co- and cross- polarized far fields in the first operational antenna state ($S := 1$). Note that the maximum of the co-polarized beampattern, located at $\varphi = +90°$, corresponds to the direction of the load in the OFF state. The simulated and measured co- and cross-

polarized beampatterns are in good agreement, as shown in Fig 10. Because of the SPA symmetrical structure and the reactance pair antisymmetry, the other antenna beampattern should simply be a mirror image of the first beampattern around the $\varphi = 0^\circ - 180^\circ$ axis, which is well verified by the measured prototype as can be seen in Fig. 11.

### *D. Experimental Results*

The proposed antenna prototype has been successfully used for spatially multiplexing two BPSK datastreams *over the air* at $2.6$ GHz. The experiments constitute to the best of the authors' knowledge the first MIMO transmission with a single RF source yet to be proposed. The first train was modulated into a BPSK symbol stream (using a raised-cosine waveform with 0.3 roll-off factor) and up-converted to 2.6 GHz. The high frequency signal was modulated to the central element within a modulation bandwidth of $533$ kHz. The second binary train was XORed with the first binary train in the baseband domain and the output baseband control signal was amplified and used for switching the SPA loads. A simple zero-forcing decoding was implemented by the receiver which was equipped with two distant omnidirectional monopole antennas separated from each other by 23cm or $2\lambda$, and both are located several wavelengths from the SPA (the receiver is located in the broadside direction of the SPA, but completely blocked from the transmitter in the sense that no line-of-sight between the transmitter and the receiver exists). The receiver first estimates the receive antennas' responses to the two beampatterns $\mathcal{G}_1(\varphi, \vartheta)$ and $\mathcal{G}_2(\varphi, \vartheta)$ using classical training, then the response to the basis is obtained from (10a,10b). Finally the $2 \times 2$ complex channel matrix is inverted and used for equalizing the received signal. A total bit rate of $820$ kbps was obtained with arbitrarily low error, thus a spectral efficiency of $1.54$ b/s/Hz can be claimed. Although this seems far from the target upperbound of $5$ b/s/Hz, it is well justified by the fact of using real signaling with uniform distribution rather than complex signaling with Gaussian distribution. The details of the experiments' setup are detailed in [25].

Fig. 12 shows the received signal constellations after equalization (spatial separation), onto which the transmitted signals (red dots) are also projected, for comparison reasons. Every demodulated signal comprises of two noisy clouds such that $\widehat{\mathbf{x}}_1 = \mathbf{c}_1 \cup \mathbf{c}_2$ and $\widehat{\mathbf{x}}_2 = \mathbf{c}_3 \cup \mathbf{c}_4$. The receive SNR of the $i$th cloud is calculated as

$$\text{SNR}_i = \frac{\mathbb{E}\left\{\mathbf{c}_i^H \mathbf{c}_i\right\} - \text{Var}\left\{\mathbf{c}_i\right\}}{\text{Var}\left\{\mathbf{c}_i\right\}} \qquad (21)$$

where $\mathbb{E}\{.\}$ returns the sample mean of the operand and $\text{Var}\{.\}$ returns the sample variance of the operand. The four clouds have almost the same SNR and the mean of the four SNRs is finally considered. The bit SNR referred to as $E_b/N_o$, is calculated by adding $10\log_{10}(0.5\mathcal{K})$ to the average SNR (in dB), where $\mathcal{K}$ is the number of samples per one symbol whereas the $0.5$ factor is due to using real signaling. In this experiment, $\mathcal{K}$ was set to $5$ samples per symbol such that each transmission has $410$ symbols or equivalently $2048$ samples. On the other hand, Fig. 13 shows the bit probability of error

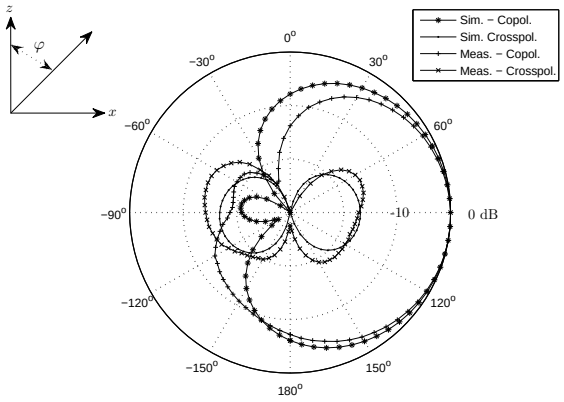


Fig. 10. Simulated and measured co- and cross- polarization components of the beampattern $\mathcal{G}_1(\vartheta, \varphi)$ in the H-plane i.e. $\mathcal{G}_1(\vartheta = \frac{\pi}{2}, \varphi)$, at $f = 2.6$ GHz.

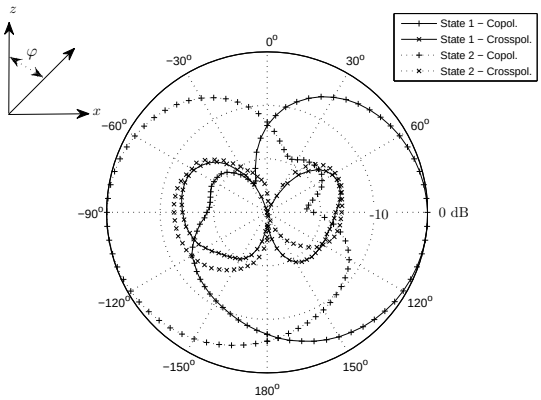


Fig. 11. Measured co- and cross- polarization components of the beampatterns $\mathcal{G}_1(\vartheta = \frac{\pi}{2}, \varphi)$ and $\mathcal{G}_2(\vartheta = \frac{\pi}{2}, \varphi)$ at $f = 2.6$ GHz. Notice that $\mathcal{G}_1(\vartheta = \frac{\pi}{2}, \varphi) \approx \mathcal{G}_2(\vartheta = \frac{\pi}{2}, -\varphi)$, resulting in a MIPP.

($P_b$) versus $E_b/N_o$ obtained by measurements as well as the performance of a $2 \times 2$ BPSK-MIMO with a Rayleigh channel of independent and identically distributed coefficients, and zero-forcing decoding[8]. The figure shows that the performance of the beamspace MIMO is comparable to the conventional one, thus validating the importance of such a new approach for realizing single radio compact-sized MIMO transceivers.

## VI. Conclusion

The paper generalized a previously reported approach for transmitting multiple signals using a single RF source. The idea is to obtain an orthogonal or orthonormal basis out of MIPPs. The paper also provided design steps for an example of a 3-element SPA, capable of forming a MIPP that are mirror images of each other. The SPA was optimized for BPSK signaling by deriving a criterion that maximizes the SPA

[8]Theoretically, $P_b$ of a $2 \times 2$ BPSK-MIMO under Rayleigh fading and a zero-forcing receiver is unsurprisingly identical to the performance of $1 \times 1$ BPSK-SISO i.e $P_b = 0.5\left(1 - \sqrt{\frac{E_b/No}{E_b/No+1}}\right)$ [26].

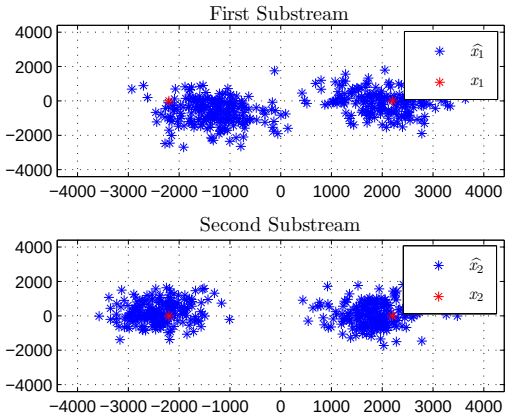


Fig. 12. Scatter plot of received signal constellation after equalization.

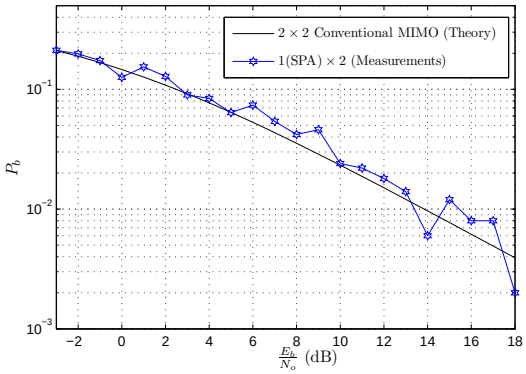


Fig. 13. Probability of error versus the transmit SNR (per bit).

efficiency and minimizes the power imbalance between the basis functions, simultaneously. A reconfigurable impedance was designed and a fully operational SPA for single radio MIMO transmission was demonstrated for the first time. The measured SPA parameters are in good agreement with the target values, regarding the SPA return loss and the radiation patterns in the different SPA states. Finally, the SPA has been successfully used for multiplexing two BPSK datastreams with a total bit rate of 820 kbps.

## ACKNOWLEDGMENT

The authors like to thank Pablo Pardo for fabricating and measuring the variable load circuit, and Pavel Miskovsky for his help in the antenna measurement, both at CTTC.

J. Perruisseau-Carrier thanks the Swiss National Science Foundation (SNSF) for financial support through its professorship program. Finally, the authors express their deepest gratitude to the editor and to the anonymous reviewers for their helpful and constructive comments and suggestions.

## APPENDIX

In this part we prove that the cross-correlation of a MIPP in a uniform field is *real*.

*Proof:* : Assuming a MIPP over the $\varphi$ angular domain, where $\varphi$ is the azimuth polar system of coordinates with a reference axis taken from the MIPP axis of symmetry (the $\vartheta$ can be dropped for simplicity). The MIPP can generally be written as $\mathcal{G}_1(\varphi)$ and $\mathcal{G}_2(\varphi) = \mathcal{G}_1(-\varphi)$. The $\mathcal{G}_1(\varphi)$ can be further written as $\mathcal{G}_R(\varphi) + j\mathcal{G}_I(\varphi)$, where $\mathcal{G}_R(\varphi)$ and $\mathcal{G}_I(\varphi)$ are the real and imaginary parts of $\mathcal{G}_1(\varphi)$. The cross-correlation of the MIPP becomes

$$\begin{aligned}
\varrho_{12} &= \frac{1}{2\pi P}\int_{\varphi} \mathcal{G}_1(\varphi)\,\mathcal{G}_2^*(\varphi)\cdot d\varphi \\
&= \frac{1}{2\pi P}\int_{\varphi} \mathcal{G}_1(\varphi)\,\mathcal{G}_1^*(-\varphi)\cdot d\varphi \\
&= \frac{1}{2\pi P}\int_{\varphi} \left(\mathcal{G}_R(\varphi)+j\mathcal{G}_I(\varphi)\right)\left(\mathcal{G}_R(-\varphi)-j\mathcal{G}_I(-\varphi)\right)\cdot d\varphi \\
&= \frac{1}{2\pi P}\int_{\varphi} \Big(\mathcal{G}_R(\varphi)\,\mathcal{G}_R(-\varphi)+\mathcal{G}_I(\varphi)\,\mathcal{G}_I(-\varphi)\Big)\cdot d\varphi \\
&\quad + j\frac{1}{2\pi P}\int_{\varphi} \Big(\mathcal{G}_R(-\varphi)\,\mathcal{G}_I(\varphi)-\mathcal{G}_I(-\varphi)\,\mathcal{G}_R(\varphi)\Big)\cdot d\varphi \\
&= \underbrace{\frac{1}{2\pi P}\int_{\varphi} \Big(\mathcal{G}_R(\varphi)\,\mathcal{G}_R(-\varphi)+\mathcal{G}_I(\varphi)\,\mathcal{G}_I(-\varphi)\Big)\cdot d\varphi}_{\text{real}}
\end{aligned}$$

■

## REFERENCES

[1] J. H. Winters,"On the capacity of radio communication systems with diversity in a Rayleigh fading environment," *IEEE J. Select Areas Commun.*, vol. SAC-5, pp. 871878, June 1987.

[2] G. J. Foschini and M. J. Gans,"Limits of wireless communication in a fading environment when using multiple antennas," *Wireless Personal Communications*, . 6, pp. 311-335, 1998.

[3] Overview of 3GPP Release 8 V0.0.3, November 2008, available online at http://www.3gpp.org/Release-8.

[4] J. Kotecha, "LTE:MIMO Techniques in 3GPP-LTE," *Freescale Semiconductor*, June 2008.

[5] M. Okoniewski, S. V. Hum, A. Sutinjo, and G. G. Messier, "A spacetime coding scheme utilizing phase shifting antennas at RF frequencies," *IEEE Antennas and Wireless Propagation Letters*, vol. 4, Page(s): 369 - 372, 2005.

[6] J. Yuan and B. Vucetic," *Space-Time Coding*, John Wiley & Sons Ltd, 2003.

[7] A. Grau, J. Romeu, M. Lee, S. Blanch, L. Jofre and F. De Flaviis, "A Dual-Linearly-Polarized MEMS-Reconfigurable Antenna for Narrowband MIMO Communication Systems," *IEEE Transactions on Antennas and Propagation*, vol. 58, no. 1, January 2010.

[8] M. Wennstorm and T. Savantesson, "An antenna solution for MIMO channels: the switched parasitic antenna," *IEEE International Symposium on Personal, Indoor and Mobile Radio Communications, 2001 12th*, vol.1, pp 159-163, September 2001.

[9] R. Vaughan, "Switched Parasitic Elements for Antenna Diversity," *IEEE Transactions on Antennas and Propagations*, vol.47, no.2, Feb-1999.

[10] T. Sawaya, K. Iigusa, M. Taromaru, T. Ohira, "Reactance diversity: proof-of-concept experiments in an indoor multipath-fading environment with a 5-GHz prototype planar ESPAR antenna," *Consumer Communications and Networking Conference*, 5-8 Jan. 2004, pp. 678-680.

[11] M. Yamamoto, M. Taromaru, H. Sadamichi and A. Shimizu, "Performance of Angle Switch Diversity Using ESPAR Antenna for Mobile Reception of Terrestrial Digital TV," *Vehicular Technology Conference*, Fall-2006.

[12] C. Sun, A. Hirata, T. Ohira, and N. C. Karmakar,"Fast Beamforming of Electronically Steerable Parasitic Array Radiator Antennas: Theory and Experiment," *IEEE Transactions on Antennas and Propagation*, vol. 52, no. 7, July 2004.

[13] A. Kalis, A. G. Kanatas and C. B. Papadias, "A novel approach to MIMO transmission using a single RF front end," IEEE Journal on Selected Areas in Communications, vol. 26, No. 6, Aug. 2008.

[14] O. N. Alrabadi C. B. Papadias, A. Kalis and R. Prasad, "A Universal Encoding Scheme for MIMO Transmission Using a Single Active Element for PSK Modulation Schemes," *IEEE Transactions on Wireless Communications*, pages: 5133 - 5142, vol. 8, No. 10, October 2009.

[15] A. S. Y. Poon, R. W. Brodersen, and D. N. C. Tse, “Degrees of freedom in multiple-antenna channels: a signal space approach,” *IEEE Trans. on Information Theory*, vol. 51, no. 2, pp. 523-536, Feb. 2005.
[16] M. L. Morris and M. A. Jensen,, “Network Model for MIMO Systems With Coupled Antennas and Noisy Amplifiers,”*IEEE Transactions on Antennas and Propagation*, vol.53, no.1, Jan. 2005.
[17] C. Waldschmidt, S. Schulteis, and W. Wiesbeck, “Complete RF System Model for Analysis of Compact MIMO Arrays,” *IEEE Trans. on Veh. Tech.*, vol. 53, no. 3, May 2004.
[18] D. M. Pozar, “The active element pattern”, *IEEE Trans. on Antennas and Propagation*, vol. 42, no. 8, Aug 1994.
[19] L. Petit, L. Dussopt and J. Laheurte, “MEMS-Switched Parasitic-Antenna Array for Radiation Pattern Diversity,” *IEEE Transactions on Antennas and Propagation*, vol. 54, no. 9, Sep 2006.
[20] D. S. Shiu, G. J. Foschini, M. J. Gans and J. M. Kahn, “Fading correlation and its effect on the capacity of multielement antenna systems,” *IEEE Trans. Commun.*, vol. 48, no. 3, pp. 502-513, Mar. 2000.
[21] Y. Fei, Y. Fan, B. K. Lau, and J. S. Thompson, “Optimal Single-Port Matching Impedance for Capacity Maximization in Compact MIMO Arrays,” *IEEE Trans. Antennas and Propagation*, vol. 56, no. 11, Nov. 2008.
[22] A. Paulraj, R. Nabar and D. Gore, “Introduction to Space-Time Wireless Communications,” *Cambridge, U.K.: Cambridge Univ. Press*, 2003.
[23] R. A. Horn, “Matrix analysis,” *Cambridge university press*, 1996.
[24] J. Perruisseau-Carrier, O. N. Alrabadi, and A. Kalis,“Implementation of a Reconfigurable Parasitic Antenna for Beam-Space BPSK Transmissions,” *2010 European Microwave Conference (EuMA)*, Paris, France, September 2010, Page(s): 644 - 647.
[25] O. N. Alrabadi et al, “Spatial Multiplexing with a Single Radio: Proof-of-Concept Experiments in an Indoor Environment with a 2.6 GHz Prototype,” *IEEE Communications Letters*, pp. 178-180, vol. 15, no. 2, 17 Dec. 2010.
[26] D. Tse and P. Viswanath, “Fundamentals of Wireless Communication,” *Cambridge University Press*, 2005.